Phenotypic Antimicrobial Susceptibility Testing Based on Nucleic Acid Analysis

Thesis by

Nathan Garrett Schoepp

In Partial Fulfillment of the Requirements for

the degree of

Doctor of Philosophy

CALIFORNIA INSTITUTE OF TECHNOLOGY

Pasadena, California

2019

(Defended May 10, 2019)

Nathan Garrett Schoepp
ORCID: 0000-0002-2406-3693

ACKNOWLEDGEMENTS

There have been countless people who have helped me learn and mature until this point in my life. Nothing is done in isolation and I am extremely grateful for everyone who has helped, supported, and taught me. I am thankful for all the individuals (named and not named below) who I have learned from. I have been privileged in so many ways, and especially to be able to do work that I enjoy and I try to remember that every day.

First and foremost, I would like to thank my family for their love and constant support. My mom Julie, my dad Scott, and my brother Tim have given me so much even though I take them for granted far too often. They have provided me with the foundation to succeed, and have made so many parts of my life easy. I am forever grateful for this and hope in the future I can provide even a fraction of the support I was given. My family has helped me through stressful times and hard decisions. They have taught me the values I hold today, and they are as much responsible for my drive and motivation as anyone. I hope they feel some ownership over this work as well.

I would also like to thank the partners and friends who have supported me and given me much needed breaks from the difficulties of lab. These were important and memorable moments that kept me going.

All members of the Ismagilov lab also deserve a special thanks. Without them there would be no lab environment, no lab jokes, and no lab discussion. I value all of these, and my PhD would have been much less enjoyable without them. I have learned many technical and personal skills from each of you. Specifically, I would like to thank Travis Schlappi, Justin Rolando, Said Bogatyrev, Asher Preska Steinberg, Erik Jue, Emily Savela, Eric Liaw, Jesus Rodriguez Manzano, Daan Witters, and Natasha Shelby. I would like to especially acknowledge Travis Schlappi, for setting the bar for a model colleague and friend. I hope to get to work with more people like you.

I would like to thank the mentors in my life up to now. I have had the incredible fortune of working with many fabulous scientists and advisors. It seems the role of advisor/mentor is often underappreciated and thankless, and there is no way this paragraph does them justice. First, I would like to thank my advisor Rustem and my committee. Thank you Rustem for teaching me scientific rigor and excellence, providing truly exceptional resources, and for always being available. I would also like to thank my committee Jim Heath, Dave Tirrell, and Jared Leadbetter for their continued guidance and support throughout my PhD and their willingness to always take time when I need advice. I would also like to thank some exceptional individuals not on my committee but who have never hesitated to offer guidance or support: Mikhail Shapiro and Justin Bois. Both of you have been model mentors and I have the utmost respect for you.

Collaborations significantly increase the speed of scientific progress and I have seen this first-hand during my PhD. I would like to thank the UCLA microbiology lab (specifically Romney Humphries, Shelley Miller, and Janet Hindler) who provided clinical samples and participated in countless discussions. You made collaboration easy and smooth. I would also like to thank S.O. at the University of Washington for his passion and involvement in the ongoing work with *Neisseria gonorrhoeae*.

ABSTRACT

Antimicrobial resistance (AMR) is one of the most widely recognized threats to global health, and one that continues to grow as new mechanisms of resistance evolve and resistant pathogens spread. Antibiotics are a cornerstone of modern medicine, but their misuse and overuse has constantly and consistently reduced their efficacy to the critically low levels we observe today. As a result, the rate of mortality as a direct result of AMR is approaching over a million deaths annually, with 20-year projections in the ten-millions. Rapid, phenotypic antimicrobial susceptibility testing (AST) that could be performed at the point of care (most notably in ≤ 30 min) would decrease the overuse of antimicrobials, allow physicians to make informed choices about which antimicrobials to prescribe, and improve patient outcomes. Today no such method exists. The ultimate goal of the below work is to allow physicians to choose, instead of guess, which antibiotics to use. We envision that development of these tests into distributable diagnostics will drastically improve patient outcomes, curb the spread of resistance, strengthen global antibiotic stewardship, and forestall the post-antibiotic era.

PUBLISHED CONTENT AND CONTRIBUTIONS

Chapter II: Nathan G. Schoepp†, Eugenia M. Khorosheva†, Travis S. Schlappi, Matthew S. Curtis, Romney M. Humphries, Janet A. Hindler, and Rustem F. Ismagilov. "Digital Quantification of DNA Replication and Chromosome Segregation Enables Determination of Antimicrobial Susceptibility after only 15 Minutes of Antibiotic Exposure." Angewandte Chemie 2016, 55 (33), 9557-9561. DOI: 10.1002/anie.201602763

This chapter describes the use of digital quantification of nucleic acids to shorten the required antibiotic exposure time needed to determine the antibiotic susceptibility phenotype of *E. coli* clinical isolates. Nathan G. Schoepp: 1. Major contributor to selecting DNA replication as AST marker, contributed knowledge on AST state of the art and effects of antibiotics on replication, contributed to digital resolution hypothesis, contributor to chromosome segregation hypothesis 2. Optimized antibiotic exposure protocols 3. Performed all antibiotic exposures 4. Maintained bacterial isolates 5. Performed all bulk and digital quantification experiments 6. Contributed all data to figures 1, 2, 3, S1, S2, S3, and table S2, contributed all non-sheared data to figure 4 7. Drew figures 1, 2, 3, 4, S1, S2, S3, and constructed table S2 8. Contributed to writing abstract, introduction, results/discussion, and conclusion sections of manuscript 9. Contributed to writing of supplemental information Eugenia Khorosheva: 1. Major contributor to selecting DNA replication as AST marker, major contributor of knowledge on AST state of the art and effects of antibiotics on replication, contributed to selecting 23S gene as a target of choice, contributed to digital resolution hypothesis, contributed to chromosome segregation hypothesis 2. Selected experimental protocols for maintenance and growth of isolates 3. Established initial AST protocols and experimental workflow from exposure to extraction 4. Selected and optimized protocols for amplification with Enterobacteriaceae specific 23S primers. 5. Contributed to optimizing DNA shearing experiments. 6. Contributed to writing introduction, results/discussion, and conclusion sections of manuscript Travis S. Schlappi: 1. Contributed knowledge on AST statistics, contributed to digital resolution hypothesis 2. Connected FDA guidelines for establishing new antimicrobial susceptibility determination methods to statistical hypothesis testing for both qPCR and dPCR. 3. Performed statistical analysis (p-

values and error bars) for all data presented in the manuscript and supplemental information. 4. Performed preliminary digital PCR experiments showing that dPCR can resolve differences in concentration after 15min exposure that qPCR cannot. 5. Contributed to writing of supplemental information. Matthew S. Curtis: 1. Contributed to selecting DNA replication as AST marker, contributed knowledge on AST state of the art and effects of antibiotics on replication, contributed to digital resolution hypothesis, major contributor to chromosome segregation hypothesis 2. Selected and optimized shearing protocols on extracted DNA for the analysis of chromosome structure. 3. Performed shearing experiments to generate data for figure 4. 4. Contributed to statistical analysis 5. Contributed to writing of the introduction, results/discussion, and conclusion of the manuscript

Chapter III: Nathan G. Schoepp[†], Travis S. Schlappi[†], Matthew S. Curtis, Slava S. Butkovich, Shelley Miller, Romney M. Humphries, and Rustem F. Ismagilov. "Rapid pathogen-specific phenotypic antibiotic susceptibility testing using digital LAMP quantification in clinical samples." Science Translational Medicine 2017, 9 (410). DOI: 10.1126/scitranslmed.aal3693

This chapter describes the use of rapid digital LAMP assay to determine phenotypic antibiotic susceptibility of bacteria directly from clinical urinary tract infection samples in less than 30 min. The order of co-first authors was determined by coin toss. T.S.S., N.G.S., and R.F.I. contributed to the design and/or interpretation of the reported experiments or results. T.S.S., N.G.S., M.S.C., S.S.B., and R.F.I. contributed to the acquisition and/or analysis of the data. T.S.S., N.G.S., R.M.H., and R.F.I. contributed to the drafting and/or revising of the manuscript. M.S.C. was primarily responsible for real-time imaging acquisition and analysis. S.M. and R.M.H. were primarily responsible for acquiring clinical samples and performing gold standard broth microdilution ASTs. R.F.I. and R.M.H. contributed administrative, technical, and supervisory support.

Chapter IV: Tahmineh Khazaei, Jacob T. Barlow, Nathan G. Schoepp, and Rustem F. Ismagilov. "RNA markers enable phenotypic test of antibiotic susceptibility in *Neisseria*

gonorrhoeae after 10 minutes of ciprofloxacin exposure." Scientific Reports 2018, 8 (1), DOI: 10.1038/s41598-018-29707-w

This chapter describes the discovery and use of RNA biomarkers to determine the phenotypic susceptibility of *Neisseria gonorrhoeae* to ciprofloxacin after a short antibiotic exposure. Tahmineh Khazaei: Co-designed the study with NGS; Developed the computational pipeline for processing and analyzing RNA sequencing data and for selection of RNA markers. Using this pipeline, identified porB and rpmB as the top markers for this study; Established the RNA extraction protocol for *Neisseria gonorrhoeae* samples (e.g. best kit/protocol to use); Performed RNA extraction of *Neisseria gonorrhoeae* samples from all the AST experiments in this study for RNA sequencing and performed the quality assessment of the extracted RNA. (This step was after the initial AST exposures performed by NGS or JTB.); Wrote the manuscript and generated all the final figures for publication. Jacob T. Barlow: Worked side-by-side with TK on day-to-day experimental optimization of RNA AST pipeline on CDC strains, including choice of using 16S rRNA as a control marker; Generated glycerol stocks used for the 50 CDC strains using NGS's protocol; Set up all cultures and ran all antibiotic exposures for the 50 CDC strains using NGS's protocols; Ran all qPCR and dPCR experiments for assessing changes in RNA markers; Designed and implemented statistical thresholding method for determination of differential genes; Used thresholding method to choose 4 additional markers tested; Designed and optimized primers for the additional markers; Generated visualization strategy for plots in figures 2, 3, 4, and 5 before handing off to TK to prepare final versions for paper. Nathan G. Schoepp: Designed "high throughput" sample handling and exposure workflow for isolates used by JTB and TK; Obtained initial set of *Neisseria gonorrhoeae* isolates from UCLA; Established *Neisseria gonorrhoeae* culturing and quantification methods which included 1) selecting and screening medias (including the one ultimately used in AST experiments) and 2) selecting and testing primers from literature for specificity, speed, and LOD; Performed initial AST exposures using *Neisseria gonorrhoeae* isolates, which TK then extracted and sequenced; Designed primers used in final manuscript for rpmB and porB markers; Assisted JTB in primer design for other markers by demonstrating primer design workflow and tools; Made minor

contributions to manuscript including minor edits, and providing TK with graphics used in Fig. 1.

Chapter V: Nathan G. Schoepp, Eric J. Liaw, Emily S. Savela, and Rustem F. Ismagilov. "Differential DNA accessibility to polymerase enables 30-minute phenotypic β-lactam antibiotic susceptibility testing of carbapenem-resistant Enterobacteriaceae." *Submitted*.

This chapter describes the use of a novel polymerase-accessibility method using loop-mediated isothermal amplification (LAMP) to determine phenotypic antibiotic susceptibility of clinical Enterobacteriaceae isolates to β-lactams in less than 30 min. All authors contributed to conceiving the method, revising the manuscript, and interpretation of experimental results. NGS developed the sample handling workflow and performed all experiments for comparison of amplification methods, validation, and timed sample-to-answer experiments. NGS was the major contributor to manuscript preparation and prepared all figures. EJL performed filtration experiments, reviewed relevant medical literature, and contributed to manuscript writing. ESS performed early experimental work to link beta-lactam exposure to differential nucleic acid readout, analyzed data from validation experiments, and developed TTPD metrics. RFI supervised and guided the project, and helped compose the manuscript.

Chapter VI: Nathan G. Schoepp[†], Emily S. Savela[†], Justin C. Rolando, Olusegun O. Soge, and Rustem F. Ismagilov. "Surfactant-enhanced DNA accessibility to nuclease accelerates phenotypic β-lactam antibiotic susceptibility testing of *Neisseria gonorrhoeae*." *Submitted*.

This chapter describes the use of a novel nuclease-accessibility method using a surfactant-based enhancement step to determine phenotypic antibiotic susceptibility of clinical *Neisseria gonorrhoeae* isolates to β-lactams in less than 30 min (sum of steps). N.G.S. guided initial testing of enhancers and developed two-step nuc-aAST workflow; selected and performed initial testing of surfactant enhancers; optimized sample handling during ABX exposure; performed and analyzed no-enhancer time-course experiments (Fig. 2); designed

LAMP primers and contributed to the optimization of LAMP conditions for dLAMP experiments (Fig. 5); wrote the manuscript and created figures. E.S.S. performed initial enhancer testing experiments;. selected and performed initial testing of osmotic, autolysis, and surfactant enhancers; optimized sample handling prior to ABX exposure; performed and analyzed enhancer testing and nuc-aAST experiments (Figs. 3, 4, 5), and assisted in performing dLAMP experiments (Fig. 5); performed data analysis, selected the readout metric of percentage accessibility, and selected optimal conditions for nuc-aAST; contributed to writing the manuscript and figure design and wrote the methods section. N.G.S., E.S.S., and R.F.I. conceived of the project and discussed design and interpretation of experiments. J.C.R. optimized digital LAMP conditions, and performed and analyzed all digital LAMP experiments for Fig. 5. O.O.S. provided isolates and guided discussion on gold-standard AST and current treatment practices for *Ng*, and performed agar-dilution AST. R.F.I. supervised and guided the project, and helped compose the manuscript. All authors read and edited the manuscript.

Chapter VII: Erik Jue, Nathan G. Schoepp, Daan Witters, and Rustem F. Ismagilov. "Evaluating 3D printing to solve the sample-to- device interface for LRS and POC diagnostics: example of an interlock meter-mix device for metering and lysing clinical urine samples." Lab on a Chip 2016, 16 (10), 1852-60. DOI: 10.1039/c6lc00292g

This chapter describes the use of a 3D-printed metering and mixing device for transfer and lysis of urine samples. Erik Jue (EJ) contributed to the invention, design, and validation of the meter-mix device. This includes the invention and design of the plunger system (chambers, plungers, valves, stoppers), invention and design of the multivalve and interlock system, design of the sealing mechanisms, design of the static mixer, and the design of the urine suction tube. EJ validated device function, user operation, device assembly, urine suction tube anti-drip feature, accurate metering and dispensing, mixer efficacy, and compatibility with qPCR. Nathan Schoepp (NS) contributed to the invention of the multivalve and interlock system as well as testing of the meter-mix device using biological samples, including development and validation of polymerase chain reaction (PCR) and

loop-mediated isothermal amplification (LAMP) assays for the detection of Ct and Ng. All device validation and control experiments extracting urine spiked with either Ct or Ng prior to mixing with the device were performed by NS. Amplification of extracted nucleic acids using either PCR or LAMP was performed by NS, including data analysis. Daan Witters (DW) contributed to the initial invention and design of the meter-mix device as well as the writing, editing, and finalization of both the outline and manuscript.

Chapter VIII: Travis S. Schlappi[†], Stephanie E. McCalla[†], Nathan G. Schoepp, and Rustem F. Ismagilov. "Flow-through Capture and in Situ Amplification Can Enable Rapid Detection of a Few Single Molecules of Nucleic Acids from Several Milliliters of Solution." Analytical Chemistry 2016, 88 (15), 7647-7653. DOI: 10.1021/acs.analchem.6b01485

This chapter describes the development of a method to capture and amplify single nucleic acid molecules from large volumes of solution. Travis S. Schlappi: 1. Contributor to method/protocol development for capture experiments and in situ amplification experiments. 2. Major contributor to simulation and theory development. 3. Performed all simulations for Figures 1 and 2. 4. Developed protocol for DNA capacity measurements and performed all experiments for Figure 3. 5. Contributed to experiments and data accumulation for Figure 5. 6. Major contributor to outline, manuscript, and supporting information writing. 7. Major contributor to figure and manuscript revisions. 8. Made all figures and tables in the manuscript and supporting information. Stephanie E. McCalla: 1. Major contributor to concept of chitosan-based flow-through capture and in situ amplification for low concentration detection. 2. Major contributor to method/protocol development for chitosan functionalization (hydrogel and monolayer), capture experiments, and in situ amplification experiments. 3. Major contributor to simulation and theory development. 4. Performed preliminary experimental work on in situ amplification and flow-through capture. 5. Performed preliminary simulations for Figure 1c. 6. Contributed to outline writing. 7. Contributed to manuscript revisions. Nathan G. Schoepp: 1. Major contributor to method/protocol development for chitosan hydrogel synthesis. 2. Contributor to method/protocol development for capture experiments, and in-situ amplification. 3.

Contributor to experiments and data accumulation for Figure 5. 4. Minor contributor to manuscript writing. 5. Minor contributor to manuscript revisions.

Chapter IX: Justin C. Rolando, Erik Jue, Nathan G. Schoepp, and Rustem F. Ismagilov. "Real-Time, Digital LAMP with Commercial Microfluidic Chips Reveals the Interplay of Efficiency, Speed, and Background Amplification as a Function of Reaction Temperature and Time." Analytical Chemistry 2018, 91 (1), 1034-1042. DOI: 10.1021/acs.analchem.8b04324

This chapter investigates the use of commercial microfluidic chips to optimize real-time digital LAMP assays. J.C.R. conceptualized the method, generated and analyzed data. Wrote the paper, constructed figures, and performed all revisions. E.J. wrote the MATLAB software script for automated analysis of digital LAMP image sequences. Provided minor input to experimental design; and minor edits and inputs to the figures and manuscript. N.G.S. prepared and quantified nucleic acid stocks. Optimized buffer conditions for Bst 2.0. Provided minor input to experimental design and minor edits and inputs to the figures and manuscript.

†These authors contributed equally

TABLE OF CONTENTS

Chapter 1

Introduction

Antibiotic resistance is potentially the greatest global health threat facing humanity today, with a direct annual mortality rate of > 700,000[1]. Antibiotics are a foundational part of modern medicine[2-4]. Without antibiotics, it would be impossible to treat fatal infections, perform surgery, or protect immunosuppressed patients. The current gold-standard practice requires days to determine the phenotypic susceptibility profile of a patient's infection, meaning physicians do not have this information when choosing which antibiotic to prescribe[5]. There is an international need for solutions to this problem that is currently unmet[3,6,7]. The primary focus of my research has been to develop antibiotic susceptibility tests (ASTs) that could be performed at the point of care, *before antibiotic are prescribed*, in order to allow physicians to make informed prescriptions[8]. Providing clinicians with this information would i) re-enable the use of older antibiotics, ii) improve patient outcomes (save lives), and iii) dramatically slow the spread of antibiotic resistance.

Antibiotic resistance is a natural phenomenon, and one that will occur as long as antibiotics are used. The problem is not the existence of antibiotic resistance, but the rate at which it is emerging and spreading[9]. This rate is directly proportional to the amount of antibiotics used. The more any single antibiotic is used, the greater the chance that bacteria evolve resistance, and that resistance will spread. In order to ensure patient safety, physicians treat with broad-spectrum and even last-line antibiotics (according to consensus guidelines issued by the CDC[10] and WHO[11,12]), which further drives resistance. When resistance does emerge, it does not mean all infections are immediately resistant. However, even when rates of resistance are low (5-10%), physicians cannot risk prescribing an antibiotic that will not cure their patient's infection. Therefore, antibiotic treatment is escalated, and antibiotics that would otherwise be reserved for serious infections are used in routine cases. The use of these second- and third-line antibiotics

then increases the rates of resistance, leading to further escalation. This cycle (Figure 1-1) has led to the current global health emergency we face today. An antibiotic susceptibility test that could be performed before antibiotic prescriptions are made would enable physicians to make the most rational antibiotic choice while ensuring positive patient outcome.

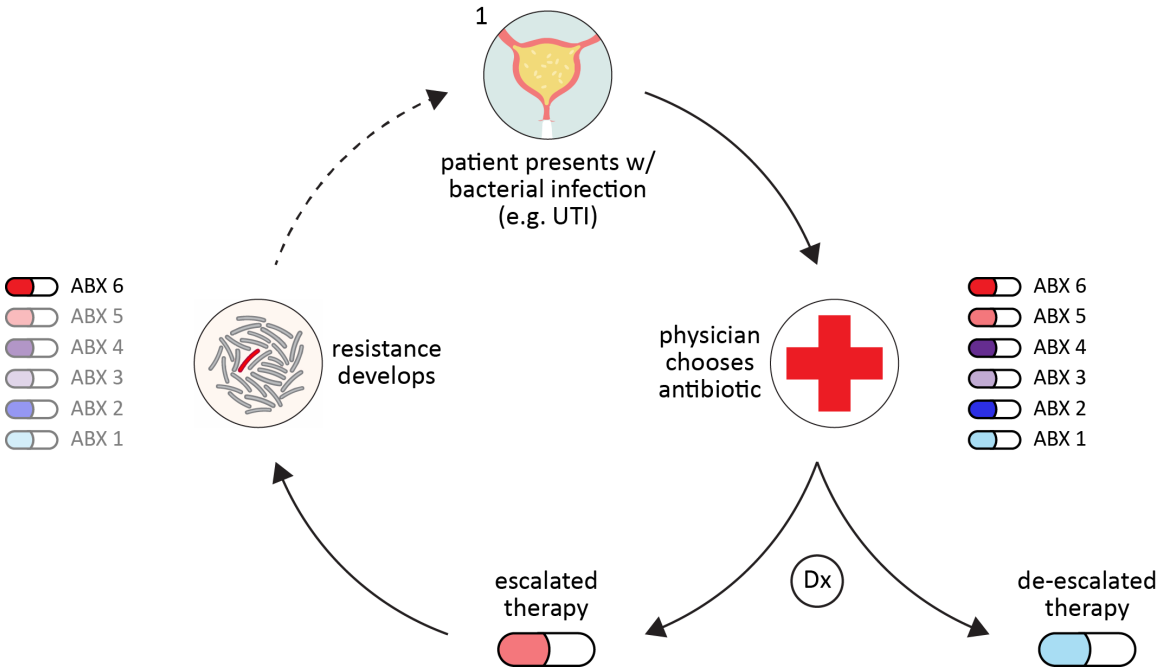

Figure 1-1. The antibiotic resistance cycle. Sufficiently fast diagnostics would allow physicians to make informed choices about which antibiotics to prescribe. This would lead to de-escalated treatments and preservation of antibiotics.

There are two types of antibiotic susceptibility tests: phenotypic and genotypic. The gold standard method in antibiotic susceptibility testing is broth or agar microdilution[13,14], a phenotypic method[15]. Phenotypic methods measure the response of the infecting pathogen to antibiotics, and are thus agnostic to the mechanism of resistance. These culture-based methods provide the most general and complete antibiotic susceptibility profiles; however, they currently require isolation and cultivation of the infecting pathogen and are thus too slow to be used at the point of care. Genotypic tests predict resistance based on the presence or absence of known resistance genes. Genotypic tests

can never prove susceptibility, they can only predict resistance with a given predictive value. However, because genotypic tests only require isolation and amplification of nucleic acids (and do not require the isolation of viable bacteria), they can be fast in certain scenarios. However, they remain under-utilized due to their lack of generality[6,7]. The goal of the majority of my thesis work has been to develop methods that determine phenotype (thus achieving the same general and complete susceptibility information achieved with culture-based gold-standard methods) using molecular methods after a short antibiotic exposure (thus achieving the same or faster time-scales as genotypic tests).

Chapters II and III of this work summarize our efforts to design a rapid phenotypic antibiotic susceptibility test suitable for use (in terms of assay time and simplicity) at the point of care. The method described in these chapters is based on measuring total nucleic acid concentration following a short antibiotic exposure in order to determine phenotypic antibiotic susceptibility. We first demonstrate that the antibiotic exposure step, a required step for any phenotypic test, can be shortened to 15 min[16]. We demonstrate this is possible for the four major classes of antibiotics used to treat urinary tract infections (UTIs) if digital nucleic acid quantification methods are used to assess DNA replication. Digital quantification was critical in shortening the antibiotic exposure step due to its higher precision and inherent partitioning step, which was important in the case of the β-lactam amoxycillin.

We then demonstrate that direct measurement of clinical samples is possible[17]. We show that extremely rapid readout of nucleic acid concentration is achievable using an isothermal nucleic acid amplification chemistry we have optimized, capable of amplifying and counting single DNA molecules in < 5 min in a microfluidic format suitable for implementation at the point of care. This unique combination of short exposure and ultra-fast digital quantification allows the susceptibility profile of bacteria in urine samples from patients with UTIs to be determined in less than 30 min. This

breakthrough shortens the time required to obtain AST results from 48 hours (the shortest possible time using culture-based methods) to the time span of a patient visit.

Chapter IV describes our work discovering and using RNA markers to test for ciprofloxacin susceptibility in *Neisseria gonorrhoeae*[18]. The use of RNA presents several challenges compared to DNA. However, we demonstrate that through screening and selection of appropriate RNA markers, susceptibility can be determined after an extremely short antibiotic exposure time.

Chapters V and VI describe two related but distinct methods for measuring susceptibility to β-lactams based on quantifying nucleic acid accessibility. The first is a novel test we have developed for measuring phenotypic β-lactam susceptibility in carbapenem-resistant Enterobacteriaceae (CRE)[19]. CRE represent some of the most lethal antibiotic-resistant infections encountered in the healthcare setting. We demonstrate determination of β-lactam susceptibility in all three major genera of CRE (*E. coli*, *K. pneumonia*, and *Enterobacter* spp.) in less than 30 min, and show that the method is completely agnostic to genotype. The second method is a nucleic acid accessibility-based test for measuring susceptibility of *Neisseria gonorrhoeae* to β-lactams[20]. We show that susceptibility can be measured much faster than cell division using a surfactant-based enhancement step in the presence of exogenously added nuclease, following antibiotic exposure. This method allows us to determine the phenotypic susceptibility of *Neisseria gonorrhoeae* isolates to β-lactams on unprecedented time scales.

Chapters VII – IX of this work summarize additional methods for improving nucleic acid diagnostic workflows. Chapter VII describes the design and validation of a 3D printed meter-mix device for use with clinical samples[21]. Chapter VIII describes a method for the capture and detection of extremely low concentrations of nucleic acids from large volumes of solution[22]. Chapter IX describes validation of a digital loop-mediated isothermal amplification (LAMP) system based on commercially available parts[23]. This system can be used to optimize LAMP assays or perform rapid digital quantification.

References

1 O'Neill, J. Tackling Drug-Resistant Infections Globally: Final Report and Recommendations. *Review on Antimicrobial Resistance* (2016). <https://amr-review.org/Publications.html>.

2 Marston, H. D., Dixon, D. M., Knisely, J. M., Palmore, T. N. & Fauci, A. S. Antimicrobial Resistance. *JAMA* **316**, 1193-1204, doi:10.1001/jama.2016.11764 (2016).

3 WHO. *Global Action Plan on Antimicrobial Resistance*, <https://www.who.int/antimicrobial-resistance/global-action-plan/en/> (2015).

4 Laxminarayan, R. *et al.* Antibiotic resistance-the need for global solutions. *Lancet Infect Dis* **13**, 1057-1098, doi:10.1016/S1473-3099(13)70318-9 (2013).

5 van Belkum, A. *et al.* Developmental roadmap for antimicrobial susceptibility testing systems. *Nature Reviews Microbiology*, doi:10.1038/s41579-018-0098-9 (2018).

6 Piddock, L. J. V. Assess drug-resistance phenotypes, not just genotypes. *Nature Microbiology* **1**, 16120, doi:10.1038/nmicrobiol.2016.120 (2016).

7 Bard, J. D. & Lee, F. Why Can't We Just Use PCR? The Role of Genotypic versus Phenotypic Testing for Antimicrobial Resistance Testing. *Clinical Microbiology Newsletter* **40**, 87-95, doi:10.1016/j.clinmicnews.2018.05.003 (2018).

8 O'neill, J. Rapid Diagnostics: Stopping Unnecessary Use of Antibiotics. *Review on Antimicrobial Resistance* (2015). <https://amr-review.org/Publications.html>.

9 Jorgensen, P. S. *et al.* Use antimicrobials wisely. *Nature* **537**, 159-161 (2016).

10 CDC. Sexually Transmitted Diseases Treatment Guidelines. (2015).

11 WHO. Guidelines for the Management of Sexually Transmitted Infections. (2003).

12 WHO. Treatment of Neisseria gonorrhoeae. (2016).

13 CDC. Agar Dilution Antimicrobial Susceptibility Testing. (2017).

14 CLSI. M100 Performance Standards for Antimicrobial Susceptibility Testing. (2017).

15 Jorgensen, J. H. & Ferraro, M. J. Antimicrobial susceptibility testing: a review of general principles and contemporary practices. *Clin Infect Dis* **49**, 1749-1755, doi:10.1086/647952 (2009).

16 Schoepp, N. G. *et al.* Digital Quantification of DNA Replication and Chromosome Segregation Enables Determination of Antimicrobial Susceptibility after only 15 Minutes of Antibiotic Exposure. *Angew Chem Int Ed Engl* **55**, 9557-9561, doi:10.1002/anie.201602763 (2016).

17 Schoepp, N. G. *et al.* Rapid pathogen-specific phenotypic antibiotic susceptibility testing using digital LAMP quantification in clinical samples. *Sci Transl Med* **9**, doi:10.1126/scitranslmed.aal3693 (2017).

18 Khazaei, T., Barlow, J. T., Schoepp, N. G. & Ismagilov, R. F. RNA markers enable phenotypic test of antibiotic susceptibility in Neisseria gonorrhoeae after 10 minutes of ciprofloxacin exposure. *Sci Rep* **8**, 11606, doi:10.1038/s41598-018-29707-w (2018).

19 Schoepp, N. G., Liaw, E. J., Savela, E. S. & Ismagilov, R. F. Differential DNA accessibility to polymerase enables 30-minute phenotypic β-lactam antibiotic susceptibility testing of carbapenem-resistant Enterobacteriaceae. *Under review* (2019).

20 Schoepp, N. G., Savela, E. S., Rolando, J. C., Soge, O. O. & Ismagilov, R. F. Surfactant-enhanced DNA accessibility to nuclease accelerates phenotypic β-lactam antibiotic susceptibility testing of Neisseria gonorrhoeae. *Under review* (2019).

21 Jue, E., Schoepp, N. G., Witters, D. & Ismagilov, R. F. Evaluating 3D printing to solve the sample-to-device interface for LRS and POC diagnostics: example of an interlock meter-mix device for metering and lysing clinical urine samples. *Lab Chip* **16**, 1852-1860, doi:10.1039/c6lc00292g (2016).

22 Schlappi, T. S., McCalla, S. E., Schoepp, N. G. & Ismagilov, R. F. Flow-through Capture and in Situ Amplification Can Enable Rapid Detection of a Few Single Molecules of Nucleic Acids from Several Milliliters of Solution. *Anal Chem* **88**, 7647-7653, doi:10.1021/acs.analchem.6b01485 (2016).

23 Rolando, J. C., Jue, E., Schoepp, N. G. & Ismagilov, R. F. Real-Time, Digital LAMP with Commercial Microfluidic Chips Reveals the Interplay of Efficiency, Speed, and

Background Amplification as a Function of Reaction Temperature and Time. *Anal Chem*, doi:10.1021/acs.analchem.8b04324 (2018).

Chapter II

Digital Quantification of DNA Replication and Chromosome Segregation Enables Determination of Antimicrobial Susceptibility After Only 15 Minutes of Antibiotic Exposure[1]

Abstract

Rapid antimicrobial susceptibility testing (AST) would decrease misuse and overuse of antibiotics. To achieve the "holy grail" of AST, a phenotype-based test that can be performed within a doctor visit, requires determining a pathogen's susceptibility after a short antibiotic exposure. We used digital PCR (dPCR) to test whether assessing DNA replication of the target pathogen via digital single-molecule counting would shorten the required antibiotic exposure. Partitioning bacterial chromosomal DNA into many small volumes during dPCR enabled AST via (i) precise quantification and (ii) a measure of how antibiotics affect the states of macromolecular assembly of bacterial chromosomes. This digital AST (dAST) determined susceptibility of clinical isolates from urinary tract infections (UTI) after 15 min of exposure for all four antibiotic classes relevant to UTI. This work lays the foundation to develop a rapid, point-of-care AST and strengthen global antibiotic stewardship.

Introduction, Results, and Discussion

The increasingly liberal use and misuse of antibiotics (ABX) has led to widespread development of antibiotic resistance.[1] To address this crisis, we need rapid and reliable tests of a pathogen's susceptibility to the drugs available (antimicrobial susceptibility test, AST) to provide correct, life-saving treatment, facilitate antibiotic stewardship[2] and drastically decrease hospital costs.[1a,3] Having a rapid AST that provides results within

---

[1]This chapter was first published in *Angewandte Chemie* with authorship belonging to Nathan G. Schoepp, Eugenia M. Khorosheva, Travis S. Schlappi, Matthew S. Curtis, Romney M. Humphries, Janet A. Hindler and Rustem F. Ismagilov. The original manuscript can be found at: http://dx.doi.org/10.1002/anie.201602763.

the period of a doctor visit would lead to improved patient outcomes and reduced spread of antibiotic resistance.[4] Development of a rapid AST is currently the focus of significant research efforts[5] that aim to supplant traditional clinical methods. To reduce the spread of resistance, one urgently needed AST is for urinary tract infections (UTIs), which are among the most common bacterial infections, yet can progress to pyelonephritis or sepsis.[6]

Two types of ASTs are currently used in clinical settings: traditional culture-based methods and genotypic methods. Culture-based tests remain the gold standard for determining antibiotic susceptibility because they detect phenotypic susceptibility to a drug, however these tests require a long period of antibiotic exposure (typically 16–24 h).[7] We[8] and others[5a,5b,5k,9] have proposed using confinement of single, or a small number of, bacterial cells in small volumes to reduce the duration of antibiotic exposure required to read out the phenotype of the target pathogen. However, these methods typically do not differentiate between the pathogen and the potential contamination of the sample with commensal bacteria. Alternative genotypic methods (detecting genes responsible for known mechanisms of resistance) are more rapid than culture-based approaches.[10] However, these resistance genes constitute only a fraction of all possible mechanisms of resistance,[11] and new forms of resistance evolve quickly.[12] Therefore, predicting resistance by analyzing a few known resistance genes is not a general solution.[13]

To develop more rapid and specific phenotypic tests, hybrid approaches have been proposed that use quantification of nucleic acids to determine the susceptibility or resistance phenotype after a short antibiotic exposure. These tests do not rely on detecting specific resistance genes.[5g,5i] For example, quantification of RNA has allowed determination of susceptibility to ciprofloxacin (cip) and rifampin,[5i] which impair transcription, after exposures as short as 15 min. However, these methods require longer incubation times when using antibiotics with different mechanisms of action. Using quantitative PCR (qPCR), quantification of DNA after 2–9 h of antibiotic exposure was

used to detect bacterial growth and determine susceptibility,[5d,5e] however an ideal exposure time would be shorter than one cell division.

Here we tested the hypothesis that digital methods of nucleic acid quantification,[14] such as digital PCR (dPCR), would enable use of DNA markers to perform a phenotypic AST after short antibiotic exposure. Digital methods partition bacterial chromosomal DNA into thousands of compartments and then use targeted amplification to determine the number of "positive" compartments containing DNA carrying one or more copies of the target gene. This partitioning should enable more precise and robust measurements of concentrations of bacterial DNA, achieving higher statistical power with fewer replicates relative to qPCR.[14c,15] Further, we hypothesized that this partitioning would provide unique capabilities for AST when analyzing target genes present in a macromolecular assembly, such as a bacterial chromosome during replication. In contrast to qPCR, dPCR results should reflect the state of the macromolecular assembly, providing a different count for a pair of segregated chromosomes (two positives) vs the chromosomal assembly just prior to segregation (one positive). We test our hypotheses in the context of four of the main antibiotics used in UTI treatment: ciprofloxacin (cip), nitrofurantoin (nit), sulfamethoxazole/trimethoprim (sxt), and amoxicillin/clavulanic acid (amc).[6a,7b,16]

We first determined the minimum antibiotic exposure time necessary to differentiate susceptible and resistant clinical UTI isolates using qPCR analysis of DNA after incubation in the presence ("treated") or absence ("control") of antibiotics (see SI). Cycle thresholds were used to calculate relative fold change

compared to t = 0 min (Fig. 2-1). When treated with cip, DNA replication in susceptible isolates was significantly inhibited, resulting in an increasing difference in fold change between target concentration in treated and control samples. If the isolate was resistant, DNA replication continued regardless of exposure. To align with FDA requirements for very major errors[17] we used a conservative alpha, 0.02 (see SI). Susceptibility to cip could be determined after 15 min of exposure. We obtained similar results using isolates pre-cultured in media and in urine (SI Fig. 2-S1), and chose to conduct all subsequent experiments in media in order to reduce the work with human samples and to ensure reproducibility. The focus of this work is to evaluate the differences in minimum antibiotic exposure time necessary to determine susceptibility when quantification of changes in DNA is performed with qPCR vs dPCR.

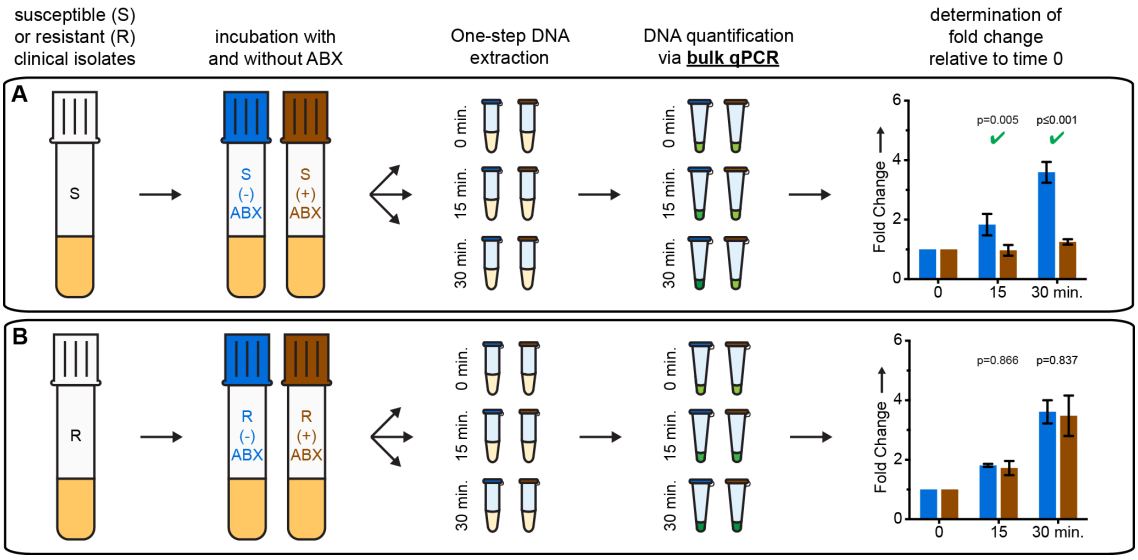

Figure 2-1. Quantitative PCR (qPCR) time course for exposure of (A) susceptible and (B) resistant UTI *E. coli* isolates to ciprofloxacin. For cycle thresholds (Ct) error bars are 2.8 S.D. (see SI), N=3. Fold change values represent change from t = 0 min; error bars represent the upper and lower bounds of the 98% C.I. (see SI), N=2. Significant differences (p-value ≤ 0.02) are marked with a green check.

These results are the first evidence of detection of phenotypic susceptibility based on DNA quantification after only 15 min of antibiotic exposure. The rapid effect of cip on DNA replication is logical because the drug's mechanism of action is to inhibit DNA-

gyrase and topoisomerase IV, producing double stranded breaks in DNA and directly inhibiting DNA replication.[18] To test generality, we evaluated AST with three other antibiotics: nit,[19] sxt,[20] and amc (which is not known to specifically affect DNA replication) (see SI). Using qPCR, 15 min of exposure to these three antibiotics was not sufficient to detect a significant difference in DNA replication in susceptible isolates (Fig. 2-2 B–D), while statistically significant differences were detectable with cip treatment (Fig. 2-2 A).

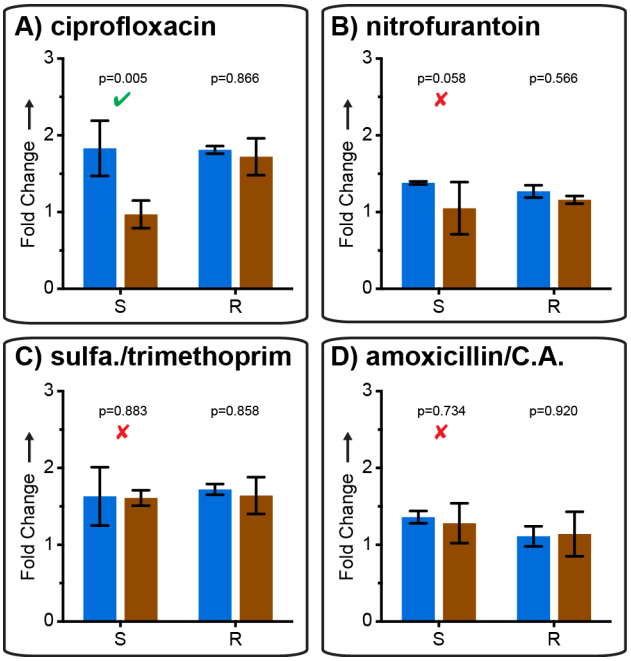

Figure 2-2. Comparison of susceptible and resistant isolates from UTI samples after a 15 min exposure with each of four antibiotics, analyzed by quantitative PCR. Fold change values represent change from t = 0 min; error bars are 98% C.I. (see SI), N=3. Significant (p-value $\leq$ 0.02) and nonsignificant differences detected using the susceptible isolate are marked with a green check and red x respectively.

We then tested AST with digital quantification by quantifying the same DNA samples using digital PCR (Fig. 2-3). For cip, we observed a more statistically significant difference (smaller p value) between target concentrations in treated and control susceptible isolates (Figure 2-3A), while target concentrations did not differ between

treated and control resistant isolates (Figure 2-3B). A significant difference was also detected after 15 min exposures to nit (Figure 2-3C) or sxt (Fig. 2-3C).

Interestingly, neither qPCR or dPCR detected susceptibility after exposure to amc when samples were denatured and treated with protease during extraction (SI Figure 2-S2). This confirmed that genome replication proceeded (resulting in an increase in the total number of amplifiable targets) during incubation with amc regardless of phenotype. We therefore tested the hypothesis that dPCR would be sensitive not only to the total gene copy number, but also to the state of macromolecular assembly of chromosomal DNA. If exposure to amc causes changes in chromosome segregation, even without affecting replication, dPCR should still be able to differentiate susceptible and resistant phenotypes. To preserve chromosome structure and macromolecular complexes, we performed DNA extraction in non-denaturing conditions without protease treatment. Under these conditions, dPCR provided susceptibility phenotype after 15 min of exposure to amc (Figure 2-3D).

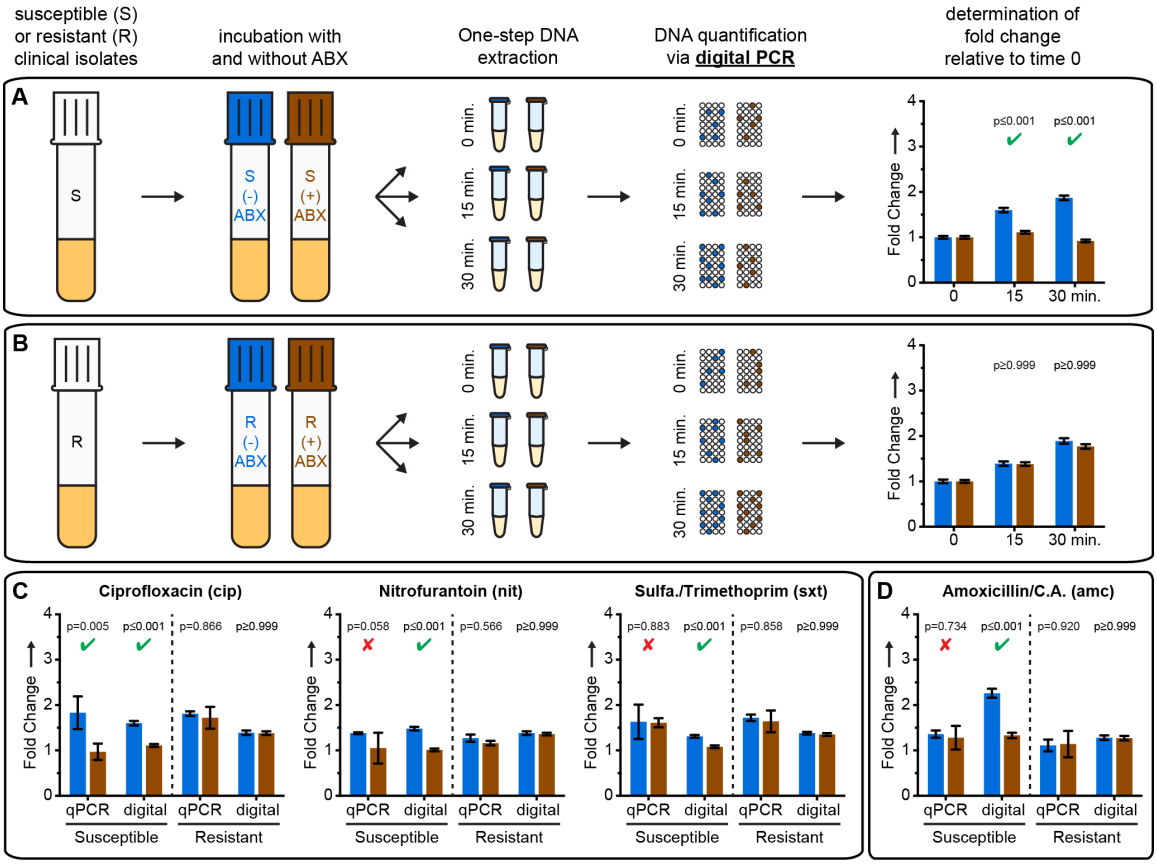

Figure 2-3. AST results using dPCR. (A,B) Time course results for exposure of susceptible (A) and resistant (B) UTI *E. coli* isolates to ciprofloxacin. (C,D) Fold changes after treatment with all four antibiotics tested. Significant (p-value ≤ 0.02) and nonsignificant p-values for susceptible isolates are denoted with a green check and red x respectively. Samples treated with amoxicillin/clavulanic acid (D) were extracted using a non-denaturing protocol. Concentrations are calculated using Poisson statistics. Fold change values represent change from t = 0 min; all error bars are 98% C.I. (see SI), N=3 for qPCR, N=2 for dPCR.

To test whether dPCR differentiated susceptible and resistant isolates via quantifying macromolecular assemblies, we designed control experiments in which all assemblies were sheared into ~1000 bp DNA fragments, much smaller than the average distance between 23S genes within the genome (see SI). As expected, shearing caused an increase in measured target concentration when quantified using dPCR, but not using qPCR (Fig. 2-4 A–B). In samples that were not sheared, dPCR detected the susceptible phenotype

after 15 min of amc exposure (Fig. 4C). Shearing these samples to disrupt macromolecular assemblies eliminated the ability to detect susceptibility (Fig. 4D); qPCR measurements confirmed this was not due to loss of DNA. This suggests that in amc-susceptible isolates short exposure to amc does not result in a change of the total number of target gene copies, but does change the macromolecular assembly of these copies.

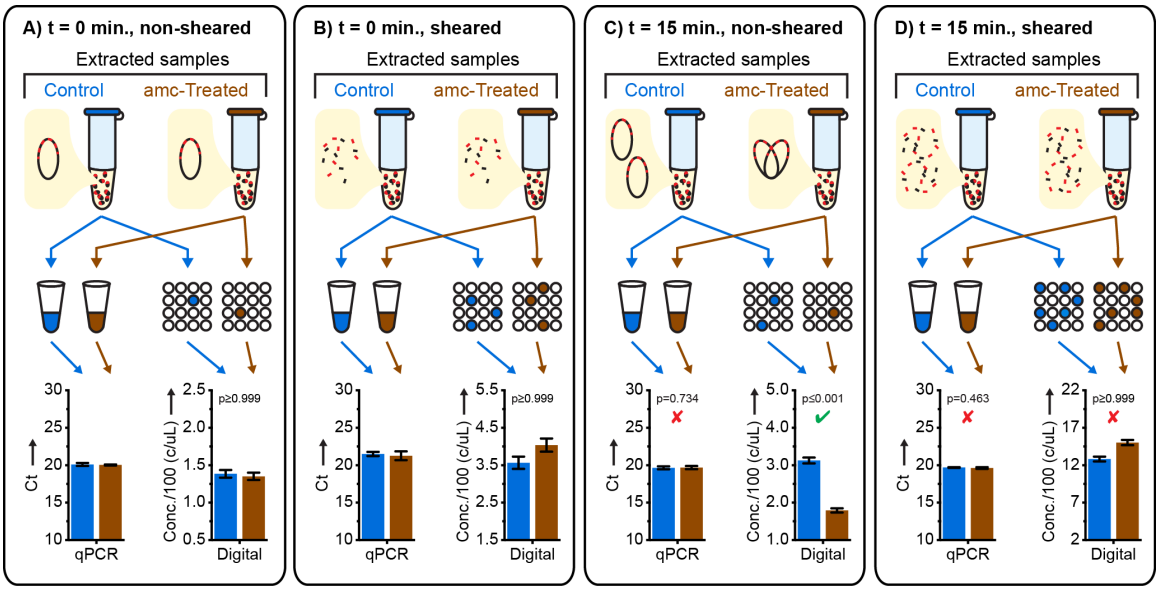

Figure 2-4. A mechanistic investigation of AST by digital PCR (dPCR) after beta lactam exposure and non-denaturing DNA extraction using shearing to disrupt macromolecular assemblies; error bars for qPCR are 2.8 S.D. (see SI), N=3; error bars are 98%C.I. for dPCR (see SI), N=2. Significant (p-value ≤ 0.02) and nonsignificant p-values for susceptible isolates quantified using dPCR are denoted with a green check and red x respectively (see SI).

Our results suggest a previously unknown effect of brief beta-lactam antibiotic exposure: a delay in chromosome segregation. Using dPCR (but not qPCR) this effect can be quantified by counting the number of macromolecular DNA assemblies containing 23S target genes, and used for AST. The high resolution of digital quantification enables measuring small (less than two-fold) changes in chromosome replication and segregation after antibiotic exposure shorter than the average time of cell division. The dAST approach developed here adds chromosome segregation to the list of the phenotypic markers suitable for rapid antibiotic susceptibility detection. The ability to partition macromolecular assemblies allows dAST to be used even when genome replication proceeds on the timescale of antibiotic exposure, while the high precision of digital quantification allows accurate determination of susceptibility after shorter exposure times than would be required using less-precise methods such as qPCR.

These dAST results warrant a follow-up study with a wide range of Gram-positive and Gram-negative bacterial isolates from urine, blood, and other sample types, and then a clinical study comparing dAST directly from patient samples to the gold standard culture-based methods. Elucidating the effects of using variable clinical samples with a range of background matrices is a critical next step in the development of a rapid, sample-to-answer AST. Ultimately, a sample-to-answer AST at the point of care must be robust, rapid, and require minimal sample handling and instrumentation. Ideally, such a workflow will integrate sample handling, antibiotic exposure, and quantification into a single device. We anticipate that digital isothermal amplification chemistries will replace dPCR in dAST.[15a,21] When integrated with sample preparation[22] and combined with simple readouts,[23] we envision that digital quantification will establish a new paradigm in rapid point of care AST.

Acknowledgements

This research was supported by DARPA Cooperative Agree- ment HR0011-11-2-0006, NIH Grant R01EB012946, and a grant from the Joseph J. Jacobs Institute for Molecular Engineering for Medicine. We thank Shelley Miller for advice and experimental assistance. We thank Natasha Shelby for contributions to writing and editing this manuscript.

References

[1] a) CDC, *Antibiotic Resistance Threats in the United States*, U. S. Department of Health
and Human Services, Centers for Disease Control and Prevention, **2013**, p. pp. 114; b) R. Laxminarayan*, et al.*, *Lancet Infect. Dis.* **2013**, *13*, 1057-1098.
[2]White House, *National Action Plan for Combating Antibiotic-Resistant Bacteria*, Washington D.C., **2015**, p. 62.
[3]R. R. Roberts*, et al.*, *Clin. Infect. Dis.* **2009**, *49*, 1175-1184.
[4]B. Spellberg*, et al.*, *Clin. Infect. Dis.* **2011**, *52 Suppl 5*, S397-428.
[5] a) J. D. Besant, E. H. Sargent, S. O. Kelley, *Lab Chip* **2015**, *15*, 2799-2807; b) Y. Lu, J. Gao, D. D. Zhang, V. Gau, J. C. Liao, P. K. Wong, *Anal. Chem.* **2013**, *85*, 3971-3976; c) C. Zhu, Q. Yang, L. Liu, S. Wang, *Angew. Chem. Int. Ed. Engl.* **2011**, *50*, 9607-9610; d) J. R. Waldeisen, T. Wang, D. Mitra, L. P. Lee, *PLoS One* **2011**, *6*, e28528; e) J. M. Rolain, M. N. Mallet, P. E. Fournier, D. Raoult, *J. Antimicrob. Chemother.* **2004**, *54*, 538-541; f) A. Mezger, E. Gullberg, J. Goransson, A. Zorzet, D. Herthnek, E. Tano, M. Nilsson, D. I. Andersson, *J. Clin. Microbiol.* **2015**, *53*, 425-432; g) K. E. Mach, R. Mohan, E. J. Baron, M. C. Shih, V. Gau, P. K. Wong, J. C. Liao, *J. Urol.* **2011**, *185*, 148-153; h) V. Ivančić*, et al.*, *J. Clin. Microbiol.* **2008**, *46*, 1213-1219; i) C. Halford, R. Gonzalez, S. Campuzano, B. Hu, J. T. Babbitt, J. Liu, J. Wang, B. M. Churchill, D. A. Haake, *Antimicrob. Agents Chemother.* **2013**, *57*, 936-943; j) A. K. Barczak*, et al.*, *Proc. Natl. Acad. Sci. U. S. A.* **2012**, *109*, 6217-6222; k) I. Sinn, P. Kinnunen, T. Albertson, B. H. McNaughton, D. W. Newton, M. A. Burns, R. Kopelman, *Lab Chip* **2011**, *11*, 2604-

2611; l) T. S. Mann, S. R. Mikkelsen, *Anal. Chem.* **2008**, *80*, 843-848; m) Y. Tang, L. Zhen, J. Liu, J. Wu, *Anal. Chem.* **2013**, *85*, 2787-2794.

[6]a) T. M. Hooton, *N. Engl. J. Med.* **2012**, *366*, 1028-1037; b) F. M. Wagenlehner, A. Pilatz, W. Weidner, *Int. J. Antimicrob. Agents* **2011**, *38 Suppl*, 51-57.

[7] a) J. M. Andrews, *J. Antimicrob. Chemother.* **2001**, *48 Suppl 1*, 5-16; b) Clinical and Laboratory Standards Institute (CLSI), *Performance Standards for Antimicrobial Susceptibility Testing; Seventeenth Informational Supplement*, **2007**.

[8]J. Q. Boedicker, L. Li, T. R. Kline, R. F. Ismagilov, *Lab Chip* **2008**, *8*, 1265-1272.

[9]C. H. Chen, Y. Lu, M. L. Sin, K. E. Mach, D. D. Zhang, V. Gau, J. C. Liao, P. K. Wong, *Anal. Chem.* **2010**, *82*, 1012-1019.

[10] a) S. G. Beal, J. Ciurca, G. Smith, J. John, F. Lee, C. D. Doern, R. M. Gander, *J. Clin.*
Microbiol. **2013**, *51*, 3988-3992; b) O. Altun, M. Almuhayawi, M. Ullberg, V. Özenci, *J. Clin. Microbiol.* **2013**, *51*, 4130-4136; c) A. J. Blaschke*, et al.*, *Diagn. Microbiol. Infect. Dis.* **2012**, *74*, 349-355; d) T. Spanu*, et al.*, *J. Clin. Microbiol.* **2012**, *50*, 2783-2785; e) T. Kostic, M. Ellis, M. R. Williams, T. M. Stedtfeld, J. B. Kaneene, R. D. Stedtfeld, S. A. Hashsham, *Appl. Microbiol. Biotechnol.* **2015**, *99*, 7711-7722.

[11]a) C. Walsh, *Nature* **2000**, *406*, 775; b) M. A. Webber, L. J. V. Piddock, *J. Antimicrob. Chemother.* **2003**, *51*, 9-11.

[12]R. T. Cirz, J. K. Chin, D. R. Andes, V. de Crecy-Lagard, W. A. Craig, F. E. Romesberg, *PLoS Biol.* **2005**, *3*, e176.

[13] a) N. Tuite, K. Reddington, T. Barry, A. Zumla, V. Enne, *J. Antimicrob. Chemother.* **2014**, *69*, 1729-1733; b) M. R. Pulido, M. Garcia-Quintanilla, R. Martin-Pena, J. M. Cisneros, M. J. McConnell, *J. Antimicrob. Chemother.* **2013**, *68*, 2710-2717.

[14] a) M. Baker, *Nature Methods* **2012**, *9*, 541-544; b) J. F. Huggett*, et al.*, *Clin. Chem.* **2013**, *59*, 892-902; c) A. S. Whale, J. F. Huggett, S. Cowen, V. Speirs, J. Shaw, S. Ellison, C. A. Foy, D. J. Scott, *Nucleic Acids Res.* **2012**, *40*, e82.

[15]a) D. A. Selck, M. A. Karymov, B. Sun, R. F. Ismagilov, *Anal. Chem.* **2013**, *85*,

11129-11136; b) B. Vogelstein, K. W. Kinzler, *Proc. Natl. Acad. Sci. U. S. A.* **1999**, *96*, 9236-9241; c) S. Weaver, S. Dube, A. Mir, J. Qin, G. Sun, R. Ramakrishnan, R. C. Jones, K. J. Livak, *Methods* **2010**, *50*, 271-276.

[16]K. Gupta*, et al.*, *Clin. Infect. Dis.* **2011**, *52*, e103-120.

[17] FDA, *Class II Special Controls Guidance Document: Antimicrobial Susceptibility Test (AST) Systems*, **2007**.

[18]A. Fàbrega, S. Madurga, E. Giralt, J. Vila, *Microb Biotech* **2009**, *2*, 40-61.

[19]D. R. Guay, *Drugs* **2001**, *61*, 353-364.

[20] P. A. Masters, T. A. O'Bryan, J. Zurlo, D. Q. Miller, N. Joshi, *Arch. Intern. Med.* **2003**, *163*, 402-410.

[21] a) A. Gansen, A. M. Herrick, I. K. Dimov, L. P. Lee, D. T. Chiu, *Lab Chip* **2012**, *12*, 2247-2254; b) J. Jarvius, J. Melin, J. Goransson, J. Stenberg, S. Fredriksson, C. Gonzalez-Rey, S. Bertilsson, M. Nilsson, *Nature Methods* **2006**, *3*, 725-727; c) F. Shen, E. K. Davydova, W. Du, J. E. Kreutz, O. Piepenburg, R. F. Ismagilov, *Anal. Chem.* **2011**, *83*, 3533-3540; d) B. Sun, J. Rodriguez-Manzano, D. A. Selck, E. Khorosheva, M. A. Karymov, R. F. Ismagilov, *Angew. Chem. Int. Ed. Engl.* **2014**, *53*, 8088-8092.

[22] J. R. Buser, A. Wollen, E. K. Heiniger, S. A. Byrnes, P. C. Kauffman, P. D. Ladd, P. Yager, *Lab Chip* **2015**, *15*, 1994-1997.

[23] J. Rodriguez-Manzano, M. A. Karymov, S. Begolo, D. A. Selck, D. V. Zhukov, E. Jue, R. F. Ismagilov, *ACS Nano* **2016**, *10*, 3102-3113.

Supporting Information

Experimental Section

Materials and reagents

All reagents purchased from commercial sources were used as received unless otherwise stated. BBL Trypticase Soy Agar plates with 5% Sheep Blood and Bacto Brain Heart Infusion (BHI) media were purchased from BD (Franklin Lakes, NJ, USA). BHI was dissolved in deionized water at the manufacturers recommended concentration and

autoclaved prior to use. All antibiotic stock solutions and PCR reactions were prepared using sterile, nuclease-free water (NF-H_2O) purchased from Thermo Fisher (Waltham, MA, USA).

All antibiotics and clavulanic acid were purchased from Sigma-Aldrich (St. Louis, MO, USA), with the exception of amoxicillin, which was purchased from Alfa-Aesar (Ward Hill, MA, USA). Ciprofloxacin and clavulanic acid were prepared as a 1 mg/mL stock solutions in NF-H_2O. Nitrofurantoin was prepared as a 10 mg/mL stock solution in dimethylformamide (DMF). Sulfamethoxazole was prepared as a 10 mg/mL stock solution in dimethyl sulfoxide (DMSO). Trimethoprim was prepared as a 1 mg/mL stock solution in DMSO. All antibiotic stock solutions were stored at -20 °C. Amoxicillin was prepared fresh as a 1 mg/mL stock solution in NF-H_2O before each experiment.

QuickExtract DNA Extraction Solution and QuickExtract RNA Extraction Kit were purchased from Epicentre (Madison, WI, USA). SsoFast EvaGreen Supermix (2X) and QX200 ddPCR EvaGreen Supermix was purchased from Bio-Rad Laboratories (Hercules, CA, USA) and used for all qPCR and dPCR experiments respectively.

Pooled human urine (catalog no. 991-03-P) was obtained from Lee Biosolutions (Maryland Heights, MO, USA).

Isolate maintenance

Ten *E. coli* isolated from the urine of 10 unique patients were obtained from the University of California Los Angeles (UCLA) Clinical Microbiology Laboratory with approval from the UCLA and Veterans Affairs Institutional Review Boards and appropriate Health Insurance Portability and Accountability Act exemptions. All isolates were identified as *E. coli* using the Vitek2 GNID panel (bioMerieux, Durham, NC, USA), and chosen for use based on their determined MICs. Urine cultures were performed by routine semi-quantitative methods, by inoculating 1 μL of urine to a BBL Trypticase Soy Agar plate with 5% Sheep Blood (BAP, BD, Sparks MD) and a MacConkey plate

followed by overnight incubation at 35 +/-2 °C in ambient air. In all cases, the *E. coli* grew in pure culture at >100,000 colony forming units. Minimum inhibitory concentrations (MIC) for each isolate was determined by UCLA for ciprofloxacin (cip), nitrofurantoin (nit), sulfamethoxazole/trimethoprim (sxt), and amoxicillin/clavulanic acid (amc) using the Clinical and Laboratory Standards Institute (CLSI) reference broth microdilution method,[1] in panels prepared by UCLA with cation-adjusted Mueller-Hinton broth (MHB). BMD tests were incubated at 35 +/- 2 ºC in ambient air conditions for 16-20 h. MICs were interpreted using CLSI M100S 26th edition breakpoints.[1] *E. coli* isolates were stored at -80 °C in Brucella broth with 20% glycerol (Becton, Dickinson, Sparks, MD, USA). Isolates were subcultured twice on BAP and well-isolated colonies were used for antibiotic exposure time course experiments.

Antibiotic exposure time course experiments

In order to generate liquid culture for use in experiments, *E. coli* isolates were cultured overnight (10-12 hours) after scraping a small portion of the plate and inoculating in 4 mL BHI. Overnight cultures were re-inoculated into 4 mL of fresh BHI and grown for an additional 4–6 h until early logarithmic phase. Cultures were then diluted 10 fold into pre-warmed BHI, and optical density (600 nm) was measured using a portable spectrophotometer (GE Healthcare Ultrospec 10). OD was converted to approximate cell count using the correlation factor OD600 1.0 = 8.0*10^8 cells/mL). The dilutions prepared for OD measurements were then immediately diluted a second time into 2 mL polypropylene tubes to a final volume of 500 µL (dilution factor dependent on desired final cell concentration). These tubes were incubated for 5 min at 37 °C with shaking at 500 rpm in a heating/shaking block (Thermo Fisher Digital Heating Shaking Drybath) to ensure thorough mixing. During this time, separate 2 mL polypropylene tubes containing 450 µL of BHI with and without antibiotics were prepared. All exposure time courses were conducted with antibiotic concentrations above the minimum inhibitory concentration (MIC) of the susceptible isolate and below the MIC of the resistant isolate being tested. Ciprofloxacin exposure in media and urine was conducted at a final antibiotic concentration of 2.00 and 0.75 µg/mL respectively. Nitrofurantoin experiments

were performed at 64.00 μg/mL. Sulfamethoxazole/trimethoprim experiments were performed at 76.00/4.00 μg/mL. For amoxicillin experiments, susceptible isolates were exposed to a final concentration of 12.00 μg/mL, and resistant isolates were exposed to a final concentration of 14.00 μg/mL. Cultures were then diluted a final 10 fold (50 μL culture into 450 μL) into single tubes containing media with or without antibiotics, and time was started. 10 μL aliquots were removed at 0, 15, and 30 min., and immediately mixed with 90 μL of a one-step extraction buffer suitable for direct use in PCR. Denaturing extraction conditions used Epicentre QuickExtract DNA Extraction Solution. Cells were mixed with Epicentre QuickExtract DNA Extraction Solution, pipette mixed, incubated at 65 °C for 6 min., 98 °C for 4 min., then chilled on ice. Non-denaturing extraction conditions used Epicentre Quick Extract RNA Extraction solution. Aliquots were mixed with RNA extraction immediately via pipette, gently vortexed to ensure thorough mixing, and chilled on ice. All samples were stored at -20 °C for several days during use before being moved to -80 °C for long-term storage.

DNA fragmentation

DNA was fragmented to a predicted 1000 bp fragment size using a Covaris 220M ultrasonicator. Samples were diluted 10 fold into a 130 μL microTUBE AFA Fiber Snap-Cap, and sheered for 90 seconds at 20 °C with a Peak Incident Power of 50 W, duty factor of 2%, and 200 cycles per burst. This size was chosen to ensure that all copies of the 23S gene will be separated from each other. Based on an analysis of 11 *E.coli* strains isolated from UTIs, the average distance between 23S genes is 1,169 kb with the closest genes being 38 kb apart. These genomes may be accessed with the following accession numbers: CP011018.1; HG941718.1; CP007265.1; CP007391.1; CP002797.2; CP002212.1; CP001671.1; CU928163.2; CP000247.1; CP000243.1; CP011134.1.

DNA quantification

All qPCR reactions were performed using a Roche LightCycler 96. All reactions contained only SsoFast EvaGreen Supermix at a final concentration of 1X, forward and reverse primers (forward primer TGCCGTAACTTCGGGAGAAGGC, reverse primer

TCAAGGCTCAATGTTCAGTGTC) specific for Enterobacteriaceae[2] at a final concentration of 500 nM, template DNA at variable concentrations, and NF-H_2O. A single master mix containing supermix, primers, and NF-H_2O was prepared and aliquoted into PCR tubes. Template was then added, bringing the final volume to 30 µL. Each tube was then mixed thoroughly via pipette and technical triplicates (9 µL each) were aliquoted into the 96 well plate. Cycling conditions consisted of an initial denaturation step at 95 °C for 3 min. followed by 30 cycles of 95 °C for 20 s, 62 °C for 20 s, and 72 °C for 20 s. Following amplification a continuous melt curve was obtained between 55 and 95 °C. Total cycling time (including melt analysis) was 60 min.

Digital PCR reactions were carried out in a BioRad QX200 Droplet Digital PCR system according to the manufacturer's instructions. Samples were prepared in identical fashion as those prepared for qPCR. For each sample, two wells of the droplet generation chip and well plate were used to generate and thermocycle droplets, respectively. This resulted in approximately 40,000 droplets being analyzed for each sample. Cycling conditions consisted of an initial denaturation step at 95 °C for 5 min followed by 40 cycles of 95 °C for 30 s, 60 °C for 30 s, and 72 °C for 30 s. Following initial thermocycling, the sample was cooled to 4 °C for 5 min followed by a final heating step at 95 °C for 5 min. All thermocycling steps were performed with a 2 °C/s ramp rate. Total cycling time was 115 min.

Statistical analyses

Raw Ct values are not normally distributed; therefore, a typical plot showing the mean Ct +/- 2·SD does not mean that the true mean will lie in the confidence interval 95% of the time. Understanding this fact, we would still like to represent the variability in qPCR measurements for the raw Ct plot. We did this with a standard confidence interval calculation:

$$Ct_{U/L} = Ct_{avg} \pm t_{crit} \cdot \frac{s_{Cq}}{\sqrt{n}} \quad (1)$$

The critical t value (t_{crit}) for a 98% confidence interval with 2 degrees of freedom is 4.85; with $n = 3$ replicates, this results in the SD being multiplied by 2.80 for the confidence intervals. This does not mean that the true Ct is within this interval 98% of the time, but it does give a representation of the variability in Ct measurements.

In order to calculate the p-value for comparing treated and untreated samples, the raw Ct values (which are exponential) were linearized into a relative quantity (FC) with t = 0 min as the reference point using $FC = 2^{Ct(t)-Ct(0)}$. The log ratio of these linearized quantities was compared to ln(1.1) using a one-tailed t test. A one-tailed test was chosen because the untreated sample should have a higher concentration than the treated sample; if by some random event the treated sample has a statistically significant higher concentration than untreated, we don't want to draw the false conclusion that the isolate is susceptible. To account for pipetting variation (the treated sample could have randomly had 10% more bacteria pipetted into its media at time = 0 than the untreated sample), the null hypothesis is $\ln\left(\frac{FC_{ut}}{FC_t}\right) - \ln(1.1) = 0$ instead of $\ln\left(\frac{FC_{ut}}{FC_t}\right) = 0$. This makes the AST more conservative (reducing very major errors) by requiring that the untreated sample have at least 1.1 fold more copies than the treated sample. P-values for digital PCR were calculated with a one-tailed Z test comparing $\ln\left(\frac{FC_{ut}}{FC_t}\right)$ to $\ln(1.1)$, with FC_{ut} representing the fold change in concentration of the untreated sample with respect to time = 0 and FC_t representing the same quantity, but for the treated sample.

Discussion of mechanism of action of antibiotics tested

In addition to ciprofloxacin, we evaluated three other antibiotics used in the treatment of UTIs: (i) nitrofurantoin, which is reduced to a reactive radical inside the cell, reacting with multiple cellular targets including enzyme involved in DNA synthesis[3], which would directly affect replication; (ii) the combination of sulfamethoxazole and trimethoprim, which synergistically inhibit folic acid biosynthesis, subsequently impairing multiple metabolic reactions including thymidine synthesis[4]; and (iii)

amoxicillin, which disrupts the synthesis of the peptidoglycan layer of bacterial cell walls leading to lysis[5], but is not known to specifically affect DNA replication.

Figures and Tables

Isolate Number	Specimen	AMC	CIP	NIT	SXT
1	urine	<=2	<=.25	<=16	<=1
2	urine	<=2	<=.25	<=16	<=1
3	urine	<=2	<=.25	<=16	<=1
5	urine	<=2	<=.25	<=16	<=1
6	urine	>16	>2	<=16	<=1
8	urine	<=2	>2	64	>8
10	urine	4	>2	<=16	>8
11	urine	ND	>2	>256	>8

Table 2-S1. Minimum inhibitory concentrations for all isolates tested, as determined by broth dilution. AMC = amoxicillin/clavulanic acid, CIP = ciprofloxacin, NIT = nitrofurantoin, SXT = sulfamethoxazole/trimethoprim. ND = not determined.

Isolate Number	S or R	ABX	[ABX] (ug/mL)	DNA Extraction Type	Control or Treated	Fold Change (qPCR)	Upper Bound 98% CI (qPCR)	Lower Bound 98% CI (qPCR)	p-val (qPCR)	Fold Change (dPCR)	Upper Bound 98% CI (dPCR)	Lower Bound 98% CI (dPCR)	p-val (dPCR)
1	S	cip	2.00	denaturing	control	1.41	0.19	0.19	0.006	1.15	0.03	0.03	<0.001
					treated	0.99	0.02	0.02		0.78	0.02	0.02	
5	S	cip	2.00	denaturing	control	1.83	0.36	0.36	0.005	1.60	0.05	0.05	<0.001
					treated	0.97	0.18	0.18		1.11	0.03	0.03	
10	R	cip	2.00	denaturing	control	1.81	0.05	0.05	0.866	1.39	0.05	0.05	>0.999
					treated	1.72	0.24	0.24		1.38	0.04	0.04	
2	S	nit	64.00	denaturing	control	1.38	0.02	0.02	0.058	1.48	0.04	0.04	<0.001
					treated	1.05	0.34	0.34		1.01	0.03	0.03	
3	S	nit	24.00	denaturing	control	2.93	0.67	0.67	0.027	1.58	0.10	0.10	<0.001
					treated	1.87	0.09	0.09		1.00	0.04	0.04	
11	R	nit	64.00	denaturing	control	1.27	0.08	0.08	0.566	1.38	0.04	0.04	>0.999
					treated	1.16	0.05	0.05		1.36	0.03	0.03	
3	S	sxt	76.00	non-denaturing	control	1.34	0.07	0.07	0.302	3.37	0.25	0.25	0.001
					treated	1.19	0.17	0.17		2.67	0.19	0.19	
5	S	sxt	76.00	denaturing	control	1.63	0.38	0.38	0.883	1.31	0.03	0.03	<0.001
					treated	1.61	0.10	0.10		1.08	0.03	0.03	
8	R	sxt	76.00	denaturing	control	1.72	0.07	0.07	0.858	1.38	0.03	0.03	>0.999
					treated	1.64	0.24	0.24		1.35	0.03	0.03	
1	S	amc	12.00	denaturing	control	1.60	0.17	0.17	0.973	1.49	0.04	0.04	>0.999
					treated	1.60	0.02	0.02		1.62	0.05	0.05	
1	S	amc	12.00	non-denaturing	control	1.36	0.08	0.08	0.734	2.26	0.10	0.10	<0.001
					treated	1.28	0.26	0.26		1.33	0.06	0.06	
1	S	amc	12.00	non-denaturing*	control	3.50	0.72	0.72	0.463	3.60	0.19	0.19	>0.999
					treated	3.14	1.45	1.45		3.72	0.18	0.18	
3	S	amc	14.00	non-denaturing	control	1.60	0.20	0.20	0.535	6.56	0.28	0.28	<0.001
					treated	1.46	0.55	0.55		1.37	0.07	0.07	
6	R	amc	14.00	non-denaturing	control	1.11	0.13	0.13	0.920	1.15	0.04	0.04	>0.999
					treated	1.14	0.29	0.29		1.24	0.04	0.04	

Table 2-S2. Raw data and additional experiments performed with multiple isolates. "S or R" refers to susceptible or resistant as determined by MIC. ABX = antibiotic. * indicates samples were sheared prior to quantification (see methods section of SI). Experiment exposing isolate 1 to ciprofloxacin was performed in 1:1 media:urine, all other experiments were performed in media.

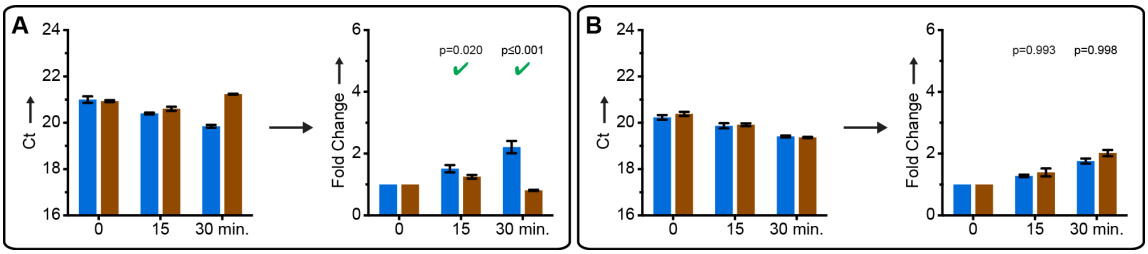

Figure 2-S1. qPCR time course for exposure of (A) susceptible and (B) resistant UTI *E. coli* isolates to ciprofloxacin pre-cultured in urine and exposed to antibiotics in 1:1 urine:BHI. Raw cycle thresholds represent the average of technical triplicates; error bars represent 2.8 standard deviations (see SI). Fold change values represent change from t = 0 min; error bars represent the upper and lower bounds of the 98% confidence interval. Significance was defined as a p-value <= 0.02 when comparing the fold change in 23S concentration of samples incubated without antibiotics (blue) to 1.1 times the fold change in 23S concentration of samples with antibiotics (brown) at a specific time point. Significant differences detected using the susceptible isolate are marked with a green check.

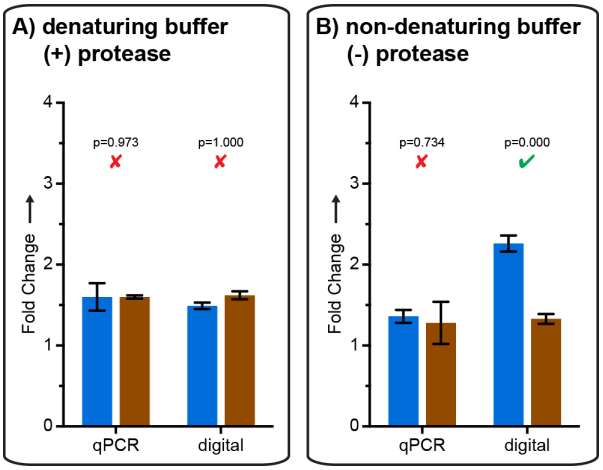

Figure 2-S2. Comparison of susceptible isolate analyzed by qPCR and digital PCR after a 15 min exposure to amoxicillin/clavulanic acid and extracted using a denaturing buffer with protease treatment (A) and a non-denaturing buffer without protease treatment (B). Fold change values represent change from t = 0 min; error bars are 98% confidence intervals. Significance was defined as a p-value <= 0.02 when comparing the fold change

in 23S concentration of samples incubated without antibiotics (blue) to 1.1 times the fold change in 23S concentration of samples with antibiotics (brown) at a specific time point. Significant and non-significant differences are marked with a green check and red x respectively.

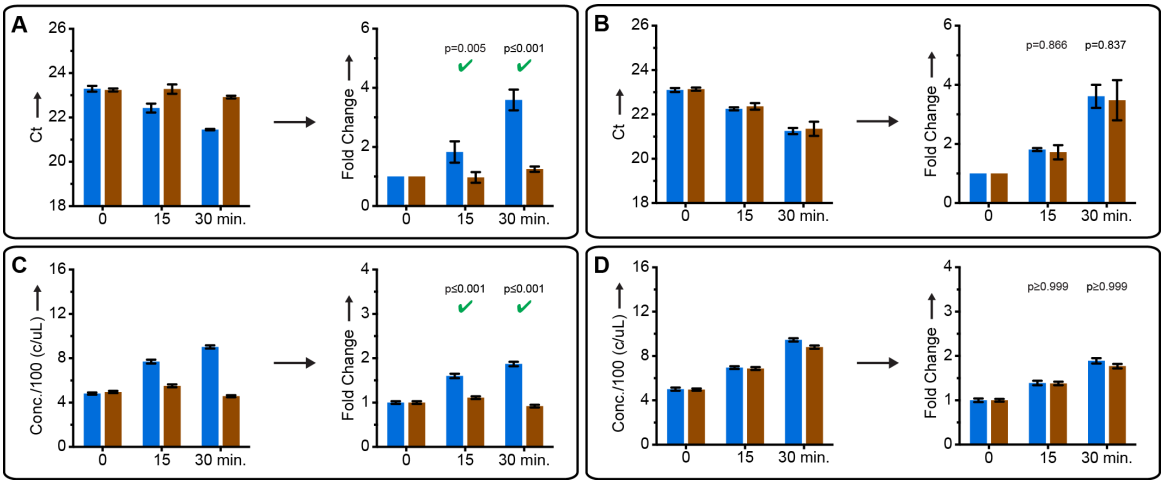

Figure 2-S3. Fold change plots from Figures 1 and 3 with corresponding Ct and concentration plots to demonstrate conversion from either Ct or concentration to fold change. (A, B) AST results using qPCR. Time course for exposure of (A) susceptible and (B) resistant UTI *E. coli* isolates to ciprofloxacin. For cycle thresholds (Ct) error bars are 2.8 S.D. Fold change values represent change from t = 0 min; error bars represent the upper and lower bounds of the 98% C.I. Significant differences (p-value ≤ 0.02) are marked with a green check. (C, D) AST results using dPCR. Time course for exposure of susceptible (C) and resistant (D) UTI *E. coli* isolates to ciprofloxacin. Concentrations are calculated using Poisson statistics; error bars represent the upper and lower bounds of the 98% C.I. Fold change values represent change from t = 0 min; error bars represent the upper and lower bounds of the 98% C.I. Significant (≤ 0.02) p-values for susceptible isolates are denoted with a green check.

Contributions of non-corresponding authors

Nathan G. Schoepp:

- Major contributor to selecting DNA replication as AST marker, contributed knowledge on AST state of the art and effects of antibiotics on replication, contributed to digital resolution hypothesis, contributor to chromosome segregation hypothesis
- Optimized antibiotic exposure protocols
- Performed all antibiotic exposures
- Maintained bacterial isolates
- Performed all bulk and digital quantification experiments
- Contributed all data to figures 1, 2, 3, S1, S2, S3, and table S2, contributed all non-sheared data to figure 4
- Drew figures 1, 2, 3, 4, S1, S2, S3, and constructed table S2
- Contributed to writing abstract, introduction, results/discussion, and conclusion sections of manuscript
- Contributed to writing of supplemental information

Eugenia Khorosheva:

- Major contributor to selecting DNA replication as AST marker, major contributor of knowledge on AST state of the art and effects of antibiotics on replication, contributed to selecting 23S gene as a target of choice, contributed to digital resolution hypothesis, contributed to chromosome segregation hypothesis
- Selected experimental protocols for maintenance and growth of isolates
- Established initial AST protocols and experimental workflow from exposure to extraction
- Selected and optimized protocols for amplification with Enterobacteriaceae specific 23S primers.
- Contributed to optimizing DNA shearing experiments.

- Contributed to writing introduction, results/discussion, and conclusion sections of manuscript

Travis S. Schlappi:

- Contributed knowledge on AST statistics, contributed to digital resolution hypothesis
- Connected FDA guidelines for establishing new antimicrobial susceptibility determination methods to statistical hypothesis testing for both qPCR and dPCR.
- Performed statistical analysis (p-values and error bars) for all data presented in the manuscript and supplemental information.
- Performed preliminary digital PCR experiments showing that dPCR can resolve differences in concentration after 15min exposure that qPCR cannot.
- Contributed to writing of supplemental information.

Matthew S. Curtis:

- Contributed to selecting DNA replication as AST marker, contributed knowledge on AST state of the art and effects of antibiotics on replication, contributed to digital resolution hypothesis, major contributor to chromosome segregation hypothesis
- Selected and optimized shearing protocols on extracted DNA for the analysis of chromosome structure.
- Performed shearing experiments to generate data for figure 4.
- Contributed to statistical analysis
- Contributed to writing of the introduction, results/discussion, and conclusion of the manuscript.

Romney M. Humphries and Janet A. Hindler contributed microbiological and AST expertise.

SI References

[1]Clinical and Laboratory Standards Institute, *M100S Performance Standards for Antimicrobial Susceptibility Testing*, 26th ed., Wayne, Penn., USA, **2016**.

[2]K. Matsuda, H. Tsuji, T. Asahara, Y. Kado, K. Nomoto, *Appl. Environ. Microbiol.* **2007**, *73*, 32-39.

[3]D. R. Guay, *Drugs* **2001**, *61*, 353-364.

[4]P. A. Masters, T. A. O'Bryan, J. Zurlo, D. Q. Miller, N. Joshi, *Arch. Intern. Med.* **2003**, *163*, 402-410.

[5]A. Tomasz, *Annu. Rev. Microbiol.* **1979**, *33*, 113-137.

Chapter III

Rapid pathogen-specific phenotypic antibiotic susceptibility testing using digital LAMP quantification in clinical samples [2]

Abstract

Rapid antimicrobial susceptibility testing (AST) is urgently needed for informing treatment decisions and preventing the spread of antimicrobial resistance resulting from the misuse and overuse of antibiotics. To date, no phenotypic AST exists that can be performed within a single patient visit (30 min) directly from clinical samples. We show that AST results can be obtained by using digital nucleic acid quantification to measure the phenotypic response of Escherichia coli present within clinical urine samples exposed to an antibiotic for 15 min. We performed this rapid AST using our ultrafast (~7 min) digital real-time loop-mediated isothermal amplification (dLAMP) assay [area under the curve (AUC), 0.96] and compared the results to a commercial (~2 hours) digital polymerase chain reaction assay (AUC, 0.98). The rapid dLAMP assay can be used with SlipChip microfluidic devices to determine the phenotypic antibiotic susceptibility of E. coli directly from clinical urine samples in less than 30 min. With further development for additional pathogens, antibiotics, and sample types, rapid digital AST (dAST) could enable rapid clinical decisionmaking, improve management of infectious diseases, and facilitate antimicrobial stewardship.

Introduction

[2]This chapter was first published in *Science Translational Medicine* with authorship belonging to Nathan G. Schoepp, Travis S. Schlappi, Matthew S. Curtis, Slava S. Butkovich, Shelley Miller, Romney M. Humphries, and Rustem F. Ismagilov. The original manuscript can be found at: http://dx.doi.org/10.1126/scitranslmed.aal3693.

The emergence of antibiotic resistance is an impending threat to global health. It is projected to cause 10 million deaths and more than $1 trillion in total economic impact by 2050 if left unchecked (1, 2). To combat antimicrobial resistance, facilitate stewardship, and improve patient outcomes, health care providers need to be able to determine antibiotic susceptibility rapidly and ideally at the point of care (POC) (3–6). The need for rapid antimicrobial susceptibility testing (AST) to guide antibiotic treatment is recognized by all major health organizations, including the Centers for Disease Control and Prevention and the World Health Organization (7–11).

Urinary tract infections (UTIs) are among the most common bacterial infections, accounting for ~8 million primary care visits annually, and are almost always treated with antibiotics (12, 13). In the absence of a rapid AST, UTIs are among the many infections that are treated with second-line antibiotics, such as the fluoroquinolone ciprofloxacin (cip), instead of first-line antibiotics, such as nitrofurantoin (nit) (14). This increased use of fluoroquinolones is accompanied by the emergence of fluoroquinolone resistance, limiting treatment options, which is especially critical in life-threatening cases, such as when UTIs progress to sepsis. Thus, UTIs are a specific clinical scenario where an inexpensive and rapid (within the ~30-min duration of a patient visit) AST would notably improve patient outcomes and antimicrobial stewardship.

No such AST diagnostic currently exists. Phenotypic AST methods based on culture of the target pathogen are the current gold standard but are too slow to support immediate treatment decisions or to be implemented at the POC (15). Genotypic methods, which detect known resistance genes, are faster because they do not require a culturing step (16–18). Genotypic methods have shown promise in select clinical settings where the presence of a single gene yields high predictive value, such as testing for mecA to detect methicillin-resistant Staphylococcus aureus (19–21). However, genotypic tests have not been implemented more broadly because they are not generalizable to different pathogens or mechanisms of resistance, especially in the case of Gram-negative bacteria, for which more than 800 resistance genes are known for b-lactam class antibiotics alone (22).

An ideal AST would test the phenotypic response of a pathogen to antibiotics in a pathogen-specific manner and provide an AST answer (susceptible or resistant) in less than 30 min (23, 24). This is a critical bar to meet because if the AST result can be obtained within the time span of a patient visit, then the information can be used to inform treatment and facilitate antimicrobial stewardship at the POC. Additionally, in some infections, such as sepsis, accelerated time to treatment is correlated with improved patient outcome (25). To achieve this speed, the AST method needs to work directly from a clinical sample. Several methods, including our previous work (26), have improved the speed of individual steps of the phenotypic AST workflow (such as pathogen isolation and identification, antibiotic exposure time, sample preparation, and readout), but few of these papers report performing the entire workflow from start to finish using a clinical sample.

To date, no phenotypic AST has achieved a sample-to-answer result in less than 30 min directly from a clinical sample. Most of the methods under development were validated with clinical isolates of pathogens, which before the assay were grown in culture to a high density and not directly with clinical samples. Among the rapid phenotypic AST methods used with clinical samples, one microscopy-based method could differentiate susceptible and resistant isolates after only 10 min of antibiotic exposure but did not test clinical samples (27). A similarly rapid microscopy-based method could detect differences in bacterial growth during antibiotic treatment after as short as 6 min of antibiotic exposure using isolates, but the total assay time for a clinical sample was 155 min (28). As discussed in (28), clinical sample matrices, such as urine, present a challenge for rapid microscopy-based ASTs, affecting the speed and sensitivities (required cell concentrations) of these assays.

Furthermore, identification and differentiation of target pathogens from commensal organisms can be challenging if these steps rely only on imaging, without the molecular specificity offered by other methods. A microfluidic-based microscopy method using

isolates reported AST in ~3 to 4 hours without an identification step and estimated that the total assay time from a clinical sample would be 52 hours (29). Another microscopy-based method in clinical testing performs identification and AST from a positive culture in 5 to 6 hours, with additional overnight or longer time required to first grow the culture from a clinical sample (30, 31). An electrochemical method was used to determine susceptibility in as short as 25 min using nonspecific redox markers for reference strains (32), but the workflow lacked a pathogen identification step and the AST was not pathogen-specific. Other electrochemical methods are pathogen-specific but require at least 45 min of assay time when using isolates (33). Pathogen-specific electrochemical methods have also been used to determine susceptibility from clinical samples, but assay times were on the order of hours (34). Methods that perform phenotypic AST by quantifying nucleic acids (NAs) are promising because they provide molecular specificity, but so far, most have required long antibiotic exposures (~2 hours or more) in addition to the time required for measurement, which was as fast as 1.5 hours using isothermal amplification (35–37). This promise of an NA-based AST was highlighted in a study that used RNA gene expression markers and demonstrated antibiotic exposure times as short as 10 min for isolates and as short as 30 min for clinical samples, although in that landmark study, the total assay time was more than 23 hours as a result of using slow quantification technology (38).

We have shown previously that the antibiotic exposure time in a phenotypic AST can be shortened to 15 min by measuring DNA concentrations in a digital format (26). That work was performed with bacterial UTI isolates and required a 2-hour measurement step using commercial droplet digital polymerase chain reaction (dPCR). The transition from cultures of clinical isolates to clinical samples is invariably challenging for phenotypic AST methods, and previous works have highlighted these challenges (28, 38, 39).

Here, we asked and answered two salient questions: For clinical samples, (i) can digital single-molecule counting of pathogen DNA enable phenotypic AST after a short (15 min) antibiotic exposure, and (ii) is there a quantification strategy faster than PCR that can be

used in a digital format to achieve a pathogen-specific, sample-toanswer phenotypic AST within 30 min directly from a clinical sample? To answer these questions, we developed an ultrafast digital isothermal amplification assay to shorten the readout step and demonstrated that the entire contiguous sample-to-answer workflow could enable an AST result in less than 30 min from a clinical UTI urine sample. We tested the rapid digital loop-mediated isothermal amplification (dLAMP) assay we developed with 51 clinical UTI urine samples and compared the results to commercial dPCR analysis.

Results

Key processes and operational space of digital AST

A phenotypic AST consists of two key processes: antibiotic exposure and measurement of the AST marker. To meet the demands of a rapid AST, these two processes, plus sample handling, must occur within 30 min. The workflow of the digital AST (dAST) method involved the following steps: aliquoting and diluting a clinical urine sample into two equal volumes of media—one with an antibiotic and a control without antibiotic; incubation at 37°C for 15 min; quantification of a target NA sequence (AST marker) in each sample; and calculation of the ratio of the marker concentrations in the control and antibiotic-treated samples, defined as the control/treated (CT) ratio (Fig. 1A).

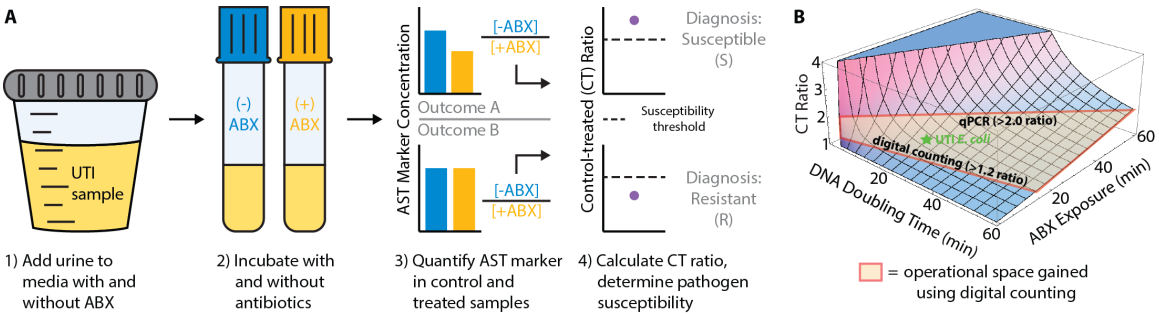

Fig. 3-1. Experimental workflow of the dAST method and computationally estimated operational space. (A) The workflow for detecting antibiotic susceptibility by measuring the quantity of a specific NA sequence (AST marker). Urine samples are incubated

without and with antibiotics (ABX) (steps 1 and 2), AST markers are quantified in control (−ABX) and treated (+ABX) samples (step 3), and the CT ratios are analyzed (step 4). (B) Theoretical model that predicts a CT ratio as a function of pathogen DNA doubling time and antibiotic exposure time. The operational space gained by using digital counting compared with qPCR is outlined in red.

Antibiotic susceptibility was determined by comparing a CT ratio to a previously determined threshold value (susceptibility threshold). Sample pairs that yield a CT ratio that falls above this threshold are called susceptible, and samples with a ratio below this threshold are called resistant. A CT ratio that is higher than the susceptibility threshold shows that DNA replication continued in the control (−ABX) sample but was slowed or halted in the antibiotic-treated (+ABX) sample, indicating that the sample was susceptible to that antibiotic. CT ratios lower than the susceptibility threshold indicate that DNA replication continued in both the control (−ABX) and antibiotictreated (+ABX) samples at the same rate, indicating that the sample was resistant to that antibiotic (Fig. 1A, step 4).

The time period of the antibiotic exposure step affects the resolution requirements for the quantification step: a shorter antibiotic exposure results in a smaller difference in the concentration of the target AST marker between the antibiotic-treated and control samples. Thus, at shorter exposure periods, quantification with higher resolution is required to reliably quantify an AST marker. To illustrate the interplay of antibiotic exposure time and required measurement resolution, we explored the trade-off of these three parameters (exposure time, required resolution, and DNA replication rate) computationally and made predictions about the resolution needed to detect susceptibility. We defined this combination of parameters as the operational space (Fig. 1B). For simplicity, we assumed that for an antibiotic-susceptible pathogen, DNA replication halts upon exposure to the antibiotic. Under this assumption, the DNA replication rate (which differs for different pathogens) directly determines the CT ratio at a given antibiotic exposure time. We also assumed that there was no lag phase upon

transitioning from urine to liquid media; if there is a lag phase, then the requirements for resolution become even more stringent, further emphasizing the need for high-precision digital measurements. For example, if the measurement method is limited to twofold resolution, such as in quantitative PCR (qPCR), and the pathogen's DNA doubles every 30 min, then the minimum exposure time necessary to achieve a CT ratio of 2 is 30 min. If the measurement method can instead resolve a 1.2-fold difference in concentrations, then the minimum exposure time decreases to 8 min. Measuring changes in DNA concentration with high resolution therefore allows the detection of a pathogen's response to antibiotic even faster than cell division time (26). Compared with bulk methods (such as qPCR or isothermal amplification), digital quantification can resolve the difference between the two concentrations with greater precision (26, 40, 41), which in turn enables shorter antibiotic exposure times (26).

Digital quantification achieves higher resolution by partitioning target molecules into thousands of compartments such that each compartment contains a single molecule. Amplifying each partitioned molecule to a detectable concentration and counting the number of positive compartments at the end point yield precise quantification. Resolution can be increased, and antibiotic exposure time reduced, by increasing the number of digital compartments. However, the benefit of adding more digital compartments decreases beyond ~1000 compartments, and additional compartments are better used for multiplexing of multiple markers or antibiotics. For example, at UTI-relevant concentrations of DNA (106 copies/ml), 1000 digital compartments with 1-nl volume each provides 1.23-fold resolution. Increasing the number of these compartments to 10,000 or 100,000 while correspondingly reducing their volumes to 0.1 and 0.01 nl each, to maintain the same sample volume and total number of target molecules, provides 1.18and 1.17-fold resolution, respectively (fig. S1). With 10,000 1-nl compartments, the resolution is 1.08, whereas 2000 1-nl compartments provide a resolution of 1.16 each, enabling a fourplex dAST (one control and four antibiotic-treated samples) to be performed with the same number of wells (fig. S1C).

We have previously demonstrated that a 15-min exposure step is sufficient to generate detectable differences in DNA concentrations between the control and antibiotic-treated samples using UTI isolates and four antibiotics commonly prescribed for UTIs (26). For a 15-min exposure period, which is shorter than the fastest reported uropathogenic Escherichia coli doubling time of 16 min (42), we predicted the DNA concentration in the control sample to increase 1.4× to 1.6× (Fig. 1B, green star). Other uropathogenic organisms have doubling times of 13 min (Klebsiella pneumoniae), 25 min (Proteus mirabilis), and 29 min (Staphylococcus saprophyticus) (43, 44). Therefore, theoretical estimates suggested that a 15-min exposure should provide a 1.4to 2.2-fold change, which is within the resolution of digital measurements. Historically, such measurements have required 90 min or more (45, 46). For the total assay time to remain less than 30 min, digital NA quantification must be performed in less than 10 min, assuming sample handling (including NA extraction) of at least 5 min and an antibiotic exposure of 15 min. On the basis of these theoretical calculations, we developed a method of digital NA quantification that could be performed in less than 10 min.

dAST in the presence of commensal organisms

A factor that may challenge phenotypic ASTs that are run directly on clinical samples is that commensal or contaminating organisms present in the sample may respond differently to a given antibiotic than the target pathogen. If the measurement method cannot differentiate between the response of the target pathogen and commensals, then susceptibility cannot be determined accurately. NA amplification can be designed to target a sequence specific to a potential pathogen species or families of interest. Therefore, we hypothesized that when using a pathogen-specific NA target, the CT ratio (and, therefore, the determination of the pathogen as susceptible or resistant by the AST) would not be affected by varying amounts of commensal bacteria. dAST was performed in the presence of Lactobacillus jensenii (Lj), a common commensal bacterium found in urine. An E. coli culture [~106 colony-forming units (CFU)/ml] was mixed with each of the three concentrations of Lj (0.1×, 1×, and 10× the optical density of the target

pathogen) and exposed to cip for 15 min. The response was measured using droplet dPCR, and susceptibility of E. coli was determined correctly at all concentrations of the commensal organism (Fig. 2).

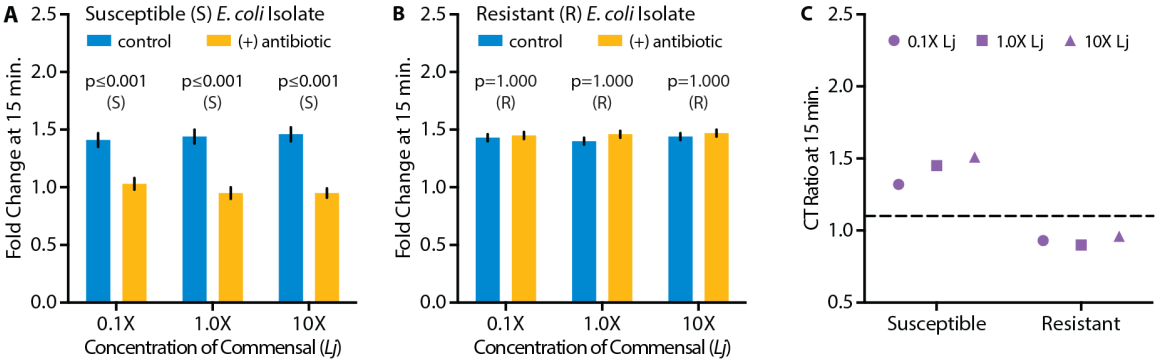

Fig. 3-2. dAST using dPCR is robust to the presence of high concentrations of commensal bacteria due to the specificity of NA amplification. (A) A cip-susceptible E. coli isolate and (B) a cip-resistant E. coli isolate from the urine of patients diagnosed with UTIs were exposed to cip (1.0 mg/ml) in the presence of varying amounts of Lj, a common urine commensal. Fold changes relative to time 0 were compared as described in (26) and used to determine susceptibility. (C) Susceptibility determined using the CT ratios after 15 min of antibiotic exposure for each concentration of Lj tested. n = 2 technical replicates for each biological sample. Error bars are 98% confidence intervals.

Optimization of isothermal amplification (LAMP)

We next focused on shortening the measurement time from 2 hours (time of amplification using dPCR) to <10 min. We investigated dLAMP first because it has been demonstrated previously by us and others (40, 47–50). However, these dLAMP assays previously took >45 min and were not shown to resolve small differences (~1.5×) in NA concentrations. Fast LAMP reactions often show background amplification in negative control experiments, so we aimed to also solve this problem.

We designed primers and optimized real-time LAMP in bulk solutions to maximize amplification speed while eliminating background amplification. At very high NA concentrations, real-time bulk LAMP assays have been reported to be as fast as 5 min (18, 51), but at the lower concentrations of a single target molecule present in a single digital partition (~1 copy/nl = 106 copies/ml), amplification takes 10 min or more (52–55). To mimic the concentration of a template in a single digital partition, we performed our bulk optimization experiments at ~106 copies/ml. We selected the E. coli 23S ribosomal DNA gene as the pathogen-specific NA sequence (dAST marker) and as the target for primer design because we showed previously that this was a reliable marker for DNA replication in the context of AST (26). PanEnterobacteriaceae primers would be useful for targeting other UTI pathogens. Although we did not purposefully design our primers to exclude other Enterobacteriaceae pathogens, we were able to detect K. pneumoniae and P. mirabilis in pilot experiments using the same primers. Sensitivity and specificity of these primers remain to be further validated for additional pathogens and commensals.

The LAMP optimization process (Fig. 3A) consisted of four steps: (1) screening multiple LAMP primer sets for speed and lack of background amplification, (2) screening multiple loop primer pairs with the selected primer set from step 1 for speed and lack of background amplification, (3) testing the selected LAMP and loop primers with a range of magnesium ion (Mg) concentrations, and (4) selecting the optimal amplification temperature from the data obtained in step 3. Each parameter was tested using a temperature gradient, which proved to be critical to minimizing the time to positive (TTP), the reaction time to detect a positive sample. Of the four tested LAMP primer sets, we selected set B because it showed the fastest amplification and no background amplification (Fig. 3A, step 1). No loop primer pair showed much earlier TTPs than any other pair, and no pair showed theoretical or experimental evidence of primer-dimers, so we arbitrarily chose the loop A set (Fig. 3A, step 2). Four concentrations of Mg were tested using the DNA polymerase Bst 3.0. The resulting TTPs varied by as much as 11 min depending on the amplification temperature. This optimization process resulted in

TTPs as fast as ~4 to 5 min for ~700 target copies in a 6-ml amplification volume, with the fastest TTP (4.4 min) obtained using 6 mM Mg at 71°C.

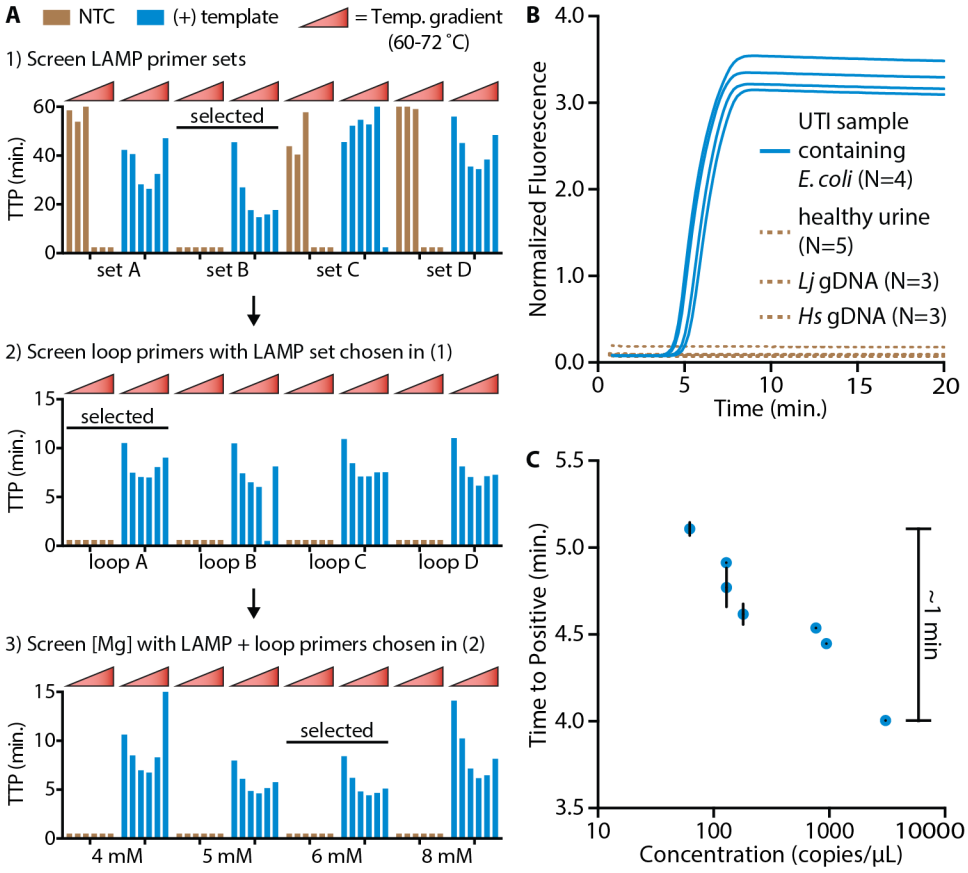

Fig. 3-3. Real-time LAMP optimization and compatibility with clinical samples. (A) Assay optimization protocol used to reduce the TTP from 15 to <5 min. Optimization was performed at a template concentration of ~700 or 0 copies per reaction. NTC, no template control. A value of 0.5 indicates that no amplification was observed. n = 1 for all TTP values. (B) Real-time fluorescence readout of amplified DNA for UTI urine samples containing E. coli (blue lines), healthy urine samples, urine samples containing gDNA of Lj, and urine samples containing human (Hs) gDNA (dashed brown lines). (C) TTP values for clinical UTI urine samples containing a range of pathogen concentrations. Error bars represent a single SD from the average of technical triplicates. n = 3 technical replicates for each TTP value.

Once LAMP primers and protocols had been optimized, we further tested their specificity for the dAST marker. No positive signals were obtained when we ran real-time LAMP using Lj genomic DNA (gDNA), human gDNA, or urine from healthy donors without any symptoms of UTI (Fig. 3B). When testing clinical UTI samples, a positive signal was only obtained when E. coli DNA was present. TTPs ranged from 4 to 5 min for clinical UTI samples (Fig. 3C). However, using this LAMP method in a standard well-plate format to resolve a 1.5× difference in concentration would require detecting a difference in TTP of ~8 s, which is difficult in practice to perform robustly (40).

dAST using ultrafast single-molecule counting (dLAMP)

Our next goal was to test whether using this optimized LAMP chemistry in a digital format would yield an accurate determination of antibiotic susceptibility while preserving the speed observed in bulk solutions. This would require the ability to resolve small changes in NA concentrations that occur after a 15-min exposure to antibiotic, despite any heterogeneity in TTPs (the difference in amplification kinetics of individual molecules), which has been observed previously (50, 56). Because sample matrices might increase the heterogeneity in TTPs and thus decrease the resolution, we tested clinical urine samples, which can contain urea, proteins, blood (including heme as a potent PCR inhibitor), and other cellular components that can interfere with assay detection. To eliminate extracellular DNA present in clinical urine as a potential source of error, we modified the dAST procedure that we previously developed for isolates (26) to include deoxyribonuclease (DNase) during the exposure step to digest any extracellular DNA (see the Supplementary Materials). We used the optimized LAMP assay (Fig. 3) with SlipChip microfluidic devices in a digital format (57). The SlipChip partitioned the samples into 1280 digital compartments. In each compartment, single molecules were amplified if present, and the total number of positive compartments was counted in real time (56). In a clinical setting, decisions are typically made from single assay runs, and thus, we tested whether differences in NA concentrations between the control and

antibiotic-treated samples could be resolved reliably using a single 1280-well SlipChip for each measurement.

Using dLAMP (Fig. 4), most (>80%) single molecules amplified between 4 and 10 min, as shown by the fluorescence curves plotted in Fig. 4 (A and F). As expected, heterogeneity in TTP was observed, likely as a result of the stochasticity of single-molecule amplification (50, 58). Despite heterogeneity and matrix effects of clinical urine, we detected a significant difference in NA concentration ($P = 6.1 \times 10{-}4$) after only 5 min of amplification time for the cip-susceptible clinical urine sample (Fig. 4C). For the cip-resistant sample, no significant difference in concentration was detected during the dLAMP assay ($P > 0.05$) (Fig. 4H). In both samples, the CT ratios were stable after 6 min and 40 s (6.7 min) of amplification (Fig. 4, D and I), were consistent with the ratios obtained by dPCR (Fig. 4, E and J), and yielded the correct AST call (susceptible or resistant). We then repeated this dLAMP assay for one nit-susceptible and one nit-resistant clinical urine sample. After 6.7 min of dLAMP amplification time, the CT ratios for both samples were stable, and the correct antibiotic-susceptibility call was determined (fig. S2). This demonstrates that the optimized dLAMP assay yields correct AST calls in only 6.7 min, below the 10-min limit necessary to achieve a 30-min dAST. Further, individual DNA target molecules were detected, and the DNA concentration was accurately quantified even after dilution during antibiotic exposure and sample preparation (table S1).

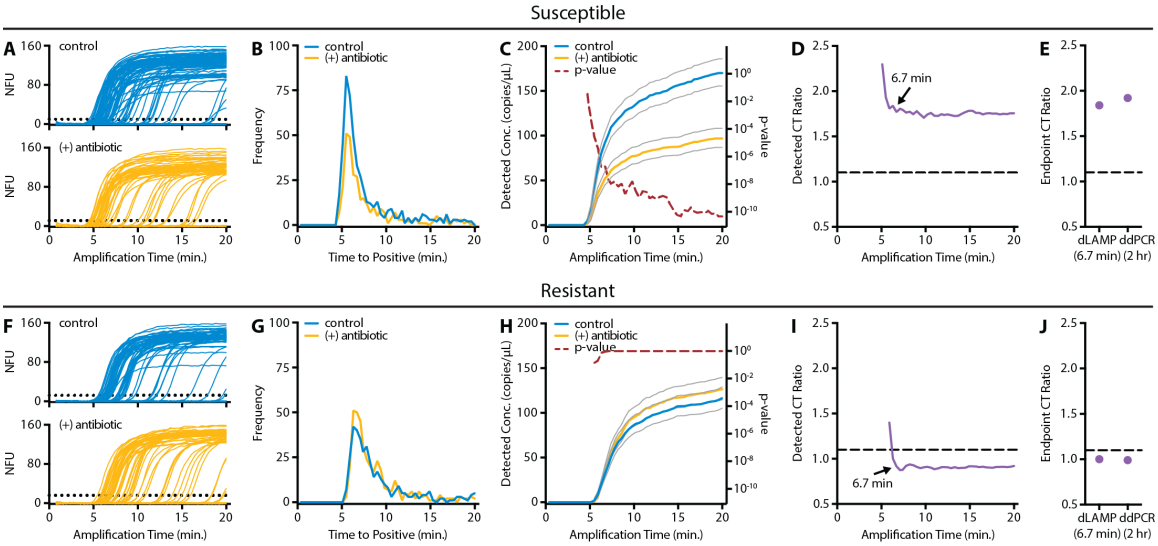

Fig. 3-4. High-resolution single-molecule NA amplification using ultrafast dLAMP for dAST of clinical UTI urine samples. UTI urine samples with (A to E) antibiotic-susceptible and (F to J) antibiotic-resistant E. coli. (A and F) Real-time fluorescence amplification traces (200 of 1280 traces shown for clarity). NFU, normalized fluorescence units; dotted line, positive threshold. When the normalized fluorescence intensity of a compartment crosses the threshold, that compartment is counted as positive. (B and G) TTP distribution determined by counting the number of compartments that crossed the positive threshold at each time point. (C and H) Detected concentrations of the target dAST marker in control and antibiotic-treated samples for successive image cycles. Note that these curves are distinct from the amplification curves shown in (A) and (F). Gray lines represent 95% confidence intervals. P values were calculated using a Z test (see Statistical analysis). (D and I) Detected CT ratios over time. Dashed line indicates susceptibility threshold. (E and J) Comparison of the CT ratios for droplet digital PCR (ddPCR) after 2 hours and dLAMP after 6.7 min of amplification.

Thirty-minute sample-to-answer dAST directly from clinical urine samples

Next, we tested whether the entire dAST workflow (antibiotic exposure, sample preparation, measurement, and data analysis) could be performed in less than 30 min (Fig. 5). To accomplish this goal, we shortened the sample preparation time from 10 to 2

min while maintaining compatibility with dLAMP. In parallel with antibiotic exposure of a clinical sample, rapid real-time LAMP was used to confirm the presence of E. coli and to measure the approximate NA concentration of the dAST marker in the sample (Fig. 5B). This step provided the identification of the pathogen and could be used to select the amount of NAs loaded on the chip to maximize the performance of the digital assay without adding time to the workflow; it also avoided the AST quantification step for the samples lacking the pathogen or containing subclinical amounts. We also modified the real-time image analysis software we developed previously (56) to calculate the concentrations of the dAST marker in real time from each image, instead of after completion of amplification.

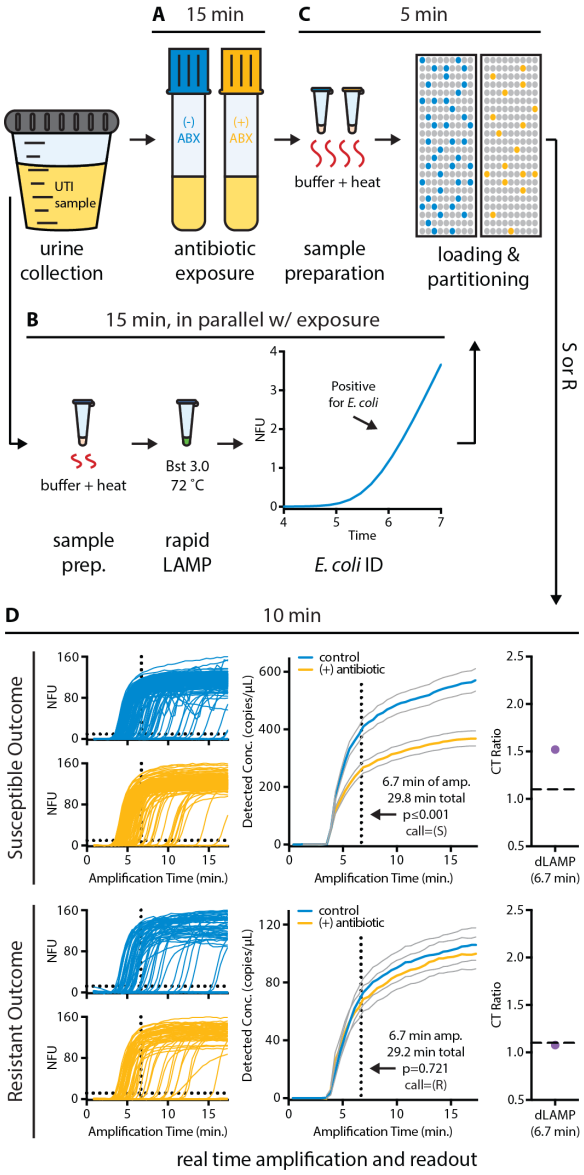

Fig. 3-5. Workflow of a sample-to-answer AST performed in less than 30 min. (A) A clinical UTI sample was added to media with and without cip and incubated for 15 min. (B) During the antibiotic exposure step, the optimized bulk LAMP as- say was performed on NAs prepared from an aliquot of the urine sample. Amplification indicated the presence of E. coli at clinically relevant concentrations. (C) Aliquots of the control and antibiotic-treated samples were added to extrac- tion buffer, NAs were prepared for quantification using dLAMP, and samples were rapidly partitioned using SlipChips. (D) dLAMP was monitored in real time, and a susceptibility call was determined after 6.7

min of amplification; data for one resist- ant and one susceptible sample are shown. P values were calculated using a Z test (see Statistical analysis). Gray lines represent 95% confidence intervals.

After these modifications, we calculated that all steps could be performed within ~24 min [15 min (exposure) + 2 min (sample preparation) + 6.7 min (readout)]. We tested whether these steps could be performed in succession to provide a full sample-to-answer workflow, including all fluid transfer steps and data analysis, within 30 min. We started a timer when an infected clinical urine sample was added to media with and without cip. After 29.8 min of total elapsed time (6.7 min of dLAMP amplification time), the software reported the control and treated concentrations for the cip-susceptible sample to be significantly different ($P = 7.4 \times 10{-}10$), with a CT ratio of 1.59. For the cip-resistant sample, no significant difference in concentration was reported through the entire dLAMP assay ($P > 0.05$). At 29.2 min (6.7 min of dLAMP amplification time), the CT ratio for the cip-resistant sample was 1.08 (Fig. 5D). This result shows how a combination of rapid partitioning, fast isothermal amplification, and high-resolution digital measurements enabled antibiotic susceptibility to be determined in less than 30 min.

dAST using a set of 51 clinical samples

Having established that the dAST method could be performed, sampleto-answer, in less than 30 min, we next tested dAST with 51 clinical samples using both dPCR and dLAMP readouts. Samples were exposed to antibiotic for 15 min, and NA extraction was performed on a total of 51 clinical UTI samples containing $\geq 5 \times 104$ CFU/ml E. coli (17 cip-susceptible, 14 cip-resistant, 18 nit-susceptible, and 5 nit-resistant). Three clinical samples were tested separately with cip and nit, for a total of 54 tests. We focused on categorical agreement of our binary susceptibility determination (susceptible or resistant) and did not test intermediate samples due to the variability in minimum inhibitory concentration (MIC) determination of gold standard AST methods (59, 60). It is common

to only challenge new AST methods against susceptible and resistant samples (34, 35, 61), which excludes a small fraction of samples for cip (62). To ensure that there were no special issues with bacteria with intermediate MICs, we used the dAST method on a small set of cip-intermediate isolates to better understand its performance (fig. S3).

We quantified the DNA AST marker of the control and treated extractions on all 54 samples with both dPCR and dLAMP. For each sample, the CT ratio was calculated and compared to a susceptibility threshold [1.10; determined in (26)] to classify the samples as resistant or susceptible (Fig. 6A). Discordant CT ratios were observed for five samples when compared with the gold standard broth microdilution method. To resolve the discrepancy, we reran three of these five discordant samples, averaging the second CT ratio with the CT ratio from the first run to obtain a consensus value of the CT ratio (table S2, samples #28, #29, and #36). As a control, we also reran one sample that was not discordant (table S2, sample #122). To ensure clinical samples yielded reproducible CT ratios, we used the dAST method to test a small set of cip-susceptible isolates in triplicate (fig. S4).

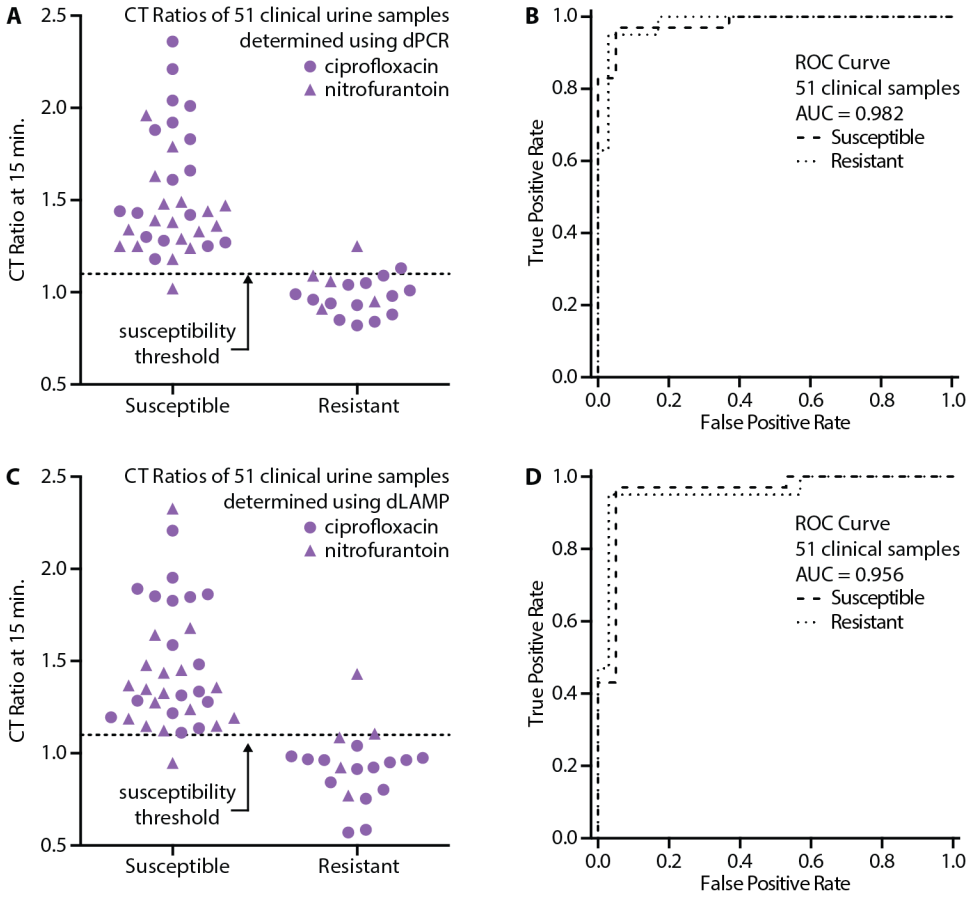

Fig. 3-6. dAST directly from clinical samples using dPCR and dLAMP for quantification. (A and C) Antibiotic suscep- tibility of 51 clinical E. coli–infected UTI samples determined using the CT ratios after 15 min of exposure to nit and cip (35 susceptible and 19 resistant; 3 samples were tested for both antibiotics). NA concentrations were quantified with dPCR (A) and dLAMP (C). (B and D) ROC curves for the dAST method as measured by dPCR (B) and dLAMP (D).

With 1.10 as the susceptibility threshold for dPCR measurements, the dAST method returned 51 correct calls (94.4% categorical agreement), 2 very major errors for 19 resistant samples (10.5%), and 1 major error for 35 susceptible samples (2.9%). Because 1.10 was a threshold based on experiments with isolates (26), we generated a receiver operating characteristic (ROC) curve to inform the optimal threshold for clinical UTI samples (Fig. 6B). ROC curves show the ability of a diagnostic test to discriminate

positives and negatives based on a threshold: Values below the threshold are called negative (resistant), and values above the threshold are called positive (susceptible). The area under the curve (AUC) for the generated ROC was 0.98. Using the optimal threshold given by the ROC curve (1.14), 53 of 54 dAST calls matched the gold standard AST call (98.1% categorical agreement) with 1 very major error (5.3%) and 0 major errors (0%).

We also used dLAMP to quantify the same 54 samples. The CT ratios at 6.7 min were calculated and plotted in Fig. 6C, along with the ROC curve for dLAMP (Fig. 6D). With 1.10 as the susceptibility threshold for dLAMP measurements at 6.7 min, the dAST method returned 51 correct calls (94.4% categorical agreement), 2 very major errors for 19 resistant samples (10.5%), and 1 major error for 35 susceptible samples (2.6%). The AUC for the generated ROC curve was 0.96. Using the optimal threshold given by the ROC curve (1.11), 52 of 54 dAST calls matched the gold standard AST call (96.3% categorical agreement) with 1 very major error (5.3%) and 1 major error (2.9%). These data show that although the optimal thresholds derived from the ROC curves (1.14 for dPCR and 1.11 for dLAMP) slightly improve the categorical agreement, they are consistent with the threshold established for isolates [1.10 (26)] and are consistent with each other. Quantifying DNA with dLAMP at 6.7 min produces similar CT ratios and susceptibility calls as dPCR.

Discussion

Here, we solved three problems to determine phenotypic antibiotic susceptibility in clinical samples within 30 min. First, we used digital quantification of a DNA marker to reduce the antibiotic exposure time to 15 min. Second, we showed that dAST is robust to the presence of commensal bacteria and clinical urine matrices. Third, we developed and optimized a rapid, high-resolution measurement method for quantifying NA targets that shortens the measurement step to less than 10 min.

The dLAMP assay developed here was capable of amplifying single target DNA molecules in less than 5 min. Despite the heterogeneity of single-molecule amplification times, high-resolution measurements were obtained even before all partitions with a target DNA molecule had amplified (~6.7 min). This makes dLAMP a strong tool for real-time, high-resolution, rapid measurements of NAs. Rapid, high-resolution measurements increase the information gained in shorter times and will be invaluable for other assays, such as viral load measurements and genotyping (50, 63, 64). LAMP was chosen for translation to a digital format because it is a well-established amplification chemistry (51, 65, 66) with several readout methods (67–70). If necessary, other amplification chemistries—including NASBA (NA sequencebased amplification), RPA (recombinase polymerase amplification), NEAR (nicking enzyme amplification reaction), and HDA (helicase-dependent amplification)—could be tested and optimized for a digital format and used to measure a marker of interest. Additionally, we show that the LAMP assay is compatible with a rapid, one-step extraction method, which considerably reduces the sample preparation time. Because of the speed of extraction and amplification, the same LAMP assay can be used in a real-time bulk format for rapid pathogen identification in parallel with the 15-min antibiotic exposure step. This step, completed in <10 min including sample preparation, did not extend the total assay time but provided two critical pieces of information before digital quantification: (i) whether a sample was infected with the pathogen of interest and (ii) whether a sample contained clinically relevant concentrations of the pathogen. UTI-positive samples gave TTP values of 4 to 5 min (corresponding to ~10^5 to ~10^6 DNA copies/ml, n = 7) (Fig. 3C), whereas healthy urine samples remained negative for at least 20 min (n = 5) (Fig. 3B). This specificity is critical in working with clinical samples because it enables the dAST to provide information specific to the pathogens of interest rather than commensals, contaminating organisms, or mixtures of pathogens. Additionally, using dLAMP to calculate the CT ratios and determine susceptibility was informative for estimating pathogen concentration in the urine sample (see table S1).

Most of the previous rapid AST methods used cultures of clinical isolates instead of clinical samples (see table S3 for a quantitative summary of the published state of the art). The introduction of commensal or contaminating organisms and clinical sample matrices to diagnostic workflows can cause major challenges in the development and translation of laboratory methods. It is therefore critical to prove that AST methods are compatible with clinical samples. Here, we have shown that the dAST method is compatible with a wide range of urine samples. Urine color of the samples included colorless, yellow, dark yellow, and red; pH ranged from <5.0 to 8.0; and protein concentrations ranged from 0.0 to 1.0 mg/ml (71). Additionally, red and white blood cell counts were as high as >106 cells/ml each in separate samples, and several samples demonstrated elevated glucose. One sample contained a lactose-positive Gram-negative rod bacterium (3 × 104 CFU/ml) in addition to the infecting E. coli. Although this study warrants more extensive follow-up investigation into more detailed correlations between urine composition and dAST speed and does not establish whether this method would work in a more complex matrix like whole blood, our results indicate that dAST is compatible with a wide range of urine matrices and contaminants in clinical samples.

The dAST method described herein was demonstrated with a specific scenario, and thus, there are inherent limitations to the extrapolations we can make to other pathogens and antibiotics. These limitations will guide future work in this area. We demonstrated dAST using a single clinical sample set of UTI urine samples infected with E. coli, which causes 80% of UTIs, using a threshold of 1.10 previously established with isolates. This is similar to other studies at this stage of technology development (72–74); multiple clinical sets should be run in the future.

Cip was chosen because it has become one of the most commonly prescribed antibiotics for UTIs, despite being a second-line therapy that should be preserved for more severe cases (12, 13, 75). Nit was chosen because it is the recommended treatment for acute uncomplicated cystitis (6). Nit is a highly effective first-line antibiotic that is often overlooked because of a lack of susceptibility data. The lack of AST data becomes

especially important because nit is sometimes used as a prophylactic treatment for recurrent UTIs and, despite its effectiveness, is not used to treat acute cases due to susceptibility concerns (12). Multiplexing with more pathogens and antibiotics in a blinded study is an important next step that, if successful, would further validate and prove the clinical utility of this rapid dAST assay.

Other UTI pathogens may have slower growth rates and smaller differences in control and treated concentrations (Fig. 1B); however, these differences are theoretically resolvable with digital NA quantification. Furthermore, alternative dAST markers might yield larger CT ratios after shorter antibiotic exposure times. In particular, changes in RNA in response to antibiotic exposure have been shown to be both large and fast (38) and should be rapidly discernable with digital methods such as the ones described here. For example, we have demonstrated quantification of viral RNA on digital SlipChips (64, 76), including a 5-plex chip for multiplexed measurements. With chip designs properly adjusted for appropriate multiplexing and desired resolution (fig. S1), multiplexed measurements could be useful for analyzing combinations of RNA markers (38). Additionally, RNA markers (38) and alternative DNA markers may be required for antibiotics with different mechanisms of action, such as b-lactams (26), to achieve a 30-min sample-to-answer dAST.

Pathogen concentration is also considered when working with clinical samples. Quantifying NAs with high resolution is challenging if the NA concentration drops below the optimal dynamic range of the system. For example, in sepsis, the concentration of pathogens in blood can be as low as ~1 to 10 CFU/ml (77). Although blood cultures, which require overnight or longer incubations, are currently used to increase the concentration of pathogens, they are too slow to inform the initial treatment because each additional hour of delayed treatment in sepsis results in a 7.6% increase in mortality (25), emphasizing the need for rapid AST. This major challenge of low concentrations of pathogens must be overcome to perform dAST in cases of sepsis and will require alterations to the methodology, such as the addition of a pathogen-concentrating step

before antibiotic exposure. Last, we have not tested dAST against heteroresistant microbial populations, which have been documented in Gram-positive organisms (78) but are not common in Gram-negative organisms.

We have streamlined many aspects of the workflow for the dAST demonstration and believe this workflow can be performed by trained personnel in diagnostic laboratories. However, because this process requires several pipetting and handling steps, operator error is possible. We anticipate that dAST would have the greatest impact on antibiotic stewardship if it could be performed by minimally trained personnel at the POC. This would require integration of the dAST workflow into an inexpensive, simple-to-use device operated with inexpensive equipment. An integrated dAST device would increase throughput and reduce the potential biohazard risks associated with open pipetting steps, which are a limitation of our current protocol. Although not demonstrated here, an integrated device should be feasible due to the straightforward nature of the dAST workflow. Isothermal digital quantification can be performed using a range of technologies and amplification chemistries (40, 47, 49, 63, 79), including SlipChips, which are compatible with untrained users (80) and can be read with inexpensive optics such as a camera phone (40, 70). Whereas reusable glass SlipChips require cleaning (76), disposable injection-molded SlipChips further simplify the workflow. Furthermore, the SlipChip platform supports multiplexed digital measurements (45), which is desired to perform AST on multiple antibiotics and/or pathogens simultaneously. Finally, the robustness of isothermal digital amplification to temperature, imaging conditions, reaction time (40), sample preparation methods (81, 82), and inhibitors (83–85) could further simplify the instrument requirements. This rapid dAST, if fully developed and validated for additional microorganisms, antibiotics, and sample types and transitioned to a Clinical Laboratory Improvement Amendments– waived POC device approved by the regulatory bodies, would enable rapid clinical decision-making, improve management of infectious diseases, and increase antimicrobial stewardship.

Materials and Methods

Study design

The objective of this study was to develop a rapid phenotypic AST using digital NA quantification. The two key hypotheses of this work were as follows: (i) 15 min of antibiotic exposure can cause sufficient differences in pathogen-specific DNA concentrations between control and antibiotic-treated samples such that a high-resolution digital quantification measurement method such as dPCR can reliably detect a difference in NA concentrations for a susceptible sample and (ii) a rapid dLAMP assay can resolve these small differences in NA concentration in less than 10 min. To test the first hypothesis, 51 clinical human urine samples were tested using the dAST method (three samples run with both antibiotics for a total of 54 antibiotic-susceptibility calls), and the results were compared to the gold standard broth microdilution. Clinical UTI samples with E. coli as the pathogen of interest were chosen as a test case for the dAST method using one first-line antibiotic (nit) and one second-line antibiotic (cip). To test the second hypothesis, the rapid dLAMP assay was compared with a commercial dPCR system for calculating the CT ratios and determining antibiotic susceptibility from clinical UTI samples.

To calculate the sample size, the methods and Equation 5 from (86) were used. We define the true-positive rate (sensitivity) as the proportion of gold standard–susceptible samples that are correctly identified as susceptible by the dAST method and the true-negative rate (specificity) as the proportion of gold standard–resistant samples that are correctly identified as resistant by the dAST method. We suspected that the specificity and sensitivity of the dAST method would be 95% with a desired margin of error of ±10%. Under these conditions, 18.2 (or 19) samples must be tested with the dAST method and compared to the gold standard. We tested 19 resistant samples and 35 susceptible samples. Experimental details of LAMP primer design, optimization, and specificity and the rapid dLAMP assay are described in the Supplementary Materials.

dAST in the presence of commensal organisms

Antibiotic-susceptible and antibiotic-resistant isolates of E. coli from patients diagnosed with UTIs were obtained from the University of California, Los Angeles, Clinical Microbiology Laboratory (UCLA CML). These isolates were treated separately with and without antibiotics (±ABXs) in the presence of varying concentrations of Lj (also isolated from a clinical UTI urine sample by the UCLA CML). Lj was spiked into clinical urine samples at varying concentrations relative to the concentration of E. coli. Concentrations were determined by measuring the optical density at 600 nm. Samples were exposed to cip (1 mg/ml; Sigma-Aldrich) for 30 min (26). A 10-ml aliquot of the sample was removed after 0, 15, and 30 min of exposure and added to 90 ml of QuickExtract DNA Extraction Solution (Epicentre). Target DNA was quantified using droplet dPCR (26). The fold change in the concentration of target DNA after 15 min of antibiotic exposure relative to time 0 in the control and antibiotic-treated samples was compared (Fig. 2, A and B), measuring the significance of this difference by P value as described previously (26). The CT ratios at 15 min (Fig. 2C) were calculated as the ratios of the marker concentrations in the control and antibiotic-treated samples.

The primers used for all dPCR amplification experiments target the 23S gene of the Enterobacteriaceae family (26). The concentrations of the components in the dPCR mix used for these experiments and all subsequent dPCR experiments were as follows: 1× QX200 ddPCR EvaGreen Supermix (Bio-Rad), 500 nM forward primer, and 500 nM reverse primer. The NA extraction comprised 10% of the final volume in the dPCR mix. The remaining volume was nuclease-free water (NF-H2O).

dAST using clinical UTI samples.

Clinical urine samples were obtained under an approved institutional review board (IRB) protocol at the UCLA CML (#15-001189) and analyzed at the California Institute of Technology (Caltech) under an approved protocol (IRB #15-0566). Samples were

deidentified before being transported to Caltech. Samples were stored in Vacutainer Plus C&S Boric Acid Sodium Borate/Formate tubes (Becton Dickinson), transported at ambient temperature, and stored at 4°C once received at Caltech. Urine samples were from otherwise healthy patients suspected of having a UTI (based on urinalysis results). The presence of E. coli was confirmed by the UCLA CML, and MICs were determined as described previously (26). Urine samples were selected for dAST analysis based on the determined MIC of the infecting E. coli. Samples were considered cip-susceptible if the determined MIC was ≤0.25 mg/ml and considered cip-resistant if the MIC was ≥4 mg/ml. Samples were considered nit-susceptible if the MIC was ≤16 mg/ml and considered nit-resistant if the MIC was ≥128 mg/ml. Viable bacteria are a requirement of phenotypic ASTs. Nonviable samples were excluded if a decrease in DNA concentration was observed (indicating digestion of DNA from nonviable cells). If the change in DNA concentration was not easily discernible by dPCR after 15 min of growth in media, then the DNA concentration at 30 min was measured to determine whether the sample was viable (DNA concentration increased at 30 min) or nonviable (DNA concentration decreased at 30 min).

Before the start of each experiment, urine as received, still containing boric acid, was warmed to 37°C over 30 min to mimic the temperature of fresh urine samples. At the start of each dAST experiment (t = 0), warmed urine was added to media (prewarmed to 37°C) with or without antibiotics (±ABXs) to initiate DNA replication and begin exposure. This addition to media dilutes the boric acid in the transport media, allowing bacterial replication to proceed. The final 500-ml sample mixture in the control and treated tubes contained 250 ml of brain heart infusion media (Becton Dickinson), 25 ml of DNase I (New England Biolabs), 5 ml of DNase buffer (100 mM trisHCl, 25 mM MgCl2, and 5 mM CaCl2), and an aliquot of the urine, with the remaining volume of NF-H2O. Either cip (1 mg/ml) or nit (16 mg/ml) was added to the +ABX sample, with an equal volume of NF-H2O (in the case of cip) or dimethylformamide (in the case of nit) added to the control sample (−ABX). Antibiotic concentrations were chosen on the basis of our previous work with isolates (26) and are near the Clinical and Laboratory

Standards Institute and European Committee on Antimicrobial Susceptibility Testing breakpoints. A 10-ml aliquot of urine was added to control and treated tubes in the cip treatments, and a 25-ml aliquot was added in the nit treatments. Samples were shaken at 750 rpm at 37°C for 30 min. After 0, 15, and 30 min of exposure, 10-ml aliquots of the control and treated samples were removed and added to 90 ml of QuickExtract DNA Extraction Solution. The extracted samples were heated according to a modified version of the manufacturer's protocol (65°C for 6 min, 95°C for 4 min, and chilled on ice), vortexed, and centrifuged. Next, 5 ml of each extraction was added to 45 ml of ddPCR mix and quantified using dPCR. If the DNA concentration of the sample was too high, then the template was diluted in NF-H2O and dPCR was rerun. The CT ratios were calculated; if the dAST call did not match the gold standard AST call, then the sample was rerun several hours later on the same day. For the four samples that were rerun, only the second set of NA extractions were quantified by dLAMP.

Sample-to-answer dAST in less than 30 min

Clinical urine samples were treated with ("treated") and without ("control") cip (1 mg/ml) for 15 min as described above. A timer was started as soon as urine was added to the media with and without cip. After 0 and 15 min, a 20-ml aliquot of each sample was added to 80 ml of QuickExtract DNA Extraction Solution (Epicentre). The two samples were then heated at 65°C for 1 min followed by 98°C for 1 min, after which they were chilled by incubation on an ice block for 30 s, vortexed, and centrifuged.

In parallel with the 15-min antibiotic exposure step, we used the semiquantitative ability of quantitative LAMP to predict the appropriate dilution factor for our 1280-well digital SlipChips. A 2-ml aliquot from each of the control and treated DNA extractions from time 0 was added to 8 ml of LAMP mix. The samples, along with two standards with known DNA concentrations (S1, 128.5 copies/ml; S2, 766.0 copies/ml), were then incubated at 72°C for 5 min on a Roche LightCycler 96, and fluorescent traces were monitored in real time. If the TTP of the average of the samples was earlier than the TTP

of S1, then 3 ml of the NA aliquot extracted at 15 min was added to 24 ml of dLAMP mix, along with 3 ml of NF-H2O. If the TTP of the sample was between the TTPs of S1 and S2, then 6 ml of the 15-min NA extraction was added to 24 ml of dLAMP mix, with no additional NF-H2O added. This step was completed within the 15 min of antibiotic exposure. In the experiments with both antibiotic-resistant and antibiotic-susceptible samples (Fig. 5), the TTP was earlier than the TTP of S1.

After semiquantification and mixture of the dLAMP mix with the template, the dLAMP solutions were pipette-mixed, loaded into SlipChips, partitioned into 1280 compartments, and placed on the thermal cycler of a digital real-time imaging instrument at 72°C.

Images were taken every 26 s, and concentrations were calculated on the basis of the number of positive and negative wells [as described in Rapid digital LAMP (dLAMP) in the Supplementary Materials]. Software developed in (56) was modified to enable realtime image processing and concentration calculations as each image was taken instead of after the assay completed. The CT ratios were also calculated for each time point; the value of the CT ratio after 6.7 min of amplification time is plotted in Fig. 5D and was compared to a threshold of 1.10 to determine susceptibility or resistance. The timer was stopped at this time point; 29.8 min had elapsed when running dAST with the susceptible sample, and 29.2 min had elapsed with the resistant sample.

Statistical analysis

Poisson statistics was used to calculate the 95 or 98% confidence interval of the NA concentration for each digital measurement (45). To calculate the error in fold change, we used standard error propagation methods (87). With l as a concentration and s as the SD, the equation is

$$\sigma_{ratio} = \sqrt{\left(\frac{\sigma_{\lambda_2}}{\lambda_1}\right)^2 + \left(\frac{\lambda_2 \cdot \sigma_{\lambda_1}}{\lambda_1^2}\right)^2}$$

Kreutz et al. (45) demonstrated that results from a Z test (assuming a normal distribution) and a permutation test are in very good agreement for various SlipChip designs; therefore, it is appropriate to calculate P values comparing digital NA concentrations with a one-sided Z test. This Z test asks whether the control NA concentration (l) control is 1.10× higher than the treated NA concentration (lABX) (26, 45).

$$Z = \frac{\ln(\lambda_{control}) - \ln(1.10 \cdot \lambda_{ABX})}{\sqrt{\sigma^2_{\ln(\lambda_{control})} + \sigma^2_{\ln(\lambda_{ABX})}}}$$

Concentration (l) and SD (s) for each digital NA measurement were calculated from the number of positive and negative compartments with Poisson statistics as described in (45) for single-volume digital NA quantification. A significance level of 0.05 was used.

References

1. R. Laxminarayan, A. Duse, C. Wattal, A.K. Zaidi, H.F. Wertheim, N. Sumpradit, E. Vlieghe, G.L. Hara, I.M. Gould, H. Goossens, C. Greko, A.D. So, M. Bigdeli, G. Tomson, W. Woodhouse, E. Ombaka, A.Q. Peralta, F.N. Qamar, F. Mir, S. Kariuki, Z.A. Bhutta, A. Coates, R. Bergstrom, G.D. Wright, E.D. Brown, O. Cars. Antibiotic resistance--the need for global solutions. *Lancet Infect. Dis.* **13**, 1057-1098 (2013).

2. J. O'Neill, *Tackling Drug-Resistant Infections Globally: Final Report and Recommendations* https://amr-review.org/Publications.html (2016)

3. J. O'Neill, *Rapid Diagnostics: Stopping Unnecessary Use of Antibiotics* https://amr-review.org/Publications.html (2015)

4. S.E. Cosgrove. The relationship between antimicrobial resistance and patient outcomes: mortality, length of hospital stay, and health care costs. *Clin. Infect. Dis.* **42 Suppl 2**, S82-89 (2006).

5. K.K. Perez, R.J. Olsen, W.L. Musick, P.L. Cernoch, J.R. Davis, G.A. Land, L.E. Peterson, J.M. Musser. Integrating rapid pathogen identification and antimicrobial stewardship significantly decreases hospital costs. *Arch. Pathol. Lab. Med.* **137**, 1247-1254 (2013).

6. K. Gupta, T.M. Hooton, K.G. Naber, B. Wullt, R. Colgan, L.G. Miller, G.J. Moran, L.E. Nicolle, R. Raz, A.J. Schaeffer, D.E. Soper, A. Infectious Diseases Society of, M. European Society for, D. Infectious. International clinical practice guidelines for the treatment of acute uncomplicated cystitis and pyelonephritis in women: A 2010 update by the Infectious Diseases Society of America and the European Society for Microbiology and Infectious Diseases. *Clin. Infect. Dis.* **52**, e103-120 (2011).

7. CDC, "Antibiotic Resistance Threats in the United States," Centers for Disease Control Office of Infectious Diseases, Atlanta, GA, https://www.cdc.gov/drugresistance/pdf/ar-threats-2013-508.pdf (2013).

8. Nesta, *Longitude Prize: How can we prevent the rise of resitance to antibiotics?* https://longitudeprize.org/challenge/antibiotics (2014).

9. CDDEP, "State of the World's Antibiotics," (Center for Disease Dynamics, Economics and Policy, Washington, D.C., http://cddep.org/sites/default/files/swa_2015_final.pdf 2015).

10. The White House, "National Action Plan for Combating Antibiotic-Resistant Bacteria," https://obamawhitehouse.archives.gov/sites/default/files/docs/national_action_plan_for_combating_antibotic-resistant_bacteria.pdf (2015).

11. WHO, "Global Antimicrobial Resistance Surveillance System - Manual for Early Implementation," http://apps.who.int/iris/bitstream/10665/188783/1/9789241549400_eng.pdf (2015).

12. A.E. Barber, J.P. Norton, A.M. Spivak, M.A. Mulvey. Urinary tract infections: current and emerging management strategies. *Clin. Infect. Dis.* **57**, 719-724 (2013).

13. T.M. Hooton. Uncomplicated urinary tract infection. *N. Engl. J. Med.* **366**, 1028-1037 (2012).

14. M. Kobayashi, D.J. Shapiro, A.L. Hersh, G.V. Sanchez, L.A. Hicks. Outpatient antibiotic prescribing practices for uncomplicated urinary tract infection in women in the United States, 2002-2011. *Open Forum Infect. Dis.* **3**, 1-7 (2016).

15. J.H. Jorgensen, M.J. Ferraro. Antimicrobial susceptibility testing: a review of general principles and contemporary practices. *Clin. Infect. Dis.* **49**, 1749-1755 (2009).

16. T. Kostic, M. Ellis, M.R. Williams, T.M. Stedtfeld, J.B. Kaneene, R.D. Stedtfeld, S.A. Hashsham. Thirty-minute screening of antibiotic resistance genes in bacterial isolates with minimal sample preparation in static self-dispensing 64 and 384 assay cards. *Appl. Microbiol. Biotechnol.* **99**, 7711-7722 (2015).

17. T. Ikeuchi, M. Seki, Y. Akeda, N. Yamamoto, S. Hamaguchi, T. Hirose, K. Yamanaka, M. Saito, K. Tomono, E. Tamiya. PCR-based method for rapid and minimized electrochemical detection of mecA gene of methicillin-resistant *Staphylococcus aureus* and methicillin-resistant *Staphylococcus epidermidis*. *General Medicine: Open Access* **3**, 215 (2015).

18. Y. Zboromyrska, A. Vergara, C. Cosgaya, G. Verger, N. Mosqueda, M. Almela, C. Pitart, I. Roca, F. Marco, J. Vila. Rapid detection of beta-lactamases directly from positive blood cultures using a loop-mediated isothermal amplification (LAMP)-based assay. *Int J Antimicrob Ag* **46**, 355-356 (2015).

19. L.R. Peterson, D.M. Schora. Methicillin-Resistant Staphylococcus aureus Control in the 21st Century: Laboratory Involvement Affecting Disease Impact and Economic Benefit from Large Population Studies. *J. Clin. Microbiol.* **54**, 2647-2654 (2016).

20. A. van der Zee, W.D. Hendriks, L. Roorda, J.M. Ossewaarde, J. Buitenwerf. Review of a major epidemic of methicillin-resistant Staphylococcus aureus: the costs of screening and consequences of outbreak management. *Am. J. Infect. Control* **41**, 204-209 (2013).

21. M. Spencer, S. Barnes, J. Parada, S. Brown, L. Perri, D. Uettwiller-Geiger, H.B. Johnson, D. Graham. A primer on on-demand polymerase chain reaction technology. *Am. J. Infect. Control* **43**, 1102-1108 (2015).

22. J. Davies, D. Davies. Origins and evolution of antibiotic resistance. *Microbiol. Mol. Biol. Rev.* **74**, 417-433 (2010).

23. H.D. Marston, D.M. Dixon, J.M. Knisely, T.N. Palmore, A.S. Fauci. Antimicrobial Resistance. *JAMA* **316**, 1193-1204 (2016).

24. J.M. Hicks, R. Haeckel, C.P. Price, K. Lewandrowski, A.H.B. Wu. Recommendations and opinions for the use of point-of-care testing for hospitals and primary care: summary of a 1999 symposium. *Clin. Chim. Acta* **303**, 1-17 (2001).

25. A. Kumar, D. Roberts, K.E. Wood, B. Light, J.E. Parrillo, S. Sharma, R. Suppes, D. Feinstein, S. Zanotti, L. Taiberg, D. Gurka, A. Kumar, M. Cheang. Duration of hypotension before initiation of effective antimicrobial therapy is the critical determinant of survival in human septic shock. *Crit Care Med.* **34**, 1589-1596 (2006).

26. N.G. Schoepp, E.M. Khorosheva, T.S. Schlappi, M.S. Curtis, R.M. Humphries, J.A. Hindler, R.F. Ismagilov. Digital Quantification of DNA Replication and Chromosome Segregation Enables Determination of Antimicrobial Susceptibility after only 15 Minutes of Antibiotic Exposure. *Angew. Chem. Int. Ed. Engl.* **55**, 9557-9561 (2016).

27. O. Baltekin, A. Boucharin, E. Tano, D.I. Andersson, J. Elf. Antibiotic susceptibility testing in less than 30 min using direct single-cell imaging. *Proc. Natl. Acad. Sci. U. S. A.*, (2017).

28. M. Fredborg, K.R. Andersen, E. Jorgensen, A. Droce, T. Olesen, B.B. Jensen, F.S. Rosenvinge, T.E. Sondergaard. Real-time optical antimicrobial susceptibility testing. *J. Clin. Microbiol.* **51**, 2047-2053 (2013).

29. J. Choi, J. Yoo, M. Lee, E.G. Kim, J.S. Lee, S. Lee, S. Joo, S.H. Song, E.C. Kim, J.C. Lee, H.C. Kim, Y.G. Jung, S. Kwon. A rapid antimicrobial susceptibility test based on single-cell morphological analysis. *Sci. Transl. Med.* **6**, 267ra174 (2014).

30. I.S. Douglas, C.S. Price, K.H. Overdier, R.F. Wolken, S.W. Metzger, K.R. Hance, D.C. Howson. Rapid automated microscopy for microbiological surveillance of ventilator-associated pneumonia. *Am. J. Respir. Crit. Care. Med.* **191**, 566-573 (2015).

31. C. Chantell. Multiplexed automated digital microscopy for rapid identification and antimicrobial susceptibility testing of bacteria and yeast directly from clinical samples. *Clin. Microbiol. Newsl.* **37**, 161-167 (2015).

32. P. Ertl, E. Robello, F. Battaglini, S.R. Mikkelsen. Rapid antibiotic susceptibility testing via electrochemical measurement of ferricyanide reduction by *Escherichia coli* and *Clostridium sporogenes*. *Anal. Chem.* **72**, 4957-4964 (2000).

33. C. Halford, R. Gonzalez, S. Campuzano, B. Hu, J.T. Babbitt, J. Liu, J. Wang, B.M. Churchill, D.A. Haake. Rapid antimicrobial susceptibility testing by sensitive detection of precursor rRNA using a novel electrochemical biosensing platform. *Antimicrob. Agents. Chemother.* **57**, 936-943 (2013).

34. K.E. Mach, R. Mohan, E.J. Baron, M.C. Shih, V. Gau, P.K. Wong, J.C. Liao. A biosensor platform for rapid antimicrobial susceptibility testing directly from clinical samples. *J. Urol.* **185**, 148-153 (2011).

35. A. Mezger, E. Gullberg, J. Goransson, A. Zorzet, D. Herthnek, E. Tano, M. Nilsson, D.I. Andersson. A general method for rapid determination of antibiotic susceptibility and species in bacterial infections. *J. Clin. Microbiol.* **53**, 425-432 (2015).

36. J.M. Rolain, M.N. Mallet, P.E. Fournier, D. Raoult. Real-time PCR for universal antibiotic susceptibility testing. *J Antimicrob. Chemother.* **54**, 538-541 (2004).

37. I. Steinberger-Levy, O. Shifman, A. Zvi, N. Ariel, A. Beth-Din, O. Israeli, D. Gur, M. Aftalion, S. Maoz, R. Ber. A Rapid Molecular Test for Determining Yersinia pestis Susceptibility to Ciprofloxacin by the Quantification of Differentially Expressed Marker Genes. *Front. Microbiol.* **7**, (2016).

38. A.K. Barczak, J.E. Gomez, B.B. Kaufmann, E.R. Hinson, L. Cosimi, M.L. Borowsky, A.B. Onderdonk, S.A. Stanley, D. Kaur, K.F. Bryant, D.M. Knipe, A. Sloutsky, D.T. Hung. RNA signatures allow rapid identification of pathogens and antibiotic susceptibilities. *Proc. Natl. Acad. Sci. U. S. A.* **109**, 6217-6222 (2012).

39. M. Fredborg, F.S. Rosenvinge, E. Spillum, S. Kroghsbo, M. Wang, T.E. Sondergaard. Rapid antimicrobial susceptibility testing of clinical isolates by digital time-lapse microscopy. *Eur. J. Clin. Microbiol. Infect. Dis.* **34**, 2385-2394 (2015).

40. D.A. Selck, M.A. Karymov, B. Sun, R.F. Ismagilov. Increased robustness of single-molecule counting with microfluidics, digital isothermal amplification, and a mobile phone versus real-time kinetic measurements. *Anal. Chem.* **85**, 11129-11136 (2013).

41. A.S. Whale, J.F. Huggett, S. Cowen, V. Speirs, J. Shaw, S. Ellison, C.A. Foy, D.J. Scott. Comparison of microfluidic digital PCR and conventional quantitative PCR for measuring copy number variation. *Nucleic Acids Res.* **40**, e82 (2012).

42. D. Haake, B. Churchill, C. Halford, "Amdinocillin for rapid determination of susceptibility to beta-lactam antibiotics," PCT/US2014/047684, international filing date 7/22/2014.

43. R.J. Almeida, J.H. Jorgensen. Comparison of adherence and urine growth rate properties of Staphylococcus saprophyticus and Staphylococcus epidermidis. *Eur. J. Clin. Microbiol.* **3**, 542-545 (1984).

44. M.S. Lawlor, C. O'Connor, V.L. Miller. Yersiniabactin is a virulence factor for Klebsiella pneumoniae during pulmonary infection. *Infect. Immun.* **75**, 1463-1472 (2007).

45. J.E. Kreutz, T. Munson, T. Huynh, F. Shen, W. Du, R.F. Ismagilov. Theoretical design and analysis of multivolume digital assays with wide dynamic range validated experimentally with microfluidic digital PCR. *Anal. Chem.* **83**, 8158-8168 (2011).

46. S. Weaver, S. Dube, A. Mir, J. Qin, G. Sun, R. Ramakrishnan, R.C. Jones, K.J. Livak. Taking qPCR to a higher level: Analysis of CNV reveals the power of high throughput qPCR to enhance quantitative resolution. *Methods* **50**, 271-276 (2010).

47. P. Xu, X. Zheng, Y. Tao, W. Du. Cross-Interface Emulsification for Generating Size-Tuneable Droplets. *Anal. Chem.* **88**, 3171-3177 (2016).

48. F. Schuler, C. Siber, S. Hin, S. Wadle, N. Paust, R. Zengerle, F. von Stetten. Digital droplet LAMP as a microfluidic app on standard laboratory devices. *Anal. Methods* **8**, 2750-2755 (2016).

49. T.D. Rane, L. Chen, H.C. Zec, T.H. Wang. Microfluidic continuous flow digital loop-mediated isothermal amplification (LAMP). *Lab. Chip* **15**, 776-782 (2015).

50. B. Sun, J. Rodriguez-Manzano, D.A. Selck, E. Khorosheva, M.A. Karymov, R.F. Ismagilov. Measuring fate and rate of single-molecule competition of amplification and restriction digestion, and its use for rapid genotyping tested with hepatitis C viral RNA. *Angew. Chem. Int. Ed. Engl.* **53**, 8088-8092 (2014).

51. N.A. Tanner, T.C. Evans, Jr. Loop-mediated isothermal amplification for detection of nucleic acids. *Curr. Protoc. Mol. Biol.* **105**, Unit 15 14 (2014).

52. M. Imai, A. Ninomiya, H. Minekawa, T. Notomi, T. Ishizaki, M. Tashiro, T. Odagiri. Development of H5-RT-LAMP (loop-mediated isothermal amplification) system for rapid diagnosis of H5 avian influenza virus infection. *Vaccine* **24**, 6679-6682 (2006).
53. Y. Kurosaki, N. Magassouba, O.K. Oloniniyi, M.S. Cherif, S. Sakabe, A. Takada, K. Hirayama, J. Yasuda. Development and Evaluation of Reverse Transcription-Loop-Mediated Isothermal Amplification (RT-LAMP) Assay Coupled with a Portable Device for Rapid Diagnosis of Ebola Virus Disease in Guinea. *PLoS Negl. Trop. Dis.* **10**, e0004472 (2016).
54. A. Buhlmann, J.F. Pothier, F. Rezzonico, T.H. Smits, M. Andreou, N. Boonham, B. Duffy, J.E. Frey. Erwinia amylovora loop-mediated isothermal amplification (LAMP) assay for rapid pathogen detection and on-site diagnosis of fire blight. *J. Microbiol. Methods* **92**, 332-339 (2013).
55. G.P. Wu, S.H. Chen, R.E. Levin. Application of ethidium bromide monoazide for quantification of viable and dead cells of Salmonella enterica by real-time loop-mediated isothermal amplification. *J. Microbiol. Methods* **117**, 41-48 (2015).
56. D.A. Selck, R.F. Ismagilov. Instrument for Real-Time Digital Nucleic Acid Amplification on Custom Microfluidic Devices. *PLoS One* **11**, e0163060 (2016).
57. F. Shen, W. Du, J.E. Kreutz, A. Fok, R.F. Ismagilov. Digital PCR on a SlipChip. *Lab. Chip* **10**, 2666-2672 (2010).
58. D.T. Gillespie. Stochastic simulation of chemical kinetics. *Annu. Rev. Phys. Chem* **58**, 35-55 (2007).
59. CLSI, "M100-S25 Performance Standards for Antimicrobial Susceptibility Testing," (Clinical Laboratory Standards Institute, 2015).
60. J. Turnidge, D.L. Paterson. Setting and revising antibacterial susceptibility breakpoints. *Clin. Microbiol. Rev.* **20**, 391-408, table of contents (2007).
61. V. Ivancic, M. Mastali, N. Percy, J. Gornbein, J.T. Babbitt, Y. Li, E.M. Landaw, D.A. Bruckner, B.M. Churchill, D.A. Haake. Rapid antimicrobial susceptibility determination of uropathogens in clinical urine specimens by use of ATP bioluminescence. *J. Clin. Microbiol.* **46**, 1213-1219 (2008).

62. EUCAST, "Antimicrobial wild type distributions of microorganisms," European Society of Clinical Microbiology and Infectious Disease, https://mic.eucast.org/Eucast2/ (2017).

63. F. Shen, E.K. Davydova, W. Du, J.E. Kreutz, O. Piepenburg, R.F. Ismagilov. Digital isothermal quantification of nucleic acids via simultaneous chemical initiation of recombinase polymerase amplification reactions on SlipChip. *Anal. Chem.* **83**, 3533-3540 (2011).

64. B. Sun, F. Shen, S.E. McCalla, J.E. Kreutz, M.A. Karymov, R.F. Ismagilov. Mechanistic evaluation of the pros and cons of digital RT-LAMP for HIV-1 viral load quantification on a microfluidic device and improved efficiency via a two-step digital protocol. *Anal. Chem.* **85**, 1540-1546 (2013).

65. T. Notomi, Y. Mori, N. Tomita, H. Kanda. Loop-mediated isothermal amplification (LAMP): principle, features, and future prospects. *J. Microbiol.* **53**, 1-5 (2015).

66. N.A. Tanner, T.C. Evans, "Compositions and Methods for Reducing Background DNA Amplification," US20130323793, filing date 3/13/2013.

67. A. Martin, K.B. Grant, F. Stressmann, J.-M. Ghigo, D. Marchal, B. Limoges. Ultimate Single-Copy DNA Detection Using Real-Time Electrochemical LAMP. *ACS Sensors* **1**, 904-912 (2016).

68. N.A. Tanner, Y. Zhang, T.C. Evans, Jr. Simultaneous multiple target detection in real-time loop-mediated isothermal amplification. *Biotechniques* **53**, 81-89 (2012).

69. N.A. Tanner, Y. Zhang, T.C. Evans, Jr. Visual detection of isothermal nucleic acid amplification using pH-sensitive dyes. *Biotechniques* **58**, 59-68 (2015).

70. J. Rodriguez-Manzano, M.A. Karymov, S. Begolo, D.A. Selck, D.V. Zhukov, E. Jue, R.F. Ismagilov. Reading Out Single-Molecule Digital RNA and DNA Isothermal Amplification in Nanoliter Volumes with Unmodified Camera Phones. *ACS Nano* **10**, 3102-3113 (2016).

71. J.A. Simerville, W.C. Maxted, J.J. Pahira. Urinalysis: a comprehensive review. *Am. Fam. Physician* **71**, 1153-1162 (2005).

72. A. Courbet, D. Endy, E. Renard, F. Molina, J. Bonnet. Detection of pathological biomarkers in human clinical samples via amplifying genetic switches and logic gates. *Sci. Transl. Med.* **7**, 289ra283 (2015).

73. T. Laksanasopin, T.W. Guo, S. Nayak, A.A. Sridhara, S. Xie, O.O. Olowookere, P. Cadinu, F. Meng, N.H. Chee, J. Kim, C.D. Chin, E. Munyazesa, P. Mugwaneza, A.J. Rai, V. Mugisha, A.R. Castro, D. Steinmiller, V. Linder, J.E. Justman, S. Nsanzimana, S.K. Sia. A smartphone dongle for diagnosis of infectious diseases at the point of care. *Sci. Transl. Med.* **7**, 273re271 (2015).

74. N.N. Watkins, U. Hassan, G. Damhorst, H. Ni, A. Vaid, W. Rodriguez, R. Bashir. Microfluidic CD4+ and CD8+ T lymphocyte counters for point-of-care HIV diagnostics using whole blood. *Sci. Transl. Med.* **5**, 214ra170 (2013).

75. A.J. Kallen, H.G. Welch, B.E. Sirovich. Current antibiotic therapy for isolated urinary tract infections in women. *Arch. Intern. Med.* **166**, 635-639 (2006).

76. F. Shen, B. Sun, J.E. Kreutz, E.K. Davydova, W. Du, P.L. Reddy, L.J. Joseph, R.F. Ismagilov. Multiplexed quantification of nucleic acids with large dynamic range using multivolume digital RT-PCR on a rotational SlipChip tested with HIV and hepatitis C viral load. *J. Am. Chem. Soc.* **133**, 17705-17712 (2011).

77. A.L. Walsh, M.D. Smith, V. Wuthiekanun, Y. Suputtamongkol, W. Chaowagul, D.A.B. Dance, B. Angus, N.J. White. Prognostic significance of quantitative bacteremia in septicemic melioidosis. *Clin. Infect. Dis.* **21**, 1498-1500 (1995).

78. A.C. Musta, K. Riederer, S. Shemes, P. Chase, J. Jose, L.B. Johnson, R. Khatib. Vancomycin MIC plus heteroresistance and outcome of methicillin-resistant Staphylococcus aureus bacteremia: trends over 11 years. *J. Clin. Microbiol.* **47**, 1640-1644 (2009).

79. F. Schuler, F. Schwemmer, M. Trotter, S. Wadle, R. Zengerle, F. von Stetten, N. Paust. Centrifugal step emulsification applied for absolute quantification of nucleic acids by digital droplet RPA. *Lab. Chip* **15**, 2759-2766 (2015).

80. D. Witters, B. Sun, S. Begolo, J. Rodriguez-Manzano, W. Robles, R.F. Ismagilov. Digital biology and chemistry. *Lab. Chip* **14**, 3225-3232 (2014).

81. K. Hayashida, K. Kajino, L. Hachaambwa, B. Namangala, C. Sugimoto. Direct blood dry LAMP: a rapid, stable, and easy diagnostic tool for Human African Trypanosomiasis. *PLoS Negl. Trop. Dis.* **9**, e0003578 (2015).

82. J. Jevtusevskaja, K. Krolov, I. Tulp, U. Langel. The effect of main urine inhibitors on the activity of different DNA polymerases in loop-mediated isothermal amplification. *Expert. Rev. Mol. Diagn.*, 1-8 (2017).

83. T.C. Dingle, R.H. Sedlak, L. Cook, K.R. Jerome. Tolerance of droplet-digital PCR vs real-time quantitative PCR to inhibitory substances. *Clin. Chem.* **59**, 1670-1672 (2013).

84. R.H. Sedlak, J. Kuypers, K.R. Jerome. A multiplexed droplet digital PCR assay performs better than qPCR on inhibition prone samples. *Diagn. Microbiol. Infect. Dis.* **80**, 285-286 (2014).

85. A.S. Whale, A.S. Devonshire, G. Karlin-Neumann, J. Regan, L. Javier, S. Cowen, A. Fernandez-Gonzalez, G.M. Jones, N. Redshaw, J. Beck, A.W. Berger, V. Combaret, N. Dahl Kjersgaard, L. Davis, F. Fina, T. Forshew, R. Fredslund Andersen, S. Galbiati, A. Gonzalez Hernandez, C.A. Haynes, F. Janku, R. Lacave, J. Lee, V. Mistry, A. Pender, A. Pradines, C. Proudhon, L.H. Saal, E. Stieglitz, B. Ulrich, C.A. Foy, H. Parkes, S. Tzonev, J.F. Huggett. International Interlaboratory Digital PCR Study Demonstrating High Reproducibility for the Measurement of a Rare Sequence Variant. *Anal. Chem.* **89**, 1724-1733 (2017).

86. S. Banoo, D. Bell, P. Bossuyt, A. Herring, D. Mabey, F. Poole, P.G. Smith, N. Sriram, C. Wongsrichanalai, R. Linke, R. O'Brien, M. Perkins, J. Cunningham, P. Matsoso, C.M. Nathanson, P. Olliaro, R.W. Peeling, A. Ramsay, T.D.R.D.E.E. Panel. Evaluation of diagnostic tests for infectious diseases: general principles. *Nat. Rev. Microbiol.* **4**, S21-31 (2006).

87. H.H. Ku. Notes on the use of propagation of error formulas. *Journal of Research of the National Bureau of Standards, Section C: Engineering and Instrumentation* **70C**, 263-263 (1966).

88. T. Stenholm, A.J. Hakanen, E. Hakanen, H. Harma, M. Osterblad, J. Vuopio, P.E. Hanninen, P. Huovinen, K. Rankakokko-Jalava, P. Kotilainen. High-throughput

screening of colonization samples for methicillin-resistant Staphylococcus aureus. *Scand. J. Infect. Dis.* **45**, 922-929 (2013).
89. Y. Lu, J. Gao, D.D. Zhang, V. Gau, J.C. Liao, P.K. Wong. Single cell antimicrobial susceptibility testing by confined microchannels and electrokinetic loading. *Anal. Chem.* **85**, 3971-3976 (2013).
90. J.D. Besant, E.H. Sargent, S.O. Kelley. Rapid electrochemical phenotypic profiling of antibiotic-resistant bacteria. *Lab. Chip* **15**, 2799-2807 (2015).
91. C.H. Chen, Y. Lu, M.L. Sin, K.E. Mach, D.D. Zhang, V. Gau, J.C. Liao, P.K. Wong. Antimicrobial susceptibility testing using high surface-to-volume ratio microchannels. *Anal. Chem.* **82**, 1012-1019 (2010).
92. M.A. Broeren, Y. Maas, E. Retera, N.L. Arents. Antimicrobial susceptibility testing in 90 min by bacterial cell count monitoring. *Clin. Microbiol. Infect.* **19**, 286-291 (2013).
93. I. Sinn, P. Kinnunen, T. Albertson, B.H. McNaughton, D.W. Newton, M.A. Burns, R. Kopelman. Asynchronous magnetic bead rotation (AMBR) biosensor in microfluidic droplets for rapid bacterial growth and susceptibility measurements. *Lab. Chip* **11**, 2604-2611 (2011).
94. C.Y. Liu, Y.Y. Han, P.H. Shih, W.N. Lian, H.H. Wang, C.H. Lin, P.R. Hsueh, J.K. Wang, Y.L. Wang. Rapid bacterial antibiotic susceptibility test based on simple surface-enhanced Raman spectroscopic biomarkers. *Sci. Rep.* **6**, 23375 (2016).
95. T.T. Liu, Y.H. Lin, C.S. Hung, T.J. Liu, Y. Chen, Y.C. Huang, T.H. Tsai, H.H. Wang, D.W. Wang, J.K. Wang, Y.L. Wang, C.H. Lin. A high speed detection platform based on surface-enhanced Raman scattering for monitoring antibiotic-induced chemical changes in bacteria cell wall. *PLoS One* **4**, e5470 (2009).
96. N.K. Shrestha, N.M. Scalera, D.A. Wilson, G.W. Procop. Rapid differentiation of methicillin-resistant and methicillin-susceptible Staphylococcus aureus by flow cytometry after brief antibiotic exposure. *J. Clin. Microbiol.* **49**, 2116-2120 (2011).
97. I. Faria-Ramos, M.J. Espinar, R. Rocha, J. Santos-Antunes, A.G. Rodrigues, R. Canton, C. Pina-Vaz. A novel flow cytometric assay for rapid detection of extended-spectrum beta-lactamases. *Clin. Microbiol. Infect.* **19**, E8-E15 (2013).

98. C. Lange, S. Schubert, J. Jung, M. Kostrzewa, K. Sparbier. Quantitative matrix-assisted laser desorption ionization-time of flight mass spectrometry for rapid resistance detection. *J. Clin. Microbiol.* **52**, 4155-4162 (2014).
99. T.S. Mann, S.R. Mikkelsen. Antibiotic susceptibility testing at a screen-printed carbon electrode array. *Anal. Chem.* **80**, 843-848 (2008).
100. Y. Tang, L. Zhen, J. Liu, J. Wu. Rapid antibiotic susceptibility testing in a microfluidic pH sensor. *Anal. Chem.* **85**, 2787-2794 (2013).
101. B.L. Roth, M. Poot, S.T. Yue, P.J. Millard. Bacterial viability and antibiotic susceptibility testing with SYTOX green nucleic acid stain. *Appl. Environ. Microbiol.* **63**, 2421-2431 (1997).

Acknowledgements

We thank N. Shelby for contributions to manuscript writing and editing, M. Lee at the Clinical Microbiology Laboratory at UCLA for assistance with clinical sample and data acquisition, SlipChip Corp. for providing injection-molded SlipChips for dLAMP quantification, and W. Liu and D. Capule of SlipChip Corp. for providing technical assistance and expertise. Funding: This research was supported by the Defense Advanced Research Projects Agency (DARPA) Cooperative Agreement HR0011-11-2-0006, NIH grant R01EB012946, a Burroughs Wellcome Fund Innovation in Regulatory Science award, an NIH National Research Service Award (NRSA) (5T32GM07616NSF) to N.G.S., and a grant from the Joseph J. Jacobs Institute for Molecular Engineering for Medicine. Author contributions: The order of co-first authors was determined by coin toss. T.S.S., N.G.S., and R.F.I. contributed to the design and/or interpretation of the reported experiments or results. T.S.S., N.G.S., M.S.C., S.S.B., and R.F.I. contributed to the acquisition and/or analysis of the data. T.S.S., N.G.S., R.M.H., and R.F.I. contributed to the drafting and/or revising of the manuscript. M.S.C. was primarily responsible for real-time imaging acquisition and analysis. S.M. and R.M.H. were primarily responsible for acquiring clinical samples and performing gold standard broth microdilution ASTs. R.F.I. and R.M.H. contributed administrative, technical, and supervisory support.

Competing interests: R.F.I., T.S.S., M.S.C., and N.G.S. are inventors on a patent (PCT/US2015/059344) filed by Caltech and SlipChip Corp. and on provisional patent applications 62/399,196 and 62/460,625 filed by Caltech that cover devices and methods for rapid digital antibiotic susceptibility testing. R.F.I. has a financial interest in SlipChip Corp. and is a consultant for SlipChip Corp. Data and materials availability: Requests for additional information should be addressed to R.F.I. (rustem.admin@caltech.edu).

Supplementary Materials

Materials and Methods

Supplementary materials and sample handling

Materials and reagents

All reagents purchased from commercial sources were used as received unless otherwise stated. BBL trypticase soy agar (TSA) plates with 5% sheep blood and Bacto brain heart infusion (BHI) media were purchased from BD Biosciences. All antibiotic stock solutions and nucleic acid amplification reactions were prepared using sterile, nuclease-free water (NF-H2O) purchased from Thermo Fisher. Ciprofloxacin was purchased from Sigma-Aldrich and prepared as a 1 mg/mL stock solution in NF-H2O. Nitrofurantoin was purchased from Sigma-Aldrich and prepared as a 10 mg/mL stock solution in NF-H2O. QuickExtract DNA Extraction was purchased from Epicentre. QX200 ddPCR EvaGreen Supermix was purchased from Bio-Rad Laboratories. Bst 3.0 and 10 mM dNTPs were purchased from NEB. Pooled healthy human urine was obtained from Lee Biosolutions. Primer sequences were ordered as dried stocks from IDT.

Digital quantification with dPCR

Droplet digital PCR reactions were carried out as described previously (*26*).

Design, fabrication and preparation of SlipChips

Details of the design, fabrication, preparation, and assembling of the single-volume 1,280-well SlipChip glass devices are described in previous work (*50*). For this manuscript, the workflow in Fig. 5 was performed with lab-made reusable glass microfluidic chips (Samples 28-29,48-51). To run the rest of the 54 samples with the rapid dLAMP assay, we obtained a set of disposable injection molded chips (5,376 2.4-nL compartments) from SlipChip Corp, which enabled shorter turnaround times between experiments (Samples 1-27,30-47).

Clinical sample handling and gold-standard broth microdilution AST

Urine from patients suspected of having urinary tract infections (UTIs) was collected and transported in a BD Vacutainer Urine Collection Tube containing formate and borate as preservatives. Next, pathogens from the urine samples were isolated and identified using mass spectrometry. Broth microdilution AST was performed on samples positive for *E. coli*.

dAST with clinical samples

One modification to our original dAST protocol (*26*) is the addition of DNase to digest extracellular DNA. We did this to eliminate the confounding effect that extracellular DNA could have on the CT ratio. Consider an antibiotic-susceptible sample with 500 cop/μL of cell-free DNA and 300 cop/μL DNA inside cells. If the genomes replicate 1.5X over a 15 min exposure time, then the CT ratio in the case where cell-free DNA is also detected would be 950 cop/uL ÷ 800 cop/uL = 1.19; in the case where cell-free DNA is digested by DNase and not detected, the CT ratio would be 450 cop/uL ÷ 300 cop/uL = 1.50.

If discordant AST calls (compared to the gold-standard) were noticed on the same day, we re-ran that sample to resolve the discordancy. Some reruns are accepted even in the FDA submissions of diagnostic AST devices, so rerunning samples in itself is not a problem. It would have been better to rerun the samples twice, to get a third measurement as a tie-breaker. Unfortunately, we could not do so due to the limitations of our protocols and the concern for aging of clinical samples over time (and we were not able to rerun all of the samples).

Because our data provide a quantitative measurement (CT ratio), we averaged the two runs to obtain a consensus value of the CT ratio. When we do this (using dPCR values as an example), we find that three samples (#28, #29, #43) returned average CT ratios (1.48, 1.07, 1.48) that were in agreement with the gold standard (S, R, S). For a fourth sample (#36), the average CT ratio (1.09) was also discordant with the gold standard (S) and we recorded it as an error in our analysis for both dPCR and dLAMP (see Table S1).

Isolate maintenance and exposure experiments.

For all experiments involving isolates (Fig. 2), isolates were maintained and antibiotic exposure carried out as described in previous work (*26*). All *E. coli* isolates were maintained on solid or liquid BHI media (BD), all *Lactobacillus jensenii* isolates were maintained on solid or liquid MRS media (BD).

Intermediate samples

In this manuscript, we focus on categorical agreement of our binary susceptibility determination (susceptible or resistant). We chose to design our study this way and to exclude intermediate samples for the following reasons:

The current gold-standard antibiotic susceptibility testing method is broth dilution. This method, used every day in central clinical laboratories, is only accurate to +/one dilution

step. For example, *E. coli* with an initially determined ciprofloxacin MIC of 2.0 μg/mL might have an MIC of 1, 2, or 4 μg/mL if tested again using the same gold-standard method. According to the CLSI standards used in the US, 1.0 μg/mL is considered "susceptible", while 2 μg/mL is considered "intermediate" and 4.0 μg/mL is considered resistant. This is well-known in the clinical microbiology community. In fact, the CLSI manual (*59*) states that one of the roles of the intermediate category is to include a buffer zone which should prevent small, uncontrollable, technical factors from causing major discrepancies in interpretation. Furthermore, when gold standard broth dilution vs gold standard inhibition zone diameter is compared, intermediate samples do not show consistent results (see Fig. 4 of (*60*); of the five samples tested with intermediate MICs (as determined by the goldstandard), the inhibition zone method called one of them resistant, two intermediate, and two susceptible (*60*)).

A further issue is the discrepancy of the meaning "resistant and susceptible" around these concentrations. For example, using EUCAST standards, susceptible isolates are those with ciprofloxacin MIC of 0.25 μg/mL and below, while intermediate isolates have MIC of 0.5 μg/mL and resistant isolates are 1.0 μg/mL and above.

We chose to exclude samples with MICs of 0.5, 1.0, and 2.0 μg/mL to ensure that the gold standard method would not frequently switch between a susceptible and resistant call if repeated.

Importantly, this approach is still applicable to "real world" samples and does not correspond to only looking at extremes of MIC. Excluding these samples only eliminates a small percentage of *E. coli* samples based on epidemiological data [see "Ciproflaxin / *Escherichia coli* international MIC distribution" reference database (62)], with the caveat that these distributions may change at different times in different locations. For example: a broader range of antibiotic concentrations is tested when generating epidemiological data than is tested in clinical microbiology laboratories. The cut-off MIC for defining resistant and susceptible organisms is different between the epidemiological and clinical

microbiological data. Epidemiological cut-off is defined relative to the wild-type susceptibility whereas the clinical cut-off is defined relative to clinically relevant susceptibility. These data should not be used to infer the rates of resistance in a particular geographical location at a particular time (62).

For nitrofurantoin (nit), MIC of >=128 is considered resistant and MIC of <= 32 is considered susceptible. Similarly, we chose to exclude the minimal possible number of samples with MICs that might switch between a susceptible or resistant call when repeated. For this reason, we excluded samples with MICs of 32 and 64 μg/mL.

Therefore, it should not be surprising that when validating a new AST method with clinical samples, it is common to challenge the method only against susceptible and resistant samples that are above or below the MIC breakpoints, while avoiding intermediate samples (*34, 35, 61*).

To test whether intermediate or near-intermediate samples provide any unexpected results, we did run a small separate study of 8 clinical isolates (2 operators with 4 isolates each) with intermediate and near-intermediate MICs using dPCR readout. We exposed these isolates with (1.0 μg/mL ciprofloxacin) and without antibiotics for 15 min and measured the nucleic acid concentrations with dPCR. Isolates with MIC of 1.0 μg/mL are clustering very close to the threshold and slightly below, while isolates with MIC of 0.5 μg/mL are comfortably above the threshold and would be read as susceptible (fig. S3).

Theoretical analysis of phenotypic AST

To explore the tradeoffs among antibiotic exposure time, the growth rate of the bacteria in question, and the required resolution of the measurement method, we developed a simple model to inform optimal AST methods when DNA replication is used as the differentiating marker between susceptible and resistant bacteria. We assumed that i) a sample containing bacteria with an initial concentration of a specific NA sequence, C0

[mol/L], has a DNA doubling time of tdouble [min] when incubated in media for tinc [min], ii) an antibioticsusceptible bacteria sample incubated in media with antibiotics does not grow at all, and iii) antibiotic-resistant bacteria grow at the same rate with and without antibiotics.

Under these assumptions, the ratio of the NA concentrations of a control sample (*Ccontrol*) compared to an antibiotic-treated sample (*CABX*)—the control–treated ratio (*CT ratio*)—after a certain time of antibiotic exposure (*tinc*) would be:

$$CT\ ratio = \frac{C_{control}(t_{inc})}{C_{ABX}(t_{inc})} = \frac{C_0 \cdot 2^{t_{inc}/t_{double}}}{C_0} = 2^{t_{inc}/t_{double}}$$

Plotting CT ratio as a function of *tinc* and *tdouble* yields Fig. 1B. Typically, qPCR is capable of resolving 2-fold differences in concentration, whereas digital PCR (dPCR) can resolve as low as 1.2-fold differences in concentration (*41*). Due to the higher resolving power of dPCR, phenotypic AST can be performed with shorter antibiotic exposure times than if qPCR was used as the measurement method.

Experimental details for LAMP primer design, optimization, and specificity.

LAMP primer optimization experiments (Fig. 3A, steps 1–2) were performed on a Roche LightCyler 96 using the SYBR Green I channel for readout, 6 µL reaction volumes, and the following concentrations of reagents: 20 mM Tris-HCl pH 8.8, 50 mM KCl, 10 mM (NH4)2SO4, 0.1% Tween-20, 1.4 mM dNTPs, 2 µM Syto-9, 400 U/mL Bst 2.0 (New England Biolabs), ~700 copies/µL *E. coli* gDNA, and 8 mM MgSO4. All samples were run across a temperature gradient spanning 60 – 72℃.

The experiments optimizing magnesium concentration (Fig. 3A, step 3) were performed using the same protocol as above with the following concentrations of reagents: 20 mM Tris-HCl pH 8.8, 150 mM KCl, 10 mM (NH4)2SO4, 0.1% Tween-20, 1.4 mM dNTPs, 2

μM Syto-9, 360 U/mL Bst 3.0 (New England Biolabs), ~700 copies/μL *E. coli* gDNA, and variable concentrations of MgSO4 (Fig. 3A). All samples were run across a temperature gradient spanning 60–74℃.

Primer concentrations were kept constant in all experiments: 1.6 μM FIP/BIP, 0.2 μM FOP/BOP, and 0.4 μM loopF/loopB (when included). The final selected primer set was as follows: GGCGTTAAGTTGCAGGGTAT (FOP), TCACGAGGCGCTACCTAA (BOP), CGGTTCGGTCCTCCAGTTAGTGTTTTCCCGAAACCCGGTGATCT (FIP), TAGCGGATGACTTGTGGCTGGTTTTTCGGGGAGAACCAGCTATC (BIP), ACCTTCAACCTGCCCATG (LoopF), GTGAAAGGCCAATCAAACC (LoopB).

Identification and specificity experiments were performed using the same concentration of reagents as the experiments to optimize MgSO4 concentration, but were run with 5 mM MgSO4. Although 6 mM MgSO4 yielded the fastest TTP, 5 mM MgSO4 was used in subsequent experiments in order to minimize the risk of background amplification. We have not observed background amplification with the primers described here, but other primer sets are sensitive to MgSO4 concentration. The optimal TTP using 5 mM MgSO4 was only 12 s slower than when using 6 mM MgSO4.

BLAST was used to evaluate primer specificity against the families *Enterobacteriaciae*, *Staphylococcaceae*, and *Enterococcaceae*. The specificity of the LAMP primers targeting the *E. coli* 23S rDNA gene was tested against human genomic DNA (*Hs* gDNA), *Lj* gDNA, urine from healthy donors, and water (Fig. 3A,B). *Hs* gDNA was tested at 0.002, 0.02, and 0.2 ng/μL final reaction concentration as measured using a NanoDrop 2000c (Thermo Fisher Scientific). *Lj* gDNA was tested at final reaction concentrations of 0.16, 0.8, and 1.6 ng/μL, as measured using a NanoDrop 2000c. Urine from healthy donors was run at 10% final reaction volume. Real-time LAMP amplification was performed using a range of concentrations of *E. coli* gDNA (*Ec* gDNA) prepared from clinical UTI urine samples and quantified using droplet digital PCR (Fig. 3C).

Rapid digital LAMP (dLAMP)

Clinical urine samples were treated with and without 1 μg/mL cip or 16 μg/mL nit for 15 min and nucleic acids extracted as described above. The dLAMP mix consisted of 20 mM Tris-HCl pH 8.8, 150 mM KCl, 10 mM (NH4)2SO4, 0.1% Tween-20, 1.4 mM dNTPs, 1X EvaGreen (Biotium), 360 U/mL Bst 3.0, 1X RNase Cocktail (ThermoFisher), 5 mM MgSO4, and 1 mg/mL BSA prepared in NF-H2O. Aliquots of NA extractions composed 10% or 20% of the final volume in the dLAMP mix. Two aliquots of dLAMP mix containing equal volumes of NA extractions from the control and treated samples were simultaneously loaded into two separate SlipChip devices. The top piece of each SlipChip was moved relative to the bottom piece, which partitioned the solution into 1,280 3-nL compartments (lab made glass SlipChips) or 5,376 2.4-nL compartments (injection-molded plastic SlipChips) (see Supplementary Materials). When using the injection-molded plastic SlipChips, the treated chip was loaded 30 s after the control chip. The SlipChips were then placed onto the thermal cycler of a digital real-time imaging instrument and incubated at 72 °C for 20 min (*56*). Amplification time was recorded starting from when the thermal cycler reached 72 °C.

Images were taken every 20 s and the fluorescent intensity was measured for each compartment (Fig. 4A/F) with LabView software as described in (*56*). Wells that showed liquid movement or bubbles were excluded from analysis. If there was a spatial amplification gradient (i.e., positives in one area of the chip appeared before other areas), then the experiment was excluded. The concentration of the target was calculated using Poisson statistics and was based on the number of "positive" compartments that exceeded the fluorescence intensity threshold, for time points where 13 or more compartments were positive. The concentration of the control and treated samples was calculated in real-time, along with a *P* value representing the probability that the ratio of concentrations being greater than 1.10 was a result of random chance (Fig. 4C/H). If $P < 0.05$, we can be reasonably certain that the bacteria are susceptible to the antibiotic. If the P-value remains > 0.05, we can be reasonably certain that the bacteria are resistant to the

antibiotic. The CT ratio was calculated and plotted for each 20 s interval in Fig. 4 D/I for one susceptible sample and one resistant sample. For Fig. 6C, the CT ratio at 6.7 min was calculated and plotted for all 54 dAST experiments.

In some cases, the TTP distribution (Fig. 4 B/G) of one chip was delayed relative to the other chip. If this happened, the TTP maximums were aligned to normalize the data before concentrations and CT ratios calculated.

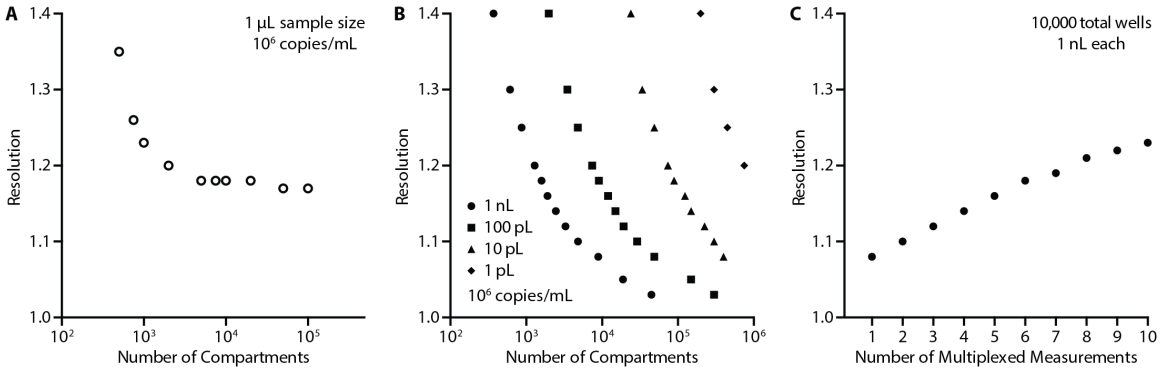

Fig. 3-S1. Resolution of digital devices. The resolution of digital quantification depends on the number and volume of compartments. Simulations were performed with the methods described in (45). A) For a fixed sample size, and fixed input concentration of 106 cop/mL relevant to UTIs, increasing the number of compartments (and reducing the volume of each compartment accordingly) beyond 1,000 does not improve resolution in a useful way. B) For fixed compartment volume, and fixed input concentration of 106 copy/mL relevant to UTIs, the resolution improves with increasing number of compartments, although this increase requires a larger input of sample and amplification reagents. C) Dependence of resolution on the number of multiplexed measurements made for a constant number of total wells. For example, while 10,000 of 1 nL compartments provide 1.08 resolution, 2,000 of 1 nL compartments provide 1.16 resolution each, enabling a 4- plex dAST (1 control and 4 ABX treated samples) to be performed.

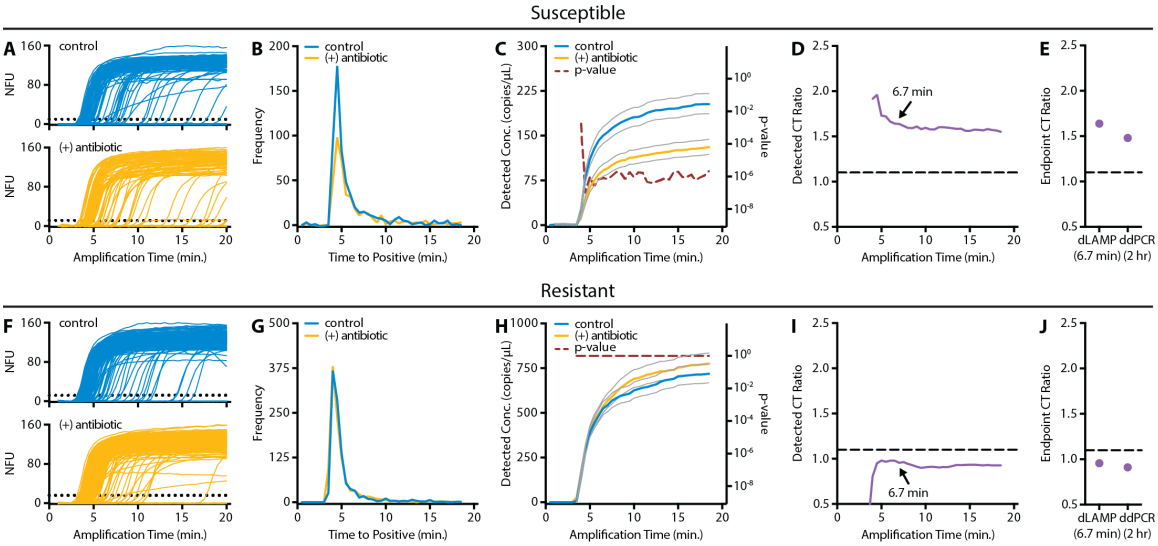

Fig. 3-S2. Real-time dLAMP DNA quantification of a UTI sample with nit treatment. High-resolution single- molecule nucleic acid amplification was performed using ultrafast digital LAMP (dLAMP) for digital antimicrobial susceptibility test (dAST) of clinical UTI urine samples with antibiotic-susceptible (A–E) and antibiotic-resistant (F–J) *E. coli*. Aliquots of a clinical UTI sample were treated with and without 16 µg/mL nitrofurantoin. After 15 min, DNA was extracted and quantified with digital LAMP on SlipChips. The protocols followed and materials used are described in Materials and Methods, "Digital AST (dAST) using clinical UTI samples" and Supplementary Materials Section 5. (**A,F**) Real-time fluorescence amplification traces (only 200 of 1,280 traces shown for clarity). NFU = normalized fluorescence units; dotted line = positive threshold; when the normalized fluorescence intensity of a compartment crosses the threshold, that compartment is counted as positive. (**B,G**) Time-to-positive (TTP) distribution was determined by counting the number of compartments that crossed the positive threshold at each time point. (**C,H**) Detected concentrations of the target dAST marker in control and antibiotic-treated samples for successive image cycles. Grey lines represent 95% confidence intervals. Note these curves are not the amplification curves shown in A and F. (**D,I**) Detected control–treated (CT) ratios over time. Dashed line indicates susceptibility threshold. (**E,J**) Comparison of CT ratios for droplet digital PCR (dPCR) after 2 h and dLAMP (after 6.7 min of amplification).

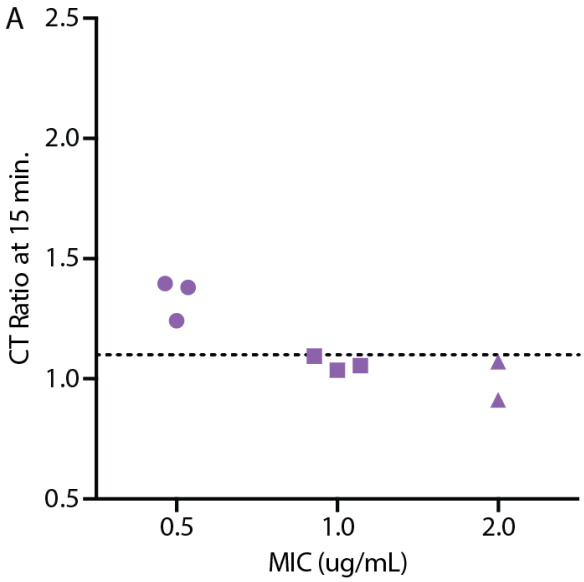

Fig. 3-S3. The dAST method tested with isolates with near-intermediate MICs. The digital AST (dAST) method was tested with clinical isolates from urinary tract infections(UTIs) using a 15 min treatment of 1 µg/mL ciprofloxacin. Eight isolates with three near-intermediate MICs were analyzed with the dAST method (two operators with four isolates each). Control–treated (CT) ratios were calculated from dPCR 23S DNA concentration measurements.

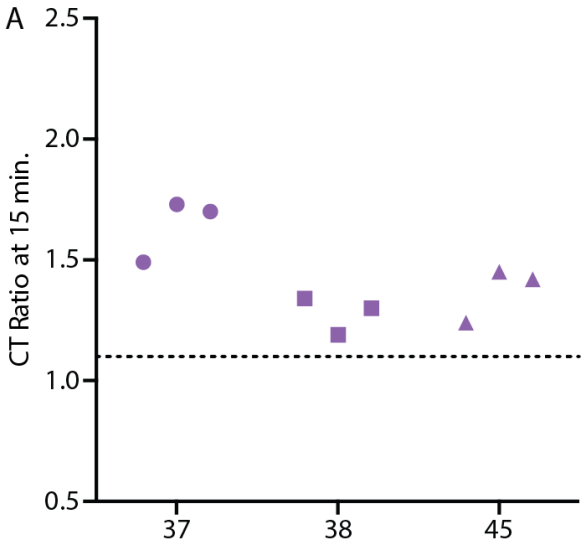

Fig. 3-S4. Reproducibility of the dAST method with clinical urine samples. Three ciprofloxacin-susceptible samples (#37, #38, #45 from table S1) were analyzed with the

dAST method in triplicate and control–treated (CT) ratios were calculated from DNA concentration measurements using digital droplet PCR.

Table 3-S1. Concentration of clinical urine samples. Pathogen-specific 23S DNA concentration as determined by digital LAMP after 6.7 min of amplification time (Fig. 4C/H). Taking into account the number of rDNA copies per *E. coli* chromosome, and the efficiency of dLAMP in counting DNA in 6.7 min, the concentration of full genomes is ~6 times lower than the number reported in this table. CFU/mL was determined by plate counting at the UCLA Clinical Microbiology Laboratory.

Caltech Sample #	23S Conc. (cop/mL)	CFU/mL	Caltech Sample #	23S Conc. (cop/mL)	CFU/mL
1	1.59E+07	>100,000	27	4.63E+07	>100,000
2	2.52E+07	>100,000	28	3.62E+07	>100,000
3	3.94E+07	>100,000	29	6.21E+06	>100,000
4	5.63E+07	>100,000	30	2.38E+07	>100,000
5	3.14E+07	>100,000	31	2.98E+07	>100,000
6	7.86E+06	>100,000	32	9.57E+07	>100,000
7	7.07E+06	>100,000	33	1.08E+08	>100,000
8	5.08E+07	>100,000	34	1.13E+08	>100,000
9	1.72E+07	>100,000	35	4.84E+07	>100,000
10	2.64E+07	>100,000	36	5.73E+07	>100,000
11	7.44E+06	>100,000	37	1.59E+07	>100,000
12	2.75E+07	>100,000	38	8.49E+07	>100,000
13	2.07E+07	>100,000	39	3.18E+06	50,000
14	1.55E+07	>100,000	40	2.45E+07	>100,000
15	2.12E+08	>100,000	41	1.02E+08	>100,000
16	1.59E+07	>100,000	42	1.26E+07	>100,000
17	5.12E+07	>100,000	43	4.97E+06	>100,000
18	1.44E+07	>100,000	44	1.69E+08	>100,000
19	2.62E+07	>100,000	45	2.46E+08	>100,000
20	4.52E+06	>100,000	46	8.78E+06	>100,000
21	4.25E+07	>100,000	47	8.58E+06	>100,000
22	1.30E+08	>100,000	48	1.21E+07	>100,000
23	3.04E+07	>100,000	49	1.41E+07	>100,000
24	2.38E+07	>100,000	50	3.06E+06	>100,000
25	4.19E+07	>100,000	51	8.02E+06	>100,000
26	1.92E+07	>100,000			

Table 3-S2. Clinical samples used in this study. Clinical urinary tract infection (UTI) urine samples tested for ciprofloxacin (cip) or nitrofurantoin (nit) susceptibility testing by gold-standard broth microdilution and by digital AST (dAST). Nucleic acids were quantified with both digital PCR (dPCR) and digital LAMP (dLAMP). Sample reruns (indicated by a "(2)") were performed several hours later on the same day when the

control- treated ratio was discordant with the gold-standard AST call (CT ratio > 1.10 for a resistant sample or < 1.10 for a susceptible sample). S = antibiotic-susceptible; R = antibiotic-resistant; *major error; **very major error.

Caltech Sample #	UCLA ID #	Description (Color, Turbidity)	ABX	MIC (µg/mL)	Gold-standard AST call	CT Ratio (dPCR)	dAST call (dPCR)	CT Ratio (dLAMP, 6.7 min)	dAST call (dLAMP)
1	15-31A-020	red, clear	nit	<16	S	1.48	S	1.64	S
2	15-31A-022	light yellow, clear	cip	<=0.25	S	1.44	S	1.34	S
3	15-31A-025	light yellow, clear	nit	<16	S	1.33	S	1.33	S
4	15-31A-026	light yellow, clear	nit	<16	S	1.36	S	1.35	S
5	15-31A-027	light yellow, clear	nit	<16	S	1.25	S	1.24	S
6	15-31A-031	colorless, clear	cip	>=4	R	1.09	R	0.95	R
6	15-31A-031	colorless, clear	nit	256	R	0.95	R	0.77	R
7	15-31A-039	light yellow, clear	cip	>=4	R	0.99	R	0.84	R
8	15-31A-040	light yellow, clear	nit	128	R	1.06	R	1.09	R
9	15-31A-042	dark yellow, clear	cip	<=0.25	S	1.92	S	1.83	S
10	15-31A-043	light yellow, clear	cip	<=0.25	S	1.66	S	1.85	S
10	15-31A-043	light yellow, clear	nit	128	R	0.91	R	0.92	R
11	15-31A-049	light yellow, clear	cip	>=4	R	0.96	R	1.04	R
12	15-31A-050	dark yellow, cloudy	cip	>=4	R	0.88	R	0.96	R
13	15-31A-051	light yellow, cloudy	cip	>=4	R	0.98	R	0.97	R
14	15-31A-054	light yellow, cloudy	cip	<=0.25	S	1.42	S	1.48	S
15	15-31A-056	light yellow, cloudy	nit	256	R	1.09	R	1.106	S**
16	15-31A-060	light yellow, cloudy	cip	<=0.25	S	1.83	S	1.31	S
17	15-31A-063	yellow, cloudy	cip	<=0.25	S	1.28	S	1.111	S
18	15-31A-066	yellow, cloudy	cip	>=4	R	0.85	R	0.80	R
19	15-31A-067	light yellow, cloudy	cip	>=4	R	0.82	R	0.59	R
20	15-31A-068	light yellow, cloudy	cip	>=4	R	0.84	R	0.57	R
21	15-31A-071	light yellow, cloudy	cip	>=4	R	1.04	R	0.92	R
22	15-31A-079	light yellow, cloudy	nit	128	R	1.25	S**	1.43	S**
23	15-31A-084	yellow, clear	cip	>=4	R	1.01	R	0.96	R
24	15-31A-086	yellow, cloudy	cip	<=0.25	S	2.01	S	2.21	S
25	15-31A-088	yellow, cloudy	cip	<=0.25	S	1.25	S	1.22	S
26	15-31A-089	light yellow, clear	cip	>=4	R	0.94	R	0.91	R
27	15-31A-091	yellow, cloudy	cip	<=0.25	S	1.18	S	1.19	S
28	15-31A-093	orange/red, clear	cip	<=0.25	S	1.08	R	-	-
28(2)	15-31A-093	orange/red, clear	cip	<=0.25	S	1.88	S	1.59	S
28 avg	15-31A-093	orange/red, clear	cip	<=0.25	S	1.48	S	-	-
29	15-31A-096	light yellow, cloudy	cip	>=4	R	1.20	S	-	-
29(2)	15-31A-096	light yellow, cloudy	cip	>=4	R	0.93	R	0.98	R
29 avg	15-31A-096	light yellow, cloudy	cip	>=4	R	1.07	R	-	-
30	15-31A-097	light yellow, cloudy	cip	>=4	R	1.13	S**	0.98	R
31	15-31A-101	light yellow, clear	nit	<16	S	1.39	S	1.19	S
32	15-31A-102	dark yellow, clear	nit	<16	S	1.63	S	1.68	S
33	15-31A-103	light yellow, clear	nit	<16	S	1.38	S	1.28	S
34	15-31A-105	light pink, cloudy	nit	<16	S	1.47	S	1.44	S
35	15-31A-108	yellow, cloudy	nit	<16	S	1.29	S	1.37	S
36	15-31A-111	yellow, clear	nit	<16	S	1.02	R*	-	-
36(2)	15-31A-111	yellow, clear	nit	<16	S	1.16	S	0.95	R*
36 avg	15-31A-111	yellow, clear	nit	<16	S	1.09	R	-	-
37	15-31A-112	yellow, clear	nit	<16	S	1.49	S	1.12	S
38	15-31A-114	light yellow, clear	nit	<16	S	1.34	S	1.36	S
39	15-31A-115	yellow, clear	nit	<16	S	1.44	S	1.48	S
40	15-31A-116	dark yellow, cloudy	cip	>=4	R	1.05	R	0.75	R
40	15-31A-116	dark yellow, cloudy	nit	<16	S	1.96	S	2.33	S
41	15-31A-118	yellow, clear	nit	<16	S	1.25	S	1.15	S
42	15-31A-119	light yellow, clear	cip	<=0.25	S	2.21	S	1.95	S
43	15-31A-122	light yellow, clear	nit	<16	S	1.17	S	-	-
43(2)	15-31A-122	light yellow, clear	nit	<16	S	1.79	S	1.45	S
43 avg	15-31A-122	light yellow, clear	nit	<16	S	1.48	S	-	-

44	15-31A-123	yellow, cloudy	nit	<16	S	1.18	S	1.15	S
45	15-31A-126	light yellow, clear	nit	<16	S	1.24	S	1.19	S
46	15-31A-131	light yellow, clear	cip	<=0.25	S	1.61	S	1.28	S
47	15-31A-132	dark yellow, clear	cip	<=0.25	S	1.27	S	1.14	S
48	15-31A-133	dark yellow, cloudy	cip	<=0.25	S	1.30	S	1.29	S
49	15-31A-134	dark yellow, clear	cip	<=0.25	S	2.36	S	1.85	S
50	15-31A-136	light yellow, clear	cip	<=0.25	S	2.04	S	1.89	S
51	15-31A-137	dark yellow, clear	cip	<=0.25	S	1.43	S	1.28	S

Table 3-S3. Rapid phenotypic AST literature summary showing the state of the art. Phenotypic antibiotic susceptibility tests using clinical samples, blood culture, contrived samples, clinical isolates, or reference strains with reported total assay time less than 3.5 hrs (210 min). References are sorted by sample type and then by combined time of all steps. NR = not reported. Literature from 1997–2017.

Sample Type	*Method*	*Pre-assay Enrichment Time (min)*	*Minimum ABX Exposure Time (min)*	***Combined Time of All Steps (min)***	*Fastest Reported Sample-to-Answer Time (min)*	*Reference*
Clinical Samples	dAST (using dLAMP)	0	15	24	29	*This work*
Clinical Samples	ATP Bioluminescence	0	90	105	NR	(*61*)
Clinical Samples	Microscopy	120	30	155	NR	(*28*)
Clinical Samples	NA Quantification	0	120	204[a]	NR	(*35*)
Clinical Samples	Microscopy	0	206	206[b]	NR	(*88*)
Clinical Samples	Electrochemical	0	150	NR	210	(*34*)
Contrived Samples	Microfluidics	0	60	60	NR	(*89*)
Contrived Samples	Electrochemical	0	60	100	NR	(*90*)
Contrived Samples	Microfluidics	0	120	120	NR	(*91*)
Blood Culture	Microscopy	0	40	45[c]	NR	(*39*)
Clinical Isolates	Microscopy	0	10	<30[d]	NR	(*27*)
Clinical Isolates	Microscopy	0	40	40	NR	(*39*)
Clinical Isolates	Electrochemical	0	15	45	NR	(*33*)
Clinical Isolates	FACS	0	90	95	NR	(*92*)
Clinical Isolates	Magnetic Bead Rotation	90	15	120[e]	NR	(*93*)
Clinical Isolates	Microscopy	120	6	126	NR	(*28*)
Clinical Isolates	Raman Spectroscopy	0	120	130[f]	NR	(*94*)
Clinical Isolates	Raman Spectroscopy	0	120	130[f]	NR	(*95*)
Clinical Isolates	dAST (using dPCR)	0	15	140	NR	(*26*)
Clinical Isolates	FACS	0	120	150	NR	(*96*)
Clinical Isolates	FACS	0	60	180	NR	(*97*)
Clinical Isolates	Mass Spectrometry	0	60	180	NR	(*98*)
Clinical Isolates	Microscopy	0	180	200[g]	NR	(*29*)
Clinical Isolates	Electrochemical	0	90	NR	NR	(*34*)
Reference Strains	Microscopy	0	3	<30[d]	NR	(*27*)
Reference Strains	Electrochemical	0	10	25	NR	(*32*)
Reference Strains	Raman Spectroscopy	0	20	25[f]	NR	(*95*)
Reference Strains	Electrochemical	0	20	42	NR	(*99*)
Reference Strains	Microfluidics	0	60	60	NR	(*100*)
Reference Strains	FACS	0	120	120[h]	NR	(*101*)
Reference Strains	Raman Spectroscopy	0	120	130[f]	NR	(*94*)

[a]time does not include washing and centrifugation steps

[b]detailed times of each step not reported, listed time is median time reported for all samples

[c]does not include time of overnight blood culture growth

[d]total time of all steps reported as “less than 30 min.”

[e]time does not include washing steps

[f]washing, imaging, and agarose embedding time not included

[g]reported as "clinical samples" in the abstract, but methods clearly state that all work was performed with clinical isolates: "We tested 189 clinical isolates...Before testing, each isolate was subcultured on cation-adjusted MHA for 20-24 hours"

[h]does not include time of FACS measurement

Chapter IV

RNA Markers Enable Phenotypic Test of Antibiotic Susceptibility in *Neisseria gonorrhoeae* After 10 Minutes of Ciprofloxacin Exposure[3]

Abstract

Rapid antimicrobial susceptibility testing (AST) is urgently needed for informing treatment decisions and preventing the spread of antimicrobial resistance resulting from the misuse and overuse of antibiotics. To date, no phenotypic AST exists that can be performed within a single patient visit (30 min) directly from clinical samples. We show that AST results can be obtained by using digital nucleic acid quantification to measure the phenotypic response of Escherichia coli present within clinical urine samples exposed to an antibiotic for 15 min. We performed this rapid AST using our ultrafast (~7 min) digital real-time loop-mediated isothermal amplification (dLAMP) assay [area under the curve (AUC), 0.96] and compared the results to a commercial (~2 hours) digital polymerase chain reaction assay (AUC, 0.98). The rapid dLAMP assay can be used with SlipChip microfluidic devices to determine the phenotypic antibiotic susceptibility of E. coli directly from clinical urine samples in less than 30 min. With further development for additional pathogens, antibiotics, and sample types, rapid digital AST (dAST) could enable rapid clinical decisionmaking, improve management of infectious diseases, and facilitate antimicrobial stewardship.

Introduction

Neisseria gonorrhoeae is the second most common sexually transmitted bacterial infection in the United States, with about 460,000 cases reported in 2016, an 18.5% rise

[3]This chapter was first published in *Scientific Reports* with authorship belonging to Tamineh Kazaei, Jacob T. Barlow, Nathan G. Schoepp, and Rustem F. Ismagilov.

since 2015Prevention [1]. Worldwide, it is estimated that about 78 million new *N. gonorrhoeae* infections occur annually[2]. *N. gonorrhoeae* infections can lead to heart and nervous system infections, infertility, ectopic pregnancies, newborn blindness, and increased risk for other sexually transmitted infections, including HIV[3]. The CDC has identified *N. gonorrhoeae* as one of the three most urgent drug-resistant bacterial threats[3]. *N. gonorrhoeae* has developed resistance to all of the most commonly used antibiotics (including penicillins, sulfonamides, tetracyclines, and fluoroquinolones) leaving only one last effective class of antibiotics: cephalosporins. However, there have even been worldwide reported cases of decreased susceptibility to the cephalosporin ceftriaxone[4-8], and therefore an imminent threat of widespread untreatable *N. gonorrhoeae*. An important factor leading to the widespread development of antibiotic resistance is the liberal use and misuse of antibiotics. Critically needed is a rapid antibiotic susceptibility test (AST) that can guide treatment at the point-of-care — both to provide correct treatment and to facilitate antibiotic stewardship.

The gold standard for determining *N. gonorrhoeae* susceptibility to antibiotics is the culture-based agar dilution test, which is unacceptably slow (1–2 days). More rapid genotypic approaches, involving detection of gene mutations, are available for a subset of antibiotics in *N. gonorrhoeae*[9,10], but such approaches are inherently limiting, as they require knowledge of the mechanisms of resistance. Moreover, *N. gonorrhoeae* is naturally competent for transformation, and can take up gonococcal DNA from the environment and recombine it with its own genome, resulting in frequent gene mutations[11,12]. Given the high rate at which new resistance emerges, relying solely on genotypic methods is not an acceptable long-term solution. Phenotypic methods involving growth measurements have enabled faster ASTs that are independent of resistance mechanisms[13-16]. However, such growth-based methods are challenging for *N. gonorrhoeae*, which is slow-growing and fastidious[17]. Another phenotypic approach for antibiotic susceptibility testing is quantification of nucleic acids[18,19]. We have previously demonstrated a rapid (30 min) phenotypic AST using quantification of DNA replication by digital PCR (dPCR) to assess the antibiotic susceptibility of *Escherichia coli* in

clinical urine samples[20]. However, AST methods that quantify changes in DNA replication require a longer antibiotic-exposure step for slow-growing pathogens such as *N. gonorrhoeae,* which has a doubling time of about 60 min[21], compared with the 20 min doubling time of *E. coli*[22].

A complementary approach to DNA quantification is measuring the pathogen's RNA response to antibiotic exposure. Transcriptional responses are among the earliest cellular changes upon exposure to antibiotics[23], far before phenotypic changes in growth can be observed. Quantifying changes in RNA signatures is therefore a particularly appealing approach for slow-growing organisms. RNA has previously been used to differentiate antibiotic susceptibility and resistance in organisms where the transcriptional response is well characterized[24,25]. More recently, RNA sequencing (RNA-Seq) has been used to measure the transcriptome response of *Klebsiella pneumoniae* and *Acinetobacter baumanii* to antibiotic exposure[25]. Although the *N. gonorrhoeae* transcriptome has been previously sequenced[26,27], to our knowledge, no one has characterized the transcriptome response of *N. gonorrhoeae* to antibiotic exposure. Unlike most bacteria, *N. gonorrhoeae* lacks the classic transcriptional SOS response to DNA damage whereby DNA repair is induced and the cell cycle is arrested[28,29]. The SOS response promotes survival to certain antibiotic classes, such as the fluoroquinolones, which act by directly inhibiting DNA synthesis[30]. The recA or recA-like proteins are essential for the induction of the SOS response[28]. However, neither *recA* transcripts nor recA protein levels increase in *N. gonorrhoeae* upon exposure to DNA damaging agents[31,32].

In this work, we explore the transcriptome response of *N. gonorrhoeae* upon exposure to ciprofloxacin. Ciprofloxacin is a fluoroquinolone and functions by inhibiting the enzymes topoisomerase II (DNA gyrase) and topoisomerase IV, thereby inhibiting cell division[33]. Ciprofloxacin was chosen in this study to gain insight into transcriptional changes that occur upon DNA damage in an organism lacking the classic SOS response. Here, we address the following questions: (1) How does the transcriptome of *N. gonorrhoeae* respond to ciprofloxacin exposure? (2) What is the shortest antibiotic exposure time at

which we can still observe significant changes (>4-fold) in RNA expression? (3) Which transcripts provide the largest and most abundant fold-changes per cell, which is an important consideration for clinical samples that have low numbers of pathogens? (4) Will candidate markers respond consistently across a large pool of isolates with wide genetic variability?

Results

We used RNA-seq to study the transcriptome response of susceptible and resistant isolates of *N. gonorrhoeae* after 5, 10, and 15 min of ciprofloxacin exposure (Fig. 1). Each clinical isolate was initially split into two tubes, where one tube was exposed to the antibiotic (+) and the other served as the control with no antibiotic exposure (-). Samples were collected for RNA-seq prior to antibiotic exposure and every 5 min for 15 min. We calculated the fold change in gene expression between the control and treated samples – defined as the control:treated ratio (C:T ratio); genes that demonstrated significant fold-change differences between the susceptible and resistant isolates were identified as differentially expressed. To account for biological variability, three pairs of susceptible and resistant isolates were used in this study. Candidate markers were selected from the pool of differentially expressed genes and were validated using droplet dPCR (see Methods).

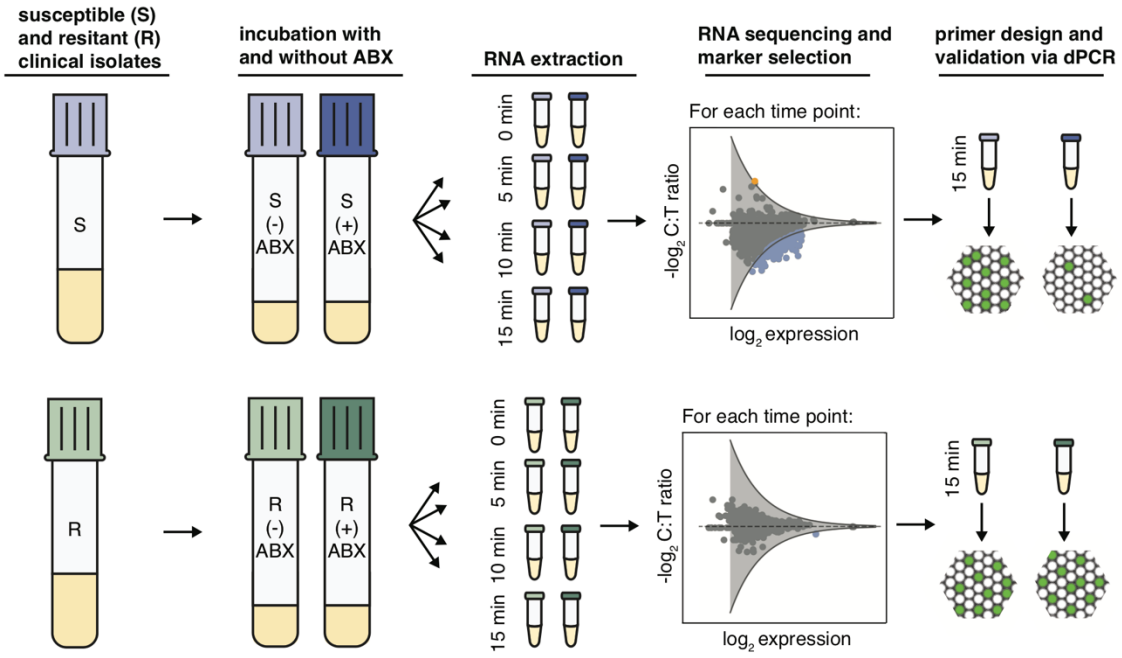

Figure 4-1. The work flow for selection and validation of RNA markers for phenotypic measurements of antibiotic susceptibility and resistance. Susceptible and resistant isolates of *Neisseria gonorrhoeae* are exposed to antibiotics (ABX) for 5, 10, and 15 min. Samples are collected for RNA sequencing at time zero and every 5 min thereafter. Genes demonstrating fold changes in expression (control:treated ratio (C:T ratio)) greater than the threshold of significance (gray line) are identified as differentially expressed (blue: downregulated and orange: upregulated). Candidate markers are selected from the pool of differentially expressed genes and validated by digital PCR.

Temporal shifts in global gene expression upon antibiotic exposure

We observed global shifts in RNA expression in susceptible isolates in as early as 5 min after antibiotic exposure (Fig. 2a). The distribution of fold changes in gene expression levels (C:T ratios) indicated global shifts toward negative $\log_2$ fold-change values (downregulation). The magnitude of fold change at which most genes were distributed was approximately 2-fold. The tail of the distribution illustrates that a few genes

responded to antibiotic exposure with changes as large as 6-fold within 5 min. Increasing the antibiotic exposure time further shifted the distribution to larger negative $\log_2$ fold-change values. The transcriptional response in resistant isolates was tightly distributed around a fold-change value of 1 at every time point, indicating that the transcriptome of the resistant isolates did not respond significantly to antibiotic exposure (Fig. 2a).

To identify genes that were differentially expressed between control and treated samples, we defined a threshold of significance (Fig. 2b). The threshold of significance took into account technical variability and was calculated from the C:T ratios at t = 0 min of all biological replicates that were sequenced (three susceptible and three resistant isolates). For each of the six gene expression datasets (one for each isolate), we plotted the $-\log_2$(C:T ratio) against the $-\log_2$(expression) for all genes and fit a negative exponential curve to the outer edge of each plot. We then averaged the curves from all six datasets and added a 90% confidence interval to the average curve by assuming a Gaussian fit for the error distribution, which we define as our threshold of significance. Genes with a $-\log_2$(C:T ratio) value above or below the upper and lower thresholds were identified as differentially expressed. Downregulated genes (fold changes below the significance threshold) appeared as early as 5 min after antibiotic exposure (blue dots, Fig. 2b). Two upregulated genes (fold changes above the significance threshold) appeared after 10 min of exposure (orange dots, Fig. 2b).

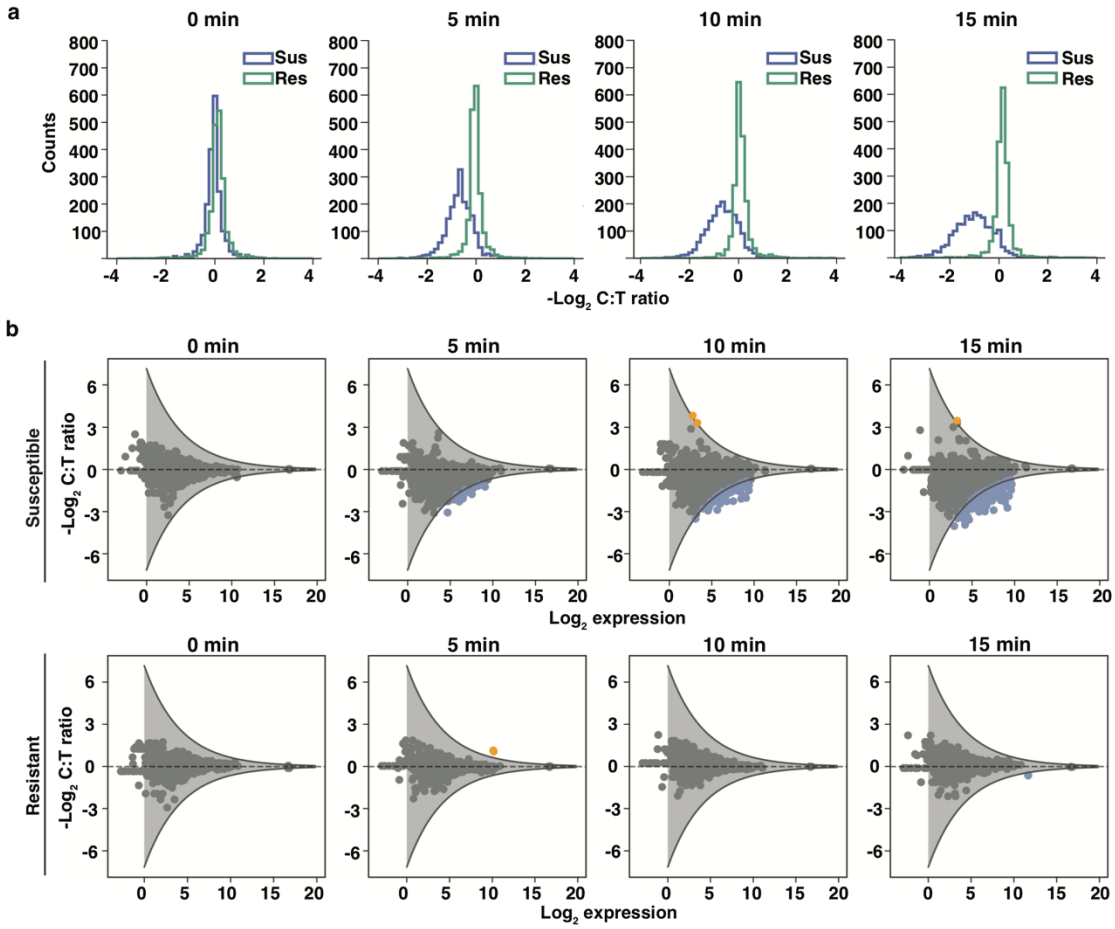

Figure 4-2. Temporal shifts in global gene expression upon ciprofloxacin exposure in *Neisseria gonorrhoeae*. (**a**) The distribution of −log2(C:T ratios) for a susceptible isolate (Sus) and resistant isolate (Res) at 0, 5, 10, and 15 min. (**b**) The fold change in gene expression between control and treated samples (C:T ratio) versus expression in the control sample at 0, 5, 10, and 15 min for one susceptible isolate and one resistant isolate. Genes with C:T ratios above or below the significance threshold are identified as differentially expressed (blue: downregulated; orange: upregulated). Thresholds for statistical significance of fold change (gray lines) are determined by fitting a negative exponential curve (with 90% confidence interval) to the outer edge of the −log2 C:T ratios measured at time zero (see Methods).

Selection of candidate markers that are consistent in response and abundant

RNA expression in response to antibiotics can be heterogeneous among different isolates of the same species[34]; thus, it is important to select candidate markers from differentially expressed genes that respond consistently across isolates of *N. gonorrhoeae.* To identify these candidate markers, we exposed three different pairs of susceptible isolates (minimum inhibitory concentrations (MICs) <= 0.015mg/mL) and resistant isolates (MICs 2.0 mg/mL, 4.0mg/mL, and 16.0mg/mL) to ciprofloxacin for 15 min and extracted RNA for sequencing (see workflow in Fig. 1). We found 181, 41, and 410 differentially expressed genes in susceptible isolates 1, 2, and 3, respectively (Fig. 3a). Among the differentially expressed genes, 38 genes responded consistently across the three pairs of susceptible and resistant isolates (i.e. responses overlapped in all three susceptible isolates, whereas all three resistant isolates were non-responsive) (Supplementary Table S1 online). These genes spanned a variety of biochemical functions in the cell. We selected six candidate transcript markers for further analysis based on the following criteria: (1) high fold change; (2) high expression levels (>75 transcripts per million, TPM); and (3) representative of different biochemical pathways. The selected candidate markers were: *porB* (membrane protein), *rpmB* (ribosomal protein), *tig* (molecular chaperone), *yebC* (transcriptional regulator), *pilB* (pilus assembly ATPase), and *cysK* (cysteine synthase). The candidate marker with the highest abundance and largest fold change upon antibiotic exposure was *porB*, which is a membrane channel forming protein and the site of antibiotic influx into the cell[35].

A high level of gene expression was one of our criteria for selection of candidate markers from the sequencing data. High expression of candidate markers is not only important for sensitivity and limits of detection, but is particularly important for clinical samples with low numbers of pathogen cells. One of the advantages of RNA compared with DNA as a nucleic acid marker is its natural abundance in the cell. Because the gene expression values obtained from sequencing are relative values, our next step was to quantify the absolute copies per cell for the candidate markers. In our quantification approach we plated clinical isolate samples after 15 min of ciprofloxacin exposure to obtain cell

numbers in colony forming units (CFU/mL). We designed primers for the candidate markers (see Methods and Supplementary Table S2) and measured their absolute concentration using dPCR. The concentrations were converted to per cell values using the cell counts from plating (Fig. 3b). Additionally, we used the RNA sequencing data to obtain transcriptome-wide estimates of transcript copies per cell. In the sequencing approach, we added external RNA control consortium (ERCC) spike-ins to the lysis buffer step of the extraction protocol in order to capture any loss of RNA throughout the extraction steps. By linear regression we captured the relationship between ERCC copies added to the samples and ERCC quantified by sequencing. Using the linear regression, we converted gene expression values from RNA sequencing (in TPM) to approximate copy numbers per cell (see Methods). The transcript copies per cell estimated for the candidate markers using the sequencing approach were within the same order of magnitude as the absolute copies per cell measured by digital PCR (Fig. 3b).

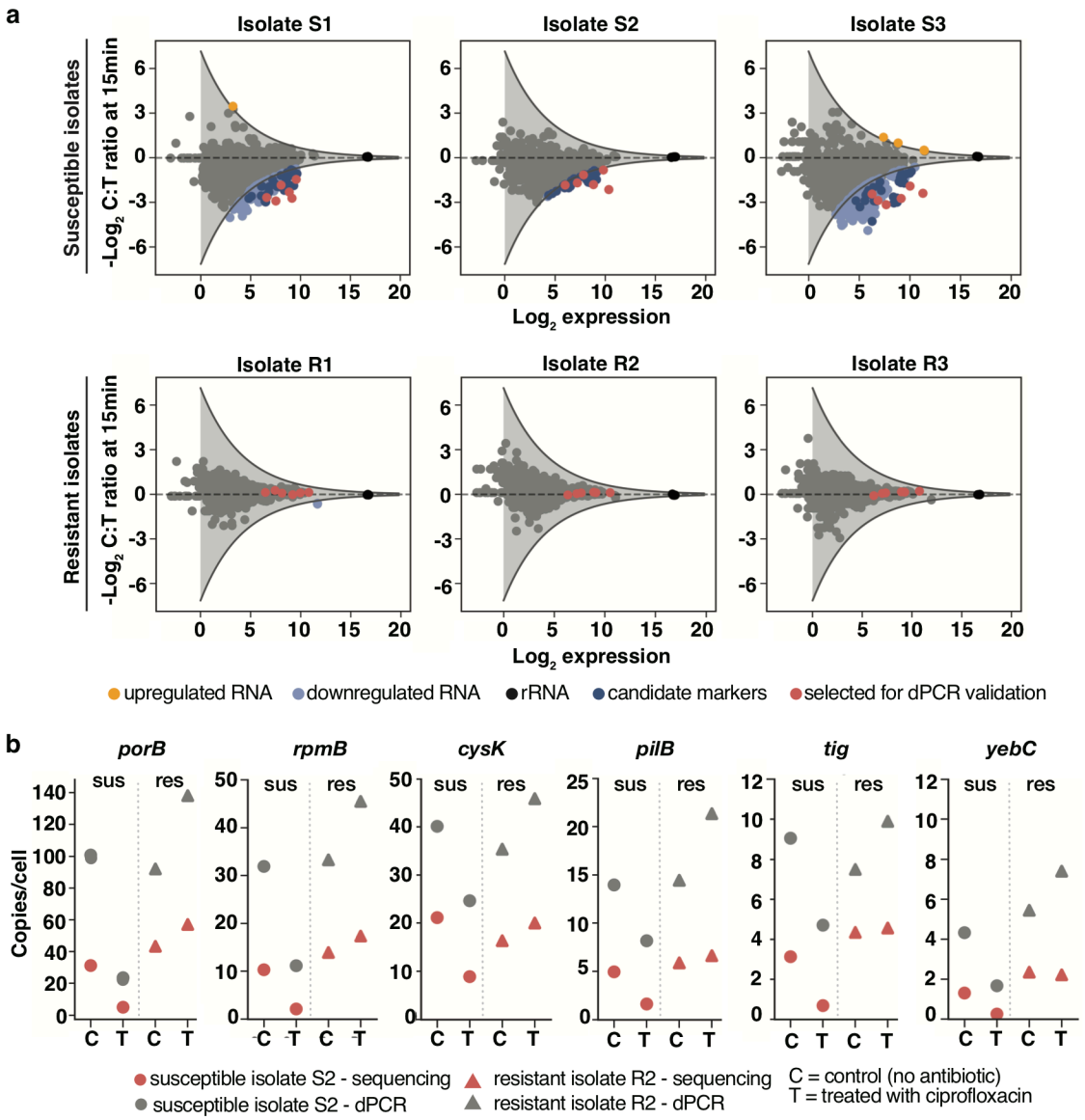

Figure 4-3. Selection of candidate RNA markers for phenotypic antibiotic susceptibility testing in *Neisseria gonorrhoeae* and measurements of candidate marker abundances per cell (**a**) Genes that are differentially expressed (light blue) across three pairs of resistant and susceptible clinical isolates are identified as candidate markers (dark blue). Six candidate markers that span different biological functions were selected for validation (red). (**b**) Copies/cell values for the candidate markers are determined from RNA sequencing (red) and dPCR (gray) (see Methods). Data is shown for one pair of susceptible (S2) and resistant (R2) isolates at 15 min of ciprofloxacin exposure.

Validation of candidate markers by dPCR

We next asked how the relative changes observed through RNA-seq compare with direct gene expression measurements by dPCR. We designed dPCR assays for candidate markers, which involved measuring the absolute expression of the candidate marker in both control and treated samples, and calculating the C:T ratio. In this assay, the 16S rRNA was also measured and used to normalize the C:T ratio of the candidate markers. In the three susceptible isolates that were sequenced we found that rRNA consistently showed the smallest fold change (<1.06) in response to ciprofloxacin compared with all other genes in *N. gonorrhoeae*. Therefore, to account for experimental variations in the antibiotic exposure and RNA extraction steps between control and treated samples, we used the 16S rRNA as an intracellular control for normalizing the C:T ratios (see Methods). We found that the C:T ratios measured by the dPCR assay agreed with the C:T ratios obtained through sequencing (Fig. 4), confirming that both approaches accurately capture the transcriptional response to antibiotic exposure.

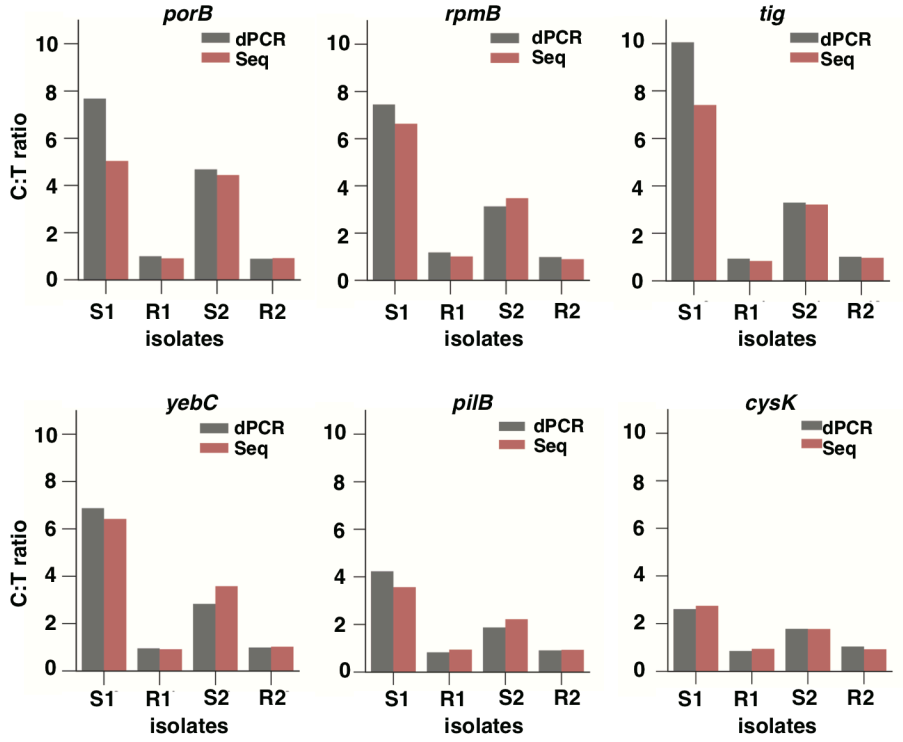

Figure 4-4. Validation of the RNA sequencing approach using digital PCR (dPCR) with six candidate markers. Control:treated ratios (C:T ratios) determined by RNA sequencing (red) were validated against C:T ratios measured by dPCR (gray). The dPCR C:T ratios were normalized using ribosomal RNA (rRNA) by dividing the C:T ratio of the candidate marker by the C:T ratio of 16S rRNA. This normalization step is not required for sequencing data because the values are normalized by sequencing depth (see Methods). Markers were validated using two susceptible (S1 and S2) and two resistant (R1 and R2) isolates at 15 min of ciprofloxacin exposure.

Validation of RNA markers across CDC isolates

Finally, we asked whether candidate markers respond consistently across a large pool of isolates with genetic variability. We chose the two candidate markers with the highest abundances and fold changes (*porB* and *rpmB*) to determine the susceptibility of 49 clinical isolates, with a wide range of MIC values (Supplementary Table S3 online), from the *N. gonorrhoeae* panel of the Centers for Disease Control (CDC) Antimicrobial

Resistance Isolate Bank. The MIC values were representative of the population-wide distribution values reported by the European Committee on Antimicrobial Susceptibility Testing[36]. We exposed each clinical isolate to ciprofloxacin for 10 min and measured the fold change in expression of the two candidate markers between the control and treated sample using dPCR (Fig. 5). Both markers correctly classified all 49 CDC isolates, based on Clinical and Laboratory Standards Institute (CLSI) breakpoint values, as 9 susceptible and 40 resistant strains.

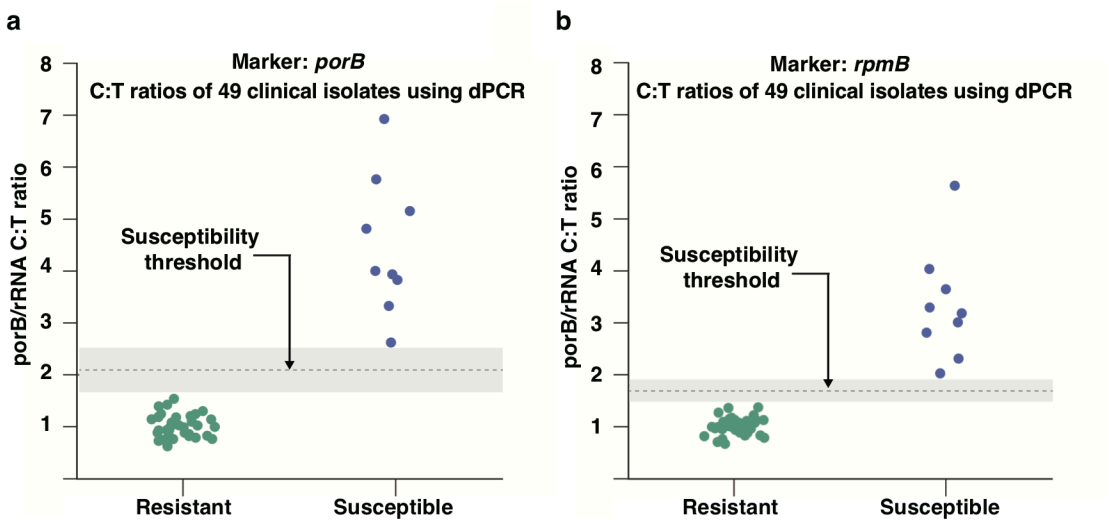

Figure 4-5. Antibiotic susceptibility testing of 49 clinical isolates using (**a**) *porB*, and (**b**) *rpmB* as RNA AST markers. Antibiotic susceptibility of 49 clinical isolates (9 susceptible and 40 resistant) from the *Neisseria gonorrhoeae* panel of the CDC Antimicrobial Resistance Isolate Bank was determined using the "normalized" C:T ratios (C:T ratio of marker/C:T ratio of 16S rRNA). Clinical isolates were exposed to ciprofloxacin for 10 min and the concentration of RNA markers was measured by digital PCR.

Discussion

In this work, we demonstrate that antibiotic-responsive transcripts can be used as suitable markers for a rapid phenotypic AST in *N. gonorrhoeae.*

When characterizing the global transcriptional response of *N. gonorrhoeae* to antibiotic exposure, we observed a significant change in response in as early as 5 min. The nature of the response was a global downregulation in transcript levels. Among the candidate markers, all exhibited downregulation in response to ciprofloxacin. We specifically looked at *gyrA* and *parC*, which are known genotypic markers of resistance to ciprofloxacin, and differential expression was not observed. We also looked at the *recA* transcript because *recA* is one of the prominent genes in the SOS response, and as expected, because *N. gonorrhoeae* does not have a true SOS system[28,29], we did not find *recA* levels to increase. Whereas *recA* is a specific cellular response to overcome DNA damage, the global downregulation that we observed suggests a general shift away from growth and cell proliferation. Among the 38 candidate markers, 15 were ribosomal proteins (including one of the top markers, *rpmB*), which play a prominent role in assembly and function of the ribosomes and are essential for cell growth. Mutations in ribosomal proteins have been reported to confer resistance to different classes of antibiotics[37]. Another top marker identified in this study was *porB*, which is a membrane channel forming protein (porin) responsible for uptake of small nutrients and the site of antibiotic influx into the cell. The expression of porins is highly regulated in response to environmental stimuli[38]. Reducing permeability to decrease intracellular antibiotic concentration is a known mechanism for bacteria to confer antibiotic resistance[37]. The downregulation of *porB* observed in this study can be attributed to a halt in growth processes caused by ciprofloxacin damage and possibly an attempt to reduce influx of antibiotic.

A key aim of this study was to identify RNA markers that would yield a measurable response after only a short antibiotic exposure (<15 min) to ensure this approach can fit within the required timescale for a rapid AST. It is possible that longer exposure times could provide additional insight into the biological response of *N. gonorrhoeae* to ciprofloxacin, but this was not the focus of our study. Furthermore, the short exposure times potentially introduce a bias in selection of transcripts present at low abundances.

For transcripts present at high abundance to display the same fold change as low abundance transcripts, a substantially higher number of mRNA molecules must be transcribed, which would require longer timescales. As an example, a 4-fold change from 1 to 4 transcripts requires 3 additional mRNA to be produced, whereas a 4-fold change from 20 to 80 requires 60 mRNA to be transcribed. This bias also holds true in downregulation, where mRNA continues to be transcribed in the control samples, whereas transcript levels drop in treated samples due to degradation of RNA, and/or a reduction in the rate of transcription.

We identified candidate markers with consistent differential expression across three sets of susceptible and resistant pairs. Among the candidate markers, one of our criteria for selection was transcript abundance, which is of particular importance in clinical samples with low cell numbers. Furthermore, marker abundance affects measurement sensitivity and limits of detection, as has been previously demonstrated in AST methods based on quantification of DNA replication[20]. To measure the abundance of the candidate markers, we used both dPCR measurements and ERCC spike-ins for RNA sequencing to obtain approximate RNA copies/cell. Both methods yielded results within the same order of magnitude. To our knowledge this is the first quantitative measurement of RNA abundance per cell in *N. gonorrhoeae*.

We separately validated the performance of the two most abundant candidate markers, *porB* and *rpmB*, with 49 clinical isolates. Both markers were consistent in their ability to correctly determine susceptibility or resistance of all 49 clinical isolates. *porB* demonstrated C:T ratios between 2.5 to 7 and *rpmB* demonstrated C:T ratios between 2 and 6 after 10 min of antibiotic exposure in the nine susceptible clinical isolates. The large fold changes highlight the significance of using RNA response as an AST marker compared with quantification of DNA replication. Our previous work using dPCR quantification of DNA replication demonstrated C:T ratios between 1.2 and 2.4 for 15 min of antibiotic exposure in *E. coli*[20], which has a doubling time approximately 3 times shorter than *N. gonorrhoeae*.

We performed an alignment search of *porB* against other prokaryotes and found it to be specific to the *Neisseria* genus. AST markers should be specific to the pathogen of interest because additional bacterial species are likely to be present in clinical samples. Additional experiments with mixtures of bacteria would be required to further confirm the specificity of the markers identified in this study. We additionally measured the 16s rRNA to normalize C:T ratios, which inherently enables pathogen identification as well. A combination of identification and susceptibility testing in a single integrated platform is important for correct and rapid diagnosis.

This paper demonstrates that RNA markers can be used to determine antibiotic susceptibility of *N. gonorrhoeae* after short antibiotic exposure times, a requirement for a rapid phenotypic AST. *N. gonorrhoeae* is a fastidious slow-growing organism, presenting challenges to growth-based AST methods. Additional work will be needed to yield a clinic-ready, rapid RNA-based AST for *N. gonorrhoeae.* Additional background matrices of clinical samples, both urine and swab samples, that could possibly affect speed and sensitivity of an AST, must be further evaluated. Digital isothermal chemistries, such as digital loop-mediated isothermal amplification (dLAMP) should be considered to speed up quantification times relevant to point-of-care settings[20]. Follow-up studies should also examine the transcriptional response of *N. gonorrhoeae* to other classes of antibiotics and identify responsive RNA markers for class-specific antibiotics. Overall, as a first step, the work described here demonstrates the promise for a phenotypic RNA-based approach for a rapid AST of *N. gonorrhoeae* at the point-of-care*,* which is critically needed for disease management, surveillance, and antibiotic stewardship.

Methods

Antibiotic exposure for RNA sequencing

Antibiotic susceptible and resistant clinical isolates were obtained from the University of California, Los Angeles, Clinical Microbiology Laboratory. Isolates were plated from glycerol stocks onto Chocolate Agar plates and grown in static incubation overnight (37 °C, 5% CO_2). Cells were re-suspended in Hardy Fastidious Broth (HFB) and incubated for 45 min (37 °C, 5% CO_2) with shaking (800 rpm) to an OD_{600} between 1 and 5. Cultures were diluted (5X) into HFB. Each isolate culture was split into "treated" and "control" tubes. Ciprofloxacin was added to the "treated" tubes (final concentration of 0.5 µg/mL) and water was added to the "control" tubes; cultures were incubated (static; 37 °C, 5% CO_2) for 15 min. During incubation, samples were collected for RNA sequencing at 5, 10, and 15 min (300 µL aliquot of sample was mixed into 600 µL of Qiagen RNA Protect Reagent (Qiagen, Hilden, Germany) for immediate RNA stabilization). In addition, a sample was collected for RNA sequencing immediately before ciprofloxacin was added. To quantify CFU, the sample at t = 15 min was serially diluted (10x), plated on a Chocolate Agar plate, and incubated overnight (37 °C, 5% CO_2).

Antibiotic exposure for clinical isolates

Antibiotic susceptible and resistant clinical isolates were obtained from the *N. gonorrhoeae* panel of the CDC Antimicrobial Resistance Isolate Bank. Isolates were plated from glycerol stocks onto Chocolate Agar plates and grown in static incubation overnight (37 °C, 5% CO_2). Cells were re-suspended in pre-warmed HFB + 5 mM sodium bicarbonate and incubated for 30 min (37 °C, 5% CO_2) with shaking (800 rpm) to an OD_{600} between 1 and 5. Cultures were diluted (100X) into HFB + 5 mM sodium bicarbonate. Each isolate culture was split into treated (0.5 µg/mL final concentration of ciprofloxacin) and control (water instead of antibiotic) samples. Samples were incubated at 37 °C for 10 min on a static hot plate. A 90 µL aliquot of each sample was placed into 180 µL of Qiagen RNA Protect Reagent for immediate RNA stabilization. A 5 µL aliquot of each sample was plated onto a Chocolate Agar plate and incubated overnight (37 °C, 5% CO_2) as a control for the exposure experiments. If the expected growth phenotypes

(i.e. resistant = growth; susceptible = no growth) were not observed for any single sample in the plating control, the exposure experiment was repeated for the set of samples. From the 50 total isolates available from the *N. gonorrhoeae* panel of the CDC Antimicrobial Resistance Isolate Bank, 49 were used in this study. One isolate was excluded from this study because we suspected that it had been contaminated; we did not detect *porB* primer amplification using qPCR.

RNA sequencing and analysis

RNA was extracted using the Enzymatic Lysis of Bacteria protocol of the Qiagen RNeasy Mini Kit and processed according to the manufacturer's protocol. DNA digestion was performed during extraction using the Qiagen RNase-Free DNase Set. The quality of extracted RNA was measured using an Agilent 2200 TapeStation (Agilent, Santa Clara, CA, USA). Extracted RNA samples were prepared for sequencing using the NEBNext Ultra RNA Library Prep Kit for Illumina (New England Biolabs, Ipswitch, MA, USA) and the NEBNExt Multiplex Oligos for Illumina. Libraries were sequenced at 50 single base pair reads and a sequencing depth of 10 million reads on an Illumina HiSeq 2500 System (Illumina, San Diego, CA, USA) at the Millard and Muriel Jacobs Genetics and Genomics Laboratory, California Institute of Technology. Raw reads from the sequenced libraries were subjected to quality control to filter out low-quality reads and trim the adaptor sequences using Trimmomatic (version 0.35). The reads were aligned to the FA 1090 strain of *N. gonorrhoeae* (NCBI Reference Sequence: NC_002946.2) using Bowtie2 (version 2.2.5) and quantified using the Subread package (version 1.5.0-p1). A pseudocount of 1 was added to the gene quantification; gene expression was defined in transcripts per million (TPM).

Marker selection

For each gene, we defined the C:T ratio as the gene expression (TPM) in the control sample divided by the gene expression (in TPM) in the treated sample. We plotted the -

$\log_2$(C:T) against the -$\log_2$(expression in TPM) for all genes. To identify genes that were differentially expressed between control and treated samples, we defined a threshold of significance. The threshold of significance was calculated from the C:T ratios at t = 0 min for the biological replicates that were sequenced (three susceptible and three resistant isolates). For each of the six gene expression datasets (one for each isolate), we fit a negative exponential curve to the outer edge of each plot and then averaged the curves from all six datasets. Finally, we added a 90% confidence interval to the average curve by assuming a Gaussian fit for the error distribution, which is our threshold of significance. Genes with a -$\log_2$(C:T) value above or below the upper and lower thresholds were identified as differentially expressed. Genes that were differentially expressed consistently (either always above or always below the thresholds) among the three susceptible isolates and were not differentially expressed among the three resistant isolates were defined as candidate markers.

Copies/cell measurements from sequencing

To measure copies per cell using sequencing data, we added 2uL of (1/1000 dilution) ERCC RNA Spike-In Mix (Thermo Fisher Scientific, Waltham, MA, USA) to the lysis buffer in the RNeasy Mini Kit to each individual sample. We calculated the number of copies of each ERCC transcript in the sample, by accounting for dilution and multiplying by Avogadro's number (manufacturer's concentrations were reported in attomoles/μL). We plotted the relationship between $\log_2$(ERCC copies added) against $\log_2$(gene expression in TPM) and performed a linear regression in the region of linearity. We used the linear regression to convert TPM values to total RNA copies in each sample. Finally, using the CFU measured for each sample from plating (described in the "Antibiotic exposure for RNA sequencing" section), the total RNA copies were converted to copies per cell.

Validation with droplet digital PCR (dPCR)

Primers were designed for candidate markers using Primer-BLAST[39] and primer alignments were verified using SnapGene. Expression of candidate markers was quantified using the Bio-Rad QX200 droplet dPCR system (Bio-Rad Laboratories, Hercules, CA, USA). The concentration of the components in the dPCR mix used in this study were as follows: 1× EvaGreen Droplet Generation Mix (Bio-Rad), 150U/mL WarmStart RTx Reverse Transcriptase, 800U/mL RiboGaurd RNase Inhibitor, 500 nM forward primer, and 500 nM reverse primer. The RNA extraction comprised 5% of the final volume in the dPCR mix. The remaining volume was nuclease-free water. For each isolate, candidate marker expression was quantified in the control and treated samples and the fold-change difference (C:T ratio) was calculated. To account for potential differences between the control and treated samples that could arise from experimental variability and extraction efficiency, we used ribosomal RNA (rRNA) as an internal control because from our sequencing data, we found that rRNA was not affected by antibiotic exposure in the time frame of this study. To normalize by rRNA, we quantified the 16S rRNA in the control and treated samples by dPCR and calculated an rRNA C:T ratio. We then divided the C:T ratio of each marker by the rRNA C:T ratio. All dPCR C:T ratios reported in this paper are the normalized C:T ratios.

References

1 Prevention, C. f. D. C. a. (2017).

2 Organization, W. H. Global action plan to control the spread and impact of antimicrobial resistance in Neisseria gonorrhoeae. (2012).

3 Prevention, C. f. D. C. a. (Centres for Disease Control and Prevention, US Department of Health and Human Services, 2013).

4 Unemo, M. *et al.* High-level cefixime-and ceftriaxone-resistant Neisseria gonorrhoeae in France: novel penA mosaic allele in a successful international clone causes treatment failure. *Antimicrobial agents and chemotherapy* **56**, 1273-1280 (2012).

5 Ohnishi, M. *et al.* ceftriaxone-resistant Neisseria gonorrhoeae, Japan. *Emerging infectious diseases* **17**, 148 (2011).

6 Lahra, M. M., Ryder, N. & Whiley, D. M. A new multidrug-resistant strain of Neisseria gonorrhoeae in Australia. *New England Journal of Medicine* **371**, 1850-1851 (2014).

7 Cámara, J. *et al.* Molecular characterization of two high-level ceftriaxone-resistant Neisseria gonorrhoeae isolates detected in Catalonia, Spain. *Journal of antimicrobial chemotherapy* **67**, 1858-1860 (2012).

8 Deguchi, T. *et al.* New clinical strain of Neisseria gonorrhoeae with decreased susceptibility to ceftriaxone, Japan. *Emerging infectious diseases* **22**, 142 (2016).

9 Hemarajata, P., Yang, S., Soge, O., Humphries, R. & Klausner, J. Performance and verification of a real-time PCR assay targeting the gyrA gene for prediction of ciprofloxacin resistance in Neisseria gonorrhoeae. *Journal of clinical microbiology* **54**, 805-808 (2016).

10 Pond, M. J. *et al.* Accurate detection of Neisseria gonorrhoeae ciprofloxacin susceptibility directly from genital and extragenital clinical samples: towards genotype-guided antimicrobial therapy. *Journal of Antimicrobial Chemotherapy* **71**, 897-902 (2016).

11 Aas, F. E., Løvold, C. & Koomey, M. An inhibitor of DNA binding and uptake events dictates the proficiency of genetic transformation in Neisseria gonorrhoeae: mechanism of action and links to type IV pilus expression. *Molecular microbiology* **46**, 1441-1450 (2002).

12 Hamilton, H. L. & Dillard, J. P. Natural transformation of Neisseria gonorrhoeae: from DNA donation to homologous recombination. *Molecular microbiology* **59**, 376-385 (2006).

13 Baltekin, Ö., Boucharin, A., Tano, E., Andersson, D. I. & Elf, J. Antibiotic susceptibility testing in less than 30 min using direct single-cell imaging. *Proceedings of the National Academy of Sciences*, 201708558 (2017).

14 Liu, T.-T. *et al.* A high speed detection platform based on surface-enhanced Raman scattering for monitoring antibiotic-induced chemical changes in bacteria cell wall. *PloS one* **4**, e5470 (2009).

15 Broeren, M., Maas, Y., Retera, E. & Arents, N. Antimicrobial susceptibility testing in 90 min by bacterial cell count monitoring. *Clinical Microbiology and Infection* **19**, 286-291 (2013).

16 Fredborg, M. *et al.* Real-time optical antimicrobial susceptibility testing. *Journal of clinical microbiology* **51**, 2047-2053 (2013).

17 Spence, J. M., Wright, L. & Clark, V. L. Laboratory maintenance of Neisseria gonorrhoeae. *Current protocols in microbiology*, 4A. 1.1-4A. 1.26 (2008).

18 Mezger, A. *et al.* A general method for rapid determination of antibiotic susceptibility and species in bacterial infections. *Journal of clinical microbiology* **53**, 425-432 (2015).

19 Rolain, J., Mallet, M., Fournier, P. & Raoult, D. Real-time PCR for universal antibiotic susceptibility testing. *Journal of Antimicrobial Chemotherapy* **54**, 538-541 (2004).

20 Schoepp, N. G. *et al.* Rapid pathogen-specific phenotypic antibiotic susceptibility testing using digital LAMP quantification in clinical samples. *Science translational medicine* **9**, eaal3693 (2017).

21 Tobiason, D. M. & Seifert, H. S. The obligate human pathogen, Neisseria gonorrhoeae, is polyploid. *PLoS biology* **4**, e185 (2006).

22 Cooper, S. & Helmstetter, C. E. Chromosome replication and the division cycle of Escherichia coli Br. *Journal of molecular biology* **31**, 519-540 (1968).

23 Sangurdekar, D. P., Srienc, F. & Khodursky, A. B. A classification based framework for quantitative description of large-scale microarray data. *Genome biology* **7**, R32 (2006).

24 Barczak, A. K. *et al.* RNA signatures allow rapid identification of pathogens and antibiotic susceptibilities. *Proceedings of the National Academy of Sciences* **109**, 6217-6222 (2012).

25 Bhattacharyya, R. *et al.* in *Open forum infectious diseases.* S33-S33 (Oxford University Press US).

26 McClure, R. *et al.* The gonococcal transcriptome during infection of the lower genital tract in women. *PloS one* **10**, e0133982 (2015).

27 Remmele, C. W. *et al.* Transcriptional landscape and essential genes of Neisseria gonorrhoeae. *Nucleic acids research* **42**, 10579-10595 (2014).

28 Stohl, E. A., Gruenig, M. C., Cox, M. M. & Seifert, H. S. Purification and characterization of the RecA protein from Neisseria gonorrhoeae. *PloS one* **6**, e17101 (2011).

29 Schook, P. O., Stohl, E. A., Criss, A. K. & Seifert, H. S. The DNA-binding activity of the Neisseria gonorrhoeae LexA orthologue NG1427 is modulated by oxidation. *Molecular microbiology* **79**, 846-860 (2011).

30 Qin, T.-T. *et al.* SOS response and its regulation on the fluoroquinolone resistance. *Annals of translational medicine* **3** (2015).

31 Black, C. G., Fyfe, J. A. & Davies, J. K. Absence of an SOS-like system in Neisseria gonorrhoeae. *Gene* **208**, 61-66 (1998).

32 Stohl, E. A. & Seifert, H. S. Neisseria gonorrhoeae DNA recombination and repair enzymes protect against oxidative damage caused by hydrogen peroxide. *Journal of bacteriology* **188**, 7645-7651 (2006).

33 LeBel, M. Ciprofloxacin: chemistry, mechanism of action, resistance, antimicrobial spectrum, pharmacokinetics, clinical trials, and adverse reactions. *Pharmacotherapy: The Journal of Human Pharmacology and Drug Therapy* **8**, 3-30 (1988).

34 Gao, Q. *et al.* Gene expression diversity among Mycobacterium tuberculosis clinical isolates. *Microbiology* **151**, 5-14 (2005).

35 Quillin, S. J. & Seifert, H. S. Neisseria gonorrhoeae host adaptation and pathogenesis. *Nature Reviews Microbiology* (2018).

36 Testing, T. E. C. o. A. S.

37 Gomez, J. E. *et al.* Ribosomal mutations promote the evolution of antibiotic resistance in a multidrug environment. *Elife* **6** (2017).

38 Fernández, L. & Hancock, R. E. Adaptive and mutational resistance: role of porins and efflux pumps in drug resistance. *Clinical microbiology reviews* **25**, 661-681 (2012).

39 Ye, J. *et al.* Primer-BLAST: a tool to design target-specific primers for polymerase chain reaction. *BMC bioinformatics* **13**, 134 (2012).

Acknowledgements

This work was supported in part by a Burroughs Wellcome Fund Innovation in Regulatory Science Award, a Natural Sciences and Engineering Research Council of Canada (NSERC) fellowship [PGSD3-438474-2013] (to T.K.), an NIH National Research Service Award (NRSA) [5T32GM07616NSF] (to N.G.S.), and a grant from the Joseph J. Jacobs Institute for Molecular Engineering for Medicine. Research reported in this publication was also supported by the Department of Health and Human Services (HHS) Office of the Assistant Secretary for Preparedness and Response (ASPR) and the Wellcome Trust under the CARB-X program (federal award number IDSEP160030-02); the content is solely the responsibility of the authors and does not necessarily represent the official views of the Department of HHS Office of the ASPR. This work is funded in part by CARB-X as a collaboration between Talis Biomedical and Caltech. This work was also supported by the Millard & Muriel Jacobs Genetics and Genomics Laboratory at the California Institute of Technology and we acknowledge lab director Igor Antoshechkin for his assistance. We thank Dr. Olusegun O. Soge at the UW Neisseria Reference Laboratory, and the Clinical Microbiology Laboratory at UCLA for providing *N. gonorrhoeae* isolates. We also thank Natasha Shelby for contributions to writing and editing this manuscript.

Author Contributions

Tahmineh Khazaei

- Co-designed the study with NGS.
- Developed the computational pipeline for processing and analyzing RNA sequencing data and for selection of RNA markers. Using this pipeline, identified porB and rpmB as the top markers for this study.
- Established the RNA extraction protocol for *Neisseria gonorrhoeae* samples (e.g. best kit/protocol to use).

- Performed RNA extraction of *Neisseria gonorrhoeae* samples from all the AST experiments in this study for RNA sequencing and performed the quality assessment of the extracted RNA. (This step was after the initial AST exposures performed by NGS or JTB.)
- Wrote the manuscript and generated all the final figures for publication.

Jacob T. Barlow

- Worked side-by-side with TK on day-to-day experimental optimization of RNA AST pipeline on CDC strains, including choice of using 16S rRNA as a control marker
- Generated glycerol stocks used for the 50 CDC strains using NGS's protocol
- Set up all cultures and ran all antibiotic exposures for the 50 CDC strains using NGS's protocols
- Ran all qPCR and dPCR experiments for assessing changes in RNA markers
- Designed and implemented statistical thresholding method for determination of differential genes
- Used thresholding method to choose 4 additional markers tested
- Designed and optimized primers for the additional markers
- Generated visualization strategy for plots in figures 2, 3, 4, and 5 before handing off to TK to prepare final versions for paper

Nathan G. Schoepp

- Designed "high throughput" sample handling and exposure workflow for isolates used by JTB and TK
- Obtained initial set of *Neisseria gonorrhoeae* isolates from UCLA
- Established *Neisseria gonorrhoeae* culturing and quantification methods which included 1) selecting and screening medias (including the one ultimately used in AST experiments) and 2) selecting and testing primers from literature for specificity, speed, and LOD
- Performed initial AST exposures using *Neisseria gonorrhoeae* isolates, which TK then extracted and sequenced

- Designed primers used in final manuscript for rpmB and porB markers
- Assisted JTB in primer design for other markers by demonstrating primer design workflow and tools
- Made minor contributions to manuscript including minor edits, and providing TK with graphics used in Fig. 1

Supplementary Information

Table 4-S1. List of candidate markers and their expression in transcripts per million (TPM) and copies per cell for susceptible isolate S2 and resistant isolate R2 after 15 min of ciprofloxacin exposure. The genome used for alignment was *N. gonorrhoeae* FA1090 (NCBI Reference Sequence: NC_002946.2).

		Susceptible (S2) Control		Susceptible (S2) Treated		Resistant (R2) Control		Resistant (R2) Treated	
Locus Tag	**Gene Description**	**TPM**	**copies/cell**	**TPM**	**copies/cell**	**TPM**	**copies/cell**	**TPM**	**copies/cell**
NGO0340	cysteine synthase A (*cysK*)	894.1	21.1	505.2	8.9	551.8	16.3	600.0	20.0
NGO1837	50S ribosomal protein L4 *(rplD*)	474.9	10.8	262.2	4.4	403.6	11.9	425.4	13.8
NGO1843	elongation factor G (fusA)	433.4	9.8	224.9	3.8	432.9	12.8	503.5	16.6
NGO2024	50S ribosomal protein L13 (*rplM*)	415.0	9.4	213.5	3.6	455.3	13.5	503.5	16.6
NGO1845	30S ribosomal protein S12 (*rpsL*)	563.1	13.0	286.8	4.9	615.4	18.2	697.6	23.5
NGO1677	50S ribosomal protein L27 (rpmA)	410.7	9.3	192.2	3.2	500.6	14.8	497.6	16.4
NGO1844	30S ribosomal protein S7	520.0	11.9	241.3	4.0	520.1	15.4	651.6	21.9
NGO0171	50S ribosomal protein L19 (*rplS*)	379.2	8.5	175.0	2.9	328.5	9.7	353.2	11.3
NGO1834	30S ribosomal protein S19 (*rpsS*)	330.0	7.4	152.1	2.5	260.9	7.7	292.7	9.2
NGO0172	tRNA (guanine-N(1)-)-methyltransferase (*trmD*)	237.3	5.2	108.8	1.7	208.8	6.2	224.6	6.9
NGO1835	50S ribosomal protein L2 (*rplB*)	392.5	8.9	179.1	2.9	297.6	8.8	359.8	11.5
NGO1673	type IV pilus assembly protein (*pilB*)	225.9	4.9	101.5	1.6	199.3	5.9	214.9	6.6
NGO1833	50S ribosomal protein L22 (*rplV*)	343.8	7.7	147.9	2.4	292.1	8.6	304.3	9.6
NGO2173	50S ribosomal protein L32 (*rpmF*)	407.5	9.2	173.6	2.9	394.7	11.7	404.1	13.1
NGO0604	30S ribosomal protein S1 (*rpsA*)	437.9	9.9	185.3	3.1	456.3	13.5	493.9	16.2
NGO0016	preprotein translocase subunit (*secG*)	180.1	3.9	73.7	1.1	169.1	5.0	184.5	5.6
NGO2174	hypothetical protein	372.8	8.4	150.2	2.4	368.3	10.9	361.6	11.6
NGO2164	GMP synthase (guaA)	118.3	2.5	45.0	0.7	98.6	2.9	109.4	3.2
NGO1676	50S ribosomal protein L21 (*rplU*)	554.6	12.8	200.4	3.3	555.2	16.4	587.7	19.6
NGO1679	50S ribosomal protein L33 (*rpmG*)	283.8	6.3	101.4	1.6	298.5	8.8	284.3	8.9
NGO1658	hypothetical protein	98.4	2.1	33.8	0.5	118.3	3.5	116.1	3.4
NGO1440	macrolide transport protein MacA	143.3	3.1	48.6	0.7	132.3	3.9	139.7	4.2
NGO0174	30S ribosomal protein S16 (*rpsP*)	315.2	7.0	101.2	1.6	295.8	8.7	340.5	10.9
NGO0173	ribosome maturation factor RimM (*rimM*)	359.8	8.1	113.5	1.8	316.8	9.4	318.8	10.1
NGO0592	trigger factor (*tig*)	146.5	3.1	45.5	0.7	147.5	4.3	152.1	4.6
NGO1680	50S ribosomal protein L28 (*rpmB*)	452.8	10.3	130.3	2.1	470.2	13.9	525.4	17.3
NGO0620	aspartate alpha-decarboxylase	64.8	1.3	18.6	0.3	54.2	1.6	59.3	1.7
NGO1659	intracellular septation protein A	62.2	1.3	17.8	0.3	63.6	1.9	70.7	2.0
NGO1291	transcriptional regulator (yebC)	64.1	1.3	18.0	0.3	79.9	2.3	77.9	2.2
NGO0648	membrane protein	56.4	1.1	15.3	0.2	47.6	1.4	45.2	1.2
NGO0593	ATP-dependent Clp protease proteolytic subunit (*clpP*)	60.2	1.2	16.0	0.2	73.6	2.2	75.9	2.2
NGO1804	(3R)-hydroxymyristoyl-ACP dehydratase (*fabZ*)	91.0	1.9	24.0	0.3	74.6	2.2	73.5	2.1
NGO0618	membrane protein	81.4	1.7	20.1	0.3	66.8	2.0	70.2	2.0
NGO0619	2-dehydro-3-deoxyphosphooctonate aldolase	61.1	1.2	15.1	0.2	51.1	1.5	62.6	1.8
NGO1812	major outer membrane protein (*porB*)	1293.2	31.2	293.4	5.0	1459.1	43.3	1587.1	57.1
NGO1890	glutamate permease; sodium/glutamate symport carrier protein	35.0	0.7	7.5	0.1	40.3	1.2	48.9	1.3
NGO2098	diaminopimelate decarboxylase	26.0	0.5	4.9	0.1	18.6	0.5	18.6	0.5
NGO2100	frataxin-like protein (*cyaY*)	20.4	0.4	3.6	0.0	14.0	0.4	18.1	0.5

Table 4-S2. Primer sequences used for validation of candidate markers by digital PCR.

Candidate Marker	Gene Name	Forward Primer Sequence	Reverse Primer Sequence
porB	major outer membrane porin	GCTACGATTCTCCCGAATTTGCC	CCGCCKACCAAACGGTGAAC
rpmB	50S ribosomal protein L28	TTGCCCAACTTGCAATCACG	AGCACGCAAATCAGCCAATAC
tig	trigger factor	AAAGCCTTGGGTATTGCGG	TGACCAAAGCAACCGGAAC
yebC	YebC/PmpR family Transcriptional Regulator	GCTTTGGAAAAAGCAGCCG	GGTTTTGTTGTCGGTCAGGC
pilB	Type IV-A pilus assembly ATPase	GACTTTTGCCGCTGCTTTG	GCGCATTATTCGTGTGCAG
cysK	Cysteine synthase A	GAGGCTTCCCCCGTATTGAG	TTCAAAAGCCGCTTCGTTCG
16S rRNA	16S ribosomal RNA	ACTGCGTTCTGAACTGGGTG	GGCGGTCAATTTCACGCG

Table S3. Minimum inhibitory concentration **(**MIC) values for the 49 *Neisseria gonorrhoeae* clinical isolates acquired from the CDC and FDA Antibiotic Resistance Isolate Bank[1].

[1]CDC and FDA Antibiotic Resistance Isolate Bank. Atlanta (GA): CDC. (2018)

MIC	Number of strains	Susceptible or Resistant
0.015	8	Susceptible
0.03	1	Susceptible
4	1	Resistant
8	6	Resistant
16	33	Resistant

Chapter V

Differential DNA Accessibility to Polymerase Enables 30-minute Phenotypic β-lactam Antibiotic Susceptibility Testing of Carbapenem-resistant Enterobacteriaceae[4]

Abstract

The rise in carbapenem-resistant Enterobacteriaceae (CRE) infections has created a global health emergency, underlining the critical need to develop faster diagnostics to treat swiftly and correctly. Although rapid pathogen-identification tests are being developed, gold-standard antibiotic susceptibility testing (AST) remains unacceptably slow (1–2 days). Here, we develop the pol-aAST (polymerase-accessibility AST), a new phenotypic approach for β-lactams, the major antibiotic class for Gram-negative infections. The pol-aAST quantifies differences in accessibility of nucleic acids to polymerase during amplification after brief antibiotic exposure, yielding the fastest nucleic-acid-based phenotypic AST ever demonstrated for β-lactams. We test the three pathogens causing CRE infections using ceftriaxone, ertapenem, and meropenem, and show 100% agreement with gold-standard AST. Importantly, pol-aAST correctly categorized resistant isolates undetectable by current genotypic methods (negative for β-lactamase genes or lacking predictive genotypes). To illustrate clinical potential, we show that the pol-aAST can be performed in 30 min sample-to-answer using contrived urine samples.

Introduction

[4]This chapter was submitted for publication with authorship belonging to Nathan G. Schoepp, Eric J. Liaw, Emily S. Savela, and Rustem F. Ismagilov.

The evolution and global spread of carbapenem-resistant Enterobacteriaceae (CRE) threatens to disrupt modern healthcare systems, which rely heavily on β-lactams (especially carbapenems, the last-resort treatments) to control bacterial infections.[3-5] Mortality rates for CRE infections are as high as 30–49%[6-8], and thus the global emergence and spread of CRE infections represents a public health emergency.[9-11] The CDC places CRE in its highest ("urgent") category of antimicrobial-resistant pathogen threats[10, 13] and the World Health Organization (WHO) labels CRE as a critical-priority pathogen[9]. *Escherichia coli*, *Klebsiella pneumoniae*, and *Enterobacter* spp. compose the majority of CRE infections, and are the most commonly monitored Enterobacteriaceae[10, 14-16].

To halt the further spread of CRE, patients need to be treated swiftly and correctly at the point of care (POC); however there is no fast and general method for determining antibiotic susceptibility[17-19]. The current clinical workflow for treatment of bacterial infections consists of an identification (ID) step followed by an antibiotic susceptibility test (AST). Although progress is being made to develop faster ID tests[20-22] and a rapid 20-min ID test is on the horizon[23-25], the gold-standard for AST remains a culture-based workflow using broth or agar dilution that requires 1–2 days and is thus far too slow[26-27]. Because AST results are so delayed, health care providers usually treat empirically, leading to inappropriate prescriptions and even life-threatening outcomes,[28] and the further spread of resistance. To improve treatment and promote antibiotic stewardship, healthcare providers need a rapid phenotypic AST[29-31].

ASTs are either genotypic or phenotypic. Genotypic tests predict resistance by measuring the presence of genes known to be involved in resistance. Genotypic tests can be fast[32], but often have limited clinical utility because they target defined mechanisms of resistance. For example, rapid genotypic methods to detect Gram-negative β-lactamase genes have been developed[33-36], but these tests only detect one of the many known β-lactamase classes, and still require 30–40 min (estimated from described methods). Similarly, the commercial Cepheid Xpert® Carba-R assay, which detects five β-

lactamase gene families, and was shown to detect 50% of resistant isolates and took 88 min[37]. Moreover, although Carba-R is FDA-approved, its utility in treatment scenarios is limited (i.e., negative results are not actionable) so when prescribing antibiotics, it must be used in conjunction with a phenotypic AST[38-39]. Rapid methods for measuring the activity of specific β-lactamases also exist[40-44]. However, these tests only detect one mechanism of resistance, and sample-to-answer times have not been reported.

Phenotypic ASTs are ideal because they measure susceptibility directly by exposing the sample to antibiotics (ABX) and measuring the target organism's response. The gold-standard AST (broth microdilution[26-27]) is a phenotypic test. Most phenotypic tests require the growth of viable organisms isolated from patient samples, a process that requires days and is thus too slow for the POC. Innovative, faster phenotypic tests for β-lactams were developed based on *in situ* nucleic-acid staining or fluorescence measurements[45-47], flow cytometry[48], microscopy[49-50], and mass spectrometry[51]. However, majority of the currently proposed methods still require 60–180 min ABX-exposure steps in addition to the time needed to perform the assay, and no method has emerged that requires short (~15 min) ABX exposure, short (~15 min) assay time, and does not require excessively complex or delicate instrumentation so the method can be deployed at the POC.

Rapid phenotypic methods based on quantification of nucleic acids (NAs) have shown great promise for a rapid POC AST due to the speed, specificity, and robustness of NA detection[52-56]. There is an additional advantage to using NA quantification as a readout of the bacterial response to antibiotic: because rapid pathogen identification (ID) from clinical samples is commonly performed via NA analysis, therefore it would likely be easier to integrate NA-based phenotypic AST into a combined ID/AST workflow performed from the same clinical sample. For ABX that directly or indirectly impact NA replication on short time scales, we have demonstrated that the quantification of DNA[57-58] or RNA[59] can be used to rapidly (30 min) and reliably determine susceptibility to nitrofurantoin and/or ciprofloxacin. Subsequent efforts have targeted the β-lactam class

(the most widely prescribed class of ABX[3-4]) using these methods[60]. However, because β-lactams do not directly impact NA replication on short time scales, this direct translation of the existing NA-based technique required a two-hour antibiotic exposure, which is not sufficiently rapid for POC. For a POC AST to impact management of CRE infections, it must (i) determine susceptibility to β-lactams, including carbapenems; (ii) it must be rapid (< 30 min sample-to- answer)[61-62]; and (iii) it must be phenotypic (agnostic to resistance mechanism)[29, 63]. As discussed below, rapid pathogen ID technologies are becoming available and therefore pathogen ID is not the focus of this work.

Here, we hypothesized that a new NA-based approach could be used to develop a rapid phenotypic AST for multiple β-lactams. Knowing that susceptible bacteria have compromised cell walls as a result of exposure to β-lactams; we predicted that more NAs would be released from susceptible cells than from resistant bacteria, thus yielding faster amplification. Rather than measuring how total NA concentration is impacted by ABX exposure (as in previous NA-based ASTs), we hypothesized that we could measure the accessibility of NAs to polymerase following a short ABX exposure. To validate the method, termed pol-aAST (polymerase-accessibility AST), we perform 70 ASTs using clinical isolates of three major CRE pathogens exposed to each of three commonly prescribed β-lactams for Gram-negative infections: ceftriaxone (CRO), ertapenem (ETP), and meropenem (MEM). To further demonstrate clinical relevance (i.e., POC timescales), we perform timed sample-to-answer experiments using contrived urine samples to ensure the whole assay can be performed in < 30 min.

Results

The pol-aAST relies on differential accessibility of nucleic acids to polymerases as a result of ABX exposure. In this manuscript, we define differential accessibility to polymerase as a difference in the measured rate of amplification between control and ABX-treated samples. In the first step of pol-aAST, a single sample is split into control

and treated aliquots of equal volume, and the treated aliquot is exposed to a β-lactam. ABX-exposure is a critical step in any phenotypic AST because phenotypic tests measure the response of bacteria to ABX. If the bacteria in the sample are resistant, we hypothesized that no differences in NA amplification will be observed between control and treated aliquots. If the bacteria are susceptible, we hypothesized that ABX treatment would lead to a compromised peptidoglycan cell wall (Fig. 1a) and partial release of NAs (Fig. 1b). We hypothesized that both the compromised cell wall and partial release of NAs would increase the accessibility of NAs to polymerase in a treated ABX-susceptible aliquot. In the second step of pol-aAST, control and treated aliquots are exposed to polymerase in amplification conditions (Fig. 1c) and the rate of amplification is measured.

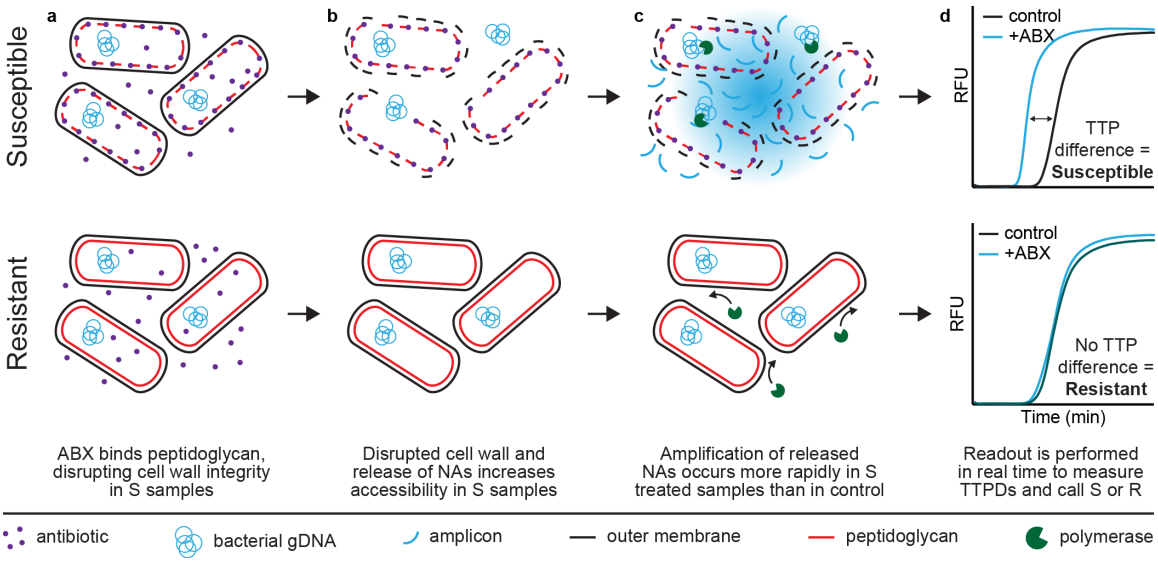

Fig. 5-1. Overview of pol-aAST shown for susceptible (S) and resistant (R) samples exposed to β-lactams. (a) Treated aliquots are exposed to a β-lactam. In susceptible samples, β-lactams compromise cell wall integrity. (b) Nucleic acids (NAs) are released from compromised cells, increasing NA accessibility to polymerase. (c) Released NAs in the susceptible treated aliquot amplify faster than NAs from intact cells in the control aliquot (not shown), resulting in a difference in time-to-positive. No difference in amplification between control and treated aliquots is observed in resistant samples. (d)

Time-to-positive difference (TTPD) between control and treated aliquots is used to assess susceptibility.

To successfully differentiate susceptible and resistant samples, ideal amplification conditions must i) not fully lyse cells, ii) enhance alterations (damage) to the cell wall caused by exposure to β-lactams, and iii) increase NA release only from ABX-damaged cells. The rate of amplification is dependent on the concentration of polymerase-accessible NA. In susceptible samples, more NAs are released in treated aliquot, leading to faster amplification in susceptible treated aliquots (Fig. 1d) relative to control. Resistant samples are not affected by the ABX, so control and treated aliquots have similar NA release and amplification rate. Amplification rate in an isothermal amplification reaction is quantified by measuring the time-to-positive (TTP), the time it takes the reaction fluorescence to reach a predetermined threshold. We found that using pol-aAST, isolates susceptible to the β-lactam being tested show increased accessibility of NAs to polymerase, manifesting in an earlier TTP relative to the control. The TTPs of any two samples, such as the control and treated aliquots, can be compared to generate a TTP difference value (TTPD), which can then be used to determine susceptibility by comparing to a susceptibility threshold. Here we use the DNA polymerase *Bst* 3.0 under loop-mediated isothermal amplification (LAMP) conditions.

We hypothesized that the chemical environment in which amplification occurs would significantly impact the result of pol-aAST, and that for pol-aAST to differentiate susceptible and resistant samples, amplification conditions should not be fully lysing. To test this, we performed pol-aAST using LAMP, and quantitative PCR (qPCR) (Fig. 2). LAMP is performed at a single temperature (70 °C), which we hypothesized would not be fully lysing, whereas qPCR is a thermocycled amplification technique reaching a maximum temperature of 95 °C, which we hypothesized would be fully lysing. Indeed, we observed that pol-aAST was successful in differentiating susceptible and resistant isolates when performed using LAMP, but not when performed using qPCR (Fig. 2). We tested qPCR with a total of two susceptible and two resistant isolates, none of which

showed a statistically significant difference in Cq between control and treated samples. When using LAMP, detectable differences were observed between control and treated aliquots when using isolates susceptible to the target β-lactam (TTPD = 1.02 min). These differences confirm that choice of amplification chemistry is critical to the success of pol-aAST.

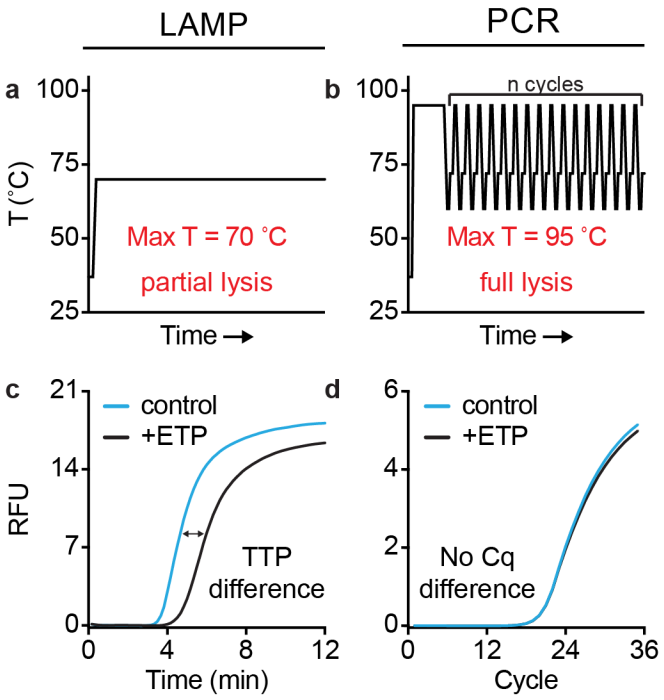

Fig. 5-2. Polymerase-accessibility AST requires non-lytic amplification conditions. (a–b) Thermal profiles of LAMP and PCR. (c–d) LAMP and PCR amplification curves for a susceptible isolate exposed to ertapenem (ETP). A difference in time-to-positive (TTP) for control and treated aliquots is observed for susceptible isolates when quantifying nucleic acids using LAMP, but not PCR.

To investigate the mechanism of pol-aAST, we performed experiments to separate free NAs from NAs contained within structurally intact cells or associated with cell debris. Susceptible and resistant clinical isolates were exposed to β-lactams for 15 min, then filtered through 0.2 μM filters to remove cells from free NAs. NAs in the sample and eluate were then quantified using droplet digital PCR (ddPCR). We observed that

following exposure to β-lactams, susceptible isolates treated with β-lactams released a significantly larger percentage of DNA than resistant samples (Fig. 3). The amount of DNA released depended on the ABX being tested. Exposure to meropenem resulted in an average of 21% of DNA being released from susceptible isolates, with a slightly smaller average percent (15%) released as a result of exposure to ertapenem. Interestingly, susceptible samples only released an average of 6% of DNA when exposed to CRO, demonstrating that NA release is dependent on choice of ABX and not, e.g., a universal stress response. These results also demonstrate that the magnitude of the effect of a β-lactam on cell wall integrity can be measured and is different depending on the ABX used, even on short exposure time scales.

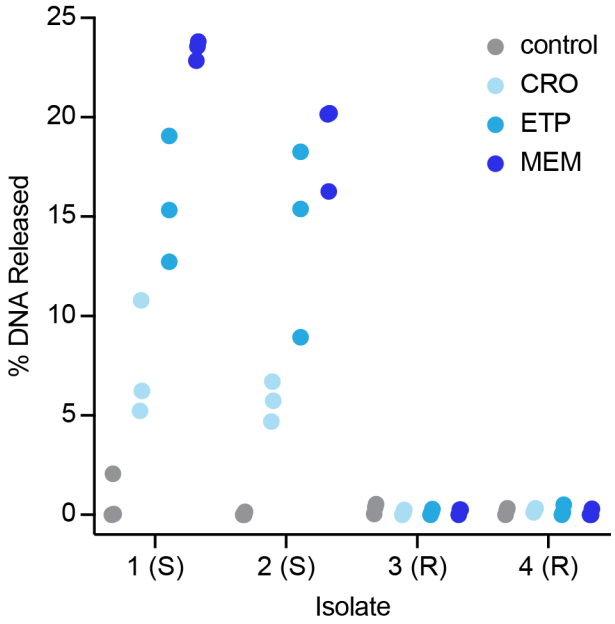

Fig. 5-3. Percentage of DNA released following antibiotic exposure. Two susceptible (S) and two resistant (R) *E. coli* isolates were exposed to no antibiotic (control), ceftriaxone (CRO), ertapenem (ETP), or meropenem (MEM) for 15 min before filtering to separate intact cells from extracellular DNA. Experiments were performed in triplicate for all isolate/antibiotic combinations.

To validate the pol-aAST method, we performed 70 ASTs using 12 clinical isolates of *Escherichia coli* (*Ec*), 8 clinical isolates of *Klebsiella pneumoniae* (*Kp*), and 5 clinical isolates of two species of *Enterobacter* (*Ebs*) and the β-lactams CRO, ETP, and MEM. The set included isolates from each genus that were susceptible and isolates that were resistant to each of the three antibiotics. In addition to isolates obtained from the UCLA Clinical Microbiology Laboratory (see Methods in SI), those tested included *Ec* and *Kp* isolates from the Centers for Disease Control (CDC) Enterobacteriaceae Carbapenem Breakpoint panel[12], as well as all available *Enterobacter* spp. isolates from the same panel. All samples were amplified using quantitative LAMP and categorical agreement was compared to gold-standard broth microdilution AST. Two approaches for determining susceptibility were investigated in all pol-aASTs performed.

The first approach we investigated was to compare the difference in TTP values of the control and treated aliquots in each pol-aAST. This difference was defined as $TTPD_{CT}$ (Fig. 4a). Using this method, we obtained 100% categorical agreement with gold-standard AST for all antibiotics tested with *Ec* (Fig. 4b), *Kp* (Fig. 4c), and *Ebs* (Fig. 4d) isolates. The values of $TTPD_{CT}$ were well-separated between susceptible and resistant isolates in all CRE-ABX combinations. Note that the threshold values separating $TTPD_{CT}$ of susceptible and resistant isolates depend on the antibiotic used (e.g. CRO gives a smaller response and therefore requires a lower threshold), as well as the pathogen tested (e.g. *K. pneumoniae* gives stronger response and requires a higher threshold). The area under the curve (AUC) of the receiver operating characteristic (ROC) curve was 1.00 for all isolates and antibiotics tested. There were no errors relative to gold-standard AST when determining susceptibility by $TTPD_{CT}$.

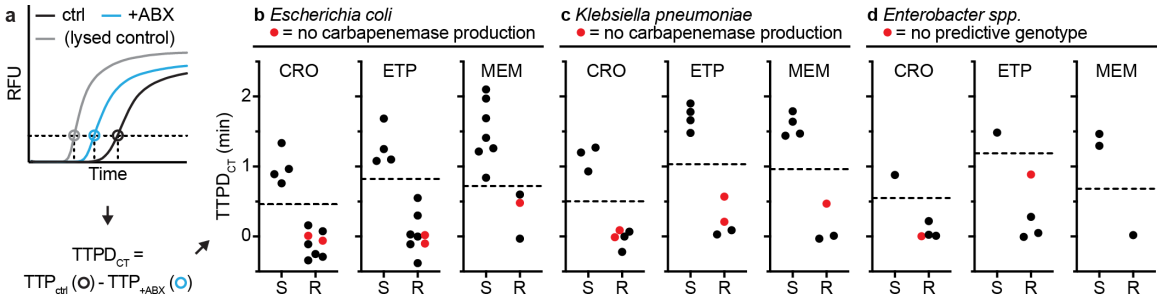

Fig. 5-4. Validation of the pol-aAST method using control (ctrl) and antibiotic-treated (+ABX) aliquots. (a) Example calculation of time-to-positive difference (TTPD) between control and treated aliquots ($TTPD_{CT}$). The TTP (in minutes) of the control and treated aliquots are used to calculate $TTPD_{CT}$. (b–d) The pol-aAST results using *Escherichia coli* (b), *Klebsiella pneumoniae* (c), and *Enterobacter* spp. (d) isolates exposed to ceftriaxone (CRO), ertapenem (ETP), and meropenem (MEM). Red points represent isolates with either no detectable carbapenemase genes (*Ec* and *Kp* isolates) according to a published genotypic assay[1] and commercial assay,[2] or no predictive genotype (*Ebs* isolates) according to the whole genome sequencing by the CDC.[12] S/R thresholds (dashed lines) were set halfway between the lowest susceptible (S) and the highest resistant (R) TTPDCT values.

The second approach we investigated was to compare the difference in the TTP of a fully lysed control aliquot and the antibiotic-treated aliquot in each pol-aAST. The fully lysed control aliquot was created by extracting NA from an aliquot of the ABX-treated sample using a single-step, LAMP-compatible extraction buffer. This difference was defined as $TTPD_{LT}$ (Fig. 5a). It is important to note that $TTPD_{LT}$ only requires the antibiotic-treated sample from the exposure step, meaning the original sample does not have to be split prior to exposure. Again, the thresholds were defined individually for each antibiotic and pathogen. Using this method, we obtained 100% categorical agreement with gold-standard AST for all antibiotics tested with *Ec* (Fig. 5b) and *Kp* (Fig. 5c) isolates. When testing *Ebs* (Fig. 5d) isolates, we observed a single error in which an isolate classified as CRO-resistant was called as susceptible, resulting in an overall categorical agreement of 92%. Because of this error, the AUC for *Ebs* isolates tested with CRO was 0.75. Aside

from this error, susceptible and resistant isolates were well separated in all cases, with AUC = 1.000 for all antibiotics tested with *Ec* and *Kp*. Although we observed a single error, using the $TTPD_{LT}$ metric still gave excellent agreement with gold-standard AST and required no splitting of the sample prior to exposure.

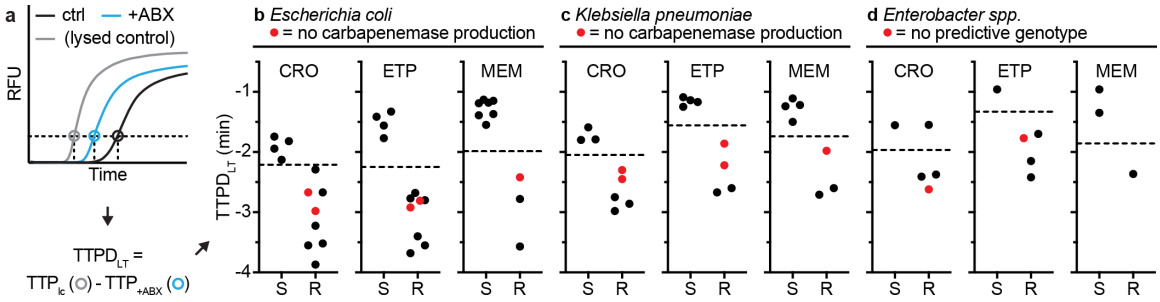

Fig. 5-5. Validation of the pol-aAST method using lysed control (lc) and antibiotic-treated (+ABX) aliquots. (a) Example calculation of time-to-positive difference (TTPD) between the lysed-control and antibiotic-treated aliquots ($TTPD_{LT}$). The TTP (in minutes) in the lysed-control and antibiotic-treated aliquots are used to calculate $TTPD_{LT}$ (b) pol-aAST results using *Escherichia coli* isolates exposed to CRO, ETP, and MEM. (c) pol-aAST results using *Klebsiella pneumonia* isolates exposed to CRO, ETP, and MEM. (d) pol-aAST results using *Enterobacter* spp. isolates exposed to CRO, ETP, and MEM. For *Ec* and *Kp* isolates, 100% categorical agreement was obtained compared to gold-standard broth microdilution AST. For *Ebs* isolates, 92% categorical agreement was obtained. Red points represent isolates with either no detectable carbapenemase genes (*Ec* and *Kp* isolates) according to a published genotypic assay[1] and commercial assay,[2] or no predictive genotype (*Ebs* isolates) according to the CDC[12]. S/R thresholds (dashed lines) were set halfway between the lowest susceptible (S) and the highest resistant (R) $TTPD_{LT}$ values.

To demonstrate one of the major differences between pol-aAST, a phenotypic method, and existing genotypic methods, we challenged the assay with five previously characterized isolates that had either i) no detectable β-lactamase genes or ii) lacked any genotypic signature predictive of β-lactam resistance. We tested two *Ec* and two *Kp*

isolates with no detectable β-lactamase genes as measured by both a published genotypic assay designed to screen for six β-lactamase gene families[1], as well as the Cepheid Xpert® Carba-R test (a commercial, FDA-approved genotypic assay designed to screen for five β-lactamase gene families).[2] These four isolates did not test positive in either assay because they lack the genes these assays screen for, despite being resistant (as determined by gold-standard broth microdilution). These four tested isolates were resistant to CRO and ETP, and one isolate from each genus was also resistant to MEM. Additionally, we tested a single resistant *Ebs* isolate from the CDC Enterobacteriaceae Carbapenem Breakpoint Panel (AR-Bank #0007). Whole genome sequencing of this isolate (performed by the CDC) revealed no known resistance markers[12], meaning the mechanism of resistance was uncharacterized. The pol-aAST performed excellently in all cases, and all 5 isolates were correctly categorized as resistant (Figs. 4, 5, red points).

To investigate the sample-to-answer time of the pol-aAST, we performed timed experiments using contrived urine samples (Fig. 6). Sample-to-answer time is a critical metric for any assay designed to be used at the point of care (POC), but is often not reported at all, even for methods claiming to be rapid. In timed experiments, we i) reduced the exposure time from 15 to 14 min to ensure all handling could be performed during the 15 min aliquoted for exposure, and ii) used an automated data-analysis spreadsheet to provide a susceptibility call as soon as the LAMP reactions reached a pre-determined threshold (indicating successful amplification). At the start of pol-aAST, a timer was started which ran for the duration of the experiment and was stopped once a susceptibility call had been made. The susceptibility of four isolates to ETP was tested simultaneously (Fig. 6a). The pol-aAST consists of only three simple handling steps (Fig. 6b-d), which allowed us to perform pol-aAST in a total time of just 29.5 min, with results in agreement with gold-standard AST (Fig. 6e).

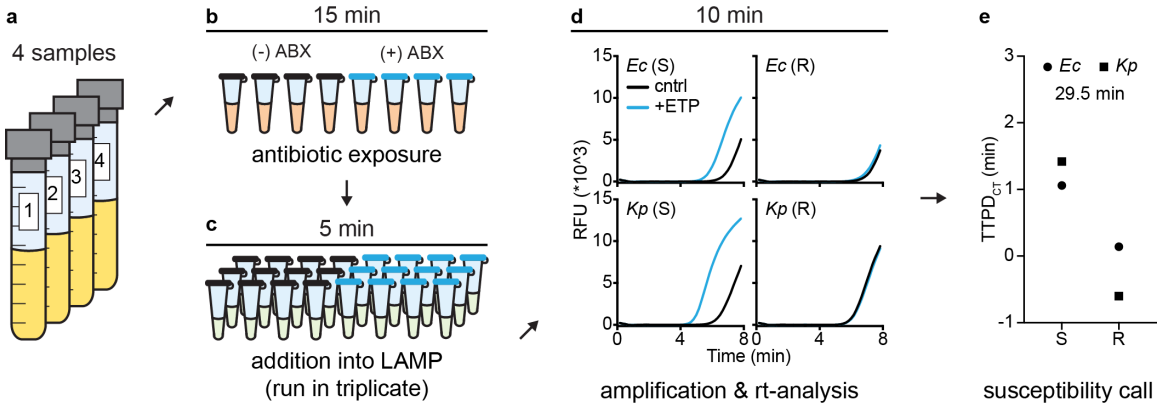

Fig. 5-6. Timed sample-to-answer pol-aAST using contrived urine samples spiked with either *E. coli* (*Ec*) or *Klebsiella pneumoniae* (*Kp*). (a) Due to the minimal sample handling throughout pol-aAST, all four contrived urine samples were run in parallel. (b) Urine samples were split into control and antibiotic-treated aliquots and incubated at 37 °C for 15 min. A timer was started immediately after sample splitting. (c) All samples were added to pre-made LAMP mix and run in triplicate. (d) Samples were amplified using LAMP and the fluorescence of reactions was monitored in real-time. Once total fluorescence passed a pre-determined threshold (indicating successful amplification), reactions were stopped and TTP values ported into an automated data-analysis spreadsheet. The timer was stopped as soon as the spreadsheet gave susceptibility calls. (e) Comparison of susceptibility calls with gold-standard AST categorization. Total assay time was 29.5 min.

Discussion

The pol-aAST method enables rapid, organism-specific measurement of susceptibility to β-lactams—the most important class of ABX for Gram-negative infections—thus providing the critically missing piece needed to develop a POC AST for this global health threat. The genera of isolates and the β-lactams used in this proof-of-concept study were intentionally chosen to broadly validate the pol-aAST: *E. coli* (*Ec*), *K. pneumoniae* (*Kp*), and the *Enterobacter* species *E. aerogenes* and *E. cloacae* (collectively *Ebs*), are responsible for the majority of CRE infections globally[10, 14-16] (in some areas of the U.S.

Kp is responsible for up to 90% of CRE infections[7]). It is for this reason that *Ec*, *Kp*, and *Ebs* together make up the majority of isolates in the CDC's Enterobacteriaceae Carbapenem Breakpoint panel, a collection of isolates designed specifically to challenge carbapenem-susceptibility tests in Enterobacteriaceae[12]. CRO, used broadly for a variety of infections because of its broad coverage and tolerability, was chosen as a representative third-generation cephalosporin. Similarly, ETP and MEM were chosen as clinically representative carbapenems[64].

The pol-aAST has two important requirements: i) amplification conditions that are not fully lytic and ii) release of NAs only from cells that are susceptible to the β-lactam to which they are exposed. If cells fully lyse, as they do in PCR, there is no difference in amplification between control and treated aliquots in susceptible isolates (Fig. 2). It is only under partial-lysis conditions, as in LAMP, that cell integrity is preserved long enough to yield a substantial TTP difference. In partial-lysis conditions, most NAs are still protected inside cells in the control aliquot, whereas a significant portion of NAs are released and start amplifying immediately in the treated aliquot. We know from previous work[58] that the speed of an optimized bulk LAMP reaction makes it is difficult to linearly correlate TTP and NA concentration, unless very sensitive real-time measurements are made. Based on the magnitude of the differences in TTP observed here and the results measuring NA release (Fig. 3), we suspect that both the state of NA (inside intact cells vs. inside or outside damaged cells) and the differences in concentration of free NA contribute to the TTP differences observed. Cell-wall defects and damage are also likely to increase the penetration of amplification reagents into DNA trapped inside the remains of susceptible treated cells especially under the elevated temperature of the amplification reaction. We chose LAMP because we have shown previously that it is a rapid and specific isothermal amplification chemistry[58]. However, other non-lytic isothermal amplification chemistries could also be investigated. Additionally, DNA release (Fig. 3) could be measured to determine susceptibility using PCR if combined with a filtration step; we have not evaluated the pros and cons of this approach in this paper.

To demonstrate the flexibility of the pol-aAST method and the simplicity of the workflow, we investigated two approaches for determining susceptibility. The first, measuring $TTPD_{CT}$, gave 100% categorical agreement and uses a standard ABX-exposure step wherein one aliquot serves as the control and the other aliquot is exposed to an ABX. The second, measuring $TTPD_{LT}$, differs in that only a single aliquot of the original sample is used during the ABX-exposure step. After exposure, this aliquot is compared with a fully lysed control aliquot, which could be extracted at any point during the assay. Using only a single aliquot of the original sample during exposure reduces the challenges of fluid handling and metering, which will be valuable when developing fully-integrated devices. When using a control and treated aliquot, both aliquots must have precisely equal volumes, and the heating required during exposure must be performed on both aliquots. Using a single aliquot means only one solution would need to incubated which i) reduces the complexity of temperature control and ii) reduces fluid handling complexity. Both methods showed excellent categorical agreement with gold-standard broth microdilution, and the choice of approach will be dictated by future device architecture.

To illustrate the generality of the method, we evaluated pol-aAST using isolates that tested negative for β-lactamase genes and isolates that lack a predictive genotype (e.g., no β-lactamase production, no modified porins, no modified penicillin-binding proteins), based on published and commercial genotypic assays,[1] and CDC classification based on the ResFinder database[65] respectively. The ABX-susceptibility of isolates lacking beta-lactamases cannot be detected by current, FDA-approved genotypic methods, yet bacteria that do not produce beta-lactamases can comprise 11–71% of CRE infections.[6, 66-67] Using pol-aAST, (which, like all phenotypic ASTs is agnostic to the mechanism of resistance), all five of these isolates were correctly categorized as resistant.

Sample-to-answer time directly reflects the speed of diagnostics in practice, and is a major factor in how likely a diagnostic is to be adopted. In general, the shorter the sample-to-answer time, the more valuable the test is, and the more feasible for use at the

POC. With urine as the contrived sample matrix, pol-aAST was able to be completed in < 30 min. This time scale is on par both with suggested time-frames for rapid POC diagnostics[61-62], and measured times of patient visits[68]. Additionally, because urine involves relatively simple sample-handling steps, we were able to perform four ASTs in parallel. The ability to run several samples in parallel demonstrates the potential to multiplex with isolates and antibiotics, which will be important for the next steps, including the design of integrated devices.

The pol-aAST method is the first demonstration of a rapid NA-based phenotypic AST for β-lactams and CREs. As with any academic report of an innovative diagnostic technology development, this work has limitations in the breadth of its scope and level of technological maturity. The following work would further extend the clinical applicability of this study, and will be necessary for translation into a system suitable for regulatory approval and clinical use. First, this proof-of-concept used contrived urine samples (clinical isolates of pathogens spiked into healthy urine) because they are easier to obtain and reduce the cost and complexity of running experiments at the early, proof-of-concept stage. Although contrived samples are accepted by the FDA as a part of regulatory clinical studies and submissions[69], the pol-aAST needs to be further evaluated with fresh clinical urine samples from patients. Urine is a relevant matrix for a CRE diagnostic because of the large number of hospital-acquired infections that involve catheters or other long-term indwelling medical devices[14], where CRE infections cause major problems. Second, to expand the scope of this approach, other sample types such as blood and blood cultures should be tested (in combination with appropriate pathogen-isolation and pathogen-enrichment technologies). Third, only categorical (S/R) agreement with the gold-standard method was tested here. While in the majority of cases a rapid categorical AST is clinically actionable, testing samples with a range of minimum inhibitory concentrations (MIC), including those with intermediate resistance, would further broaden the scope of the method. Fourth, we have not tested pol-aAST against heteroresistant samples. However, these are more common in Gram-positive organisms[70] and are not common in Gram-negative organisms. Fifth, the pol-aAST chemistry should

be integrated with microfluidic devices so the AST can be performed directly on clinical samples with minimal user intervention. Sixth, the performance of these integrated devices will need to be evaluated in pre-clinical and clinical studies.

We emphasize that the specific pol-aAST described in this paper, just like other innovative rapid ASTs,[58, 71-74] is not intended to be the sole test to guide treatment. Even though pol-aAST is based on detection of pathogen-specific nucleic acids and can therefore provide pathogen ID, we anticipate that in a clinical workflow pol-aAST would be performed after a separate rapid pathogen ID step.[20-21, 23] Furthermore, pol-aAST would likely be combined with rapid AST for other antibiotics, such as fluoroquinolones that can be used to treat CRE infections. AST methods that rely on similar underlying chemistries are more likely to be successfully integrated together. Isothermal amplification of pathogen-specific nucleic acids appears to be a promising approach for AST and we have already shown how rapid fluoroquinolone AST can be performed in 30 min using digital LAMP.[58] Upon integration with these complementary methods and translation to a distributable diagnostic, the pol-aAST will enable: i) improved antibiotic stewardship by reducing empiric use of carbapenems for Enterobacteriaceae, ii) improved patient outcomes by detecting CRE infections for which carbapenems would be ineffective, and iii) more cost-effective surveillance of CRE outbreaks.

We envision that exploratory and mechanistic research inspired by pol-aAST will lead to a new generation of AST diagnostics. Additional mechanistic studies, such as those involving visualizing bacterial response to antibiotics[75-76], would clarify the effects of different ABX on the responses measured in pol-aAST for different pathogens. To evaluate whether pol-aAST can be broadened beyond CREs and β-lactams, these studies would include organisms with cell envelopes that differ from Enterobacteriaceae (e.g., Gram-positives), and other antimicrobials that affect the cell envelope, such as antimicrobial peptides[77] or vancomycin. It would also be desirable to evaluate pol-aAST with more amplification chemistries, including modified LAMP assays[78-79] and other isothermal chemistries[80-82] that are actively being developed. Ultimately, this new

generation of AST diagnostics will be integrated with the rapid ID methods being developed[20-21, 23] and with future rapid NA-based AST methods for additional ABX and pathogens. For example, we have developed the nuc-aAST[83], which measures accessibility of DNA to nucleases and was used to perform a rapid test of antibiotic susceptibility on the fastidious organism *Neisseria gonorrhoeae*. In contrast to the pol-aAST, the nuc-aAST enhances antibiotic-induced damage using surfactants after the ABX exposure step, and performs full cell lysis. Ultimately, to address the broad diversity of antibiotic-resistant pathogens, it is clear that integrated, multiplexed POC devices that incorporate multiple rapid phenotypic AST methods are needed. Innovative methods based on antibiotic-induced accessibility of nucleic acids to enzymes are promising for generating such ASTs for multiple antibiotics and pathogens in an approach that is intrinsically compatible with other rapid AST methods[58] and with rapid pathogen ID.[20-21, 24-25]

Materials and Methods

Isolates, growth conditions, and antibiotic exposure conditions.

We obtained 25 de-identified clinical isolates from the UCLA Clinical Microbiology Laboratory (CML) and the CDC's Enterobacteriaceae Carbapenem Breakpoint panel[12]. In the case of isolates obtained from the UCLA CML, MICs were determined as described previously[57]. Genotypic testing of the two *Ec* and two *Kp* isolates selected for their lack of known β-lactamase genes was performed by UCLA CML using a previously published assay[1] and separately at the Keck School of Medicine of USC using the FDA-approved Cepheid Xpert® Carba-R test. Whole genome sequencing of the single *Ebs* isolate selected for its lack of known resistance genes was performed by the CDC[12]. All isolates were stored as glycerol stocks at -80 °C. Glycerol stocks were streaked onto Trypticase Soy Agar with 5% sheep's blood (Becton Dickinson, Franklin Lakes, NJ, USA) and grown overnight at 37 °C or resuspended directly in liquid media. Prior to experiments, a small clump of cells was resuspended from plates or glycerol stocks in 2 mL Brain Heart

Infusion Broth (BHI, Becton Dickinson) at 37 °C + 5% CO_2 with 500 rpm shaking for 2 to 4 h until visibly turbid. OD_{600} of the cultures was then measured, and working cultures prepared at an OD_{600} of 0.01–0.07 and grown for 50 – 145 min at 37 °C + 5% CO_2 with 500 rpm. Working cultures were then diluted 10X into control and treated aliquots for antibiotic exposure. For validation experiments, antibiotic exposure was performed in 100 µL volumes consisting of 80 µL Mueller Hinton II Broth (Becton Dickinson), 5 µL nuclease-free H_2O (NF-H_2O), 5 µL 20X antibiotic stock solution, and 10 µL of working culture. In control aliquots, antibiotic stock solution was replaced with NF-H_2O. For filtration experiments, antibiotic exposure was performed in 100 µL volumes consisting of 65 µL Mueller Hinton II Broth (Becton Dickinson), 21 µL nuclease-free H_2O (NF-H_2O), 4 µL 25X antibiotic stock solution, and 10 µL of working culture. In control aliquots, antibiotic stock solution was replaced with NF-H_2O.

Antibiotic stocks.

Ceftriaxone disodium salt hemi(heptahydrate) (Sigma, St. Louis, MO, USA), ertapenem sodium salt (Research Products International, VENDOR), and meropenem trihydrate (TCI, Portland, OR, USA) were used to create antibiotic stock solutions. All antibiotic stock solutions were prepared at 1.0 mg/mL antibiotic in nuclease-free H_2O (NF-H_2O) based on manufacturer reported purity, aliquoted, and stored at -80 °C. Aliquots were only thawed and used once on the days of experiments.

Comparison of amplification methods.

In order to compare amplification using LAMP and PCR, *E. coli* isolates were exposed to 0.5 µg/mL ertapenem for 15 min. Samples were then transferred directly into either PCR or LAMP mix on ice. Amplification was started immediately. Quantitative PCR (qPCR) was performed on a Roche LightCycler 96 using SsoFast EvaGreen Supermix (BioRad, Hercules, CA, USA). 10 µL reactions were used. 10% of the final reaction volume was template. Published primers were used[84] at a final concentration of 500 nM. Cycling

conditions consisted of 3.0 min at 95 °C, followed by 35 cycles of 95 °C for 10 sec, 60 °C for 10 sec, and 72 °C for 15 sec. Fluorescence was measured using the SYBR Green channel after each 72 °C extension step. LAMP was performed on a BioRad CFX96 using the following conditions: 10 µL reaction volume containing 1X Isothermal Reaction Buffer II (NEB), 5 mM $MgSO_4$ (NEB), 1.4 mM dNTPs (NEB), 320 U/mL *Bst* 3.0 (NEB), and 2 µM Syto-9 (Thermo Fisher). 10% of the reaction volume was template. Primer sequences and concentrations have been described previously[58]. Cycling conditions consisted of 2.0 min at 12 °C (while lid was heating), followed by 120 cycles of 70 °C for 10 sec. Fluorescence was measured using the SYBR Green channel every 10 sec (after each cycle).

Filtration experiments.

Filtration experiments were performed using *E. coli* isolates exposed to 0.5 µg/mL ertapenem for 15 min. Immediately following exposure, cultures were passed through 0.22 µm, 1.5 mL cellulose acetate centrifuge tube filters (Corning Costar Spin-X, Corning, NY) by adding 50 µL of sample to the filter and centrifuging for 4 minutes at 1000 rcf. DNA was extracted from both the feed and filtrate using QuickExtract DNA Extraction Solution (Lucigen, Middleton, WI, USA). Samples were diluted 10X into extraction buffer and extracted according to manufacturer instructions. The concentration of the single copy *E. coli uid*A gene was then quantified in the feed and filtrate extractions. The percentage of *E. coli* DNA in the filtrate was calculated as the filtrate concentration divided by the feed concentration. Droplet digital PCR (ddPCR) was performed using QX200 ddPCR Supermix for EvaGreen (BioRad). 10% of the final reaction volume was template. Published primers targeting the *uid*A gene in *E. coli* were used[85] at a final concentration of 500 nM. Cycling conditions consisted of 5.0 min at 95 °C, followed by 40 cycles of 95 °C for 30 sec, 60 °C for 30 sec, and 72 °C for 30 sec., with final dye stabilization steps of 4 °C for 5.0 min followed by 90 °C for 5.0 min.

pol-aAST validation.

For pol-aAST validation experiments, *E. coli* and *Enterobacter* spp. isolates were exposed to either 2.0 µg/mL ceftriaxone (CRO), 0.5 µg/mL ertapenem (ETP), or 1.0 µg/mL meropenem (MEM). *K. pneumoniae* isolates were exposed to either 2.0 µg/mL CRO, 1.0 µg/mL ETP, or 1.0 µg/mL MEM. Some isolates were run multiple times on different days. If this was the case, the average $TTPD_{CT}$ and $TTPD_{LT}$ are reported for that isolate. All isolates were exposed to ABXs for 15 min in 100 µL reaction volumes in 200 µL PCR tube strips. After 15 minutes of ABX exposure, 10 µL of samples were transferred as template to LAMP reaction mix (as described above) on ice. Amplification was immediately started.

Timed sample-to-answer using contrived urine samples.

Timed sample to answer experiments were performed in the same fashion as pol-aAST validation experiments, except with the following modifications. Following initial growth and measurement of OD, isolates were resuspended in fresh, never-frozen, pooled human urine from healthy donors (Lee BioSciences). Additionally, a timer was started as soon as samples were added to the ABX exposure conditions. *Escherichia coli* (*Ec*) and *Klebsiella pneumoniae* (*Kp*) isolates were exposed to 0.5 and 1.0 µg/mL ETP (respectively) for 13 min. 13 min was chosen to ensure all handling steps could be completed within the first 15 min of the assay. Amplification was performed until all reactions reached a fluorescence value of 1000 relative fluorescent units (RFU) or greater. Amplification was then stopped, and TTP values copied into a spreadsheet pre-populated with formulas to automatically output susceptibility calls. The timer was stopped once a susceptibility call had been determined.

Statistical analysis.

All percent release values (Fig. 3) and TTPD values (Fig. 4–6) were calculated using Microsoft Excel. Data were plotted using GraphPad Prism 8.0 software.

Conflicts of Interest

The technology described in this publication is the subject of a patent application filed by Caltech. RFI has a financial interest in Talis Biomedical Corp.

Acknowledgements

This work was funded in part by the Defense Threat Reduction Agency (DTRA) award MCDC-18-01-01-007; an effort sponsored by the U.S. Government under Other Transaction number W15QKN-16-9-1002 between the MCDC, and the Government. The US Government is authorized to reproduce and distribute reprints for Governmental purposes notwithstanding any copyright notation thereon. The views and conclusions contained herein are those of the authors and should not be interpreted as necessarily representing the official policies or endorsements, either expressed or implied, of the U.S. Government. This work was also supported by a Burroughs Wellcome Fund Innovation in Regulatory Science Award, an NIH National Research Service Award (NRSA) [5T32GM07616NSF] (to NGS), and a grant from the Joseph J. Jacobs Institute for Molecular Engineering for Medicine. We thank Omai Garner, Sukantha Chandrasekaran, Shelley Miller, and Romney Humphries at the UCLA Clinical Microbiology Laboratory for providing isolates and for discussion of gold-standard practices. We thank Jennifer Bard at the Keck School of Medicine of USC for performing Cepheid Xpert® Carba-R tests. We also thank Natasha Shelby for help with writing and editing this manuscript.

Author contributions

All authors contributed to conceiving the method, revising the manuscript, and interpretation of experimental results. NGS developed the sample handling workflow and

performed all experiments for comparison of amplification methods, validation, and timed sample-to-answer experiments. NGS was the major contributor to manuscript preparation and prepared all figures. EJL performed filtration experiments, reviewed relevant medical literature, and contributed to manuscript writing. ESS performed early experimental work to link beta-lactam exposure to differential nucleic acid readout, analyzed data from validation experiments, and developed TTPD metrics. RFI supervised and guided the project, and helped compose the manuscript.

Notes and References

1. Pollett, S.; Miller, S.; Hindler, J.; Uslan, D.; Carvalho, M.; Humphries, R. M., Phenotypic and molecular characteristics of carbapenem-resistant Enterobacteriaceae in a health care system in Los Angeles, California, from 2011 to 2013. *J. Clin. Microbiol.* **2014,** *52* (11), 4003-9.

2. Cepheid 2018. Xpert® Carba-R. http://www.cepheid.com/us/cepheid-solutions/clinical-ivd-tests/healthcare-associated-infections/xpert-carba-r

3. Van Boeckel, T. P.; Gandra, S.; Ashok, A.; Caudron, Q.; Grenfell, B. T.; Levin, S. A.; Laxminarayan, R., Global antibiotic consumption 2000 to 2010: an analysis of national pharmaceutical sales data. *Lancet Infect. Dis.* **2014,** *14* (8), 742-750.

4. Versporten, A.; Zarb, P.; Caniaux, I.; Gros, M. F.; Drapier, N.; Miller, M.; Jarlier, V.; Nathwani, D.; Goossens, H.; Global-PPS network, Antimicrobial consumption and resistance in adult hospital inpatients in 53 countries: results of an internet-based global point prevalence survey. *Lancet Glob. Health* **2018,** *6* (6), e619-e629.

5. Magill, S. S.; Edwards, J. R.; Beldavs, Z. G.; Dumyati, G.; Janelle, S. J.; Kainer, M. A.; Lynfield, R.; Nadle, J.; Neuhauser, M. M.; Ray, S. M.; Richards, K.; Rodriguez, R.; Thompson, D. L.; Fridkin, S. K.; Emerging Infections Program Healthcare-Associated, I.; Antimicrobial Use Prevalence Survey, T., Prevalence of antimicrobial use in US acute care hospitals, May-September 2011. *JAMA* **2014,** *312* (14), 1438-46.

6. Zhang, Y.; Wang, Q.; Yin, Y.; Chen, H.; Jin, L.; Gu, B.; Xie, L.; Yang, C.; Ma, X.; Li, H.; Li, W.; Zhang, X.; Liao, K.; Man, S.; Wang, S.; Wen, H.; Li, B.; Guo, Z.; Tian, J.; Pei, F.; Liu, L.; Zhang, L.; Zou, C.; Hu, T.; Cai, J.; Yang, H.; Huang, J.; Jia, X.; Huang,

W.; Cao, B.; Wang, H., Epidemiology of Carbapenem-Resistant Enterobacteriaceae Infections: Report from the China CRE Network. *Antimicrob. Agents Chemother.* **2018,** *62* (2), e01882-17.

7. Satlin, M. J.; Chen, L.; Patel, G.; Gomez-Simmonds, A.; Weston, G.; Kim, A. C.; Seo, S. K.; Rosenthal, M. E.; Sperber, S. J.; Jenkins, S. G.; Hamula, C. L.; Uhlemann, A. C.; Levi, M. H.; Fries, B. C.; Tang, Y. W.; Juretschko, S.; Rojtman, A. D.; Hong, T.; Mathema, B.; Jacobs, M. R.; Walsh, T. J.; Bonomo, R. A.; Kreiswirth, B. N., Multicenter Clinical and Molecular Epidemiological Analysis of Bacteremia Due to Carbapenem-Resistant Enterobacteriaceae (CRE) in the CRE Epicenter of the United States. *Antimicrob. Agents Chemother.* **2017,** *61* (4), e02349-16.

8. Iovleva, A.; Doi, Y., Carbapenem-Resistant Enterobacteriaceae. *Clin. Lab. Med.* **2017,** *37* (2), 303-315.

9. WHO 2017. Global Priority List of Antibiotic-resistant Bacteria to Guide Research, Discovery, and Development of New Antibiotics. https://www.who.int/medicines/publications/global-priority-list-antibiotic-resistant-bacteria/en/

10. CDC 2013. Antibiotic Resistance Threats in the United States. https://www.cdc.gov/drugresistance/pdf/ar-threats-2013-508.pdf

11. Gelband, H.; Miller-Petrie, M.; Pant, S.; Levinson, S. G. J.; Barter, D.; Laxminarayan, A. W. R. 2015. State of the World's Antibiotics. https://cddep.org/publications/state_worlds_antibiotics_2015/

12. CDC 2015. Enterobacteriaceae Carbapenem Breakpoint Panel. https://wwwn.cdc.gov/ARIsolateBank/Panel/PanelDetail?ID=7

13. CDC 2019. Antibiotic/Antimicrobial Resistance: Biggest Threats and Data. https://www.cdc.gov/drugresistance/biggest_threats.html

14. Guh, A. Y.; Bulens, S. N.; Mu, Y.; Jacob, J. T.; Reno, J.; Scott, J.; Wilson, L. E.; Vaeth, E.; Lynfield, R.; Shaw, K. M.; Vagnone, P. M.; Bamberg, W. M.; Janelle, S. J.; Dumyati, G.; Concannon, C.; Beldavs, Z.; Cunningham, M.; Cassidy, P. M.; Phipps, E.

C.; Kenslow, N.; Travis, T.; Lonsway, D.; Rasheed, J. K.; Limbago, B. M.; Kallen, A. J., Epidemiology of Carbapenem-Resistant Enterobacteriaceae in 7 US Communities, 2012-2013. *JAMA* **2015,** *314* (14), 1479-87.

15. Cerqueira, G. C.; Earl, A. M.; Ernst, C. M.; Grad, Y. H.; Dekker, J. P.; Feldgarden, M.; Chapman, S. B.; Reis-Cunha, J. L.; Shea, T. P.; Young, S.; Zeng, Q.; Delaney, M. L.; Kim, D.; Peterson, E. M.; O'Brien, T. F.; Ferraro, M. J.; Hooper, D. C.; Huang, S. S.; Kirby, J. E.; Onderdonk, A. B.; Birren, B. W.; Hung, D. T.; Cosimi, L. A.; Wortman, J. R.; Murphy, C. I.; Hanage, W. P., Multi-institute analysis of carbapenem resistance reveals remarkable diversity, unexplained mechanisms, and limited clonal outbreaks. *Proc. Natl. Acad. Sci. U. S. A.* **2017,** *114* (5), 1135-1140.

16. Weiner, L. M.; Webb, A. K.; Limbago, B.; Dudeck, M. A.; Patel, J.; Kallen, A. J.; Edwards, J. R.; Sievert, D. M., Antimicrobial-Resistant Pathogens Associated With Healthcare-Associated Infections: Summary of Data Reported to the National Healthcare Safety Network at the Centers for Disease Control and Prevention, 2011–2014. *Infect. Control Hosp. Epidemiol.* **2016,** *37* (11), 1288-1301.

17. White House 2015. National Action Plan for Combating Antibiotic-Resistant Bacteria. https://obamawhitehouse.archives.gov/sites/default/files/docs/national_action_plan_for_combating_antibotic-resistant_bacteria.pdf

18. WHO 2015. Global Action Plan on Antimicrobial Resistance. https://www.who.int/antimicrobial-resistance/global-action-plan/en/

19. O'Neill, J. Tackling Drug-Resistant Infections Globally: Final Report and Recommendations *Review on Antimicrobial Resistance* [Online], 2016. https://amr-review.org/Publications.html (accessed 12/01/2016).

20. Renner, L. D.; Zan, J.; Hu, L. I.; Martinez, M.; Resto, P. J.; Siegel, A. C.; Torres, C.; Hall, S. B.; Slezak, T. R.; Nguyen, T. H.; Weibel, D. B., Detection of ESKAPE Bacterial Pathogens at the Point of Care Using Isothermal DNA-Based Assays in a Portable Degas-Actuated Microfluidic Diagnostic Assay Platform. *Appl. Environ. Microbiol.* **2017,** *83* (4).

21. Poritz, M. A.; Blaschke, A. J.; Byington, C. L.; Meyers, L.; Nilsson, K.; Jones, D. E.; Thatcher, S. A.; Robbins, T.; Lingenfelter, B.; Amiott, E.; Herbener, A.; Daly, J.; Dobrowolski, S. F.; Teng, D. H.; Ririe, K. M., FilmArray, an automated nested multiplex PCR system for multi-pathogen detection: development and application to respiratory tract infection. *PLoS One* **2011,** *6* (10), e26047.

22. Gootenberg, J. S.; Abudayyeh, O. O.; Kellner, M. J.; Joung, J.; Collins, J. J.; Zhang, F., Multiplexed and portable nucleic acid detection platform with Cas13, Cas12a, and Csm6. *Science (New York, N.Y.)* **2018,** *360* (6387), 439-444.

23. Phaneuf, C. R.; Mangadu, B.; Piccini, M. E.; Singh, A. K.; Koh, C. Y., Rapid, Portable, Multiplexed Detection of Bacterial Pathogens Directly from Clinical Sample Matrices. *Biosensors* **2016,** *6* (4), E49.

24. Ahn, H.; Batule, B. S.; Seok, Y.; Kim, M. G., Single-Step Recombinase Polymerase Amplification Assay Based on a Paper Chip for Simultaneous Detection of Multiple Foodborne Pathogens. *Anal. Chem.* **2018,** *90* (17), 10211-10216.

25. Raja, B.; Goux, H. J.; Marapadaga, A.; Rajagopalan, S.; Kourentzi, K.; Willson, R. C., Development of a panel of recombinase polymerase amplification assays for detection of common bacterial urinary tract infection pathogens. *J. Appl. Microbiol.* **2017,** *123* (2), 544-555.

26. CLSI, *M07-A10; Methods for Dilution Antimicrobial Susceptbility Testing for Bacteria That Grow Aerobically; Approved Standard-Tenth Edition*. Clinical and Laboratory Standards Institute: 2015; Vol. 35.

27. Jorgensen, J. H.; Ferraro, M. J., Antimicrobial susceptibility testing: a review of general principles and contemporary practices. *Clin. Infect. Dis.* **2009,** *49* (11), 1749-55.

28. Blank, S.; Daskalakis, D. C., Neisseria gonorrhoeae - Rising Infection Rates, Dwindling Treatment Options. *N. Engl. J. Med.* **2018,** *379* (19), 1795-1797.

29. Piddock, L. J. V., Assess drug-resistance phenotypes, not just genotypes. *Nature Microbiology* **2016,** *1* (8), 16120.

30. Bard, J.; Lee, F., Why can't we just use PCR? The role of genotypic versus phenotypic testing for antimicrobial resistance testing. *Clin. Microbiol. Newsl.* **2018,** *40* (11), 87-95.

31. van Belkum, A.; Bachmann, T. T.; Lüdke, G.; Lisby, J. G.; Kahlmeter, G.; Mohess, A.; Becker, K.; Hays, J. P.; Woodford, N.; Mitsakakis, K.; Moran-Gilad, J.; Vila, J.; Peter, H.; Rex, J. H.; Dunne, W. M., Developmental roadmap for antimicrobial susceptibility testing systems. *Nature Reviews Microbiology* **2018**.

32. Kostic, T.; Ellis, M.; Williams, M. R.; Stedtfeld, T. M.; Kaneene, J. B.; Stedtfeld, R. D.; Hashsham, S. A., Thirty-minute screening of antibiotic resistance genes in bacterial isolates with minimal sample preparation in static self-dispensing 64 and 384 assay cards. *Appl. Microbiol. Biotechnol.* **2015,** *99* (18), 7711-22.

33. Kalsi, S.; Valiadi, M.; Tsaloglou, M. N.; Parry-Jones, L.; Jacobs, A.; Watson, R.; Turner, C.; Amos, R.; Hadwen, B.; Buse, J.; Brown, C.; Sutton, M.; Morgan, H., Rapid and sensitive detection of antibiotic resistance on a programmable digital microfluidic platform. *Lab Chip* **2015,** *15* (14), 3065-75.

34. Nakano, R.; Nakano, A.; Ishii, Y.; Ubagai, T.; Kikuchi-Ueda, T.; Kikuchi, H.; Tansho-Nagakawa, S.; Kamoshida, G.; Mu, X.; Ono, Y., Rapid detection of the Klebsiella pneumoniae carbapenemase (KPC) gene by loop-mediated isothermal amplification (LAMP). *J. Infect. Chemother.* **2015,** *21* (3), 202-6.

35. Mu, X.; Nakano, R.; Nakano, A.; Ubagai, T.; Kikuchi-Ueda, T.; Tansho-Nagakawa, S.; Kikuchi, H.; Kamoshida, G.; Endo, S.; Yano, H.; Ono, Y., Loop-mediated isothermal amplification: Rapid and sensitive detection of the antibiotic resistance gene ISAba1-blaOXA-51-like in Acinetobacter baumannii. *J. Microbiol. Methods* **2016,** *121*, 36-40.

36. Hu, C.; Kalsi, S.; Zeimpekis, I.; Sun, K.; Ashburn, P.; Turner, C.; Sutton, J. M.; Morgan, H., Ultra-fast electronic detection of antimicrobial resistance genes using isothermal amplification and Thin Film Transistor sensors. *Biosens. Bioelectron.* **2017,** *96*, 281-287.

37. Cortegiani, A.; Russotto, V.; Graziano, G.; Geraci, D.; Saporito, L.; Cocorullo, G.; Raineri, S. M.; Mammina, C.; Giarratano, A., Use of Cepheid Xpert Carba-R(R) for Rapid Detection of Carbapenemase-Producing Bacteria in Abdominal Septic Patients Admitted to Intensive Care Unit. *PLoS One* **2016,** *11* (8), e0160643.

38. Biofire 2019. The BioFire FilmArray. https://www.biofiredx.com/products/filmarray/

39. Shawar, R., 510(k) Premarket Notification for K160901 Cepheid Xpert Carba-R Assay. USA Food and Drug Administration, Department of Health and Human Services: Silver Spring, MD, 2016.
40. Lasserre, C.; De Saint Martin, L.; Cuzon, G.; Bogaerts, P.; Lamar, E.; Glupczynski, Y.; Naas, T.; Tande, D., Efficient Detection of Carbapenemase Activity in Enterobacteriaceae by Matrix-Assisted Laser Desorption Ionization-Time of Flight Mass Spectrometry in Less Than 30 Minutes. *J. Clin. Microbiol.* **2015,** *53* (7), 2163-71.
41. Bogaerts, P.; Yunus, S.; Massart, M.; Huang, T. D.; Glupczynski, Y., Evaluation of the BYG Carba Test, a New Electrochemical Assay for Rapid Laboratory Detection of Carbapenemase-Producing Enterobacteriaceae. *J. Clin. Microbiol.* **2016,** *54* (2), 349-58.
42. Robinson, A. M.; Medlicott, N. J.; Ussher, J. E., The rapid detection of cefotaxime-resistant Enterobacteriaceae by HPLC. *Future Sci OA* **2016,** *2* (4), FSO142.
43. Bernabeu, S.; Dortet, L.; Naas, T., Evaluation of the beta-CARBA test, a colorimetric test for the rapid detection of carbapenemase activity in Gram-negative bacilli. *J. Antimicrob. Chemother.* **2017,** *72* (6), 1646-1658.
44. Zhang, Y.; Lei, J. E.; He, Y.; Yang, J.; Wang, W.; Wasey, A.; Xu, J.; Lin, Y.; Fan, H.; Jing, G.; Zhang, C.; Jin, Y., Label-Free Visualization of Carbapenemase Activity in Living Bacteria. *Angew. Chem. Int. Ed. Engl.* **2018,** *57* (52), 17120-17124.
45. Santiso, R.; Tamayo, M.; Gosalvez, J.; Bou, G.; Fernandez Mdel, C.; Fernandez, J. L., A rapid in situ procedure for determination of bacterial susceptibility or resistance to antibiotics that inhibit peptidoglycan biosynthesis. *BMC Microbiol.* **2011,** *11*, 191.
46. Bou, G.; Otero, F. M.; Santiso, R.; Tamayo, M.; Fernandez Mdel, C.; Tomas, M.; Gosalvez, J.; Fernandez, J. L., Fast assessment of resistance to carbapenems and ciprofloxacin of clinical strains of Acinetobacter baumannii. *J. Clin. Microbiol.* **2012,** *50* (11), 3609-13.
47. Park, K.; Jeong, J.; Yi, S. Y.; Lee, W. S.; Shin, Y. B., FRET probe-based antibacterial susceptibility testing (F-AST) by detection of bacterial nucleases released by antibiotic-induced lysis. *Biosensors Bioelectron.* **2019**.

48. Faria-Ramos, I.; Espinar, M. J.; Rocha, R.; Santos-Antunes, J.; Rodrigues, A. G.; Canton, R.; Pina-Vaz, C., A novel flow cytometric assay for rapid detection of extended-spectrum beta-lactamases. *Clin. Microbiol. Infect.* **2013,** *19* (1), E8-E15.

49. Burnham, C. A.; Frobel, R. A.; Herrera, M. L.; Wickes, B. L., Rapid ertapenem susceptibility testing and Klebsiella pneumoniae carbapenemase phenotype detection in Klebsiella pneumoniae isolates by use of automated microscopy of immobilized live bacterial cells. *J. Clin. Microbiol.* **2014,** *52* (3), 982-6.

50. Su, I. H.; Ko, W. C.; Shih, C. H.; Yeh, F. H.; Sun, Y. N.; Chen, J. C.; Chen, P. L.; Chang, H. C., A dielectrophoresis system for testing antimicrobial susceptibility of Gram-negative bacteria to beta-lactam antibiotics. *Anal. Chem.* **2017**.

51. Lange, C.; Schubert, S.; Jung, J.; Kostrzewa, M.; Sparbier, K., Quantitative matrix-assisted laser desorption ionization-time of flight mass spectrometry for rapid resistance detection. *J. Clin. Microbiol.* **2014,** *52* (12), 4155-62.

52. Rolain, J. M.; Mallet, M. N.; Fournier, P. E.; Raoult, D., Real-time PCR for universal antibiotic susceptibility testing. *J. Antimicrob. Chemother.* **2004,** *54* (2), 538-41.

53. Mach, K. E.; Mohan, R.; Baron, E. J.; Shih, M. C.; Gau, V.; Wong, P. K.; Liao, J. C., A biosensor platform for rapid antimicrobial susceptibility testing directly from clinical samples. *J. Urol.* **2011,** *185* (1), 148-53.

54. Halford, C.; Gonzalez, R.; Campuzano, S.; Hu, B.; Babbitt, J. T.; Liu, J.; Wang, J.; Churchill, B. M.; Haake, D. A., Rapid antimicrobial susceptibility testing by sensitive detection of precursor rRNA using a novel electrochemical biosensing platform. *Antimicrob. Agents Chemother.* **2013,** *57* (2), 936-43.

55. Mezger, A.; Gullberg, E.; Goransson, J.; Zorzet, A.; Herthnek, D.; Tano, E.; Nilsson, M.; Andersson, D. I., A general method for rapid determination of antibiotic susceptibility and species in bacterial infections. *J. Clin. Microbiol.* **2015,** *53* (2), 425-32.

56. Barczak, A. K.; Gomez, J. E.; Kaufmann, B. B.; Hinson, E. R.; Cosimi, L.; Borowsky, M. L.; Onderdonk, A. B.; Stanley, S. A.; Kaur, D.; Bryant, K. F.; Knipe, D. M.; Sloutsky, A.; Hung, D. T., RNA signatures allow rapid identification of pathogens and antibiotic susceptibilities. *Proc. Natl. Acad. Sci. U. S. A.* **2012,** *109* (16), 6217-22.

57. Schoepp, N. G.; Khorosheva, E. M.; Schlappi, T. S.; Curtis, M. S.; Humphries, R. M.; Hindler, J. A.; Ismagilov, R. F., Digital Quantification of DNA Replication and Chromosome Segregation Enables Determination of Antimicrobial Susceptibility after only 15 Minutes of Antibiotic Exposure. *Angew. Chem. Int. Ed. Engl.* **2016,** *55* (33), 9557-61.

58. Schoepp, N. G.; Schlappi, T. S.; Curtis, M. S.; Butkovich, S. S.; Miller, S.; Humphries, R. M.; Ismagilov, R. F., Rapid pathogen-specific phenotypic antibiotic susceptibility testing using digital LAMP quantification in clinical samples. *Sci. Transl. Med.* **2017,** *9* (410).

59. Khazaei, T.; Barlow, J. T.; Schoepp, N. G.; Ismagilov, R. F., RNA markers enable phenotypic test of antibiotic susceptibility in Neisseria gonorrhoeae after 10 minutes of ciprofloxacin exposure. *Sci. Rep.* **2018,** *8* (1).

60. Ota, Y.; Furuhashi, K.; Nanba, T.; Yamanaka, K.; Ishikawa, J.; Nagura, O.; Hamada, E.; Maekawa, M., A rapid and simple detection method for phenotypic antimicrobial resistance in Escherichia coli by loop-mediated isothermal amplification. *J. Med. Microbiol.* **2019**.

61. Marston, H. D.; Dixon, D. M.; Knisely, J. M.; Palmore, T. N.; Fauci, A. S., Antimicrobial Resistance. *JAMA* **2016,** *316* (11), 1193-1204.

62. Hicks, J. M.; Haeckel, R.; Price, C. P.; Lewandrowski, K.; Wu, A. H. B., Recommendations and opinions for the use of point-of-care testing for hospitals and primary care: summary of a 1999 symposium. *Clin. Chim. Acta* **2001,** *303* (1-2), 1-17.

63. Bard, J. D.; Lee, F., Why Can't We Just Use PCR? The Role of Genotypic versus Phenotypic Testing for Antimicrobial Resistance Testing. *Clin. Microbiol. Newsl.* **2018,** *40* (11), 87-95.

64. Hawkey, P. M.; Livermore, D. M., Carbapenem antibiotics for serious infections. *BMJ* **2012,** *344*, e3236.

65. Zankari, E.; Hasman, H.; Cosentino, S.; Vestergaard, M.; Rasmussen, S.; Lund, O.; Aarestrup, F. M.; Larsen, M. V., Identification of acquired antimicrobial resistance genes. *J. Antimicrob. Chemother.* **2012,** *67* (11), 2640-4.

66. Chang, Y. Y.; Chuang, Y. C.; Siu, L. K.; Wu, T. L.; Lin, J. C.; Lu, P. L.; Wang, J. T.; Wang, L. S.; Lin, Y. T.; Huang, L. J.; Fung, C. P., Clinical features of patients with carbapenem nonsusceptible Klebsiella pneumoniae and Escherichia coli in intensive care units: a nationwide multicenter study in Taiwan. *J. Microbiol. Immunol. Infect.* **2015,** *48* (2), 219-25.

67. Tamma, P. D.; Goodman, K. E.; Harris, A. D.; Tekle, T.; Roberts, A.; Taiwo, A.; Simner, P. J., Comparing the Outcomes of Patients With Carbapenemase-Producing and Non-Carbapenemase-Producing Carbapenem-Resistant Enterobacteriaceae Bacteremia. *Clin. Infect. Dis.* **2017,** *64* (3), 257-264.

68. Rui, P.; Okeyode, T. 2015. National Ambulatory Care Survey: 2015 State and National Summary Tables. https://www.cdc.gov/nchs/data/ahcd/namcs_summary/2015_namcs_web_tables.pdf

69. FDA, Evaluation of Automatic Class III Designation for T2Candida Panel and T2Dx Instrument. **2014**.

70. Musta, A. C.; Riederer, K.; Shemes, S.; Chase, P.; Jose, J.; Johnson, L. B.; Khatib, R., Vancomycin MIC plus heteroresistance and outcome of methicillin-resistant Staphylococcus aureus bacteremia: trends over 11 years. *J. Clin. Microbiol.* **2009,** *47* (6), 1640-4.

71. Baltekin, O.; Boucharin, A.; Tano, E.; Andersson, D. I.; Elf, J., Antibiotic susceptibility testing in less than 30 min using direct single-cell imaging. *Proc. Natl. Acad. Sci. U. S. A.* **2017,** *114* (34), 9170-9175.

72. Choi, J.; Yoo, J.; Lee, M.; Kim, E. G.; Lee, J. S.; Lee, S.; Joo, S.; Song, S. H.; Kim, E. C.; Lee, J. C.; Kim, H. C.; Jung, Y. G.; Kwon, S., A rapid antimicrobial susceptibility test based on single-cell morphological analysis. *Sci. Transl. Med.* **2014,** *6* (267), 267ra174.

73. Etayash, H.; Khan, M. F.; Kaur, K.; Thundat, T., Microfluidic cantilever detects bacteria and measures their susceptibility to antibiotics in small confined volumes. *Nat Commun* **2016,** *7*, 12947.

74. Longo, G.; Alonso-Sarduy, L.; Rio, L. M.; Bizzini, A.; Trampuz, A.; Notz, J.; Dietler, G.; Kasas, S., Rapid detection of bacterial resistance to antibiotics using AFM cantilevers as nanomechanical sensors. *Nat Nanotechnol* **2013,** *8* (7), 522-6.

75. Pidgeon, S. E.; Pires, M. M., Vancomycin-Dependent Response in Live Drug-Resistant Bacteria by Metabolic Labeling. *Angew. Chem. Int. Ed. Engl.* **2017,** *56* (30), 8839-8843.

76. Stone, M. R. L.; Butler, M. S.; Phetsang, W.; Cooper, M. A.; Blaskovich, M. A. T., Fluorescent Antibiotics: New Research Tools to Fight Antibiotic Resistance. *Trends Biotechnol.* **2018**.

77. Deshayes, S.; Xian, W.; Schmidt, N. W.; Kordbacheh, S.; Lieng, J.; Wang, J.; Zarmer, S.; Germain, S. S.; Voyen, L.; Thulin, J.; Wong, G. C.; Kasko, A. M., Designing Hybrid Antibiotic Peptide Conjugates To Cross Bacterial Membranes. *Bioconjug. Chem.* **2017,** *28* (3), 793-804.

78. Phillips, E. A.; Moehling, T. J.; Bhadra, S.; Ellington, A. D.; Linnes, J. C., Strand Displacement Probes Combined with Isothermal Nucleic Acid Amplification for Instrument-Free Detection from Complex Samples. *Anal. Chem.* **2018,** *90* (11), 6580-6586.

79. Cai, S.; Jung, C.; Bhadra, S.; Ellington, A. D., Phosphorothioated Primers Lead to Loop-Mediated Isothermal Amplification at Low Temperatures. *Anal. Chem.* **2018,** *90* (14), 8290-8294.

80. Daher, R. K.; Stewart, G.; Boissinot, M.; Bergeron, M. G., Recombinase Polymerase Amplification for Diagnostic Applications. *Clin. Chem.* **2016,** *62* (7), 947-58.

81. Toley, B. J.; Covelli, I.; Belousov, Y.; Ramachandran, S.; Kline, E.; Scarr, N.; Vermeulen, N.; Mahoney, W.; Lutz, B. R.; Yager, P., Isothermal strand displacement amplification (iSDA): a rapid and sensitive method of nucleic acid amplification for point-of-care diagnosis. *Analyst* **2015,** *140* (22), 7540-9.

82. Reid, M. S.; Le, X. C.; Zhang, H., Exponential Isothermal Amplification of Nucleic Acids and Assays for Proteins, Cells, Small Molecules, and Enzyme Activities: An EXPAR Example. *Angew. Chem. Int. Ed. Engl.* **2018,** *57* (37), 11856-11866.

83. Schoepp, N. G.; Savela, E. S.; Rolando, J. C.; Soge, O. O.; Ismagilov, R. F., Measurement of DNA Accessibility in Neisseria gonorrhoeae Exposed to Beta-lactams Accelerates Phenotypic Antibiotic Susceptibility Testing. *In Preparation* **2018**.

84. Matsuda, K.; Tsuji, H.; Asahara, T.; Kado, Y.; Nomoto, K., Sensitive quantitative detection of commensal bacteria by rRNA-targeted reverse transcription-PCR. *Appl. Environ. Microbiol.* **2007,** *73* (1), 32-9.

85. Chern, E. C.; Siefring, S.; Paar, J.; Doolittle, M.; Haugland, R. A., Comparison of quantitative PCR assays for Escherichia coli targeting ribosomal RNA and single copy genes. *Lett. Appl. Microbiol.* **2011,** *52* (3), 298-306.

Chapter VI

Surfactant-enhanced DNA accessibility to nuclease accelerates phenotypic β-lactam antibiotic susceptibility testing of *N. gonorrhoeae*[5]

Abstract

Rapid, phenotypic antimicrobial susceptibility testing (AST) for *Neisseria gonorrhoeae* (*Ng*) is critically needed to counter widespread antibiotic resistance. However, rapid phenotypic AST for *Ng* is challenged by the pathogen's slow doubling time and the lack of methods to quickly quantify its response to β-lactams (the largest antibiotic class used to treat *Ng*). Here, we devise an innovative approach for performing a rapid phenotypic AST that measures DNA accessibility to exogenous nucleases after exposure to β-lactams. We show that DNA in antibiotic-susceptible cells has increased accessibility, and that a judiciously chosen surfactant enhanced this effect. We validated our method, termed nuc-aAST (nuclease-accessibility AST) using penicillin, cefixime, and ceftriaxone and showed 100% categorical agreement with gold-standard AST after just 15-30 min of antibiotic exposure. This proof-of-concept provides a pathway toward developing a critically needed phenotypic AST for *Ng* and these innovations can be leveraged to develop ASTs for additional global-health threats.

Introduction

Gonorrhea, caused by *Neisseria gonorrhoeae* (*Ng*), is the second most common notifiable sexually transmitted infection (STI) in the U.S.(*1*) and the third most common STI globally, affecting 78,000,000 people each year worldwide(*2*). Untreated *Ng* infections can lead to pelvic inflammatory disease, infertility, ectopic pregnancy, and neonatal

[5]This chapter was submitted for publication with authorship belonging to Nathan G. Schoepp, Emily S. Savela, Justin C. Rolando, Olusegun O. Soge, and Rustem F. Ismagilov.

blindness(*3*), and have a significant financial burden on healthcare systems(*4*). Antibiotic resistance in *Ng* emerged quickly and continues to spread unchecked because there is no rapid antibiotic susceptibility test (AST) to guide treatment. Lacking a rapid AST, clinicians are limited to making empiric prescriptions as recommended by the Centers for Disease Control and Prevention (CDC)(*5*) or World Health Organization (WHO)(*6*). When resistance to a particular ABX exceeds 5%, treatment guidelines are updated and the recommended treatment protocol is escalated to the next line of ABX(*7, 8*). As a result, *Ng* strains continue to evolve resistance, including to the last-line (dual treatment with azithromycin/ceftriaxone)(*9-11*). The global prevalence and spread of resistant *Ng* infections has led the CDC to place *Ng* in its highest ("urgent") category of antimicrobial-resistant pathogen threats(*12*) and the WHO to label *Ng* as a high-priority pathogen(*13*). Despite the threat of untreatable *Ng*(*14*) and an international call for rapid diagnostics(*15-17*), no phenotypic AST currently exists that can be performed rapidly enough for the point of care (POC).

Successful and timely treatment of *Ng* infections while providing antibiotic stewardship requires two sequential steps to be performed at the POC. First, an identification (ID) test is run on the patient's sample (typically urine or swab) to confirm that the patient is infected with *Ng.* Then, an AST must be run on the sample to determine whether the infecting strain of *Ng* is susceptible to the available ABX, so that the correct treatment can be prescribed. Substantial efforts (both academic(*18-20*) and commercial(*21, 22*)) are making great progress toward shortening the time required to identify *Ng* infections. However, there is no published path toward development of a rapid phenotypic AST for *Ng*, especially for beta-lactam antibiotics. Thus, even with swift diagnosis of an *Ng* infection, prescription of the correct antibiotics at the POC will remain bottlenecked by the lack of a rapid AST.

AST methods are either genotypic or phenotypic. Genotypic methods predict resistance by screening for the presence of known resistance genes, whereas phenotypic methods determine susceptibly and resistance by directly measuring an organism's response to an

antibiotic. Rapid genotypic methods exist for select antibiotic classes such as quinolones(*23, 24*), but the diverse mechanisms of resistance present in *Ng* would require highly multiplexed assays for most other antibiotic classes(*25, 26*), including β-lactams(*27, 28*), which are the largest class of ABX for *Ng*. For example, hundreds of β-lactamase genes are known(*29*), and new resistance genes continue to emerge, making it challenging to design a comprehensive genotypic AST, even for a single organism. Only phenotypic AST methods provide the ability to directly detect resistance, and susceptibility, regardless of the antibiotic's mechanism of action. The current gold-standard AST for *Ng* is agar dilution, a phenotypic method that takes many days and is only performed in a small number of reference laboratories(*30*). Efforts have been made to shorten the total assay time of culture-based techniques(*31-33*), but these methods still rely on multiple cell divisions and thus require many hours due to the slow doubling time (~60 min) of *Ng*.

A phenotypic AST usable at the POC would be paradigm-shifting for *Ng*(*34*) because it would provide the correct timely treatment of infections, significantly reduce disease burden, and improve global surveillance efforts(*35-37*). Until a POC diagnostic is developed for *Ng*, empiric prescribing of the last-line dual antibiotic therapy of azithromycin/ceftriaxone will likely continue, as it has in the U.S. over the last five years(*38*). Likewise, if informed antibiotic prescriptions cannot be made, resistance will continue to spread, at which point no currently available ABXs will be recommended for treatment of *Ng*. Importantly, a rapid, phenotypic AST would greatly increase treatment options because if clinicians know which ABX will be efficacious for each infection, they can once again treat with ABX that are not prescribed in the current (empiric-based) system because of the risk of resistance. For example, even though cefixime (CFM) is no longer used as a first-line therapy for *Ng*, up to 95% of infections in the U.S. are still susceptible to CFM(*1, 39*). Similarly, up to 77% of *Ng* infections are susceptible to TET(*1*). Therefore, having a POC AST would enable clinicians to once again safely prescribe CFM and other antibiotics(*40*). Several recent cases of *Ng* infections resistant to azithromycin(*41, 42*), or the currently recommended combination of

ceftriaxone/azithromycin(*9, 11*) were detected after treatment was administered, highlighting the critical need for faster diagnostics.

For an *Ng* AST to inform treatment decisions at the POC, the total assay time to determine phenotypic susceptibility must be greatly decreased(*43-45*). Quantification of pathogen-specific nucleic acid (NA) concentrations has shown major promise for the rapid determination of susceptibility phenotype(*46-49*). These methods rely on comparing the NA concentrations of control and antibiotic-treated samples, and thus work well for rapidly dividing organisms and for ABX that directly affect NA replication. NA-based phenotypic AST methods also benefit from the high sensitivity of NA amplification, and fast isothermal amplification techniques have led to short total assay times(*46*). For example, by measuring the concentration of *E. coli* DNA, we have shown that the antibiotic-exposure step for phenotypic AST can be shortened to 15 min(*50*). We also were able to achieve a phenotypic AST with a 10-min antibiotic exposure time in *Ng* by measuring changes in RNA concentration after exposure to ciprofloxacin, which directly inhibits DNA replication and downstream translation(*51*). However, for ABX that do not impact DNA replication, such as β-lactams, these NA-based AST techniques have proven difficult; the fastest published method for *Ng* still requires four hours of beta-lactam exposure(*52*). Importantly, of the ABX prescribed for *Ng*, only one, ciprofloxacin(*51*), has been demonstrated to be compatible with this existing NA-based approach.

Here, we describe an innovation that enables a rapid, NA-based phenotypic AST for β-lactams, the largest class of ABX used to treat *Ng*. We hypothesized that cell wall damage caused by exposure to β-lactams could be exploited to determine phenotypic susceptibility faster than cell division. Our method, termed nuc-aAST (nuclease-accessibility AST), measures the accessibility of intracellular *Ng* DNA to exogenously added nucleases after a short antibiotic exposure. We also wished to test whether the total time of the assay could be further decreased by including an enhancement step, defined

as a condition that would lead to greater differences in DNA accessibility between resistant (R) and susceptible (S) samples.

We chose to validate this proof-of-concept nuc-aAST using three β-lactams, penicillin (PEN), cefixime (CFM), and ceftriaxone (CRO), that represent first-line treatments at different points in the history of *Ng* treatment(*6, 53*). Additionally, CRO, in combination with azithromycin, is the current recommended (and last-line) treatment for *Ng*. Determining susceptibility to CRO is thus relevant not only for treatment, but for surveillance efforts. Urine was chosen as the matrix for contrived sample testing because it is one of the primary sample types used for *Ng* diagnosis, especially in males(*5, 6*). We chose to test only categorically S or R isolates, based on EUCAST breakpoints(*54*), because S and R isolates are more useful than intermediate isolates for gaining initial mechanistic insights into nuc-aAST, and because S and R are actionable calls in antibiotic-prescribing scenarios. Lastly, keeping in mind clinical utility, we timed each assay step to determine whether the nuc-aAST could yield a definitive susceptibility call within the time period of a patient's visit, which is usually less than an hour(*44, 45*).

Results

Design and rationale of the nuc-aAST

The nuc-aAST method measures differences in the accessibility of genomic DNA to an exogenous nuclease between control and treated samples following a short antibiotic (ABX) exposure. Like other NA-based AST methods, the nuc-aAST (Fig. 1) relies on measuring changes in the quantity of pathogen-specific NAs in response to a treatment with ABX; however, the nuc-aAST differs from existing NA-based ASTs in three aspects. First, in nuc-aAST, exposure of cells to β-lactams is performed in the presence of a DNase enzyme to degrade any DNase-accessible NAs (Fig. 1a). DNA is accessible to DNase if it is released from the cells upon cell lysis, or if the action of the antibiotic porates the cells and allows DNase to access the DNA. Second, in nuc-aAST, an

enhancement step is introduced to increase accessibility of DNA in cells that have damaged or compromised peptidoglycan caused by β-lactams; DNase is present and active during this enhancement step (Fig. 1b). Third, in nuc-aAST, lysis of the sample is performed only after DNase has degraded all accessible DNA (Fig. 1c). This lysis step also inactivates the DNase, so that the enzyme does not impact downstream quantification. Following inactivation of DNase and lysis, DNA remaining in the sample is quantified and the percentage of accessible DNA is used to determine susceptibility (Fig. 1d). The percentage of accessible DNA is quantified by subtracting the concentration of inaccessible DNA (DNA not digested) in the treated aliquot from the concentration of DNA in the control aliquot, and dividing this value by the concentration of DNA in the control. Measuring the percentage of accessible DNA is an NA-based metric that enables us to quantify the damage to the cellular envelope induced by ABX targeting cell wall biosynthesis.

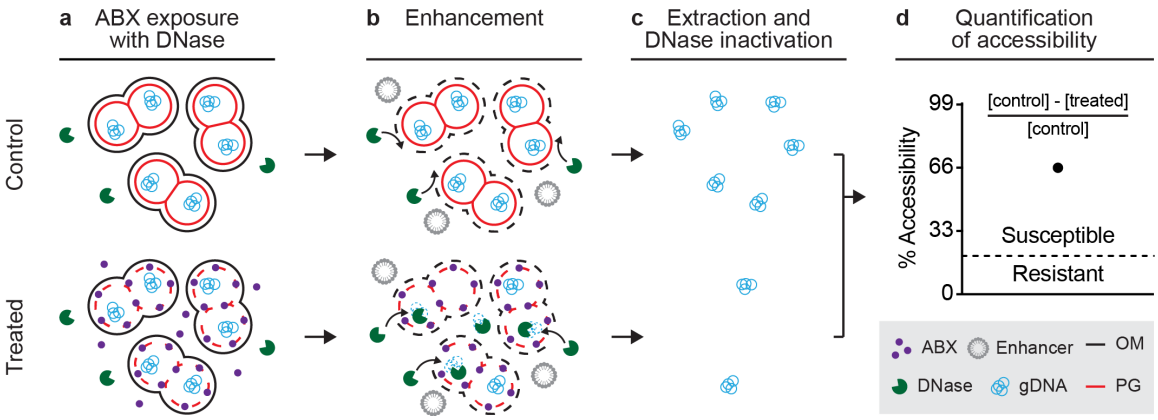

Fig. 6-1. The nuc-aAST workflow shown for a sample containing an antibiotic-susceptible pathogen. (a) A sample is split into control and treated aliquots; the treated aliquot is exposed to antibiotics (ABX) in the presence of DNase and any extracellular DNA is digested. ABX compromise peptidoglycan (PG) of cells in the treated aliquot. (b) Accessibility to nucleases is enhanced by the addition of an enhancer, which disrupts the outer membrane (OM). Genomic DNA becomes accessible and is degraded in the treated aliquot. Intact peptidoglycan in control samples (or in treated but resistant samples) prevents degradation. (c) Nucleic acids (NAs) are extracted, and DNase is inactivated. (d)

Accessibility is quantified by measuring NA concentrations in the control and treated aliquots and dividing the amount of digested DNA by the amount in the control (to yield percentage accessibility). When the percentage accessibility is greater than the threshold (dashed line), the sample is categorized as susceptible.

β-lactams should primarily affect peptidoglycan(*55*), and should not have a major impact on the outer membrane, which serves as a structural element in Gram-negative bacteria(*56*). Therefore, we expected the primary mechanism behind any increase in accessibility to be cell lysis as a result of exposure to β-lactams, leading to release of genomic DNA to the extracellular environment containing DNase. Additionally, we hypothesized that autolysis, which has been observed as an active stress response in *Ng*(*57, 58*), might accelerate changes in accessibility due to ABX exposure. We tested our hypotheses in a time-course experiment using two penicillin-susceptible (PEN-S) and two penicillin-resistant (PEN-R) *Ng* clinical isolates (Fig. 2). We observed a significant difference in the percentage accessibility between susceptible and resistant isolates after 90 min of exposure. This is the shortest incubation time for an *Ng* AST with PEN to date, and faster than existing NA-based methods that rely on DNA replication(*52*). However, the ideal length of an exposure step for an AST used at the POC would be even shorter (15-30 min) to keep the entire workflow within the time period of a patient visit. Thus, we were compelled to further accelerate changes in accessibility of DNA to nuclease as a result of β-lactam exposure in susceptible samples.

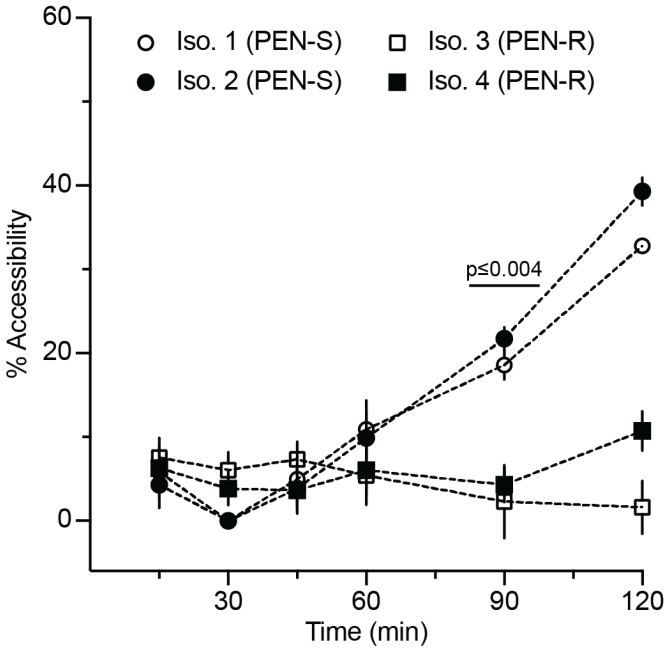

Fig. 6-2. Percentage accessibility of DNA over time using the nuc-aAST without the addition of an enhancing step. Two penicillin-susceptible (PEN-S) and two penicillin-resistant (PEN-R) *Ng* isolates were exposed to penicillin in the presence of DNase I. DNA from the control and PEN-treated aliquots was extracted and quantified using qPCR at multiple time points to calculate percentage accessibility. Error bars represent the standard deviation of the PCR triplicates.

Enhancing changes in accessibility

We next hypothesized that the differences in DNA accessibility that we observed between susceptible and resistant isolates exposed to β-lactams could be enhanced using conditions that would modify the permeability of the cell envelope. In Gram-negative organisms like *Ng*, the outer membrane (OM) presents the first, and major, permeability barrier to macromolecules (e.g. nucleases and other enzymes) entering or exiting the cell, typically allowing only small molecules with molecular weights < ~600 Da to pass through(*59, 60*). The peptidoglycan, in contrast to the OM, is a looser barrier that has been estimated to allow macromolecules up to 50 kDa to pass through(*61-63*). We thus suspected that if the OM could be compromised, damage to the peptidoglycan would

result in immediate, measurable changes in accessibility of genomic DNA to DNase, both by allowing DNase to enter and by allowing DNA fragments to exit. Therefore, we hypothesized that we could compromise the OM using an "enhancer" to decrease total assay time.

The ideal enhancer would i) increase DNA accessibility to DNase in cells that have a compromised cell wall as a result of ABX exposure, ii) result in minimal lysis of healthy cells, iii) have a consistent effect on all *Ng* isolates and iv) have no effect on downstream extraction and quantification of NAs. With these parameters in mind, we chose to test hypo-osmotic stress, stimulated autolysis, and four classes of surfactant as potential enhancers.

Hypo-osmotic stress was chosen as a method to enhance lysis of cells with damaged or compromised cell walls because osmotic stress of varying degrees is known to increase release of intracellular contents in Gram-negative bacteria,(*64-66*) although it has never been used to enhance accessibility in the context of AST. We exposed cells to hypo-osmotic conditions by diluting control and treated aliquots 20-fold in water with DNase I and 500 μM $CaCl_2$, resulting in a ~244 mOsm/kg shift from the ABX exposure conditions. Autolysis was chosen as an enhancer with the rationale of leveraging an already existing stress response in *Ng* to enhance changes in accessibility. Autolysis is a natural stress response in *Ng*, and can be accelerated by incubation in high pH conditions (e.g. Tris, pH 8.5)(*67, 68*). We hypothesized that using autolysis as an enhancer might result in large changes in NA accessibility. Surfactants were chosen as potential enhancers as a targeted chemical means of disrupting the bacterial cell membrane. We chose a representative surfactant from each of the four major charge-based classes of surfactants to investigate whether surfactant charge might lead to variability in their effectiveness due to natural variations in the OM of *Ng*. We tested the anionic surfactant sodium dodecyl sulfate (SDS), the cationic surfactant benzalkonium chloride (BAC), the non-ionic surfactant TERGITOL NP (TNP), and the zwitterionic surfactant 3-[(3-Cholamidopropyl)dimethylammonio]-1-propanesulfonate (CHAPS). Each of these

surfactant classes, with the exception of zwitterionic surfactants, have been well-studied for their ability to compromise the integrity of the cell envelope(*69*), but none have been used in the context of AST, or to change DNA accessibility on such short time scales. We chose to include the less well-studied zwitterionic surfactant CHAPS based on the diverse interactions of zwitterionic solutes with the bacterial cell envelope(*70*).

We tested each potential enhancer with respect to i) the degree of lysis caused by incubation with the enhancer alone, ii) the ability to differentiate PEN-S and PEN-R isolates using an enhancement step after exposure to PEN, and iii) the ability to differentiate CRO-S and CRO-R isolates using an enhancement step after exposure to CRO. We chose to use PEN and CRO because we expected that the degree of change in NA accessibility as a result of enhancement would depend on the type of β-lactam used during exposure. CRO and PEN bind and inhibit a different profile of penicillin-binding proteins(*40, 71*) and have different rates of killing(*72*), which we expected would lead to different effects depending on the enhancer. Each enhancer was tested using multiple isolates susceptible or resistant to either PEN or CRO. All enhancers were tested using a 5-min enhancement step after 15 min of ABX exposure. Antibiotic-exposure and enhancement steps were performed separately to decouple their effects on the *Ng* isolates.

Enhancers were first tested for the degree of lysis caused by a 5-min incubation with the enhancer alone (Fig. 3a-f). If the enhancement step lyses the majority of cells even without antibiotic exposure, then accessibility will increase in both control and treated aliquots, and any effect of the antibiotic will be diminished. We observed an average of < 50% lysis when testing all potential enhancers except BAC (Fig. 3d), which showed an average of 94% lysis across all eight isolates tested. We next measured the percentage accessibility when using each enhancer after a 15 min exposure to PEN. We evaluated the ability to differentiate PEN-S and PEN-R isolates based on the average percentage accessibility in S isolates (which we want to be large), the average percentage accessibility in R isolates (which we want to be small), and the magnitude of separation between those two values. Based on these criteria, Tris (Fig. 3h), TNP (Fig. 3k), and

CHAPS (Fig. 3l) were the most promising enhancers for differentiating PEN-S and PEN-R isolates after 15 min of exposure. However, we observed differences in accessibility in response to CRO compared with PEN depending on the enhancer used (Fig. 3m-r). Among CRO-S isolates, enhancement with TNP or CHAPS resulted in the largest average changes in accessibility. We were unable to observe consistently large changes in the seven tested CRO-S isolates using the other two ionic surfactants, SDS (Fig. 3i,o) and BAC (Fig. 3j,p), regardless of the ABX treatment. Following these tests, we chose CHAPS as the enhancer to use for validation of the nuc-aAST because it resulted in low percentage lysis, large increases in DNA accessibility for PEN-S and CRO-S isolates following exposure, and only small increases in the DNA accessibility of PEN-R and CRO-R isolates.

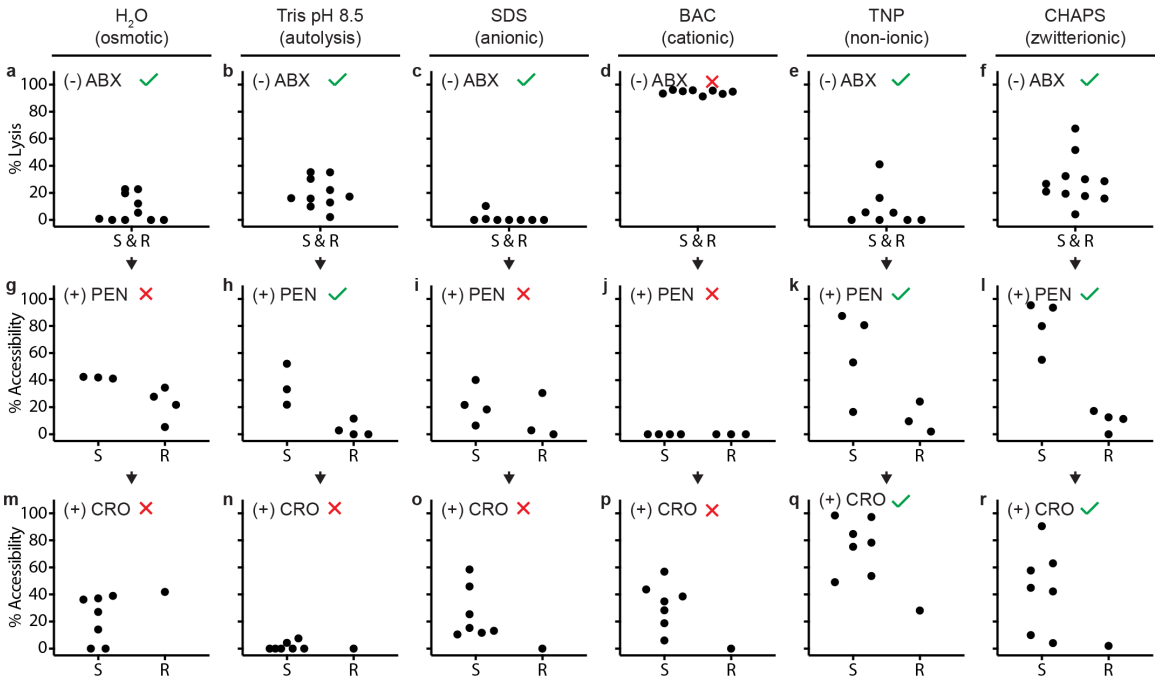

Fig. 6-3. Selection of enhancers. Six enhancers were tested for percentage of cell lysis due to enhancer alone (prior to antibiotic [ABX] exposure) (a-f), enhancement after exposure to penicillin (PEN) (g-l), and enhancement after exposure to ceftriaxone (CRO) (m-r). Each point represents the average of all biological replicates run for that condition.

Checkmarks indicate enhancers that met our criteria for inclusion in the nuc-aAST; X's indicate enhancers that did not meet our criteria.

Validation using clinical isolates

To validate the nuc-aAST we performed 34 ASTs (with multiple biological replicates each) using 13 clinical isolates of *Ng* exposed individually to PEN, CFM, or CRO for 15 min. We then compared the categorical susceptibility determined using the nuc-aAST to the susceptibility determined using gold-standard agar dilution (Fig. 4a-c). Receiver operating characteristic (ROC) plots(*73*) (not shown) were created so that the area under the curve (AUC) could be calculated for each β-lactam tested. After 15 min of exposure we obtained an AUC of 1.000 (PEN), 0.955 (CFM), and 1.000 (CRO). The AUC is determined by scanning a threshold through the ROC plot and measuring the sensitivity and specificity at each theoretical threshold value. This scanning allows one to select the threshold that would differentiate susceptible and resistant organisms with the maximum sensitivity and specificity within the given dataset. For example, an AUC of 1.000 indicates there was a threshold value that perfectly separated susceptible (S) and resistant (R) categories. However, AUC measurements do not consider the experimental noise or the magnitude of separation between S and R samples and should be applied with care to datasets with limited number of measurements, such as ours. For example, in the case of CFM, the difference between the two CFM-R isolates and the CFM-S isolates with the lowest responses (open circles in Fig. 4b) was small after 15 min of exposure, so setting the susceptibility threshold between them would be impractical. The same is true of setting a threshold between the single CRO-R isolate that was available to us and two CRO-S isolates with the lowest responses. We therefore set the thresholds for both these ABX at a more conservative 18% even though this threshold generates some errors (Fig. 4b,c; open circles) in the CFM and CRO measurements after 15 min of ABX exposure.

We then hypothesized that the differences observed in the magnitude of the response of the susceptible isolates after 15 min of exposure to each antibiotic, including the errors

observed when testing CFM and CRO (open points, Fig. 4b,c) could be the result of differences in how fast each β-lactam affects *Ng*(*72*). For example, a possible explanation for differences among isolates in their response to ABX could be phylogenetic differences(*74-76*). If isolates differ in their response times, a longer exposure would result in larger average separation between S and R isolates and potentially better categorical agreement if the S isolates were less-responsive as a result of a delayed response to antibiotic.

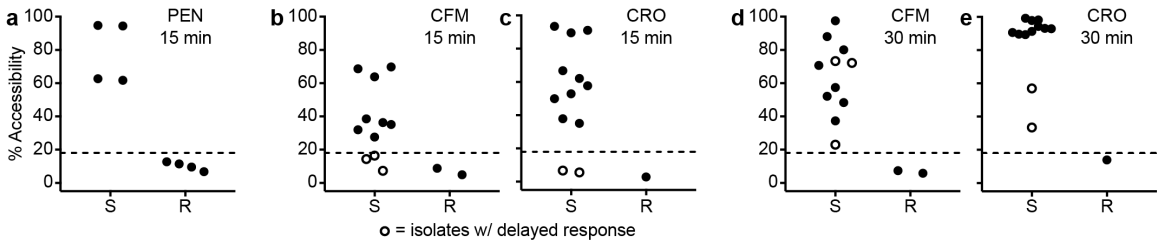

Figure 4. Validation of nuc-aAST using clinical isolates. (**a-c**) nuc-aAST results after 15 min of exposure to (**a**) penicillin (PEN), (**b**) cefixime (CFM), and (**c**) ceftriaxone (CRO). (**d-e**) nuc-aAST results after exposure to (**d**) CFM and (**e**) CRO for 30 min. All points represent the average percentage accessibility of single clinical isolates run in (at least) biological triplicate. Open points represent isolates that took longer than 15 min to respond to the β-lactam being tested. The dashed line represents the susceptibility threshold, which was set at 18% accessibility.

To test the hypothesis that there are inherent differences in isolate response time, we performed nuc-aAST using CFM and CRO with 30-min exposure times and, as predicted, we observed a larger average separation between S and R isolates and full categorical agreement with gold-standard agar dilution in all isolates. After 15 min of exposure to CFM and CRO, 73% and 83% of susceptible isolates, respectively, were classified as susceptible using nuc-aAST. After 30 min of exposure to CFM and CRO, 100% categorical agreement was obtained.

Sum-of-steps total time using contrived urine samples

To make a more realistic measure of total assay time, we modified the extraction and quantification steps of the nuc-aAST. The exposure and enhancement steps were performed as described above, but NA quantification was performed using a rapid, chip-based, digital loop-mediated isothermal amplification (dLAMP) method, as described previously(*77*). Additionally, we used a faster, single-step nucleic acid extraction method based on previous work(*46*). Both modifications made the workflow faster. Additionally, the high precision of digital quantification allowed us to make a susceptibility call as soon as there was a significant difference between the concentration of NAs in the control and treated aliquots.

We measured total assay time based on the sum of the steps of the nuc-aAST using contrived urine samples. Contrived samples mimic clinical urine samples and allowed us to better evaluate how the assay would perform in a clinical setting than assays performed with isolates in media. Samples were created using two PEN-S and two PEN-R isolates; one of the two PEN-R isolates was positive for β-lactamase activity, which we included in order to have PEN-R isolates with different mechanisms of resistance. To perform the AST, samples were first split into control and treated aliquots, and incubated at 37 °C for 15 min. Next the samples were transferred to the enhancement step, and incubated for 5 min in the presence of CHAPS. Samples were then extracted as described above and dLAMP was performed in commercial chips(*77*). Images were obtained in real time using a custom imaging system(*78*). LAMP quantification was performed using an automated data-analysis workflow in MATLAB(*77*) in which images are automatically processed and positive wells counted based on a digitized mask created from the final image (Fig. 5b). NA concentrations were used to determine percentage accessibility as soon as the measured NA concentrations in the susceptible sample became significantly different between the control and treated chips. All samples were tested in a total time (measured as the sum-of-steps) of 30 min and agreed with gold-standard agar dilution (Fig. 5c).

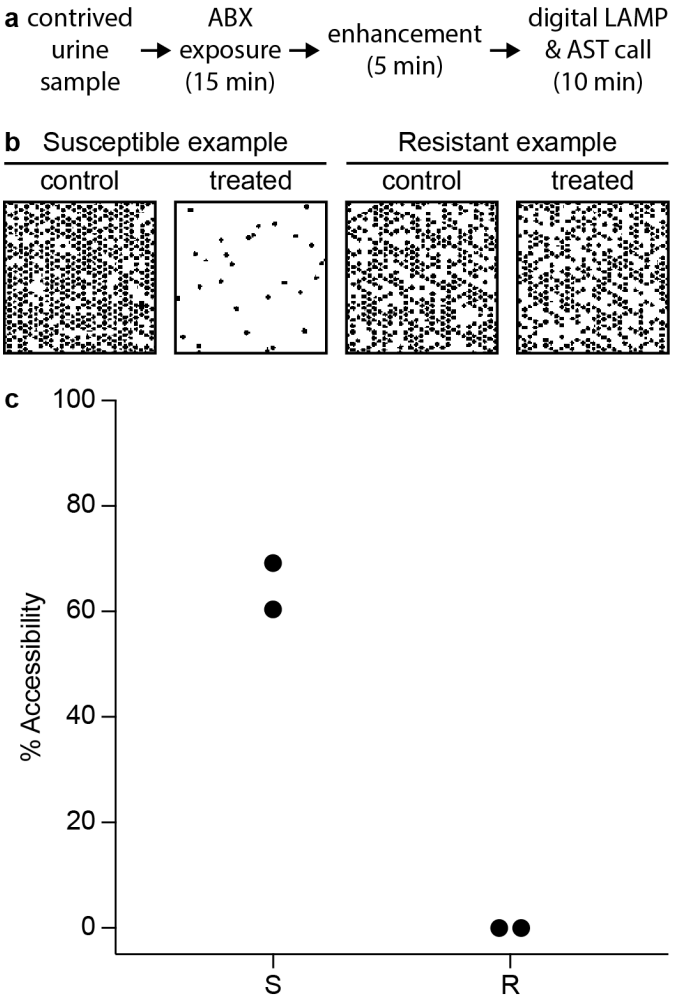

Fig. 6-5. The nuc-aAST workflow with each step timed. (a) The nuc-aAST workflow showing the time required for each step. (b) 2x2 mm subsection of masks created from chips used for performing digital LAMP (dLAMP) on control and treated aliquots of susceptible and resistant samples; as an illustration, each mask shows ~625 wells (out of ~20,000 total wells) after 10 min of amplification. Wells that showed amplification of *Ng* DNA appear black. (c) Percentage accessibility determined at earliest significance (<7 minutes of amplification, see Methods) for two susceptible and two resistant samples run using dLAMP. Each step was timed individually and the sum-of-steps of the assay was 30 min for PEN.

Discussion

Here we described a new approach—nuc-aAST—to enable developing a critically needed rapid phenotypic AST for the globally-important pathogen *Neisseria gonorrhoeae*. We show that by measuring the change in the accessibility of DNA after 15 or 30 min β-lactam exposure, the nuc-aAST yields a phenotypic susceptibility readout in less than 1 hour, as opposed to the currently available methods which require hours to days. We further show that the nuc-aAST breaks the current speed limits for nucleic-acid-based phenotypic ASTs using β-lactams (which do not directly impact NAs) by using an innovative approach: coupling cell wall damage to NA readout. The nuc-aAST thus provides a new approach for designing rapid phenotypic ASTs with NA-based readouts for ABX that impact cell envelope integrity. Overall, we envision that leveraging the nuc-aAST and combining it with other creative biological and chemical insights will result in similarly innovative approaches for other important antibiotic classes for *Ng*, such as protein-biosynthesis inhibitors like tetracycline and azithromycin. Existing NA-based approaches, such as those for ciprofloxacin(*23, 51*), can also be combined alongside the nuc-aAST.

We found that phenotypic ASTs that use NA accessibility as a readout benefit from the use of a carefully chosen enhancer. Here, the enhancement step consisted of a surfactant (CHAPS) that enabled detection of cell wall damage faster than cell division. Without the enhancement step, the cell envelope remains intact longer, so measurements of accessibility approximate the timescale of cell division (Fig. 2), which, for fastidious organisms such as *Ng,* will be too slow for POC applications. The increase in DNA accessibility in S isolates will differ based on the combination of β-lactam used and enhancer, highlighting the importance of testing multiple β-lactams with the nuc-aAST. Of the surfactants tested as enhancers, the charge-neutral surfactants TNP and CHAPS gave better results than the ionic surfactants SDS and BAC, suggesting that charge may be an important factor when designing an effective enhancement step. We also anticipate organism-specific OM chemistry and general stress responses will play a role in determining which enhancers are optimal in other organisms.

We found that for PEN, susceptibility of *Ng* could be determined after just 15 min of exposure in all isolates tested (Fig. 4a). However, for CFM and CRO, a small number of S isolates did not respond after 15 min of exposure but responded after 30 min exposure (Fig. 4b-e). We hypothesize that CFM and CRO required a longer exposure than PEN because of their differences in binding kinetics and rates of killing(*71, 72, 79*). Despite these differences, an actionable susceptibility call (i.e. determining that an isolate is susceptible to a particular ABX and therefore can be treated with that ABX) could still be made for most isolates after 15 min of exposure (100% using PEN, 77% using CFM, and 85% of cases using CRO). One approach to balance reducing assay time with minimizing errors is to perform two exposures in parallel for each ABX. The first exposure would be analyzed after 15 minutes. If a response is obtained indicating that the pathogen is susceptible (which should be the case for the majority of patients), the second exposure would be discarded. If no response or if an equivocal response is obtained, then the second exposure (after 30 min total) would be analyzed to provide the definitive susceptibility call. With this approach, the test would provide the answer after 15 min of ABX exposure for the majority of patients, and only a few patients would be delayed by the additional 15 min of ABX exposure.

Several limitations will need to be overcome in order to translate the nuc-aAST approach to an automated and distributable system. First, in this paper we used clinical isolates and contrived urine samples. Although contrived samples are a good proxy for clinical samples and are accepted by the U.S. Food and Drug Administration in certain cases(*80*), the nuc-aAST should be validated with fresh clinical samples. It remains to be tested whether the enhancer chemistry has to be modified to account for the presence of host-derived cells and metabolites that might interfere with the assay. Second, future work should test more *Ng* isolates with diverse phylogeny(*74-76*) as they are made available to researchers and characterized, as well as test isolates with intermediate resistance to PEN, CFM, and CRO. These efforts could also aim to establish a correlation in the magnitude of nuc-aAST response and minimum inhibitory concentration (MIC) of ABX, which

would provide even more detailed information at the POC. Third, in timing the sum-of-steps, we did not include handling time; future work should include optimization of handling steps and timed sample-to-answer experiments. Finally, the nuc-aAST method will need to be translated to a POC device so that larger-scale clinical evaluations can be performed. Devices for multiplexed digital quantification(*81-83*) have been demonstrated and would be useful in performing nuc-aAST for multiple ABX in parallel.

We envision that nuc-aAST would be deployed in combination with two complementary technologies: (i) the pathogen ID technologies that are being developed by others(*18, 19, 21, 22*) to identify *Ng*-positive samples that require an AST, and (ii) rapid genotypic and/or phenotypic ASTs that rely on NA readouts for other ABX used in the treatment of *Ng*, including fluoroquinolones (ciprofloxacin)(*23, 46, 75*) and protein synthesis inhibitors (tetracycline and azithromycin)(*75*). Assuming these two complementary technologies are developed and validated, further development of nuc-aAST would provide the last—and we would argue the most challenging—piece needed for a complete rapid ID/AST workflow for *Ng* based on NA readout. We chose NA readout for the nuc-aAST for two reasons. First, NA readouts will enable easy integration with pathogen ID and other NA-based AST technologies. Second, NA readouts are organism-specific[*46*], and therefore should be effective even for mixed microbial populations potentially present in clinical samples (e.g., *Ng* in the presence of commensals or other pathogens).

Implementation of a rapid phenotypic AST would dramatically improve the antibiotic stewardship of *Ng* infections and therefore impact the health of people who are infected with *Ng*; currently, there are an estimated 78,000,000 global cases of *Ng* every year(*2*). Furthermore, the nuc-aAST approach provides a framework for developing additional accessibility-based AST chemistries for other pathogens that pose global health threats but have been challenging for current phenotypic AST methods. For example, we have shown that quantifying NA accessibility to polymerases can be used to rapidly determine ABX susceptibility in Enterobacteriacea(*84*). Overall, this work highlights the diagnostic

capabilities that can be attained by developing innovative NA-based assays for AST; further expansion and application of these approaches is critically needed to address the crisis posed by antibiotic-resistant bacteria.

Materials and Methods

Isolates and agar-dilution MIC testing. Isolates were provided by the University of Washington Neisseria Reference Laboratory. MICs were determined by agar dilution according to the Clinical and Laboratory Standards Institute (CLSI) guidelines(*86*).

Reagents and culture media. BD BBL Chocolate II Agar prepared plated media (GC II Agar, with Hemoglobin and BD IsoVitaleX) was purchased from VWR International LLC (VWR, Radnor, PA, USA). Graver-Wade Medium (GWM) was prepared as described previously(*87*). Cation-adjusted Mueller Hinton II Broth (MHB) (BD, Franklin Lakes, NJ, USA) was prepared according to manufacturer instructions. All sodium bicarbonate ($NaHCO_3$) (Sigma, St. Louis, MO, USA) and calcium chloride ($CaCl_2$) (Fisher Scientific, Hampton, NH, USA) stocks were dissolved in nuclease-free water (NF-H_2O) and sterilized using 0.2-µm filters. DNase I (2000 U/mL) was obtained from New England Biolabs (NEB, Ipswich, MA, USA). Normal urine from pooled human donors was purchased from Lee Biosolutions (Maryland Heights, MO, USA) and filtered through 0.2-µM filters before use.

Antibiotic stocks were prepared and stored as single-use aliquots at -80 °C. Aliquots were thawed once and diluted in NF-H_2O before use. PEN (1 mg/mL) was prepared from penicillin G sodium salt (Sigma, St. Louis, MO, USA) in NF-H_2O. CRO (1 mg/mL) was prepared from ceftriaxone disodium salt hemi(heptahydrate) (Sigma) in NF-H_2O. CFM (5 mg/mL) was prepared from cefixime trihydrate (Sigma) in DMSO.

Unless otherwise noted, enhancer stock solutions were prepared in NF-H_2O and stored at room temperature. Tris buffer (500 mM; pH 8.5 at 37 °C) was prepared according to the

Sigma buffer reference tables(*88*) using 0.2-µm filter sterilized stocks of 1 M Tris-HCl (Sigma) and 1 M Tris base (Fisher Scientific) prepared in milliQ H_2O. TNP HLB 13.1 (100 mM) was prepared by mixing 334 µL 100 mM Tergitol NP-9 (Sigma) + 666 µL 100 mM Tergitol NP-10 (Sigma). CHAPS (200 mM) was prepared from CHAPS solid powder (Sigma). 0.1% sodium dodecyl sulfate (SDS) was prepared by diluting 10% SDS (Invitrogen, Carlsbad, CA, USA). BAC (10%) was prepared from benzalkonium chloride solid powder (MP Biomedicals, Santa Ana, CA, USA).

Nucleic acid quantification. Quantitative PCR (qPCR) was performed using ssoFast EvaGreen Supermix (BioRad, Hercules, CA, USA) in 10 µL reactions with 500 nM primers targeting the *Ng* 16S gene(*89*). DNA template composed 10% of the reaction volume. Cycling conditions consisted of 3.0 min at 95 °C, followed by 35 cycles of 15 sec at 95 °C, 15 sec at 62 °C, and 20 sec at 72 °C. All qPCR was performed on either a Roche LightCycler 96 or BioRad CFX96 instrument. The Cq values obtained from qPCR are used to compute the percentage accessibility and percentage lysis as described in the equations below. Any negative percentages were set to 0 for all analyses.

$$(1)\ \%\ Accessibility\ (control\ and\ treated) = \left((1 - 2^{(Cq_{control} - Cq_{treated})}\right) \times 100$$

$$(2)\ \%\ Lysis\ (no\ enhancer\ and\ enhancer) = \left((1 - 2^{(Cq_{no\ enhancer} - Cq_{enhancer})}\right) \times 100$$

Droplet digital PCR (ddPCR) was performed using QX200 ddPCR Supermix for EvaGreen (BioRad, Hercules, CA, USA) with the same primers and primer concentrations used in qPCR. DNA template composed 10% of the reaction volume. Cycling conditions consisted of 5.0 min at 95 °C, followed by 40 cycles of 30 sec at 95 °C, 30 sec at 60 °C, and 30 sec at 72 °C, followed by a droplet stabilization step of 4 °C for 5 min, and 95 °C for 5 min. Calculations of percentage accessibility and percentage lysis for ddPCR are given the equations below, where λ represents template concentration in copies/µL. The template concentrations are used to compute percentage accessibility

and percentage lysis as described in the equations below. Any negative percentages were set to 0 for all analyses.

$$(3)\ \%\ Accessibility\ (control\ and\ treated) = (1 - (\lambda_{treated}/\lambda_{control})) \times 100$$

$$(4)\ \%\ Lysis\ (no\ enhancer\ and\ enhancer) = (1 - (\lambda_{enhancer}/\lambda_{no\ enhancer})) \times 100$$

A dLAMP assay was performed using a previously published system(*77*). The dLAMP mix consisted of 1 µL NEB Isothermal Amplification Buffer (200 mM Tris-HCl, 20 mM $MgSO_4$, 500 mM KCl, 100 mM $(NH_4)_2SO_4$, 1% Tween 20, pH 8.8), 0.6 µL $MgSO_4$, 0.5 µL BSA (20 mg/mL), 0.4 µL Syto-9 (50 µM, prepared within two weeks of use), 1.4 µL dNTPs (10 mM each), 0.5 µL 20X primer mix, 0.4 µL NEB Bst 2.0 WarmStart, 0.2 µL Ambion RNase cocktail, 4.0 µL NF-H_2O, and 1 µL of template. Primers were designed to target the *Ng* 16S gene, and screened as described previously(*46*). Primer sequences used are as follows, with the final concentration in the amplification mix in parentheses: GCGGTGGATGATGTGGATT (forward outer primer, 0.2 µM), CCGGCAGTCTCATTAGAGTG (backward outer primer, 0.2 µM), CTCCTCCGTCTCCGGAGGATTCaaaaCGATGCAACGCGAAGAAC (forward inner primer, 1.6 µM), TCGTCAGCTCGTGTCGTGAGATttttCCCAACCGAATGATGGCA (backward inner primer, 1.6 µM), CGCACATGTCAAAACCAGG (forward loop primer, 0.4 µM), and GCAACGAGCGCAACCC (reverse loop primer, 0.4 µM). The following equation was used to compute percentage accessibility, where λ represents the template NA concentration in copies/µL as measured by dLAMP.

$$(5)\ \%\ Accessibility\ (control\ and\ treated) = (1 - (\lambda_{treated}/\lambda_{control})) \times 100$$

***Ng* culture preparation.** Isolates were streaked from glycerol stocks stored at -80 °C onto BD BBL Chocolate II Agar plates and incubated overnight in a 37 °C incubator with 5% CO_2. Isolates were then passed onto fresh BD BBL Chocolate II Agar plates and grown for 4-7 h at 37 °C with 5% CO_2. In all experiments, cells from plates passed 1-3

times were used. Several colonies were scraped and resuspended in 37 °C GWM to generate a working suspension. Optical density at 600 nm (OD_{600}) was measured, and the working suspension was diluted to create a 2 mL working culture of OD_{600} 0.05 in GWM in 15 mL polypropylene culture tubes. Cultures were incubated, with 500 rpm shaking, at 37 °C + 5% CO_2 for 3-5 h prior to ABX exposure.

nuc-aAST time-course without enhancing step. Working cultures of *Ng* isolates were prepared as described in "*Ng* culture preparation." Incubation at 37 °C was performed in 100 µL reaction volumes in PCR tube strips on a BioRad C1000 Thermal Cycler. Treated samples consisted of 77.5 µL MHB, 2.5 µL $NaHCO_3$ (200 mM), 5 µL DNase I (2 U/µL), 5 µL PEN (20 µg/mL), and 10 µL working *Ng* isolate culture. PEN was replaced with NF-H_2O in control samples. A 10 µL aliquot of each sample was extracted at 15, 30, 45, 60, 90, and 120 min and diluted 10X in QuickExtract DNA Extraction Solution (Lucigen, Middleton, WI, USA), then heated for 6 min at 65 °C followed by 4 min at 98 °C on a BioRad C1000 Thermal Cycler. All sample handling following antibiotic exposure was performed using a multichannel pipette; qPCR and calculation of % accessibility were performed as described above.

Enhancer use. Working cultures of *Ng* isolates were prepared as described in "*Ng* culture preparation." Initial exposure was performed by incubating 100 µL control and treated samples at 37 °C in PCR tube strips on a BioRad C1000 Thermal Cycler. Treated samples consisted of 75 µL MHB, 5 µL $NaHCO_3$ (100 mM), 5 µL DNase I (2 U/µL), 5 µL PEN or CRO (20 µg/mL), and 10 µL working *Ng* isolate culture. ABX were replaced with NF-H_2O in control samples. After 15 min of incubation, samples were vortexed and quick-spun, and aliquots of all samples were transferred to the enhancement step as described below. After the enhancement step, 5 or 10 µL of all samples were extracted by diluting 10X in QuickExtract DNA Extraction Solution (Lucigen) and heating for 6 min at 65 °C followed by 4 min at 98 °C on a BioRad C1000 Thermal Cycler. All sample handling following ABX exposure was performed using a multichannel pipette; qPCR and calculation of % accessibility was performed as described above.

Osmotic and autolytic enhancing steps were performed in 100 µL volumes. The osmotic enhancing step consisted of 89.75 µL NF-H_2O, 4.75 µL DNase I (2 U/uL), 0.5 µL $CaCl_2$ (100 mM, 0.2-µM filtered), and 5 µL initial exposure samples. The autolytic enhancing step consisted of 75 µL NF-H_2O, 4.75 µL $NaHCO_3$ (100 mM, 0.2-µM filtered), 10 µL Tris pH 8.5 (500 mM), 4.75 µL DNase I (2 U/uL), 0.5 µL $CaCl_2$ (100 mM), and 5 µL of the sample exposed to antibiotic.

All surfactant-enhancing steps were performed in 50 µL volumes with 25 of the 50 µL consisting of initial exposure samples. In the TNP enhancement step, the remaining 25 µL consisted of 1.25 µL DNase I (2 U/uL), 1.25 µL $NaHCO_3$ (100 mM), 20 µL MHB, and 2.5 µL TNP (100 mM). In the CHAPS enhancement step, the remaining 25 µL consisted of 1.25 µL DNase I (2 U/uL), 1.25 µL $NaHCO_3$ (100 mM), 20 µL MHB, and 2.5 µL CHAPS (200 mM). In the SDS and BAC enhancement steps, the remaining 25 µL consisted of 1.25 µL DNase I (2 U/uL), 1.25 µL $NaHCO_3$ (100 mM), 17.5 µL MHB, and either 5 µL SDS (1% w/v) or BAC (1% w/v) respectively.

Nuclease-accessibility AST validation. Working cultures were prepared, exposed to ABX, and enhancing steps performed as described for the CHAPS enhancement step in the "enhancer selection" section above. Extraction was performed as described above. Treated samples in the initial exposure step had a final concentration of 1.0 µg/mL PEN, CFM, or CRO. Samples were excluded if the percent lysis (equation 2) due to CHAPS was > 75%. Three to ten biological replicates were performed for each isolate-antibiotic combination. Biological replicates included separate antibiotic exposure, control exposure, and no-enhancer controls.

Timed sum-of-steps. Working cultures of *Ng* isolates used in Fig. 4 were prepared as described in "*Ng* culture preparation" and 1.5 mL of the cultures were pelleted at 2500 g for 2.5 min and resuspended in 150 µL normal human urine (Lee Biosciences) pre-warmed to 37 °C. Initial exposure was performed by incubating 100 µL control and

treated samples at 37 °C in PCR tube strips on a BioRad C1000 Thermal Cycler. Treated samples consisted of 65 µL MHB, 5 µL $NaHCO_3$ (100 mM), 5 µL DNase I (2 U/µL), 5 µL PEN (20 µg/mL), and 20 µL *Ng* isolate suspension in urine. NF-H_2O was used in place of PEN in control samples. A CHAPS enhancing step was performed as described above. After the enhancement step, a 20 µL aliquot from each sample was extracted by diluting 5X in QuickExtract DNA Extraction Solution (Lucigen) and heated for 1 min at 65 °C followed by 1 min at 98 °C on a BioRad C1000 Thermal Cycler. All sample handling following ABX exposure was performed using a multichannel pipette. Amplification was then performed using qPCR, ddPCR, or dLAMP. Extractions were diluted 2.5X in NF-H_2O before use in dLAMP.

Osmolarity measurements. Osmolarity measurements were performed on a Model 3320 Osmometer (Advanced Instruments Inc., Norwood, MA, USA). The instrument was calibrated with reference standards (Advanced Instruments) prior to experiments. Samples identical to the antibiotic-exposure condition (i.e., media, nuclease, etc.) and samples identical to the osmotic enhancing condition were prepared and measured. The volume that would normally be comprised of Ng culture was replaced with media.

Statistical analysis. *P*-values for Fig. 2 were calculated using GraphPad Prism 8.0 software from an unpaired, two-tailed t-test comparing the averages of the three replicates of each susceptible sample to each resistant sample. A significance value of 0.02 was used for statistical significance. ROC plots used for setting susceptibility thresholds in Fig. 4 were created using GraphPad Prism 8.0 software. Sensitivity was defined as the proportion of gold-standard susceptible samples correctly identified as susceptible by the nuc-aAST. Specificity was defined as the proportion of gold-standard resistant samples correctly identified as resistant by the nuc-aAST. Statistical analyses for Fig. 5, (dLAMP measurements) were performed as published previously(*46, 90*). As in our previous publication(*46*), the control and treated concentrations are compared as a ratio for statistical analysis.

$$(6)\ Concentration\ Ratio = \frac{\lambda_{control}}{\lambda_{treated}}$$

This concentration ratio is transformed into a percentage change for visualization purposes, but the ratio is assessed for statistical significance. Poisson statistics were used to calculate the confidence interval of the NA concentration for each measurement(*90*). The error in the concentration ratio, a term used in the calculation of percentage accessibility, is calculated with standard-error propagation methods:

$$(7)\ \sigma_{ratio} = \sqrt{\left(\frac{\sigma_{\lambda_2}}{\lambda_1}\right)^2 + \left(\frac{\lambda_2 \cdot \sigma_{\lambda_1}}{\lambda_1^2}\right)^2}$$

A one-tailed Z-test, assuming a normal distribution, is used to calculate *p*-values for digital NA concentrations. A threshold value for significance is set as a ratio of 1.22, corresponding to a percentage accessibility of 18%.

$$(8)\ Z = \frac{\ln(\lambda_{control}) - \ln(1.22\ \lambda_{treated})}{\sqrt{\sigma^2 \ln(\lambda_{control}) + \sigma^2 \ln(\lambda_{treated})}}$$

A significance value of 0.05 was used for statistical significance. The *p*-values to determine significance in dLAMP experiments were computed using Microsoft Excel's standard normal cumulative distribution function and Z-value.

References

1. CDC, Sexually Transmitted Disease Surveillance. (2017) https://www.cdc.gov/std/stats17/default.htm

2. L. Newman, J. Rowley, S. Vander Hoorn, N. S. Wijesooriya, M. Unemo, N. Low, G. Stevens, S. Gottlieb, J. Kiarie, M. Temmerman, Global estimates of the prevalence and incidence of four curable sexually transmitted infections in 2012 based on systematic review and global reporting. *PLoS One* **10**, e0143304 (2015).

3. S. J. Quillin, H. S. Seifert, Neisseria gonorrhoeae host adaptation and pathogenesis. *Nat. Rev. Microbiol.* **16**, 226-240 (2018).

4. H. W. Chesson, R. D. Kirkcaldy, T. L. Gift, K. Owusu-Edusei, Jr., H. S. Weinstock, An illustration of the potential health and economic benefits of combating antibiotic-resistant gonorrhea. *Sex. Transm. Dis.* **45**, 250-253 (2018).

5. CDC, Sexually Transmitted Diseases Treatment Guidelines: Morbidity and Mortality Weekly Report. (2015) https://www.cdc.gov/std/tg2015/tg-2015-print.pdf

6. WHO, WHO Guidelines for the treatment of Neisseria gonorrhoeae. (2016) https://www.who.int/reproductivehealth/publications/rtis/gonorrhoea-treatment-guidelines/en/

7. L. M. Newman, J. S. Moran, K. A. Workowski, Update on the management of gonorrhea in adults in the United States. *Clin. Infect. Dis.* **44 Suppl 3**, S84-101 (2007).

8. WHO, Antimicrobrial Resistance in Neisseria gonorrhoeae. (2001) https://www.who.int/csr/resources/publications/drugresist/Neisseria_gonorrhoeae.pdf

9. H. Fifer, U. Natarajan, L. Jones, S. Alexander, G. Hughes, D. Golparian, M. Unemo, Failure of Dual Antimicrobial Therapy in Treatment of Gonorrhea. *N. Engl. J. Med.* **374**, 2504-2506 (2016).

10. D. M. Whiley, A. Jennison, J. Pearson, M. M. Lahra, Genetic characterisation of Neisseria gonorrhoeae resistant to both ceftriaxone and azithromycin. *Lancet Infect. Dis.* **18**, 717-718 (2018).

11. D. W. Eyre, N. D. Sanderson, E. Lord, N. Regisford-Reimmer, K. Chau, L. Barker, M. Morgan, R. Newnham, D. Golparian, M. Unemo, D. W. Crook, T. E. Peto, G. Hughes, M. J. Cole, H. Fifer, A. Edwards, M. I. Andersson, Gonorrhoea treatment failure caused by a Neisseria gonorrhoeae strain with combined ceftriaxone and high-level azithromycin resistance, England, February 2018. *Euro Surveill.* **23**, (2018).

12. CDC, Antibiotic Resistance Threats in the United States. (2013) https://www.cdc.gov/drugresistance/pdf/ar-threats-2013-508.pdf

13. WHO, Global Priority List of Antibiotic-resistant Bacteria to Guide Research, Discovery, and Development of New Antibiotics. (2017)

https://www.who.int/medicines/publications/global-priority-list-antibiotic-resistant-bacteria/en/

14. G. A. Bolan, P. F. Sparling, J. N. Wasserheit, The emerging threat of untreatable gonococcal infection. *N. Engl. J. Med.* **366**, 485-487 (2012).

15. T. Wi, M. M. Lahra, F. Ndowa, M. Bala, J. R. Dillon, P. Ramon-Pardo, S. R. Eremin, G. Bolan, M. Unemo, Antimicrobial resistance in Neisseria gonorrhoeae: Global surveillance and a call for international collaborative action. *PLoS Med.* **14**, e1002344 (2017).

16. WHO, Global Action Plan to Control the Spread of and Impact of Antimicrobial Resistance in Neisseria gonorrhoeae. (2012) https://www.who.int/reproductivehealth/publications/rtis/9789241503501/en/

17. E. J. Weston, T. Wi, J. Papp, Strengthening Global Surveillance for Antimicrobial Drug-Resistant Neisseria gonorrhoeae through the Enhanced Gonococcal Antimicrobial Surveillance Program. *Emerg. Infect. Dis.* **23**, S47-52 (2017).

18. F. Rahimi, N. Goire, R. Guy, J. M. Kaldor, J. Ward, M. D. Nissen, T. P. Sloots, D. M. Whiley, Direct urine polymerase chain reaction for chlamydia and gonorrhoea: a simple means of bringing high-throughput rapid testing to remote settings? *Sex Health* **10**, 299-304 (2013).

19. S. Cho, T. S. Park, T. G. Nahapetian, J. Y. Yoon, Smartphone-based, sensitive microPAD detection of urinary tract infection and gonorrhea. *Biosens. Bioelectron.* **74**, 601-611 (2015).

20. J. S. Gootenberg, O. O. Abudayyeh, M. J. Kellner, J. Joung, J. J. Collins, F. Zhang, Multiplexed and portable nucleic acid detection platform with Cas13, Cas12a, and Csm6. *Science* **360**, 439-444 (2018).

21. binx, io system for clinical point of care. (2018) https://mybinxhealth.com/clinical-poc/

22. C. A. Gaydos, B. Van Der Pol, M. Jett-Goheen, M. Barnes, N. Quinn, C. Clark, G. E. Daniel, P. B. Dixon, E. W. Hook, 3rd, C. N. S. Group, Performance of the Cepheid CT/NG Xpert Rapid PCR Test for Detection of Chlamydia trachomatis and Neisseria gonorrhoeae. *J. Clin. Microbiol.* **51**, 1666-1672 (2013).

23. L. T. Allan-Blitz, X. Wang, J. D. Klausner, Wild-Type Gyrase A Genotype of Neisseria gonorrhoeae Predicts In Vitro Susceptibility to Ciprofloxacin: A Systematic Review of the Literature and Meta-Analysis. *Sex. Transm. Dis.* **44**, 261-265 (2017).

24. Z. Li, S. Yokoi, Y. Kawamura, S. Maeda, T. Ezaki, T. Deguchi, Rapid detection of quinolone resistance-associated gyrA mutations in Neisseria gonorrhoeae with a LightCycler. *J. Infect. Chemother.* **8**, 145-150 (2002).

25. S. Balashov, E. Mordechai, M. E. Adelson, S. E. Gygax, Multiplex bead suspension array for screening Neisseria gonorrhoeae antibiotic resistance genetic determinants in noncultured clinical samples. *J. Mol. Diagn.* **15**, 116-129 (2013).

26. V. Dona, J. H. Smid, S. Kasraian, D. Egli-Gany, F. Dost, F. Imeri, M. Unemo, N. Low, A. Endimiani, Mismatch Amplification Mutation Assay-Based Real-Time PCR for Rapid Detection of Neisseria gonorrhoeae and Antimicrobial Resistance Determinants in Clinical Specimens. *J. Clin. Microbiol.* **56**, (2018).

27. C. Buckley, E. Trembizki, B. Donovan, M. Chen, K. Freeman, R. Guy, M. M. Lahra, R. L. Kundu, D. G. Regan, H. V. Smith, D. M. Whiley, I. Gonorrhoea Resistance Assessment by Nucleic Acid Detection Study, Real-time PCR detection of Neisseria gonorrhoeae susceptibility to penicillin. *J. Antimicrob. Chemother.* **71**, 3090-3095 (2016).

28. L. K. Wong, P. Hemarajata, O. O. Soge, R. M. Humphries, J. D. Klausner, Real-Time PCR Targeting the penA Mosaic XXXIV Type for Prediction of Extended-Spectrum-Cephalosporin Susceptibility in Clinical Neisseria gonorrhoeae Isolates. *Antimicrob. Agents Chemother.* **61**, (2017).

29. J. Davies, D. Davies, Origins and evolution of antibiotic resistance. *Microbiol. Mol. Biol. Rev.* **74**, 417-433 (2010).

30. CDC, Agar Dilution Antimicrobial Susceptibility Testing. (2013) https://www.cdc.gov/std/gonorrhea/lab/agar.htm

31. S. Foerster, V. Desilvestro, L. J. Hathaway, C. L. Althaus, M. Unemo, A new rapid resazurin-based microdilution assay for antimicrobial susceptibility testing of Neisseria gonorrhoeae. *J. Antimicrob. Chemother.* **72**, 1961-1968 (2017).

32. V. Singh, M. Bala, M. Kakran, V. Ramesh, Comparative assessment of CDS, CLSI disc diffusion and Etest techniques for antimicrobial susceptibility testing of Neisseria gonorrhoeae: a 6-year study. *BMJ Open* **2**, e000969 (2012).
33. M. J. Siedner, M. Pandori, L. Castro, P. Barry, W. L. Whittington, S. Liska, J. D. Klausner, Real-time PCR assay for detection of quinolone-resistant Neisseria gonorrhoeae in urine samples. *J. Clin. Microbiol.* **45**, 1250-1254 (2007).
34. S. T. Sadiq, F. Mazzaferri, M. Unemo, Rapid accurate point-of-care tests combining diagnostics and antimicrobial resistance prediction for Neisseria gonorrhoeae and Mycoplasma genitalium. *Sex. Transm. Infect.* **93**, S65-S68 (2017).
35. S. M. Fingerhuth, N. Low, S. Bonhoeffer, C. L. Althaus, Detection of antibiotic resistance is essential for gonorrhoea point-of-care testing: a mathematical modelling study. *BMC Med.* **15**, 142 (2017).
36. A. R. Tuite, T. L. Gift, H. W. Chesson, K. Hsu, J. A. Salomon, Y. H. Grad, Impact of Rapid Susceptibility Testing and Antibiotic Selection Strategy on the Emergence and Spread of Antibiotic Resistance in Gonorrhea. *J. Infect. Dis.* **216**, 1141-1149 (2017).
37. K. M. Turner, H. Christensen, E. J. Adams, D. McAdams, H. Fifer, A. McDonnell, N. Woodford, Analysis of the potential for point-of-care test to enable individualised treatment of infections caused by antimicrobial-resistant and susceptible strains of Neisseria gonorrhoeae: a modelling study. *BMJ Open* **7**, e015447 (2017).
38. R. D. Kirkcaldy, A. Harvey, J. R. Papp, C. Del Rio, O. O. Soge, K. K. Holmes, E. W. Hook, 3rd, G. Kubin, S. Riedel, J. Zenilman, K. Pettus, T. Sanders, S. Sharpe, E. Torrone, Neisseria gonorrhoeae Antimicrobial Susceptibility Surveillance - The Gonococcal Isolate Surveillance Project, 27 Sites, United States, 2014. *MMWR Surveill. Summ.* **65**, 1-19 (2016).
39. R. D. Kirkcaldy, M. G. Bartoces, O. O. Soge, S. Riedel, G. Kubin, C. Del Rio, J. R. Papp, E. W. Hook, 3rd, L. A. Hicks, Antimicrobial Drug Prescription and Neisseria gonorrhoeae Susceptibility, United States, 2005-2013. *Emerg. Infect. Dis.* **23**, 1657-1663 (2017).

40. V. G. Allen, L. Mitterni, C. Seah, A. Rebbapragada, I. E. Martin, C. Lee, H. Siebert, L. Towns, R. G. Melano, D. E. Low, Neisseria gonorrhoeae treatment failure and susceptibility to cefixime in Toronto, Canada. *JAMA* **309**, 163-170 (2013).

41. A. R. Katz, A. Y. Komeya, R. D. Kirkcaldy, A. C. Whelen, O. O. Soge, J. R. Papp, E. N. Kersh, G. M. Wasserman, N. P. O'Connor, P. S. O'Brien, D. T. Sato, E. V. Maningas, G. Y. Kunimoto, J. E. Tomas, Cluster of Neisseria gonorrhoeae Isolates With High-level Azithromycin Resistance and Decreased Ceftriaxone Susceptibility, Hawaii, 2016. *Clin. Infect. Dis.* **65**, 918-923 (2017).

42. J. R. Papp, A. J. Abrams, E. Nash, A. R. Katz, R. D. Kirkcaldy, N. P. O'Connor, P. S. O'Brien, D. H. Harauchi, E. V. Maningas, O. O. Soge, E. N. Kersh, A. Komeya, J. E. Tomas, G. M. Wasserman, G. Y. Kunimoto, D. L. Trees, A. C. Whelen, Azithromycin Resistance and Decreased Ceftriaxone Susceptibility in Neisseria gonorrhoeae, Hawaii, USA. *Emerg. Infect. Dis.* **23**, 830-832 (2017).

43. L. J. Piddock, Assess drug-resistance phenotypes, not just genotypes. *Nat Microbiol* **1**, 16120 (2016).

44. J. M. Hicks, R. Haeckel, C. P. Price, K. Lewandrowski, A. H. B. Wu, Recommendations and opinions for the use of point-of-care testing for hospitals and primary care: summary of a 1999 symposium. *Clin. Chim. Acta* **303**, 1-17 (2001).

45. H. D. Marston, D. M. Dixon, J. M. Knisely, T. N. Palmore, A. S. Fauci, Antimicrobial Resistance. *JAMA* **316**, 1193-1204 (2016).

46. N. G. Schoepp, T. S. Schlappi, M. S. Curtis, S. S. Butkovich, S. Miller, R. M. Humphries, R. F. Ismagilov, Rapid pathogen-specific phenotypic antibiotic susceptibility testing using digital LAMP quantification in clinical samples. *Sci. Transl. Med.* **9**, (2017).

47. A. Mezger, E. Gullberg, J. Goransson, A. Zorzet, D. Herthnek, E. Tano, M. Nilsson, D. I. Andersson, A general method for rapid determination of antibiotic susceptibility and species in bacterial infections. *J. Clin. Microbiol.* **53**, 425-432 (2015).

48. K. E. Mach, R. Mohan, E. J. Baron, M. C. Shih, V. Gau, P. K. Wong, J. C. Liao, A biosensor platform for rapid antimicrobial susceptibility testing directly from clinical samples. *J. Urol.* **185**, 148-153 (2011).

49. C. Halford, R. Gonzalez, S. Campuzano, B. Hu, J. T. Babbitt, J. Liu, J. Wang, B. M. Churchill, D. A. Haake, Rapid antimicrobial susceptibility testing by sensitive detection of precursor rRNA using a novel electrochemical biosensing platform. *Antimicrob. Agents Chemother.* **57**, 936-943 (2013).

50. N. G. Schoepp, E. M. Khorosheva, T. S. Schlappi, M. S. Curtis, R. M. Humphries, J. A. Hindler, R. F. Ismagilov, Digital Quantification of DNA Replication and Chromosome Segregation Enables Determination of Antimicrobial Susceptibility after only 15 Minutes of Antibiotic Exposure. *Angew. Chem. Int. Ed. Engl.* **55**, 9557-9561 (2016).

51. T. Khazaei, J. T. Barlow, N. G. Schoepp, R. F. Ismagilov, RNA markers enable phenotypic test of antibiotic susceptibility in Neisseria gonorrhoeae after 10 minutes of ciprofloxacin exposure. *Sci. Rep.* **8**, 11606 (2018).

52. L. Chen, D. J. Shin, S. Zheng, J. H. Melendez, C. A. Gaydos, T. H. Wang, Direct-qPCR Assay for Coupled Identification and Antimicrobial Susceptibility Testing of Neisseria gonorrhoeae. *ACS Infect. Dis.* **4**, 1377-1384 (2018).

53. M. Unemo, W. M. Shafer, Antimicrobial resistance in Neisseria gonorrhoeae in the 21st century: past, evolution, and future. *Clin. Microbiol. Rev.* **27**, 587-613 (2014).

54. EUCAST, European Committee on Antimicrobial Susceptibility Testing: Breakpoint Tables for Interpretation of MICs and Zone Diameters (ver. 7.1). (2017) http://www.eucast.org/clinical_breakpoints/

55. M. A. Kohanski, D. J. Dwyer, J. J. Collins, How antibiotics kill bacteria: from targets to networks. *Nat. Rev. Microbiol.* **8**, 423-435 (2010).

56. E. R. Rojas, G. Billings, P. D. Odermatt, G. K. Auer, L. Zhu, A. Miguel, F. Chang, D. B. Weibel, J. A. Theriot, K. C. Huang, The outer membrane is an essential load-bearing element in Gram-negative bacteria. *Nature* **559**, 617-621 (2018).

57. W. S. Wegener, B. H. Hebeler, S. A. Morse, Cell envelope of Neisseria gonorrhoeae: penicillin enhancement of peptidoglycan hydrolysis. *Infect. Immun.* **18**, 717-725 (1977).

58. J. P. Dillard, H. S. Seifert, A peptidoglycan hydrolase similar to bacteriophage endolysins acts as an autolysin in Neisseria gonorrhoeae. *Mol. Microbiol.* **25**, 893-901 (1997).

59. H. I. Zgurskaya, C. A. Lopez, S. Gnanakaran, Permeability Barrier of Gram-Negative Cell Envelopes and Approaches To Bypass It. *ACS Infect Dis* **1**, 512-522 (2015).

60. T. J. Silhavy, D. Kahne, S. Walker, The bacterial cell envelope. *Cold Spring Harb. Perspect. Biol.* **2**, a000414 (2010).

61. P. Demchick, A. L. Koch, The permeability of the wall fabric of Escherichia coli and Bacillus subtilis. *J. Bacteriol.* **178**, 768-773 (1996).

62. A. J. Dijkstra, W. Keck, Peptidoglycan as a barrier to transenvelope transport. *J. Bacteriol.* **178**, 5555-5562 (1996).

63. D. Pink, J. Moeller, B. Quinn, M. Jericho, T. Beveridge, On the architecture of the gram-negative bacterial murein sacculus. *J. Bacteriol.* **182**, 5925-5930 (2000).

64. S. T. Harrison, Bacterial cell disruption: a key unit operation in the recovery of intracellular products. *Biotechnol. Adv.* **9**, 217-240 (1991).

65. N. Vazquez-Laslop, H. Lee, R. Hu, A. A. Neyfakh, Molecular sieve mechanism of selective release of cytoplasmic proteins by osmotically shocked Escherichia coli. *J. Bacteriol.* **183**, 2399-2404 (2001).

66. G. van den Bogaart, N. Hermans, V. Krasnikov, B. Poolman, Protein mobility and diffusive barriers in Escherichia coli: consequences of osmotic stress. *Mol. Microbiol.* **64**, 858-871 (2007).

67. B. H. Hebeler, F. E. Young, Autolysis of Neisseria gonorrhoeae. *J. Bacteriol.* **122**, 385-392 (1975).

68. W. S. Wegener, B. H. Hebeler, S. A. Morse, Cell envelope of Neisseria gonorrhoeae: relationship between autolysis in buffer and the hydrolysis of peptidoglycan. *Infect. Immun.* **18**, 210-219 (1977).

69. H. Felix, Permeabilized cells. *Anal. Biochem.* **120**, 211-234 (1982).

70. H. Nikaido, Molecular basis of bacterial outer membrane permeability revisited. *Microbiol. Mol. Biol. Rev.* **67**, 593-656 (2003).

71. S. Zhao, M. Duncan, J. Tomberg, C. Davies, M. Unemo, R. A. Nicholas, Genetics of chromosomally mediated intermediate resistance to ceftriaxone and cefixime in Neisseria gonorrhoeae. *Antimicrob. Agents Chemother.* **53**, 3744-3751 (2009).

72. S. Foerster, M. Unemo, L. J. Hathaway, N. Low, C. L. Althaus, Time-kill curve analysis and pharmacodynamic modelling for in vitro evaluation of antimicrobials against Neisseria gonorrhoeae. *BMC Microbiol.* **16**, 216 (2016).
73. K. H. Zou, A. J. O'Malley, L. Mauri, Receiver-operating characteristic analysis for evaluating diagnostic tests and predictive models. *Circulation* **115**, 654-657 (2007).
74. Y. H. Grad, S. R. Harris, R. D. Kirkcaldy, A. G. Green, D. S. Marks, S. D. Bentley, D. Trees, M. Lipsitch, Genomic Epidemiology of Gonococcal Resistance to Extended-Spectrum Cephalosporins, Macrolides, and Fluoroquinolones in the United States, 2000-2013. *J. Infect. Dis.* **214**, 1579-1587 (2016).
75. C. B. Wadsworth, M. R. A. Sater, R. P. Bhattacharyya, Y. H. Grad, Impact of population structure in the design of RNA-based diagnostics for antibiotic resistance in Neisseria gonorrhoeae. *bioRxiv*, (2019).
76. R. A. Gianecini, D. Golparian, S. Zittermann, A. Litvik, S. Gonzalez, C. Oviedo, R. G. Melano, M. Unemo, P. Galarza, G. Gonococcal Antimicrobial Susceptibility Surveillance Programme-Argentina Working, Genome-based epidemiology and antimicrobial resistance determinants of Neisseria gonorrhoeae isolates with decreased susceptibility and resistance to extended-spectrum cephalosporins in Argentina in 2011-16. *J. Antimicrob. Chemother.*, (2019).
77. J. C. Rolando, E. Jue, N. G. Schoepp, R. F. Ismagilov, Real-Time, Digital LAMP with Commercial Microfluidic Chips Reveals the Interplay of Efficiency, Speed, and Background Amplification as a Function of Reaction Temperature and Time. *Anal. Chem.* **91**, 1034–1042 (2018).
78. D. A. Selck, R. F. Ismagilov, Instrument for Real-Time Digital Nucleic Acid Amplification on Custom Microfluidic Devices. *PLoS One* **11**, e0163060 (2016).
79. S. G. Lee, H. Lee, S. H. Jeong, D. Yong, G. T. Chung, Y. S. Lee, Y. Chong, K. Lee, Various penA mutations together with mtrR, porB and ponA mutations in Neisseria gonorrhoeae isolates with reduced susceptibility to cefixime or ceftriaxone. *J. Antimicrob. Chemother.* **65**, 669-675 (2010).
80. FDA, Evaluation of Automatic Class III Designation for T2Candida Panel and T2Dx Instrument. (2014).

81. L. Li, W. Du, R. Ismagilov, User-loaded SlipChip for equipment-free multiplexed nanoliter-scale experiments. *J. Am. Chem. Soc.* **132**, 106-111 (2010).

82. F. Shen, W. Du, E. K. Davydova, M. A. Karymov, J. Pandey, R. F. Ismagilov, Nanoliter multiplex PCR arrays on a SlipChip. *Anal. Chem.* **82**, 4606-4612 (2010).

83. F. Shen, B. Sun, J. E. Kreutz, E. K. Davydova, W. Du, P. L. Reddy, L. J. Joseph, R. F. Ismagilov, Multiplexed quantification of nucleic acids with large dynamic range using multivolume digital RT-PCR on a rotational SlipChip tested with HIV and hepatitis C viral load. *J. Am. Chem. Soc.* **133**, 17705-17712 (2011).

84. N. G. Schoepp, E. J. Liaw, E. S. Savela, R. F. Ismagilov, Differential Accessibility to Polymerase During Isothermal Nucleic Acid Amplification Enables 30-Minute Phenotypic Beta-lactam Antibiotic Susceptibility Testing of Carbapenem-resistant Enterobacteriaceae (CRE). *In Submission*, (2019).

85. S. Banoo, D. Bell, P. Bossuyt, A. Herring, D. Mabey, F. Poole, P. G. Smith, N. Sriram, C. Wongsrichanalai, R. Linke, R. O'Brien, M. Perkins, J. Cunningham, P. Matsoso, C. M. Nathanson, P. Olliaro, R. W. Peeling, A. Ramsay, Evaluation of diagnostic tests for infectious diseases: general principles. *Nat. Rev. Microbiol.* **4**, S21-31 (2006).

86. CLSI, M100-S25 Performance Standards for Antimicrobial Susceptibility Testing. *CLSI* **35**, (2015).

87. J. J. Wade, M. A. Graver, A fully defined, clear and protein-free liquid medium permitting dense growth of Neisseria gonorrhoeae from very low inocula. *FEMS Microbiol. Lett.* **273**, 35-37 (2007).

88. Sigma, Buffer Reference Center. https://www.sigmaaldrich.com/life-science/core-bioreagents/biological-buffers/learning-center/buffer-reference-center.html

89. S. R. Lee, J. M. Chung, Y. G. Kim, Rapid one step detection of pathogenic bacteria in urine with sexually transmitted disease (STD) and prostatitis patient by multiplex PCR assay (mPCR). *J. Microbiol.* **45**, 453-459 (2007).

90. J. E. Kreutz, T. Munson, T. Huynh, F. Shen, W. Du, R. F. Ismagilov, Theoretical design and analysis of multivolume digital assays with wide dynamic range validated experimentally with microfluidic digital PCR. *Anal. Chem.* **83**, 8158-8168 (2011).

Acknowledgements

We thank Dr. Jeffrey Klausner at AIDS Healthcare Foundation for invaluable discussions and insight. We thank Peera Hemarajata at the UCLA Clinical Microbiology Laboratory for providing isolates and for discussion of gold-standard practices. We also thank Matthew M. Cooper for assisting in the collection of data contributing to Fig. 4, and Natasha Shelby for help with writing and editing this manuscript. **Funding**: This work was funded in part by the Department of Health and Human Services (HHS) Office of the Assistant Secretary for Preparedness and Response (ASPR) and the Wellcome Trust under the CARB-X program (federal award number IDSEP160030-02); the content is solely the responsibility of the authors and does not necessarily represent the official views of the Department of HHS Office of the ASPR. This CARB-X project is a collaboration between Talis Biomedical Corp. and Caltech. This work was also supported by a Burroughs Wellcome Fund Innovation in Regulatory Science Award, an NIH National Research Service Award (NRSA) [5T32GM07616NSF] (to N.G.S.), and a grant from the Joseph J. Jacobs Institute for Molecular Engineering for Medicine. **Author contributions**: N.G.S. guided initial testing of enhancers and developed two-step nuc-aAST workflow; selected and performed initial testing of surfactant enhancers; optimized sample handling during ABX exposure; performed and analyzed no-enhancer time-course experiments (Fig. 2); designed LAMP primers and contributed to the optimization of LAMP conditions for dLAMP experiments (Fig. 5); wrote the manuscript and created figures. E.S.S. performed initial enhancer testing experiments; selected and performed initial testing of osmotic, autolysis, and surfactant enhancers; optimized sample handling prior to ABX exposure; performed and analyzed enhancer testing and nuc-aAST experiments (Figs. 3, 4, 5), and assisted in performing dLAMP experiments (Fig. 5); performed data analysis, selected the readout metric of percentage accessibility, and selected optimal conditions for nuc-aAST; contributed to writing the manuscript and figure design and wrote the methods section. N.G.S., E.S.S., and R.F.I. conceived of the project and discussed design and interpretation of experiments. J.C.R. optimized digital

LAMP conditions, and performed and analyzed all digital LAMP experiments for Fig. 5. O.O.S. provided isolates and guided discussion on gold-standard AST and current treatment practices for *Ng*, and performed agar-dilution AST. R.F.I. supervised and guided the project, and helped compose the manuscript. All authors read and edited the manuscript. **Competing interests**: The technology described in this publication is the subject of a patent application filed by Caltech. R.F.I. has a financial interest in Talis Biomedical Corp. Caltech is a sub-awardee to Talis Biomedical Corp. on the CARB-X grant that partially funded this work. **Data and materials availability**: The authors declare that the data supporting these findings are available within the article. Any raw data for the reported results is available from the corresponding author upon request.

Chapter VII

Evaluating 3D printing to solve the sample-to-device interface for LRS and POC diagnostics: example of an interlock meter-mix device for metering and lysing clinical urine samples[6]

Abstract

This paper evaluates the potential of 3D printing, a semi-automated additive prototyping technology, as a means to design and prototype a sample-to-device interface, amenable to diagnostics in limited-resource settings, where speed, accuracy and user-friendly design are critical components. As a test case, we built and validated an interlock meter-mix device for accurately metering and lysing human urine samples for use in downstream nucleic acid amplification. Two plungers and a multivalve generated and controlled fluid flow through the device and demonstrate the utility of 3D printing to create leak-free seals. Device operation consists of three simple steps that must be performed sequentially, eliminating manual pipetting and vortexing to provide rapid (5 to 10 s) and accurate metering and mixing. Bretherton's prediction was applied, using the bond number to guide a design that prevents potentially biohazardous samples from leaking from the device. We employed multi-material 3D printing technology, which allows composites with rigid and elastomeric properties to be printed as a single part. To validate the meter-mix device with a clinically relevant sample, we used urine spiked with inactivated *Chlamydia trachomatis* and *Neisseria gonorrhoeae*. A downstream nucleic acid amplification by quantitative PCR (qPCR) confirmed there was no statistically significant difference between samples metered and mixed using the standard protocol and those prepared with the meter-mix device, showing the 3D-printed device

---

[6]This chapter was first published in *Lab on a Chip* with authorship belonging to Erik Jue, Nathan G. Schoepp, Daan Witters, and Rustem F. Ismagilov. The original manuscript can be found at: http://dx.doi.org/10.1039/c6lc00292g.

could accurately meter, mix and dispense a human urine sample without loss of nucleic acids. Although there are some limitations to 3D printing capabilities (e.g. dimension limitations related to support material used in the printing process), the advantages of customizability, modularity and rapid prototyping illustrate the utility of 3D printing for developing sample-to-device interfaces for diagnostics.

Introduction

We evaluate multi-material 3D printing for the design and prototyping of an interlock meter-mix device that meters and lyses human urine samples for a workflow compatible with limited-resource settings (LRS) and point of care (POC) diagnostic testing. 3D printing comprises a set of additive manufacturing techniques that allows the formation of complex 3D structures with minimal restrictions. The emerging technological capabilities of 3D printing bring exciting advancements in the fabrication of microand macrofluidic de vices, enabling architectures that would be difficult with conventional fabrication techniques such as soft lithography.[1,2] A primary advantage of 3D printing is the ability to rapidly prototype and iterate new designs, without needing to tool expensive molds.[3] 3D printing reduces the design and prototyping time from weeks and months down to hours and days, making prototyping more cost-effective and therefore more accessible—particularly for research labs where needs may change frequently. Because 3D printing is semi-automated, it minimizes assembly time, the requirements for labor, and reproducibility issues, therefore reducing many of the barriers that currently prevent some research labs from prototyping complex 3D parts.[2] The customizable design files generated in computer-aided design (CAD) software can be easily modified in coordination with experiments. 3D printed materials also exhibit a wide range of properties, with varying levels of rigidity, surface roughness, optical clarity, and biocompatibility to fit a diverse range of device requirements.[4] In combination, all of these advantages make 3D printing attractive for prototyping fluidic devices relevant to lab-on-a-chip and diagnostics fields.

The sample-to-device interface for diagnostics is a critical component of nucleic acid amplification testing (NAAT) in LRS, and remains an unsolved challenge.[5,6] Many NAAT technologies are not amenable to LRS, because NAAT is an intrinsically multistep process involving sample metering, lysis, nucleic acid (NA) purification, amplification, and detection.[7] To be useful in clinical practice in POC or LRS, the entire NAAT workflow should be fully automated, user-friendly (without training or pipetting steps to meet CLIA-waiver), rapid, equipment-free, sensitive, and specific. To equip a portable device with complete sample-in to answer-out functionality requires the appropriate consideration of all upstream and downstream processes. While many efforts have been taken to automate nucleic acid (NA) purification and amplification, sample metering must always be addressed because a user in LRS or at the POC cannot be asked to pipette accurately. Furthermore, combining sample transfer with the step in which the sample is mixed with the lysis buffer is attractive, because it has the advantage of minimizing the cost and complexity of an integrated diagnostic device, and could benefit such devices being developed in research labs, including our own.[8–11] Precise metering is especially critical in NAAT testing of sexually transmitted diseases (STDs), such as *Chlamydia trachomatis* (CT) and *Neisseria gonorrhoeae* (NG).[12] In 2013, there were 1 401 906 and 333 004 reported cases of CT and NG, respectively, in the United States, with many more cases unreported and undiagnosed.[13] The Centers for Disease Control and Prevention (CDC) estimates 20 million new STD infections per year in the US, accounting for $16 billion in health care costs.[13] The CDC now recommends NAAT for CT/ NG diagnosis[14] because these tests are sensitive, accurate and use non-invasive urine samples. Many of these tests need to be done under LRS or POC settings.

Currently, there is no standardized way to deliver a known amount of sample mixed with lysis buffer to an LRS- or POC-compatible NAAT diagnostic device. A method for doing so is subject to the following constraints: (i) meter a precise volume of urine with <5% coefficient of variation (CV), (ii) mix urine with premeasured, preloaded lysis buffer at a specific ratio (as determined by the extraction chemistry), (iii) transfer the lysed urine without dripping potentially infectious solution, (iv) perform these operations quickly, in

a userfriendly, equipment-free manner that minimizes potential user errors, and (v) maintain the sensitivity and specificity of the overall assay (no loss of nucleic acids to 3D printed surfaces, contamination, or leachates).

Here, we evaluate the capabilities of multi-material 3D printing to design and prototype a single-use disposable macrofluidic device that meets the above constraints. We also discuss the advantages and disadvantages of 3D printing as a research tool for device development. Multi-material printing, wherein different materials are combined into a single printed part, offer expanded capabilities, so we chose to spe cifically investigate multi-material 3D printing as a tool for building sample-to-device interfaces. We have previously demonstrated the utility of multi-material printing in the development of a pumping lid for interfacing with microfluidic devices,[15] however the pumping lid we developed was only used to compress air, and did not contact fluids directly. Here, we expand on the ability to use multi-material printed parts to generate sealed fluid cavities through the development of a multivalve and plungers used within our device.

Results and discussion

Interlock design and meter-mix device operation

To operate the meter-mix device (see ESI† video), the user performs three simple steps 1. insert urine suction tube into patient sample and pull urine plunger, 2. remove from patient sample and slide multivalve, and 3. push lysis buffer plunger to eject the mixed solution. The device can then be easily disposed of as biohazardous waste. Furthermore, the user of the device cannot accidentally perform these three operations out of order due to the presence of interlock features attached to the plungers. In the initial position, the urine plunger interlock blocks the sliding of the multivalve, and the multivalve blocks the movement of the lysis buffer plunger (Fig. 1A). When the user pulls up on the urine plunger, urine is aspirated through the suction tube, through the valve, and into the urine chamber. Pulling up on the urine plunger also releases the interlock that was blocking the

multivalve (Fig. 1B and C). The user then slides the multivalve, which disconnects the urine suction tube inlet while generating two new outlets to a static mixer, one outlet for urine and the other for lysis buffer which has been prestored on the device. By pre-storing the lysis buffer on device, we eliminate many manual pipetting steps and reduce user error.[16] The sliding of the multivalve also creates openings for the urine plunger interlock and the lysis buffer plunger interlock (Fig. 1C). In the final step, the user pushes down on the lysis buffer plunger, which also pushes the urine plunger, ejecting both urine and lysis buffer through the static mixer (Fig. 1D). The total user operating time is between 5 and 10 s.

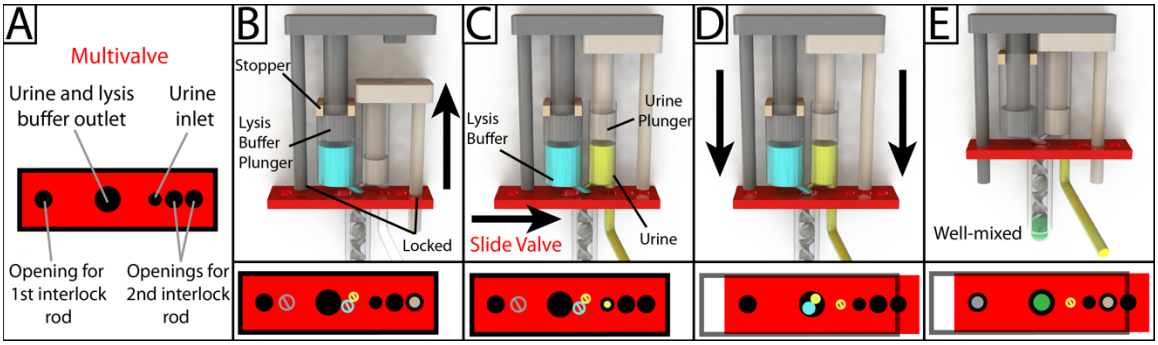

Fig. 7-1. Schematic overview of the design and operation of the 3D-printed interlock meter-mix device for metering and mixing a urine sample with lysis buffer. (A) The multivalve has five holes that are labeled accordingly. (B) Lysis buffer (blue) is preloaded into the lysis buffer chamber, where the topmost position of the lysis buffer plunger (left, grey) is pre-determined by stoppers (tan). The urine plunger interlock rod (right, beige) is posi- tioned within the multivalve, preventing the valve from sliding and simultaneously blocking the lysis buffer plunger interlock rod. The user pulls up on the urine plunger (C) until it contacts and is stopped by the lysis buffer plunger, aspirating urine and simultaneously removing the urine plunger interlock rod from the multivalve. The user slides the multivalve (D), closing off the urine suction tube, opening the lysis buffer and urine outlets to the mixer, and providing openings for both interlock rods. In the final step, the user pushes down on the lysis buffer plunger (E), ejecting urine and lysis buffer through a static mixer, wherein the solutions are well mixed before finally

being ejected from the tip of the mixer. Red blocks at the bottom of each panel show a top-down view of the multivalve. Black circles and rings indicate holes in the multivalve. Slashed circles indicate the presence of a feature that is blocked by the multivalve. Colored circles indicate the presence of an interlock rod or an open channel for the flow of a solution.

The meter-mix device is composed of eight assembled parts: 1. main enclosure, 2. lysis buffer plunger, 3. urine plunger, 4. two plunger stoppers, 5. multivalve, 6. urine suction tube, 7. static mixer elements, and 8. static mixer case (Fig. 2). All parts were designed using 3D CAD software (Solidworks 2015 Education Edition) and fabricated using an Objet 260 multi-material 3D printer (Stratasys, Eden Prairie, MN, USA). We judiciously selected two semi-transparent photopolymer materials, Veroclear and TangoPlus, corresponding to a rigid plastic, analogous to polyIJmethyl methacrylate) (PMMA), and a soft, elastomeric material, analogous to rubber, respectively. By utilizing translucent materials, fluids are visible as they are transported among chambers of the device, providing visual feedback during operation. All of the parts were composed of Veroclear, providing a strong structure. The plunger heads, stoppers, and the multivalve were printed with a combination of Veroclear and TangoPlus, which enabled us to design sliding surfaces and generate seals. With the exception of the plunger stoppers, each part underwent between seven and 25 unique design iterations. In the Fig. 2 demonstration, which shows the entire device assembly and operation, 1150 μL 0.05% (v/v) sky blue Ateco dye (August Thomson Corp., Glencove, NY, USA) was preloaded into the lysis buffer chamber and 0.1% lemon yellow Ateco dye was manually loaded into the urine chamber. These two dye solutions were run through the device and combined to form a green mixed solution (Fig. 2D).

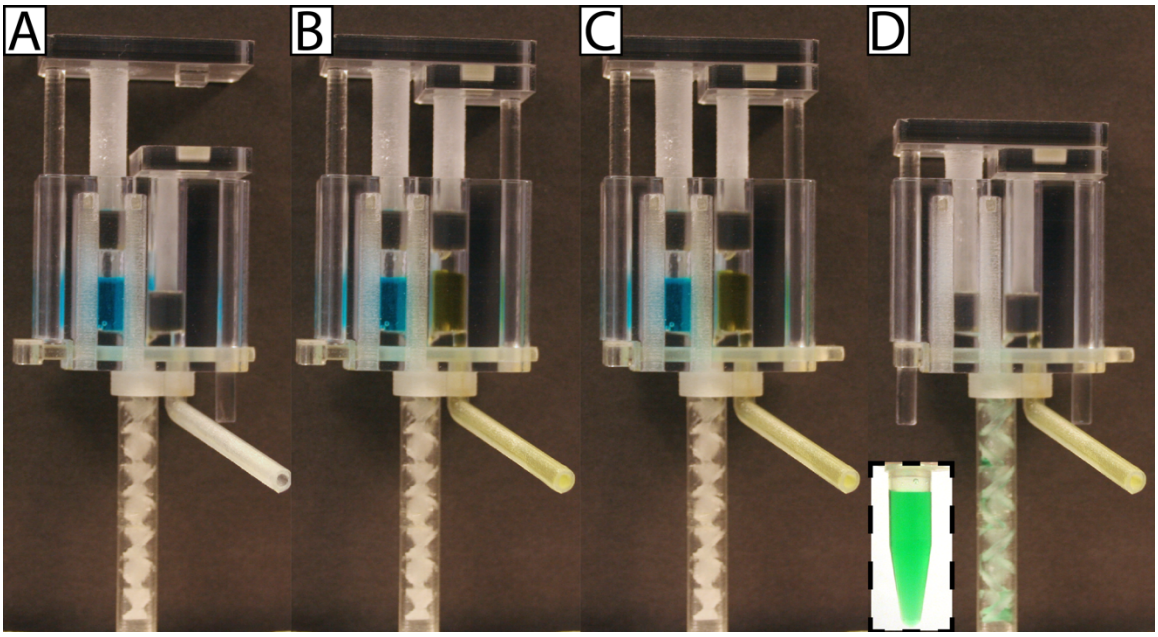

Fig. 7-2. Photographs of the device at different stages of operation. (A) In the initial position, blue dye representing lysis buffer is preloaded and the urine plunger is down. (B) In the second position, the urine plunger contacts the lysis buffer plunger and a specific volume of yellow dye representing urine is metered. (C) In the third position, the multivalve was slid 5 mm to the right, simultaneously closing and opening new connections. (D) In the final position, both plungers are down, dispensing a green solution out through the static mixer and into a 1.5 mL tube (inset).

Designing and prototyping leak-proof connections

To ensure reliable device operation, all of the seals on the device need to be hermetically sealed. We accomplish this using the capability of multi-material 3D printing to generate materials jointly composed of hard plastic (Veroclear) and soft rubber-like material (TangoPlus). We used multi-material printing for fabricating both plungers and the multivalve. The challenge with creating leak-proof connections is determining the appropriate dimensions, overlap, and the ratio of soft:hard material to create a strong leak-proof connection that is still easy to move by hand. We took advantage of the rapid prototyping capabilities of 3D printing to quickly converge on functional designs. For the

urine chamber, we found a good fit using an 8 mm diameter hole and an 8 mm diameter plunger head, where the inner diameter of the plunger head consisted of 7.2 mm Veroclear; the remaining diameter was filled with TangoPlus. For the lysis buffer chamber, we found good fit using an 11.31 mm diameter hole and an 11.31 mm diameter plunger head, where the inner diameter of the plunger head consisted of 10.18 mm Veroclear; the remaining diameter was filled with TangoPlus. These parameters made hermetically sealed connections capable of generating and holding a vacuum. We selected the dimensions of the chambers in the main enclosure to provide the desired air volumes and mixing ratios (see Accurate dispensing). To generate the multivalve seal, an open cavity was designed through the side of the main enclosure, with raised ridges around each hole for the inlets and outlets. The multivalve was 2.7 mm thick, with 0.54 mm TangoPlus (20%) layered on the top and 0.54 mm on the bottom. At the points of contact between the multivalve and the inlet/outlet ridges, there was a 0.2 mm overlap where the ridge pushed into the TangoPlus layer (by 3D CAD design). To assist sealing and sliding, we applied silicone oil to lubricate all contact points at movable interfaces (plunger heads, chambers, and the multivalve).

Plunger system and accurate metering

To accurately meter urine, we designed a plunger system with predetermined start and stop positions. During device operation, the urine plunger is pulled up until it contacts the underside of the lysis buffer plunger. The volume displaced by the plunger was calculated in CAD software, providing an estimate for the volume of urine aspirated into the device. To precisely calibrate metering, the working design was iterated by testing prototypes of the device by aspirating deionized water, weighing the device, and modifying the height of the plunger stoppers to adjust the volume displaced by the plunger. To accurately meter lysis buffer, we use a pipettor to preload the meter-mix device. When the device is set to the initial configuration, lysis buffer is sealed on both sides by the lysis buffer plunger and multivalve. This is advantageous for a disposable LRS and POC device because the filling step can be performed during manufacturing and assembly. In this

way, the end-user does not need to consider handling of the lysis buffer during device operation.

With diagnostic devices, it is important to minimize dead volumes to avoid wasting reagents, losing sample, or introducing a source of variability. One strength of 3D printing is that potential sources of dead volume can be identified and reduced during the design process. For the meter-mix device, we identified four potential sources of dead-volume: urine lost in the suction tube, urine lost in the urine chamber, lysis buffer lost in the lysis buffer chamber, and mixed solution remaining in the static mixer. We recognize that patient urine is abundant, and that it is acceptable for the meter-mix device to overfill urine; however, the final volume of urine ejected from the device must be consistent between runs. To ensure accurate, consistent ejected volumes, the dead-volume of the urine suction tube was taken into account while modifying the positions of the plunger stoppers. It should be noted that dead-volume can be reduced by changing the design of the suction tube as required. For our meter-mix device, we were concerned with dead volumes of urine remaining in the urine chamber and the static mixer, which could contribute to differences in the volumes of urine ejected between runs. In particular, a user who sees liquids trapped in the static mixer may be inclined to shake the meter-mix device, introducing error which affects the accuracy of downstream quantitative processes. To remove this dead volume, we leave a pocket of air that sits above the lysis buffer within the lysis buffer chamber. After urine is aspirated into the device, we designed the system so that the heights of the pockets of air are roughly equal (the air initially residing in the suction tube is incorporated into the device during the aspiration step). These two pockets of air produce a blow-out volume of air which removes the dead volumes of urine and lysis buffer that would otherwise remain in the chambers and static mixers.

We wanted to ensure that after urine is aspirated into the urine chamber, urine is unable to leak out through the tip of the urine suction tube. Bretherton previously examined this problem, and found the dimensionless bond number, Bo (which relates gravity to surface

tension), to be a guiding parameter.[17] The bond number is related to the density difference between the liquid and air, the diameter of the tube, and the surface tension of the liquid. He predicted that for a vertical tube that is sealed at one end, a bubble contained within will not rise if Bo < 0.842.17 Thus, in our meter-mix device, if the bond number is low, and a bubble enters the urine suction tube, the bubble will be immobile, preventing solution from dripping out through the tip of the urine suction tube. Bretherton's prediction suggests that we want to minimize the bond number, which we can do simply by reducing the diameter of the 3D-printed urine suction tube. We would not, however, want to make the diameter so small that it generates a high resistance to flow, as this would generate a noticeable delay in the filling time and negatively affect the user experience. Tube diameter is constrained with our 3D printing methods because as tube diameter decreases, it becomes increasingly difficult to remove the support material and clean inside the tube. For our device, we limited our testing to >1.5 mm diameter sized suction tubes. At the millimeter scale, there was no noticeable delay between pulling up on the urine plunger and filling of the urine chamber.

We tested the Bretherton prediction using 3D-printed parts. A simple plunger system was designed along with suction tubes of varying diameters. In multi-material 3D printing, the printing of support material can be avoided for some geometries and configurations. We printed straight suctions tubes in the vertical configuration, which does not print support within the suction tube and therefore does not require support cleaning. Although we can choose not to print some support pieces, one limitation of our multi-material printer is that it always prints support material for the bottom layer in contact with the 3D printer's build plate. When one side of the model is printed in contact with support and the other parts of the model are located on the exterior sides of the device, there may be minor differences between dimensions and surface roughness. For example, we found that when printing straight tubes upright, the diameter on the side of the tube in contact with the 3D printer's build plate was slightly smaller than the opposite opening. A discrepancy between parts of the model in contact with the build plate and parts that are open to the air is not an exclusively multimaterial 3D printing characteristic, but is common to many

types of 3D printers. Care was taken to always use the side of the tube in contact with the build plate for the connection to the body of the plunger system.

Table 7-1. Bretherton's prediction tested using 3D printed tubes of varying diameter

Fluid	Diameter (mm)	Bo	Observed behavior
Water	2	0.136	No drip
	2.5	0.212	No drip
	3	0.306	No drip
	3.5	0.416	No drip
	4	0.544	Bubble sticks
	4.5	0.688	Bubble sticks
	5	0.850	Bubble sticks/bubble rises
	5.5	1.028	Bubbles rises
Ethanol	2	0.345	Bubble sticks
	2.5	0.539	Bubble sticks
	3	0.776	Bubble sticks/bubble rises
	3.5	1.056	Bubble rises
	4	1.379	Bubble rises
	4.5	1.746	Bubble rises
	5	2.155	Liquid spills as air column rises
	5.5	2.608	Liquid spills as air column rises

To test the Bretherton prediction, we used the opposite side of the suction tube to aspirate solution into the tube. The suction tube was manually disturbed through tapping the tip in order to introduce bubbles, mimicking a real-world user experience where the user bumps the device. We found that there was general agreement between bond number and the Bretherton prediction (Table 1). Using water, for a bond number ≤ 0.416, no bubbles entered the device and no fluid dripped from the tip. For bond numbers between 0.544 and 0.688, a bubble entered the tube releasing some drops, but the bubble did not rise and the liquid–air interface at the tip regained stability. Close to the Bretherton prediction at Bo = 0.850, bubbles entered the tube and both rise and no rise of the bubble were observed, which seemed to depend on the size of the bubble incorporated. Finally, for a large bond number (1.028), drops were released when the bubble initially entered the tube, the liquid–air interface at the tip regained stability, and we saw bubble rise as predicted by Bretherton. The experiment was repeated using ethanol, which has a lower surface tension than water, with similar results. We also observed that for very large bond numbers (Bo $\geq$ 2.155), once the ethanol–air interface at the tip was disturbed, a column of air entered the suction tube, spilling all of the solution out of the tip. Accounting for Bretherton's prediction, the limitations of cleaning support material, and for the pocket of

air for blow-out, we selected a suction tube diameter of 2.3 mm in the final design. The surface tension of urine from healthy patients ranges from 48–70 mN m−1.18 Using the low value of surface tension at 48 mN m−1, a density of 1.01, and a 2.3 mm diameter gives a Bo = 0.272.

Accurate dispensing

The flow rate of each solution is determined by the design of the device chambers, plungers, and outlets. We designed each chamber of the device to undergo the same driving pressures over the entire dispensing operation. We can accomplish this by matching the solution height, air pocket height, and plunger heights in both chambers. For example, a 2 : 1 volume ratio can be obtained by making the area of one chamber twice the area of the second chamber. The crosssectional area of the channels and outlet valves should also be maintained at the 2 : 1 ratio to obtain the flow resistance and corresponding volumetric flow rate. In our device, we designed the device with a 2:1 volume ratio between lysis buffer and urine, but we were cognizant of the potential for flow irregularities near the beginning and end of the flow regime. If slight inaccuracies during filling cause urine to enter the static mixer prematurely or after all of the lysis buffer has gone through, this could leave some urine unmixed and unlysed. This could lead to inaccuracies during downstream quantification and unlysed bacteria are a biohazard. To address these concerns, we slightly overfilled the lysis buffer compartment leading to a final lysis buffer to urine volume ratio of 2.2 : 1.

We evaluated the dispensing accuracy of our device using water, green dye, spectrophometer measurements, and a balance. To examine inter-device variability, we tested three different device prototypes each run in triplicate (Table 2). There was no significant difference among devices for aspiration volume ($P = 0.46$) or the volume expelled ($P = 0.44$). Sample aspiration was found to accurately meter ∼790 μL (<1% CV). As previously described, the blow-out volume of air is responsible for ejecting the final volumes of urine and lysis buffer remaining in the chambers and the static mixer.

We found that pushing the plunger down over the course of 1–2 s led to relatively little error in the final ejection volume (<2% CV). However, pushing the plunger down faster (in <1 s) pushed bubbles through the static mixer and greater volumes of liquid remained in the device, resulting in reduced ejection volumes (~1350 μL). In real-world applications, it is important to minimize differences resulting from user operation. Future designs can address the issue of plunger speed affecting dead volume by reducing the diameter of the outlets to prevent bubbles from escaping before the fluid. The ratio of solution ejected from the lysis buffer chamber and the urine chamber was calculated by measuring the absorbance of the final ejected solution and comparing it to the green dye loaded into the lysis buffer chamber. We found that dispensed volumes out of the lysis buffer chamber and urine chamber were similar, with percent deviations of 2.5% and 6.7%.

Table 7-2. Evaluation of metering and dispensing accuracy of the meter-mix device

Device	Trial	Aspiration volume (μL)	Ejection volume (μL)	Calc. volume from lysis chamber (μL)	Calc. volume from urine chamber (μL)
1	1	782	1591	1067	524
	2	784	1613	1121	492
	3	798	1660	1135	525
2	1	796	1619	1150	469
	2	799	1630	1065	565
	3	791	1577	1120	457
3	1	788	1611	1134	477
	2	787	1586	1106	480
	3	799	1572	1099	473
AVG		792	1607	1111	496
STD		6	27	28	33
CV		0.8%	1.7%	2.5%	6.7%

Static mixer design and mixing evaluation

To simplify the user experience and eliminate mixing by pipetting or vortexing, we designed an on-device Kenics static mixer (KMS), a common mixer used for a variety of industrial applications.[19] We had previously designed the flow rates of urine and lysis buffer to exit the outlets at a consistent flow rate. We predicted that a KMS mixer placed after the lysis buffer and urine outlets would be an efficient way to mix the two streams.

The static mixer is composed of alternating leftand right-hand 180° helical twists with 90° offsets between elements. This immobile structure encased within a tube guides the flow of solutions from the center of the tube to the wall of the tube and from the wall to the center. Each element splits and recombines streams of flow, rapidly homogenizing the fluid, similar to mixing by chaotic advection in moving plugs.[14,20,21] We designed a KMS static mixer com posed of eight elements, with a diameter of 5 mm, and a length : diameter ratio of 1.25 : 1. Limited by the requirements of removing support material from 3D-printed parts, it was not feasible to print the entire mixer and tube enclosure as a single unit. Instead, we used a modular approach, printing the mixer elements and the mixer case as separate pieces. Both parts were printed in the upright configuration.

When static mixer elements were printed with the glossy finish setting, only the topmost element was glossy and had different surface roughness and dimensions than the other elements (remaining parts had the matte finish because they were printed in contact with supporting material). To address this issue, we printed the static mixer elements with the matte finish (Fig. 3A). The static mixer elements and the static mixer case were cleaned separately and assembled carefully because the static mixer elements were very prone to breaking (Fig. 3B–D).

To evaluate mixing quality, a starch iodine–thiosulfate decolorization was used. The decolorization reaction is a preferred method to evaluate mixing because any pockets of unmixed regions will be visible.[22] The initial decolorization reaction occurs quickly in a 1 : 1 iodine : thiosulfate ratio, although a secondary reaction leads to the reappearance of color so higher ratios of iodine : thiosulfate (e.g. 1 : 1.2 or 1 : 1.4) can be used.[23–25] For the meter-mix device, we used a 1 : 1.05 ratio because the design enables rapid mixing within the timescale of the device operation. The starch iodine solution was loaded into the urine chamber through the suction tube, and the sodium thiosulfate was preloaded into the lysis buffer chamber. The device mixed the two solutions within the first three to four elements (Fig. 3G). As a control, to confirm that the loss of color is due to mixing and not an artifact of the chemical or optical properties of the 3D printed part, we also

show the static mixer element fully filled and while mixing with a solution that does not cause decolorization. We ran the meter-mix device with starch iodine indicator loaded into both chambers (Fig. 3E) and in a separate experiment with starch iodine loaded into the urine chamber and water loaded into the lysis buffer chamber (Fig. 3F).

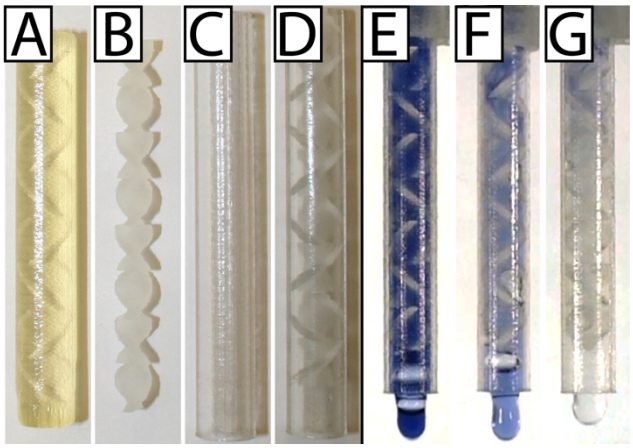

Fig. 7-3. Assembly of the static mixer (A–D) and a demonstration of its use in the meter-mix device (E–G). (A) Freshly printed static mixer ele- ments before cleaning. (B) Static mixer elements after a 15 min cleaning step to remove support material. (C) Static mixer case. (D) As- sembled static mixer with elements inserted into case. (E) Iodine– starch indicator loaded into both chambers and ejected through the static mixer. (F) Iodine–starch indicator mixing with water to show a di- lution. (G) Iodine–thiosulfate de-colorization reaction demonstrating rapid mixing within the first few static mixer elements.

Function and biocompatibility

We evaluated the meter-mix device for compatibility with a routine nucleic acid extraction kit by comparing the metering and mixing steps performed by the device with standard approaches for metering and mixing (manual pipetting and vortexing). Two concerns are the potential for nucleic acids to bind to 3D printed surfaces, and the potential for compounds from 3D printed materials to leach into the solutions, both of which can negatively affect downstream analysis of nucleic acids. We preloaded the

device with 1150 µL lysis buffer and aspirated urine spiked with 104 cells per mL of either C. *trachomatis* (CT) or N. *gonorrhoeae* (NG) through the suction tube. The multivalve was slid and the plungers were pushed manually, ejecting the solutions through the static mixer and into a 2 mL polypropylene tube. An off-device sample was tested in parallel, with 1100 µL lysis buffer and 500 µL spiked urine (see Table 2) metered by a pipettor and the solution mixed by vortex. We also ran no-template controls containing clean urine for both on and off-device conditions. After mixing, all samples were processed in parallel according to the manufacturer's instructions using the QIAamp Viral RNA Mini kit (recommended for purification of bacterial DNA from urine). Following extraction, nucleic acid concentrations were compared using routine quantitative polymerase chain reaction (qPCR) with primers previously evaluated for the detection of C. *trachomatis*[26] or N. *gonorrhoeae*.[27] The threshold cycles for vortexed and device-mixed samples were not statistically different (Fig. 4), indicating that there was no significant loss of nucleic acids and or material leaching that inhibited downstream analysis. No-template negative controls showed no amplification after 35 cycles.

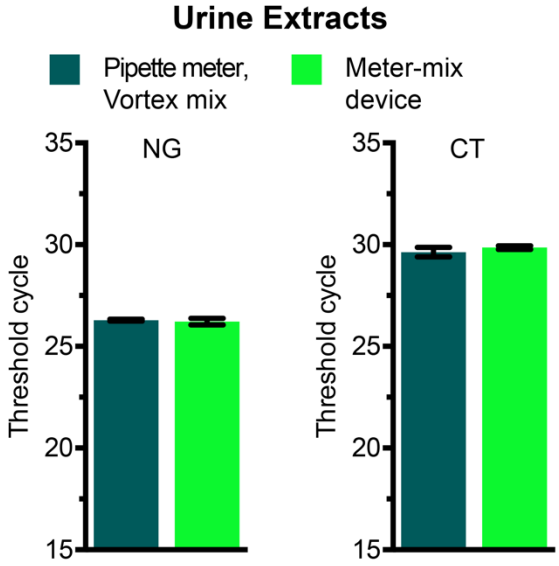

Fig. 7-4. qPCR threshold cycles on DNA extracted from urine spiked with either inactivated Chlamydia trachomatis (CT) or Neisseria gonorrhoeae (NG). Sample metering and mixing with lysis buffer was performed with either the meter-mix device

(light green bars) or stan- dard pipette and vortex (dark green bars). The remainder of the extraction protocol was identical for both conditions.

Experimental

Meter-mix device cleaning and assembly

Printed parts were cleaned using pipette tips or copper wire and rinsed with water. The urine plunger, lysis buffer plunger, multivalve, and both chambers of the main enclosure chambers were lubricated with viscous silicone oil (dimethylpolysiloxane 12500 cSt, Sigma Aldrich, St. Louis, MO, USA). To assemble, first the urine plunger was inserted into the urine chamber of the main enclosure followed by the lysis buffer plunger into the lysis buffer chamber. The two plunger stoppers were then inserted, locking the topmost position of the lysis buffer plunger. The multivalve was inserted into the main enclosure from the side, and pushed into its final position to preload 1150 μL lysis buffer through the outlet. The multivalve was then moved into its starting position, the urine plunger pushed to the bottom of the chamber, and the urine suction tube and static mixer were attached. For these joints, the outer diameter of the static mixer case (8 mm) and the outer diameter of the urine suction tube (4.5 mm) was sized exactly to the diameter of adapters on the main enclosure. After cleaning, a thin layer of support material remains at the junctions of the main enclosure. Because this support material is shed from the joints during device use, we used silicone oil to enhance the seal.

Characterization of metering and dispensing

To evaluate metering and dispensing, we loaded into the lysis buffer chamber 1150 μL 0.5% (v/v) green food color dye (The Kroger Co., Cincinnati, OH, USA) diluted in deionized water. Deionized water was aspirated into the urine chamber through the urine suction tube, and mass measured to obtain the aspirated volume (using water density of 1 g mL−1). The multivalve was pressed and the solution ejected into a pretared conical

tube to obtain the mass of the solution ejected from the device. The resulting solutions were well-mixed through vortexing. The original 0.5% (v/v) green dye and each resulting solution was diluted by 20×, loaded into a cuvette, and measured with a UV-vis spectrophotometer (Nanodrop 2000c, Thermo Scientific, Wilmington, DE, USA). Measurements were taken at the wavelength where the absorbance was maximal (630 nm), and the ratio was used to determine the volume of solutions ejected from each chamber.

Iodine–thiosulfate decolorization reaction

Iodine, starch indicator, and sodium thiosulfate solutions were prepared according to the "Handbook of industrial mixing".22 Briefly, 1150 μL sodium thiosulfate nonahydrate (0.5 mM, ThermoFisher Scientific, Waltham, MA, USA) was loaded into the the lysis buffer chamber. Starch indicator was prepared by adding 100 mg starch, soluble potato, powder (J.T. Baker, Center Valley, PA, U.S.) and 20 g potassium iodide to 10 mL deionized water. 50 μL of this starch solution was added to a 1 mL solution of iodine (1 mM, Alfa Aesar, Ward Hill, MA, USA), coloring the solution dark bluishpurple. The final ratio of iodine:thiosulfate was 1:1.05. A video was taken using a Samsung Galaxy S4 camera, and frames extracted during device operation when the flow fully filled the static mixer (Fig. 3E–G).

Qiagen extraction and qPCR experiment

In order to test device compatibility with biological samples and ensure that downstream nucleic acid analysis was not negatively affected, we compared samples that were metered and mixed on-device against traditional vortex mixing using a commercial nucleic acid extraction kit (QIAamp Viral RNA Mini Kit, 52904). Lysis buffer was loaded with 2 ng μL−1 carrier DNA (salmon sperm DNA, Thermo Fisher AM9680). Non-infectious CT and NG samples were obtained from ZeptoMetrix Corp. (NATNG-ERCM, NATCT(434)-ERCM, Buffalo, NY, USA). Quantitative PCR was performed on

a Roche LightCyler 96. PCR reactions consisted of 5 μL SsoFast EvaGreen Supermix (BioRad cat no. 1725200), 2.0 μL of template (extracted spiked urine), 0.5 μL of 20× primer stocks, and 2.5 μL nuclease-free water. The primers used26,27 were previously evaluated for the detection of either CT or NG. Final primer concentration in the reaction was 500 nM. Thermal cycling consisted of a 3 min initial denaturation step at 95 °C, followed by 40 cycles of20sat95°C,20sat62°C,and20sat72°C.Meltanalysis confirmed specific product for all reactions.

Conclusions

We showed that multi-material 3D printing can be used to prototype a disposable interlock meter-mix device that accurately meters urine and completely mixes it with lysis buffer in a format that meets the requirements for a downstream NAAT compatible with LRS and POC settings. The 3D-printed device accurately aspirated predetermined volumes into a urine chamber with a coefficient of variation of 0.8%. Urine and lysis buffer were dispensed through a KMS static mixer at a 2.2 : 1 mixing ratio. Printing with translucent materials enabled visual confirmation of fluid movement and showed that mixing occurred within the first few elements of the static mixer, with homogenization and lysis later verified by qPCR. Printing with multi-material 3D printer enabled us to use a combination of composites to create airtight seals that slide without leaking or losing vacuum pressure. Using a 3D printer also helped address the potential for sample drip ping, a biohazardous concern when working with bodily fluids and potentially dangerous solutions, as we were able to test Bretherton's prediction for bubble rising through several prototype iterations and identify optimal tube dimensions that ensured the sample did not drip.

The 3D-printed device was designed to optimize the user's experience: operation is simple (three steps); interlock features protect against user error; neither pipetting nor vortexing are required; and the entire device operation is completed within 5 to 10 s (see ESI† video). We validated our device by lysing urine samples spiked with CT/NG and

performed downstream processes to quantify nucleic acids through qPCR. These results confirmed that the 3D-printing materials (Veroclear and TangoPlus) were biocompatible; we observed no loss of nucleic acids and devices performed equally well compared with the standard protocol of pipettor metering and vortex mixing in a polypropylene tube. Finally, we demonstrated that the performance of the meter-mix device matched the performance of standard laboratory protocols for metering and mixing, with a substantially shorter time period for device operation.

The meter-mix device described here is not limited to mixing urine with lysis buffer. A common operation in biology, chemistry, and medicine is to mix two solutions of known volume. Due to the customizability of 3D printing and CAD design, it is easy to adapt the meter-mix device to different volumes or configurations. In some applications, it may be desirable to meter two different solutions at the time of use. In this example, the meter-mix device could be reconfigured with an additional suction tube appended to the lysis buffer chamber. Given the versatility of the metermix device, it may be useful in a variety of applications such as sequencing, dilutions, or chemical syntheses. Because the meter-mix device simplifies and accelerates workflow, protects against user error and provides a user-friendly experience, we foresee its future application in research labs and limited-resource settings. For example, time-sensitive laboratory measurements may require metering and mixing on the timescale of single digit seconds rather than the tens of seconds required for pipetting. In commercial applications, an important advantage of a single-use disposable device is that it can be assembled and pre-loaded with lysis buffer before it is shipped, eliminating a pipetting step for the end user.

Throughout the course of device development, the 3D printing workflow was a major advantage over analogous forms of prototyping, such as soft lithography. Prototyping with 3D printing was rapid, enabling us to design, test, redesign, and reprint a prototype in the period of a single day. For small parts that can be printed in less than a few hours, it is possible to iterate multiple designs in a single day. The ease with which parts can be modified after having developed the initial design allowed us to print multiple variations

of the meter-mix device at once and determine the optimal architecture of each part in a single experiment. This was useful for determining the diameter of the suction tube, setting the parameters for the static mixer, and adjusting the fit for the seals. Another advantage with 3D printing is that the 3D CAD models which are developed during the design stage can also be utilized and adapted for injection molding. This is important in commercial applications, where large quantities are required, because injection molding has higher start-up costs but lower costs per part than 3D printing. We also found modularity to be an important advantage with 3D printing. Parts can be built as separate components and later reassembled, reducing build time (which relies heavily on z-axis height). It is also easier, and less expensive, to validate and iterate with individual components than to redesign and reprint an entire device. Of course, the final cost of producing these devices using standard manufacturing methods (injection molding) will be even lower than prototyping costs.

The greatest limitation we faced with multi-material 3D printing pertained to the support material. We faced three specific issues: (i) wherever support material is printed in contact with the model, the printer produces a matte finish with different surface characteristics and dimensions compared with the glossy finish of parts that do not contact the support material, (ii) it can be difficult to remove the support material for some geometries, so care needs to be taken during the design to account for cleaning, and (iii) removal of the support material takes time, requiring ~45 min to clean all of the components for a single device. As new support material is developed, this limitation will diminish. For example, some companies have developed new dissolvable support materials that can be removed in a soak-and-rinse process; however, these processes are still diffusion-limited and may be difficult to implement when cleaning long, narrow channels relevant to microfluidic devices. Despite some limitations, we conclude that 3D printing is an attractive prototyping technology with great potential for solving the sample-to-device interface problem in diagnostics, especially in resource-limited settings.

Acknowledgements

This research was supported by DARPA Cooperative Agree- ment HR0011-11-2-0006. The content of this article does not necessarily reflect the position or the policy of the government, and no official endorsement should be inferred. This material is also based upon work supported by National Sci- ence Foundation Graduate Research Fellowships DGE- 1144469 (to E. J.). R. F. I. holds an Innovation in Regulatory Science Award from BWF. We thank Natasha Shelby for con- tributions to writing and editing this manuscript.

References

1 C.M.B.Ho,S.H.Ng,K.H.H.LiandY.-J.Yoon,LabChip, 2015, 15, 3627–3637.
2 B. C. Gross, J. L. Erkal, S. Y. Lockwood, C. Chen and D. M. Spence, Anal. Chem., 2014, 86, 3240–3253.
3 A. Waldbaur, H. Rapp, K. Lange and B. E. Rapp, Anal. Methods, 2011, 3, 2681–2716.
4 A. Pilipović, P. Raos and M. Šercer, Int. J. Adv. Manuf. Tech., 2007, 40, 105–115.
5 A. Niemz, T. M. Ferguson and D. S. Boyle, Trends Biotechnol., 2011, 29, 240–250.
6 P. Craw and W. Balachandran, Lab Chip, 2012, 12, 2469–2486. 7 R. W. Peeling, K. K. Holmes, D. Mabey and A. Ronald, Sex.
Transm. Infect., 2006, 82(5), v1–6.
8 D.Lee,Y.T.Kim,J.W.Lee,D.H.KimandT.S.Seo,
Biosens. Bioelectron., 2016, 79, 273–279.
9 Q.Tian,Y.Mu,Y.Xu,Q.Song,B.Yu,C.Ma,W.JinandQ.
Jin, Anal. Biochem., 2015, 491, 55–57.
10 R. C. den Dulk, K. A. Schmidt, G. Sabatte, S. Liebana and
M. W. Prins, Lab Chip, 2013, 13, 106–118.
11 A. V. Govindarajan, S. Ramachandran, G. D. Vigil, P. Yager
and K. F. Bohringer, Lab Chip, 2012, 12, 174–181.
12 W. Huang, C. A. Gaydos, M. R. Barnes, M. Jett-Goheen and

D. R. Blake, Sex. Transm. Infect., 2013, 89, 108–114.
13 CDC, Reported STDs in the United States 2012 National Data for *Chlamydia*, Gonorrhea and Syphilis, 2014, http://stacks.
cdc.gov/view/cdc/21549.
14 J. R. Papp, J. Schachter, C. A. Gaydos and B. Van Der Pol,
Recommendations for the Laboratory-Based Detection of *Chlamydia trachomatis* and *Neisseria gonorrhoeae* — 2014, 2014, vol. 63, pp. 1–19.
15 S. Begolo, D. V. Zhukov, D. A. Selck, L. Li and R. F. Ismagilov, Lab Chip, 2014, 14, 4616–4628.
16 S. Makwana, B. Basu, Y. Makasana and A. Dharamsi, Int. J. Pharm. Invest., 2011, 1, 200–206.
17 F. P. Bretherton, J. Fluid Mech., 1961, 10, 166–188.
18 C. O. Mills, E. Elias, G. H. Martin, M. T. Woo and A. F.
Winder, J. Clin. Chem. Clin. Biochem., 1988, 26, 187–194.
19 A. W. Etchells and C. F. Meyer, in Handbook of Industrial Mixing, John Wiley & Sons, Inc., 2004, ch. 7, pp. 169, 391–
477, DOI: 10.1002/0471451452.
20 H. Song, D. L. Chen and R. F. Ismagilov, Angew. Chem., Int.
Ed., 2006, 45, 7336–7356.
21 H. Song, M. R. Bringer, J. D. Tice, C. J. Gerdts and R. F.
Ismagilov, Appl. Phys. Lett., 2003, 83, 4664–4666.
22 D. A. R. Brown, P. N. Jones, J. C. Middleton, G. Papadopoulos and E. B. Arik, in Handbook of Industrial Mixing, John Wiley & Sons, Inc., 2004, ch. 4, pp. 145–256, DOI: 10.1002/0471451452.
23 A. D. Awtrey and R. E. Connick, J. Am. Chem. Soc., 1951, 73,
1341–1348.
24 S. Hashimoto, Y. Chikamochi and Y. Inoue, Chem. Eng. Sci.,
2012, 80, 30–38.
25 P. J. Carreau, I. Patterson and C. Y. Yap, Can. J. Chem. Eng.,

1976, 54, 135–142.

26 J. B. Mahony, K. E. Luinstra, J. W. Sellors and M. A. Chernesky, J. Clin. Microbiol., 1993, 31, 1753–1758.

27 B. S. Ho, W. G. Feng, B. K. Wong and S. I. Egglestone, J. Clin. Pathol., 1992, 45, 439–442.

Chapter VIII

Flow-through capture and in situ amplification can enable rapid detection of a few single molecules of nucleic acids from several milliliters of solution[7]

Abstract

Detecting nucleic acids (NAs) at zeptomolar concentrations (few molecules per milliliter) currently requires expensive equipment and lengthy processing times to isolate and concentrate the NAs into a volume that is amenable to amplification processes, such as PCR or LAMP. Shortening the time required to concentrate NAs and integrating this procedure with amplification on-device would be invaluable to a number of analytical fields, including environmental monitoring and clinical diagnostics. Microfluidic point-of-care (POC) devices have been designed to address these needs, but they are not able to detect NAs present in zeptomolar concentrations in short time frames because they require slow flow rates and/or they are unable to handle milliliter-scale volumes. In this paper, we theoretically and experimentally investigate a flow-through capture membrane that solves this problem by capturing NAs with high sensitivity in a short time period, followed by direct detection by amplification. Theoretical predictions guided the choice of physical parameters for a chitosan-coated nylon membrane; these predictions can also be applied generally to other capture situations with different requirements. The membrane is also compatible with *in situ* amplification, which, by eliminating an elution step enables high sensitivity and will facilitate integration of this method into sample-to-answer detection devices. We tested a wide range of combinations of sample volumes and concentrations of DNA molecules using a capture membrane with 2 mm radius. We

[7]This chapter was first published in *Analytical Chemistry* with authorship belonging to Travis S. Schlappi, Stephanie E. McCalla, Nathan G. Schoepp, and Rustem F. Ismagilov. The original manuscript can be found at: http://dx.doi.org/10.1021/acs.analchem.6b01485.

show that for nucleic acid detection, this approach can concentrate and detect as few as ~10 molecules of DNA with flow rates as high as 1 mL/min, handling samples as large as 50 mL. In a specific example, this method reliably concentrated and detected ~25 molecules of DNA from 50 mL of sample.

Introduction

Detection of nucleic acids (NAs) at ultra-low concentrations (few molecules per milliliter of sample) in short time intervals is invaluable to a number of analytical fields, including environmental monitoring and clinical diagnostics[1-6]. Pathogens in aqueous environmental samples are frequently present at or below zeptomolar concentrations (~1000 microorganisms per liter), requiring laborious filtration and concentration procedures before detection is possible.[7,8] In many clinical applications, including minimal residual diseases[9] and latent Hepatitis C viral (HCV) or HIV infections, target NAs are also present at < 10 molecules/mL.[10,11] Blood bank donations are typically pooled before screening, so targets may be diluted by several orders of magnitude before being screened for pathogens, generating a sample where ultra-sensitive detection is critical.[12,13] Each of these examples requires the processing of large volumes (mLs) of extremely dilute samples, and therefore the ability to concentrate NAs on the order of 1000X to reach PCR-suitable volumes (μLs). Additionally, the entire concentration process must be done within minutes and not rely on expensive equipment to be directly applicable to limited-resource settings (LRS) and at the point-of-care (POC).[14,15]

Commercial systems for the purification and concentration of nucleic acids typically involve solid phase extraction (SPE), which uses chaotropic agents to control the absorption and release of NAs on silica.[16,17] While this method is widely used, most available protocols require centralized laboratories for centrifuging samples or manipulating beads.[18] NA precipitation[19] methods are also commonly used to extract and concentrate NAs from clinical and environmental samples; however these methods are laborious and involve the use of hazardous reagents.[20] These methods are challenging to

deploy for LRS, where instrumentation is limited, or for use at the POC, where diagnostics must be rapid and require minimal sample handling.[18] To address these needs, several charge-based methods have been developed, which typically include a charged polymer matrix including chitosan, poly-L-lysine, and so on for NA capture (we are building on that work in this paper).[21-25] To increase sensitivity, these and other systems concentrate NAs and then either elute before amplification[21,22,24,25] or perform amplification *in situ*.[23,26-29] Concentration factors up to 15X[21,30] and limits-of-detection as sensitive as 10^4 copies/mL[23] or 500 cells/mL[26] have been reported. While these methods have clear advantages over traditional solid-phase extraction methods, processing time and lowest detectable concentration are still limited by their inability to handle large sample volumes (>1 mL)[26-28,31] and/or their slow processing rates, which range from μL/min to μL/hr.[18,21,22,24,32,33] Thus, current methods—whether commercialized or from literature—lack the required combination of sensitivity, speed, and ease of implementation, leaving a gap in the current NA detection workflow.

We hypothesized that pressure-driven flow and capture in a porous matrix could facilitate the handling of large samples, while retaining many of the characteristics needed for both LRS and POC. Here, we analyze this approach theoretically and experimentally to determine a regime in which rapid, convection-driven capture is possible. Using a theoretical framework to predict capture efficiency as a function of flow-through conditions, we determined the parameters necessary for a detection matrix to capture a few nucleic acid molecules (<10) from several mLs of volume in short times (<10 minutes). We tested our predictions experimentally with respect to capture efficiency, lowest detectable concentration, processing time, and total sample volume. Furthermore, we demonstrated that the capture matrix is compatible with direct amplification, eliminating the need for an elution step. The ability to amplify *in situ* makes this approach amenable to integration into sample-to-answer devices, and preserves the high concentration factors achieved during capture by preventing loss of target to the capture matrix during elution.

Experimental Section

Capture Simulations. The fraction of nucleic acid molecules captured in a membrane pore compared to the amount flowed through (capture efficiency) was simulated at steady-state using the *Transport of Diluted Species* module of *Comsol Multiphysics (version 4.4)*. A complete description of the model geometry, transport parameters, kinetics, boundary conditions, mesh, and calculations performed is included in Supporting Information.

Chitosan Membrane Fabrication. A nylon membrane (LoProdyne LPNNG810S, Pall Corp., New York City, NY) was used as a porous matrix support. Two methods were employed for chitosan functionalization of the membrane, summarized below as "Method A" and "Method B."

Method A: The LoProdyne membrane has hydroxyl surface chemistry and was functionalized with N,N carbonyldiimidazole (CDI) in methylene chloride according to the manufacturer's protocol (http://www.pall.com; Supporting Information S-VII).

Chitosan oligosaccharide lactate (No. 523682, Sigma-Aldrich, St. Louis, MO) was purified by dissolving 1.2 g chitosan in 40 mL nuclease-free (NF) water, then precipitated by adding 3 mL 1M NaOH. This solution was mixed and filtered through Whatman paper #8 (12 cm). It was then rinsed with MilliQ water until the eluant was neutral. Washed chitosan was dried for 2 h under vacuum, then a rotary evaporator was used to remove residual moisture.

The optimal pH at which to cross-link chitosan with CDI was determined to be pH 5.0. Based on the pKa of chitosan (pKa = 6.3), ~5% of the chitosan's amines will be deprotonated and able to react. At pH > 5, a larger percentage of the chitosan amines will be deprotonated, resulting in a higher degree of crosslinking to the support surface, and fewer available amines to interact with nucleic acids. At a pH of 5.0, the chitosan

polymer should crosslink to the support at either one or two positions, leaving the bulk of the polymer free in solution.

To prepare chitosan-coated supports, a 6 mg/mL solution of purified chitosan was prepared in 34 mM HCl. This solution was vortexed for 10 min until the chitosan was fully dissolved, then sonicated to remove bubbles. The pH was then raised to 5.0 by addition of NaOH while vortexing. A CDI-functionalized LoProdyne membrane was then saturated with this chitosan solution. The membrane and chitosan solution were sandwiched between two glass slides, and pressed to remove excess chitosan solution. The wet membrane was blot-dried and placed in a desiccator to dry under vacuum for 20–30 min. After drying, the membrane was placed in a 50 mL Falcon tube and rinsed with NF water. The water was poured out, 0.1 M HCl was added to quench any remaining CDI and remove non-crosslinked chitosan, and the membrane and HCl vortexed for 2 min. The HCl was poured out and the membrane was rinsed with NF water again. Next, the membrane was placed in a fresh Falcon tube, rinsed more with NF water, washed in NF water for 25 min while agitated, rinsed with NF water three more times, blot dried, then air dried in a desiccator.

Method B: To prepare hydrogel coated membranes, a 0.5% (w/v) solution of chitosan (TCI OBR6I) was prepared in 150 mM HCl. A 25% (v/v) solution of glutaraldehyde was added to this solution to a final concentration of 4 mM. The solution was rapidly mixed, and added to the LoProdyne membrane in excess. The saturated membranes were then spun on a Laurel WS-400-6NNP/Lite spin coater at 500 rpm for 5 s with an acceleration setting of 410, followed by 15 s at 2000 rpm with an acceleration setting of 820. Membranes were allowed to crosslink for 2 h in air, washed 3 times with NF water, and dried under vacuum.

Binding Capacity Measurements. 1000 ng of salmon sperm DNA (Invitrogen, Carlsbad CA) in 100 μL of 10 mM MES buffer (pH ~5) was sequentially flushed through a chitosan membrane (radius = 2 mm, fabricated with Method A) five times via a

syringe/luer lock system (Figure 4-S4). The inlet and eluate DNA concentration of each flush was measured with PicoGreen dye (Invitrogen); subtracting the eluate from the inlet and converting to mass of DNA yielded the plot in Figure 8-3.

Capture and *In Situ* Amplification. λ-phage DNA stocks were quantified via digital PCR.[34] This DNA was spiked into varying volumes of 10 mM MES buffer (pH ~5) to create concentrations ranging from 0.2 to 20 copies/mL (Table 4-S4). The solutions were flowed through chitosan-coated nylon membranes (radius = 2 mm) using syringes and luer locks (Figure 4-S4), followed twice by 100 µL MES buffer. The membranes were then removed from the syringe/luer lock system, placed in an Ilumina Eco™ well plate, and 5–10 µL of PCR mix was added to each membrane. The well plate was inserted into an Ilumina Eco™ real time PCR system (EC-101-1001, Ilumina, San Diego, CA) and thermal cycled; correct λ-phage product was verified with a gel and melt curve analysis (Figure 4-S5).

The PCR mixture used for amplification of λ-phage DNA on the chitosan-coated nylon membranes contained the following: 5 µL 2X SsoFast Evagreen SuperMix (BioRad, Hercules, CA), 1 µL of BSA (20 mg/mL), 2 µL of 10 ng/uL salmon sperm DNA (Invitrogen), 1 µL of 5 µM primers (SI-VI), and 1 µL of NF water. The PCR amplification was performed with an initial 95 °C step for 3 min and then followed by 40 cycles of: (i) 20 s at 95 °C, (ii) 20 s at 62 °C, (iii) 15 s at 72 °C.

Results and Discussion

Theoretical Analysis. To predict a regime that would enable rapid flow-through capture of nucleic acids present at low concentrations, we developed a theoretical model that takes into account the convection, diffusion, and adsorption of nucleic acid molecules onto a capture agent layered within a porous matrix (Figure 8-1a and S-I). Although the structure of the nylon membrane is spongy and non-uniform, approximating the pores as cylinders is an appropriate simplification to estimate the transport processes and has been

done previously.[35,36] The parameters governing capture dynamics in a cylindrical pore are superficial velocity U [m/s], pore radius R_p [m], membrane radius R_m [m], membrane thickness (or, equivalently, pore length) δ_m [m], diffusivity of nucleic acid molecules[37] D [m^2/s], association rate constant[38] k_{on} [m^3/(mol·s)], surface concentration of the capture agent γ [mol/m^2], and mass transfer coefficient k_c [m/s]. Instead of analyzing every relevant parameter individually, we condensed them into two dimensionless numbers:[39,40] Damköhler (*Da*) and Péclet (*Pe*). *Da* characterizes the balance between adsorption rate and transport rate (Eq. 2) while *Pe* characterizes the balance between convection rate and diffusion rate (Eq. 2).

$$Da = \frac{adsorption\ rate}{transport\ rate} = \frac{k_{on}\gamma}{k_c}, k_c = 1.62\left(\frac{UD^2}{2\delta_m R_p}\right)^{\frac{1}{3}} \quad (2)$$

$$Pe = \frac{convection\ rate}{diffusion\ rate} = \frac{U/\delta_m}{D/R_p^2} \quad (2)$$

$Da > 1$ indicates that the rate of DNA binding to the capture agent is faster than the rate of DNA transport to the pore wall; $Pe < 1$ means the rate at which molecules diffuse to the pore wall is faster than the rate at which they are convected through the pore. To capture dilute nucleic acids from large volumes in short times, two conditions must be met: i) efficient capture ($Da >> 1$), and ii) fast flow rates ($Q \sim 1$ mL/min) while maintaining $Pe < 1$.

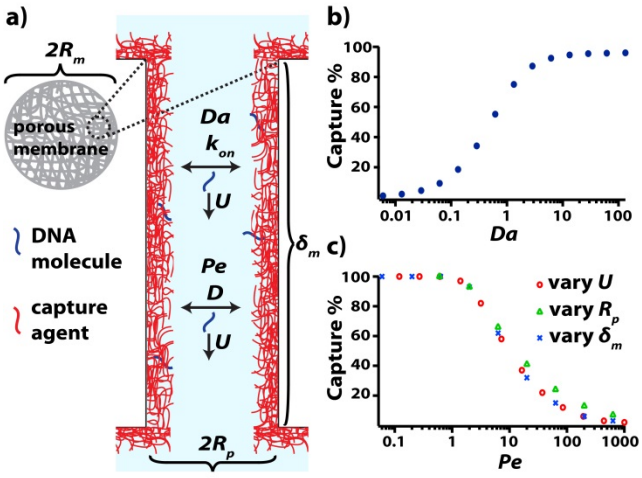

Figure 8-1. Theoretical model and numerical simulations for flow-through capture. a) A schematic drawing showing the process of capturing nucleic acids from a sample flowing through a porous membrane (which has been functionalized with a capture agent). b) Predictions for the percentage of molecules captured at the pore wall as a function of the Damköhler number (*Da*). c) Predictions for the percentage of molecules captured at the pore wall as a function of the Péclet number (*Pe*). *Pe* is changed by varying the velocity (U), pore length (δ_m), or pore diameter (R_p); all result in a similar dependence of capture percentage on *Pe*.

Capture efficiency is a factor of binding kinetics (time for the nucleic acid molecule to bind to the capture agent) and transport (time for the nucleic acid molecule to travel from the bulk solution to the pore wall coated with capture agent). High capture efficiency occurs when the transport rate is slower than the binding reaction rate (i.e., $Da >> 1$), which can occur with fast reactions or slow transport. Many passive capture processes—such as wicking through a porous matrix or mixing with beads—rely on slow transport rates to achieve high *Da*. These processes capture efficiently at small length scales in microliter volumes;[21-23,33] however, for milliliter volumes and large length scales, passive capture processes would require impractical amounts of capture agent or time for *Da* to be greater than 1. A fast binding reaction with diffusion-limited kinetics would enable higher transport rates (and thus faster flow rates) without adversely affecting capture

efficiency. Electrostatic binding and silica adsorption in the presence of Ca^{2+} are examples of diffusion-limited chemical reactions[41,42] that would maintain high *Da* without relying on slow transport rates to ensure efficient capture. Our simulations show that when a capture agent coated on a pore wall has fast binding kinetics, $Da > 10$ ensures > 95% capture of nucleic acids flowing through the pore (Figure 8-1b and S-I). To scale up efficient capture processes to larger volumes, the mass transport rate can be increased. One way to increase mass transport rate is actively forcing fluid through a porous matrix,[43] which has been used for protein capture[44] and is well established in membrane chromatography[35,36]. However, flow-through capture has not been analyzed theoretically nor tested experimentally for rapid capture and detection of zeptomolar nucleic acids. In general, high flow rates increase the transport rate, decrease *Da*, and thus reduce capture efficiency. However, the transport rate can be maintained below the adsorption rate (keeping $Da >> 1$) by manipulating other transport parameters, thus counteracting the high flow rate. These transport parameters can be analyzed together by simulating the capture efficiency as a function of *Pe* (S-I): simulations show that keeping $Pe < 1$ ensures > 90% capture efficiency (Figure 8-1c). To achieve a high convection rate and maintain $Pe < 1$, a relatively high diffusion rate is required, which ensures that the molecules don't leave the pore before having a chance to diffuse to the wall and bind. To maintain this balance of a high convection rate with an even higher diffusion rate, the membrane radius, pore radius, and membrane thickness can be adjusted. Setting $Pe < 1$ in Eq. 2 provides the following constraint on flow rate through the membrane (Q) as a function of δ_m, R_m, and R_p, where ϕ represents the porosity of the membrane (see S-II for derivation).

$$Q < \frac{\pi \phi D \delta_m R_m^2}{R_p^2} \quad (3)$$

Plotting Eq. 3 at different membrane thicknesses explores the relationship of these parameters (Figure 8-2a); trends favoring $Pe < 1$ and flow rates > 1 mL/min are decreasing pore radius, increasing membrane radius, and increasing membrane thickness. Decreasing the pore size enables faster diffusion rates and lower *Pe*, but it also increases

the resistance to flow. Figure 8-2b considers this tradeoff, showing the pressure drop required for a sample to flow through the membrane at 1 mL/min at different membrane and pore radii. The overlap of the green triangles ($Pe < 1$) with red color ($\Delta P < 1$ atm) represents an ideal combination of parameters wherein Pe is low enough and a reasonable pressure drop is achieved to flow at 1 mL/min.

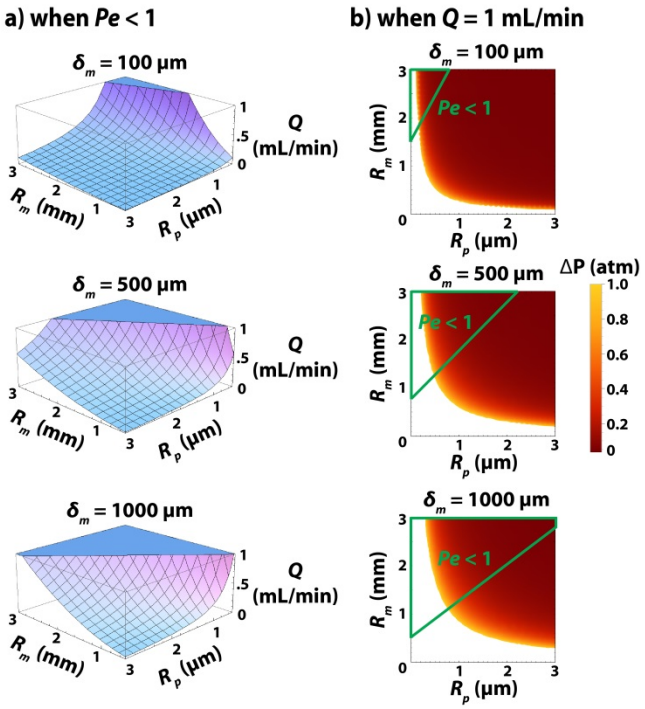

Figure 8-2. Predictions of membrane radius, pore radius, and membrane thickness tradeoffs for achieving high flow rates while also maintaining reasonable pressure drop (ΔP) and a low Péclet number (Pe). a) Combinations of membrane radius, pore radius, and flow rate that maintain $Pe < 1$ for different membrane thicknesses. Any point below the surface curvature has $Pe < 1$. b) The influence of membrane and pore radius on pressure drop with the flow rate through the membrane held constant at 1 mL/min. The overlap of the green triangle ($Pe < 1$) and red colored area represents efficient and rapid capture with a reasonable pressure drop ($\Delta P < 1$ atm). The white area signifies a combination of membrane and pore radius that results in prohibitively large pressure drops ($\Delta P > 1$ atm) necessary to achieve 1 mL/min.

Experimental Analysis. Based on these predictions, we chose an appropriate experimental system to evaluate the ability of a flow-through matrix to rapidly capture zeptomolar concentrations of nucleic acids. This matrix should be compatible with *in situ* amplification, so glass fiber, silica, and other common capture materials that inhibit amplification reactions were not considered.[45,46] Nylon membranes do not prevent nucleic acid amplification and can be purchased in various pore sizes and thicknesses. The membrane thickness for a LoProdyne nylon membrane from Pall Corporation ranges from 127.0-190.5 μm (see **Experimental Section**); at this thickness, a membrane radius of 2 mm is flexible and easily placed in a well plate for nucleic acid amplification. For a membrane thickness of 160 μm, flow rate of 1 mL/min, and membrane radius of 2 mm, Eq. 3 predicts that pore radii less than 0.76 μm would maintain $Pe < 1$. Therefore, we chose LoProdyne membranes with a pore radius of 0.6 μm; coating the membrane pores with a capture agent makes the pore size even smaller, ensuring that we were well below the 0.76 μm requirement. As described, the capture agent must have diffusion-limited kinetics. Because electrostatic binding is very fast and can easily be used for nucleic acid capture utilizing a cationic polymer to attract the negatively charged phosphate backbone of DNA, we chose chitosan as the capture agent, which has previously been used for NA capture.[21-25] Chitosan is an inexpensive biocompatible polymer with amine groups on its backbone that become positively-charged when the pH is below 6.3.[22,47] We functionalized chitosan onto the nylon membrane as described in **Experimental Section**. To verify that functionalizing the membrane with chitosan does not reduce the pore size such that the pressure drop becomes untenable (Figure 8-2b), we measured the capture efficiency at different flow rates. This experiment showed that the chitosan-functionalized nylon membrane captures > 90% of nucleic acids when solution is flowed through at 1 mL/min (see Figure 4-S2 of the Supporting Information).

To test the predictions from our analysis, we evaluated the capture efficiency as a function of Pe by flowing 500 ng/mL solutions of DNA through chitosan membranes at five different flow rates. Each flow rate was tested with three replicates and the capture efficiency along with one standard deviation is plotted in Figure 4-S2. These experiments

confirmed that the chitosan membranes capture efficiently over a range of *Pe*, with > 90% capture of DNA when *Pe* < 1 (Figure 4-S2). We also measured the DNA binding capacity of chitosan-functionalized nylon membranes and found that they have a capacity of 1000 ng or more (Figure 4-3). This capacity is much greater than needed for our target application of zeptomolar concentrations (10^{-21} M ~ 0.6 fg/mL for a bacterial genome). However, researchers in other fields may find this matrix useful in capturing large amounts of genetic material for other applications.

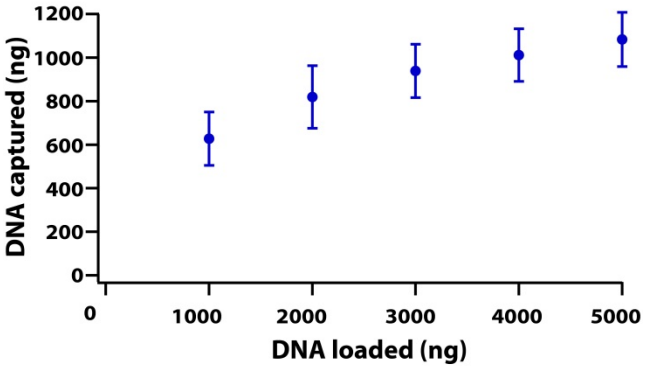

Figure 8-3. DNA binding capacity of chitosan-functionalized membranes fabricated with Method A.

Next, we tested whether *in situ* amplification would be chemically compatible with the nylon membrane that had been functionalized with chitosan. We added serial dilutions of DNA to the membrane, then submerged in amplification mix and amplified DNA via PCR. The chitosan membrane was compatible with *in situ* PCR amplification down to ~2 copies per reaction (Figure 4-S3a). We also tested the chitosan membrane compatibility with *in situ* LAMP and showed successful amplification at 20 copies per reaction (Figure 4-S3b[48]).

In this paper we did not study the location at which amplification occurs (i.e. whether amplification is initiated on the target molecules still attached to the surface of the membrane, or on the molecules released from the surface into the membrane pores, or on the molecules diffusing out of the pores). Further, we did not study the spatiotemporal

mechanism of propagation of amplification once it is initiated. Such studies could provide interesting information in subsequent research.

The final step was to use chitosan's charge-switch capability to couple rapid capture with direct amplification without eluting the nucleic acids. A sample flows through the chitosan-coated membrane at pH ~5 and the negatively-charged phosphate backbone of DNA will electrostatically bind to the positively-charged amine groups on the chitosan. Following capture of NAs, the addition of amplification mix at pH ~8 deprotonates the amine groups and releases the captured nucleic acids for amplification (Figure 8-4).

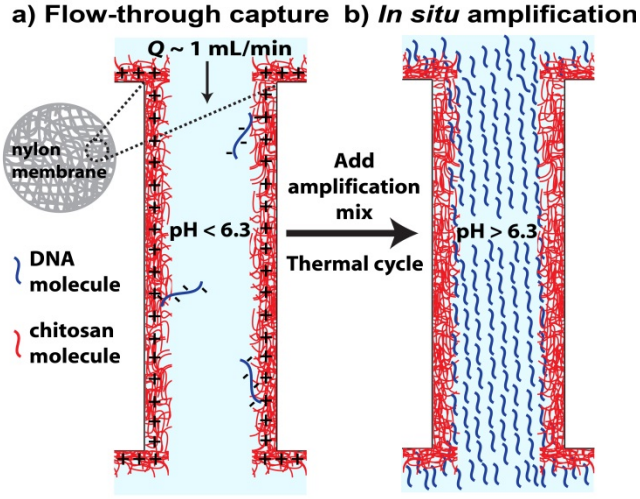

Figure 8-4. Schematic of capture and *in situ* amplification. a) Nucleic acids in a solution with pH < 6.3 will electrostatically bind to the protonated chitosan pore wall. b) Addition of amplification mix (pH ~8) deprotonates the chitosan and releases nucleic acids. Thermal cycling amplifies DNA.

We then tested this idea (combining rapid capture and *in situ* amplification via charge-switch) at ultra-low concentrations (~1 copy/mL) and fast flow rates. Various amounts of λ DNA were spiked into volumes ranging from 1 to 50 mL with 100 ng or less background DNA (Table 4-S4); the solution was then flowed through a 2 mm radius chitosan-functionalized membrane at ~1 mL/min. After capture, the amplification was

performed *in situ* with small volumes of PCR reagents (5–10 μL), as opposed to the traditional method of eluting from a capture matrix and using larger volumes of PCR reagents. DNA product was detected after thermal cycling using EvaGreen dye (see SI-V for details). This methodology detected a DNA target at concentrations as low as 0.5 copies/mL from as many as 50 mL (Figure 8-5b). Compiling data from replicate experiments run on different days, pre-concentration using the chitosan-functionalized membrane allowed detection down to 1 copy/mL over 85% of the time. Using any concentration above 10 copies/mL, detection results for the capture and amplification matrix were positive 100% of the time. No amplification was detected when flowing through buffer without DNA (see Figure 4-5a and Table 4-S4), ensuring that the λ DNA product detected is indeed from the sample flowed through the membrane and not contamination of the membrane, lab materials, or PCR reagents with λ-phage DNA.

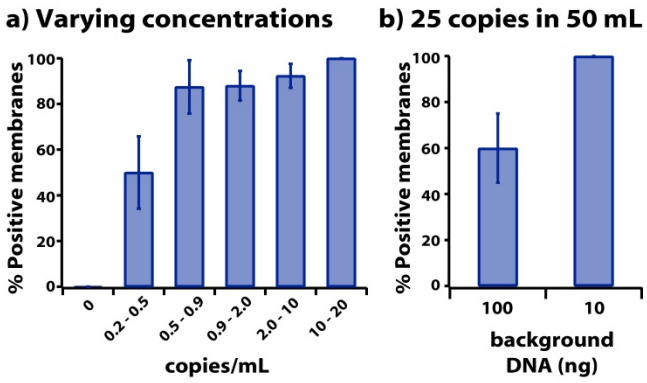

Figure 8-5. Nucleic acid detection via flow-through capture and *in situ* amplification on chitosan membranes. a) Percent of membranes that were positive for λ DNA product over different experiments on different days for varying concentrations (0.2–20 copies/mL). The volume flowed through ranged from 1 to 50 mL (Table 4-S4) and the flow rate was ~1 mL/min. Each bin of the histogram has 6–26 samples for a total of 82 samples. b) Percent of membranes that were positive for λ DNA product over different experiments on different days. 50 mL solutions with 25 copies of target DNA and 10 or 100 ng background DNA were flowed through membranes at ~0.3 mL/min. The number of replicates are N = 10 for 100 ng and N = 9 for 10 ng. All error bars are 1 S.D.

We observed that the chitosan membrane performance appeared to decrease slightly as larger volumes were flowed through (e.g., >10 mL volumes were 77% positive (23 out of 30 tests) and >20 mL volumes were 60% positive (9 out of 15 tests), see Table 4-S4). This decreased performance at higher volumes could be due to chitosan shedding off the membrane during flow or the fact that larger volumes have longer residence times and therefore more opportunity for the DNA molecule to release from its binding site and be flushed out of the membrane with the eluate. A thicker membrane with longer pores or a chitosan-functionalization method that more strongly attaches chitosan to the nylon membrane could potentially improve its performance at larger volumes; however, these parameters were not tested and are outside of the scope of this study.

Our experiments have been using stringent conditions with high flow rate (~1 mL/min) and high level of added background DNA. For some applications, these conditions might be too stringent, and high sensitivity of detection may be more valuable. For example, drinking water samples do not always have the high level of background DNA we used. The presence of high levels of background DNA can affect capture efficiency of the target molecule during flow-through and can affect amplification efficiency during PCR. We therefore also tested detection of ultra-low concentrations of nucleic acids from large volumes with reduced background DNA at 10 ng and slower flow rates at 0.3 mL/min. We compared 50 mL solutions with 100 ng background DNA to 50 mL solutions with 10 ng background DNA. These experiments showed that 25 copies in 50 mL could be consistently detected under these conditions (Figure 4-5b). We have not yet further investigated how the performance of this method depends on the interplay of flow rate, pore geometry, level of DNA background, and the details of fabrication of the chitosan coating.To test whether salts in solution could interfere with electrostatic binding and decrease the ability of chitosan membranes to capture and detect nucleic acids, we performed six preliminary experiments. The experiments were identical to those performed for Figure 4-5, but instead of using 10 mM MES buffer as the medium comprising nucleic acids, various salt solutions were used (see S-VIII for details): i)

Ringer's solution (10 and 20 copies λ DNA in 1 mL), Ringer's solution with 5 mM EDTA (10 and 20 copies λ DNA in 1 mL) and 5 mM EDTA alone (10 and 20 copies λ DNA in 1 mL). All six experiments resulted in positive amplification, indicating that the presence of salts does not disrupt capture of nucleic acids on the chitosan membrane nor their subsequent amplification.

Conclusion

We evaluated an approach for ultrasensitive detection of nucleic acids using chitosan as a charge-switch matrix that enables concentration factors up to 5000X (defined as the ratio of final detection volume to the starting sample volume, e.g., DNA from 50 mL of solution was detected in 10 μL of PCR mix) and subsequent *in situ* amplification. A theoretical model guided the parameters chosen for flow rate, membrane radius, and pore radius. Based on model predictions, membranes with specific pore and membrane radii were functionalized to capture low copy numbers of nucleic acids from large volumes in short times. Using this approach, we were able to capture zeptomolar concentrations of nucleic acids from up to 50 mL of solution at a flow rate of 1 mL/min with $\Delta P < 1$ atm. In applications with different requirements for flow rate, pressure drop, or membrane size, this theory can be applied to guide choices of membrane parameters that meet those requirements.

In addition, flowing through a matrix that is compatible with *in situ* amplification obviates the need for centrifugation or bead manipulation and simplifies the purification process by eliminating an elution step. Chitosan-functionalized nylon membranes are sturdy, flexible, and small enough to be incorporated into integrated devices for complete sample-to-answer diagnostics. In this study, we focused on the theory and the proof-of-principle experiments using solutions of purified nucleic acids in clean matrixes. However, more complex matrices are encountered in many applications. Ultrasensitive measurements of viral, bacterial, and cancer-associated nucleic acids provide important diagnostic information to clinicians, but require the extraction and detection of NAs from

milliliters of plasma and in some cases cell lysis. Combining this approach with lysis buffers and/or sample pretreatment should be tested next to evaluate the efficacy of this methodology for detection from a variety of sample matrices, such as blood, plasma, urine, and water. Additional work on integration of this approach with isothermal amplification would enable rapid and ultra-sensitive nucleic acid measurements for point-of-care and limited-resource settings.

Acknowledgements

This work was supported by DARPA Cooperative Agreement HR0011-11-2-0006. The content of this article does not necessarily reflect the position or the policy of the Government, and no official endorsement should be inferred. We thank Justin Rolando for chemistry advice and chitosan purification and Natasha Shelby for contributions to writing and editing this manuscript.

References

(1) Fearon, M.; Scalia, V.; Lane, D.; Bigham, M.; Hawes, G.; O'Brien, S.; Kadkhoda, K. *Transfusion* **2016**, *56*, 994-995.
(2) Fong, T.-T.; Lipp, E. K. *Microbiol. Mol. Biol. Rev.* **2005**, *69*, 357-371.
(3) Hodgson, S. H.; Douglas, A. D.; Edwards, N. J.; Kimani, D.; Elias, S. C.; Chang, M.; Daza, G.; Seilie, A. M.; Magiri, C.; Muia, A. *Malar. J.* **2015**, *14*, 33.
(4) World Health Organization. *Guidelines for Drinking-water Quality: Recommendations*; World Health Organization, Geneva, **2004**; Vol. 1, 3rd ed..
(5) Raboud, J. M.; Montaner, J. S.; Conway, B.; Rae, S.; Reiss, P.; Vella, S.; Cooper, D.; Lange, J.; Harris, M.; Wainberg, M. A. *AIDS* **1998**, *12*, 1619-1624.
(6) Sarmati, L.; D'Ettorre, G.; Parisi, S. G.; Andreoni, M. *Curr. HIV Res.* **2015**, *13*, 250.
(7) Jiang, S.; Noble, R.; Chu, W. *Appl. Environ. Microbiol.* **2001**, *67*, 179-184.
(8) Haramoto, E.; Kitajima, M.; Katayama, H.; Ohgaki, S. *Water Res.* **2010**, *44*, 1747-1752.

(9) Campana, D.; Pui, C.-H. *Blood*- **1995**, *85*, 1416-1434.

(10) Maggiolo, F.; Callegaro, A.; Cologni, G.; Bernardini, C.; Velenti, D.; Gregis, G.; Quinzan, G.; Soavi, L.; Iannotti, N.; Malfatto, E. *JAIDS* **2012**, *60*, 473-482.

(11) Castillo, I.; Bartolome, J.; Quiroga, J.; Barril, G.; Carreño, V. *Aliment. Pharmacol. Ther.* **2009**, *30*, 477-486.

(12) Keys, J. R.; Leone, P. A.; Eron, J. J.; Alexander, K.; Brinson, M.; Swanstrom, R. *J. Med. Virol.* **2014**, *86*, 473-477.

(13) Abubakar, A.; Ozumba, P.; Buttner, P.; Winter, J.; Abimiku, A. *Journal of Antivirals & Antiretrovirals* **2015**, *2015*.

(14) Yager, P.; Domingo, G. J.; Gerdes, J. *Annu. Rev. Biomed. Eng.* **2008**, *10*, 107-144.

(15) Urdea, M.; Penny, L. A.; Olmsted, S. S.; Giovanni, M. Y.; Kaspar, P.; Shepherd, A.; Wilson, P.; Dahl, C. A.; Buchsbaum, S.; Moeller, G. *Nature* **2006**, *444*, 73-79.

(16) Boom, R.; Sol, C.; Salimans, M.; Jansen, C.; Wertheim-van Dillen, P.; Van der Noordaa, J. *J. Clin. Microbiol.* **1990**, *28*, 495-503.

(17) Wen, J.; Legendre, L. A.; Bienvenue, J. M.; Landers, J. P. *Anal. Chem.* **2008**, *80*, 6472-6479.

(18) Dineva, M. A.; Mahilum-Tapay, L.; Lee, H. *Analyst* **2007**, *132*, 1193-1199.

(19) Chomczynski, P.; Sacchi, N. *Anal. Biochem.* **1987**, *162*, 156-159.

(20) Miller, D.; Bryant, J.; Madsen, E.; Ghiorse, W. *Appl. Environ. Microbiol.* **1999**, *65*, 4715-4724.

(21) Byrnes, S. A.; Bishop, J. D.; Lafleur, L.; Buser, J.; Lutz, B.; Yager, P. *Lab on a Chip* **2015**, *15*, 2647-2659.

(22) Cao, W.; Easley, C. J.; Ferrance, J. P.; Landers, J. P. *Anal. Chem.* **2006**, *78*, 7222-7228.

(23) Pandit, K. R.; Nanayakkara, I. A.; Cao, W.; Raghavan, S. R.; White, I. M. *Anal. Chem.* **2015**, *87*, 11022-11029.

(24) Hagan, K. A.; Meier, W. L.; Ferrance, J. P.; Landers, J. P. *Anal. Chem.* **2009**, *81*, 5249-5256.

(25) Kendall, E. L.; Wienhold, E.; DeVoe, D. L. *Biomicrofluidics* **2014**, *8*, 044109.

(26) Connelly, J. T.; Rolland, J. P.; Whitesides, G. M. *Anal. Chem.* **2015**, *87*, 7595-7601.

(27) Rodriguez, N. M.; Linnes, J. C.; Fan, A.; Ellenson, C. K.; Pollock, N. R.; Klapperich, C. M. *Anal. Chem.* **2015**, *87*, 7872-7879.

(28) Liu, C.; Geva, E.; Mauk, M.; Qiu, X.; Abrams, W. R.; Malamud, D.; Curtis, K.; Owen, S. M.; Bau, H. H. *Analyst* **2011**, *136*, 2069-2076.

(29) Rodriguez, N. M.; Wong, W. S.; Liu, L.; Dewar, R.; Klapperich, C. M. *Lab on a Chip* **2016**.

(30) Reedy, C. R.; Bienvenue, J. M.; Coletta, L.; Strachan, B. C.; Bhatri, N.; Greenspoon, S.; Landers, J. P. *Forensic science international: genetics* **2010**, *4*, 206-212.

(31) Jangam, S. R.; Yamada, D. H.; McFall, S. M.; Kelso, D. M. *J. Clin. Microbiol.* **2009**, *47*, 2363-2368.

(32) Breadmore, M. C.; Wolfe, K. A.; Arcibal, I. G.; Leung, W. K.; Dickson, D.; Giordano, B. C.; Power, M. E.; Ferrance, J. P.; Feldman, S. H.; Norris, P. M. *Anal. Chem.* **2003**, *75*, 1880-1886.

(33) Shim, S.; Shim, J.; Taylor, W. R.; Kosari, F.; Vasmatzis, G.; Ahlquist, D. A.; Bashir, R. *Biomedical microdevices* **2016**, *18*, 1-8.

(34) Shen, F.; Du, W.; Kreutz, J. E.; Fok, A.; Ismagilov, R. F. *Lab on a Chip* **2010**, *10*, 2666-2672.

(35) Thömmes, J.; Kula, M. R. *Biotechnol. Prog.* **1995**, *11*, 357-367.

(36) Unarska, M.; Davies, P.; Esnouf, M.; Bellhouse, B. *J. Chromatogr. A* **1990**, *519*, 53-67.

(37) Lukacs, G. L.; Haggie, P.; Seksek, O.; Lechardeur, D.; Freedman, N.; Verkman, A. *J. Biol. Chem.* **2000**, *275*, 1625-1629.

(38) Wink, T.; de Beer, J.; Hennink, W. E.; Bult, A.; van Bennekom, W. P. *Anal. Chem.* **1999**, *71*, 801-805.

(39) Hansen, R.; Bruus, H.; Callisen, T. H.; Hassager, O. *Langmuir* **2012**, *28*, 7557-7563.

(40) Koyayashi, T.; Laidler, K. J. *Biotechnol. Bioeng.* **1974**, *16*, 99-118.

(41) Nguyen, T. H.; Elimelech, M. *Biomacromolecules* **2007**, *8*, 24-32.

(42) Minehan, D. S.; Marx, K. A.; Tripathy, S. K. *Macromolecules* **1994**, *27*, 777-783.

(43) Chung, Y.-C.; Jan, M.-S.; Lin, Y.-C.; Lin, J.-H.; Cheng, W.-C.; Fan, C.-Y. *Lab on a Chip* **2004**, *4*, 141-147.

(44) Bhattacharjee, S.; Dong, J.; Ma, Y.; Hovde, S.; Geiger, J. H.; Baker, G. L.; Bruening, M. L. *Langmuir* **2012**, *28*, 6885-6892.
(45) Wang, W.; Wang, H. B.; Li, Z. X.; Guo, Z. Y. *J. Biomed. Mater. Res. A* **2006**, *77*, 28-34.
(46) Linnes, J.; Rodriguez, N.; Liu, L.; Klapperich, C. *Biomedical Microdevices* **2016**, *18*, 1-12.
(47) Kyung-Hee, C.; Kwang-hee, K. P. *Bulletin of the Korean Chemical Society* **1983**, *4*, 68-72.
(48) Nagamine, K.; Hase, T.; Notomi, T. *Mol. Cell. Probes* **2002**, *16*, 223-229.

Supporting Information

Flow-through capture simulations

The fraction of nucleic acid molecules captured in a membrane pore compared to the amount flowed through (capture efficiency) is a function of pore geometry, flow parameters, and adsorption kinetics (Figure 8-S6). The concentration of nucleic acids at any position in the pore, *C(r, z),* was simulated at steady-state using the *Transport of Diluted Species* module of *Comsol Multiphysics (version 4.4)* with the parameters listed in Table 4-S1. To generate the data for Figure 4-1b-c, a parametric sweep was performed with various values of $k_{on}\cdot\gamma$, U, R_p, and δ_m (Table 4-S2 and Table 4-S3). Then, the inlet flux ($J_{in} = J|_{z=\delta m}$) and outlet flux ($J_{out} = J|_{z=0}$) were evaluated and used in Eq. S-3 to calculate capture efficiency.

$$Capture\ \% = 1 - \frac{J_{out}}{J_{in}} \qquad \text{(S-3)}$$

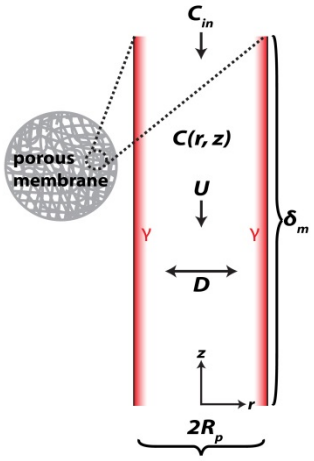

Figure 8-S6. Schematic of flow-through simulation geometry. Red represents the capture agent (γ) coated on the surface of the pore wall.

Table 4-S1. Parameters used in the flow-through capture simulations.

Parameter	Description	Value
R_p	Pore radius	0.56 – 17.78 μm
δ_m	Pore length (thickness of membrane)	0.316 – 3162 μm
U	Flow velocity	0.118 – 1000 mm/s
D	Diffusivity of nucleic acid molecule	10 $\mu m^2 \cdot s^{-1}$
k_{on}	Nucleic acid binding rate constant	10^6 $L \cdot mol^{-1} \cdot s^{-1}$
γ	Surface concentration of capture agent	10^{-7} $mol \cdot m^{-2}$
C_{in}	Inlet concentration of nucleic acids	1 μM

Table 4-S2. The product of $k_{on} \cdot \gamma$ was varied to generate Capture % as a function of Damköhler number (Da) (Figure 4-1b). R_p (1 μm), δ_m (100 μm), U (2 mm/s), D (10 $\mu m^2 \cdot s^{-1}$), and C_{in} (1 μM) were held constant.

$k_{on} \cdot \gamma$ (m/s)	k_c (m/s)	Da	J_{in} (mol/s)	J_{out} (mol/s)	Capture %
1.00E-07	1.62E-05	0.01	-3.92E-18	-3.88E-18	1.0
2.15E-07	1.62E-05	0.01	-3.92E-18	-3.83E-18	2.1
4.64E-07	1.62E-05	0.03	-3.92E-18	-3.74E-18	4.5
1.00E-06	1.62E-05	0.06	-3.92E-18	-3.55E-18	9.3

2.15E-06	1.62E-05	0.13	-3.92E-18	-3.19E-18	18.5
4.64E-06	1.62E-05	0.29	-3.92E-18	-2.58E-18	34.2
1.00E-05	1.62E-05	0.62	-3.92E-18	-1.75E-18	55.2
2.15E-05	1.62E-05	1.33	-3.92E-18	-9.77E-19	75.0
4.64E-05	1.62E-05	2.87	-3.92E-18	-5.03E-19	87.2
1.00E-04	1.62E-05	6.17	-3.92E-18	-2.94E-19	92.5
2.15E-04	1.62E-05	13.3	-3.92E-18	-2.11E-19	94.6
4.64E-04	1.62E-05	28.7	-3.92E-18	-1.78E-19	95.5
1.00E-03	1.62E-05	61.7	-3.92E-18	-1.63E-19	95.8
2.15E-03	1.62E-05	133	-3.92E-18	-1.57E-19	96.0

Table 4-S3. U, δ_m, or R_p was varied to generate Capture % as a function of Péclet number (Pe) (Figure 4-1c). C_{in} (1 μM), $k_{on}\cdot\gamma$ (10^{-4} m/s), and D (10 $\mu m^2 \cdot s^{-1}$) were held constant.

U (m/s)	δ_m (μm)	R_p (μm)	*Pe*	J_{in} (mol/s)	J_{out} (mol/s)	Capture %
1.18E-04	100	1	0.12	-2.46E-19	-2.32E-36	100.0
2.68E-04	100	1	0.27	-5.32E-19	-1.00E-26	100.0
6.11E-04	100	1	0.61	-1.20E-18	-4.11E-22	100.0
1.39E-03	100	1	1.39	-2.72E-18	-7.21E-20	97.4
3.16E-03	100	1	3.16	-6.19E-18	-1.11E-18	82.0
7.20E-03	100	1	7.20	-1.41E-17	-5.92E-18	58.0
1.64E-02	100	1	16.4	-3.21E-17	-2.02E-17	37.0
3.73E-02	100	1	37.3	-7.30E-17	-5.70E-17	22.0
8.48E-02	100	1	84.8	-1.66E-16	-1.46E-16	12.3
1.93E-01	100	1	193	-3.78E-16	-3.54E-16	6.5
4.39E-01	100	1	439	-8.60E-16	-8.32E-16	3.2
1.00E+00	100	1	1000	-1.96E-15	-1.93E-15	1.6
2.00E-03	3162	1	0.06	-3.90E-18	8.30E-39	100.0
2.00E-03	1000	1	0.20	-3.90E-18	-1.15E-28	100.0
2.00E-03	316	1	0.63	-3.90E-18	-1.72E-21	100.0
2.00E-03	100	1	2.00	-3.90E-18	-2.90E-19	92.6
2.00E-03	31.6	1	6.32	-3.90E-18	-1.50E-18	61.5
2.00E-03	10.0	1	20.0	-3.90E-18	-2.65E-18	32.1

2.00E-03	3.16	1	63.2	-3.90E-18	-3.30E-18	15.4
2.00E-03	1.00	1	200	-3.90E-18	-3.65E-18	6.4
2.00E-03	0.316	1	632	-3.90E-18	-3.80E-18	2.6
2.00E-03	100	0.56	0.63	-1.23E-18	-1.60E-21	99.9
2.00E-03	100	1.00	2.00	-3.90E-18	-2.90E-19	92.6
2.00E-03	100	1.78	6.32	-1.23E-17	-4.20E-18	65.9
2.00E-03	100	3.16	20.0	-3.90E-17	-2.30E-17	41.0
2.00E-03	100	5.62	63.2	-1.23E-16	-9.40E-17	23.6
2.00E-03	100	10.00	200	-3.90E-16	-3.40E-16	12.8
2.00E-03	100	17.78	632	-1.23E-15	-1.15E-15	6.5

Geometry: The model was assembled using a cylindrical geometry drawn in 2D axially symmetric space, with *r* as the radial component and *z* the axial component (Figure 4-S1). The radius of the cylinder (R_p) varied from 0.56 μm to 17.78 μm; the length of the cylinder (δ_m) varied from 0.316 μm to 3162 μm (Table 4-S3).

Transport: In a porous matrix, fluid flow can be approximated with a uniform velocity (U) independent of radius[1]. The flow velocity varied from $1.18 \cdot 10^{-4}$ m/s to 1 m/s (Table 4-S3). The top boundary of the cylinder ($z = \delta_m$) was an inlet and the bottom boundary ($z = 0$) was an outlet. The diffusion coefficient used was for DNA[2], 10^{-11} m^2/s.

Kinetics: The binding rate between nucleic acids and the capture agent was assumed to be second order with respect to nucleic acid concentration and capture agent surface concentration. We assumed the surface concentration of capture agent (γ) was in excess (and therefore unchanging during the course of the adsorption reaction) and estimated it to be 10^{-7} mol/m^2. With a kinetic rate constant estimated from nucleic acid-cationic polymer kinetics[3], the adsorption rate occurring at the pore wall is shown in Eq. S-4.

$$R_{ads} = k_{on} \cdot \gamma \cdot C(R_p, z) \qquad \text{(S-4)}$$

Normally, adsorption kinetics include both an on and off rate. However, in this situation, we excluded the off rate from analysis because it was insignificant compared to the on rate (kon ~ 107 $M^{-1}s^{-1}$, koff ~ 10-3 s-1, reference 38 from the manuscript).

Boundary conditions: The inlet concentration of nucleic acid molecules (C_{in} = 10^{-6} mol/L) represents a normal nucleic acid concentration in human blood plasma[4]. Axial symmetry was imposed at $r = 0$, and a flux boundary condition (Eq. S-5) was imposed at $r = R_p$ to represent the adsorption of nucleic acid molecules to the surface of the pore wall.

$$R_{ads} = D \frac{\partial C(r,z)}{\partial r}\Big|_{r=R_p} \quad \text{(S-5)}$$

Mesh and solver settings: The geometry was meshed using a Free Triangular mesh with a maximum element size of 0.0525 μm. The Direct Stationary Solver (PARDISO) was used with a nested dissection multithreaded preordering algorithm and an auto scheduling method.

Equation 3 and Figure 4-2b

The number of pores in a membrane (n_p) can be calculated from the porosity (ϕ) as in Eq. S-6.

$$\phi = \frac{n_p \pi R_p^2}{\pi R_m^2} \rightarrow n_p = \frac{\phi R_m^2}{R_p^2} \quad \text{(S-6)}$$

The flow rate through the entire membrane (Q) is the flow rate through each pore (Q_p) multiplied by the number of pores ($Q = n_p Q_p$). Using Eq. S-6 for n_p and solving for Q_p gives the following:

$$Q_p = \frac{Q R_p^2}{\phi R_m^2} \quad \text{(S-7)}$$

Eq. S-8 results from plugging Eqn S-7 into the relationship between pore flow rate and flow velocity ($Q_p = U\pi R_p^2$).

$$U = \frac{Q_p}{\pi R_p^2} = \frac{Q}{\pi \phi R_m^2} \quad \text{(S-8)}$$

Then, using Eq. S-8 in Eq. 2 and setting the condition that $Pe < 1$ yields Eq. S-9.

$$Pe = \frac{UR_p^2}{D\delta_m} = \frac{QR_p^2}{\pi\phi R_m^2 D\delta_m} < 1 \qquad \text{(S-9)}$$

Solving Eq. S-9 for Q yields Eq. 3. ϕ = 0.6 and $D = 10^{-11}$ m^2/s were assumed for all calculations.

To calculate the pressure drop as a function of pore radius (R_p) and membrane radius (R_m), Pouiselle flow was assumed (Eq. S-10). Flow rate through the pore (Q_p) was replaced with flow rate through the entire membrane (Q) using Eq. S-7. Q (1 mL/min), μ (10^{-3} Pa·s), and ϕ (0.6) were held constant; R_p and R_m were varied from 1 to 3 μm and 1 to 3 mm, respectively. The results, along with regimes of $Pe < 1$ calculated from Eq. 2, are plotted in Figure 4-2b.

$$\Delta P = \frac{8\mu Q_p \delta_m}{\pi R_p^4} = \frac{8\mu Q \delta_m}{\pi\phi R_p^2 R_m^2} \qquad \text{(S-10)}$$

DNA binding efficiency as a function of Pe

100 ng of salmon sperm DNA (Invitrogen, CA) in 200 μL of 10 mM MES buffer (pH ~5) was flushed through a chitosan membrane with a radius of 2 mm at different flow rates via the syringe/luer lock system shown in Figure 8-S9. The inlet and eluate DNA concentration of each flush was measured with PicoGreen dye (Invitrogen, CA); converting to mass (m_{DNA}), Eq. S-11 was then used to calculate the capture efficiency.

$$Capture\ \% = \left(1 - \frac{m_{DNA,out}}{m_{DNA,in}}\right) \cdot 100 \qquad \text{(S-11)}$$

Pe was calculated via Eq. 2 and the results are plotted in Figure 8-S7. This agrees with theoretical predictions that $Pe > 1$ results in reduced capture. Also, layering the nylon membrane with chitosan does not significantly hinder flow rate or require untenable pressure drops to achieve flow rates of ~ 1 mL/min and efficient capture.

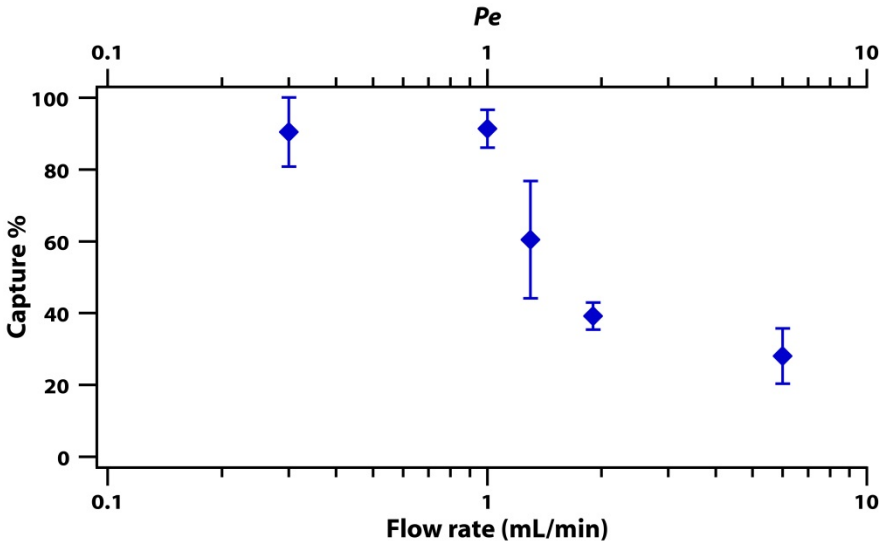

Figure 8-S7. Capture efficiency depends on flow rate.

We clarify that capture efficiencies > 90% are only possible when the capture agent is in excess of the target DNA molecule and *Pe* < 1, which is the case for 100 ng of input DNA (Figure 4-S2). On the other hand, the purpose of the experiments in Figure 4-3 was to measure the total binding capacity of the chitosan membrane (i.e., occupy all the cationic binding sites). To accomplish this, larger quantities of DNA (1000 ng) were flowed through the membrane and the capture efficiency was not expected to be high; in fact, with each successive load, it should decrease to 0% until all binding sites are occupied. Indeed, we observed that the capture efficiency in Figure 4-3 varied from 60% in the first run to 20% in the fifth run—by the time the fifth load of 1000 ng DNA was flowed through the membrane, there were fewer binding sites available and thus the recovery was much lower than the first load when all binding sites were available.

Compatibility of chitosan membrane with in situ *amplification*

To test the compatibility of chitosan membranes with *in situ* PCR amplification, 1 µL of varying concentrations of λ DNA was wetted into chitosan membrane with a radius of 2 mm. The membrane was then placed in a well plate and 10 µL PCR mix was added to the well. Replicates containing 10 µL PCR mix with the same amount of λ DNA and no membrane present were also included. The well plate was inserted into an Ilumina Eco™

real-time PCR System (EC-101-1001) and thermal cycled; correct λ-phage DNA product was verified with melt curve analysis. The PCR mix and thermal cycling conditions used were the same as described in the Experimental Section. Figure 8-S8a shows that chitosan membranes are compatible with *in situ* PCR amplification down to ~2 copies/reaction.

To test compatibility with *in situ* LAMP amplification, 20 copies of λ DNA were wetted into a chitosan membrane with a radius of 2 mm. The membrane was then placed in a well plate and 10 µL LAMP mix was added to the well. Replicates containing 10 µL LAMP mix with 20 copies of λ DNA and no membrane present were also included as solution controls. The well plate was inserted into an Ilumina Eco™ real-time PCR System and incubated for 40 min at 68 °C. Figure 8-S8b shows the real-time fluorescent traces representing DNA product.

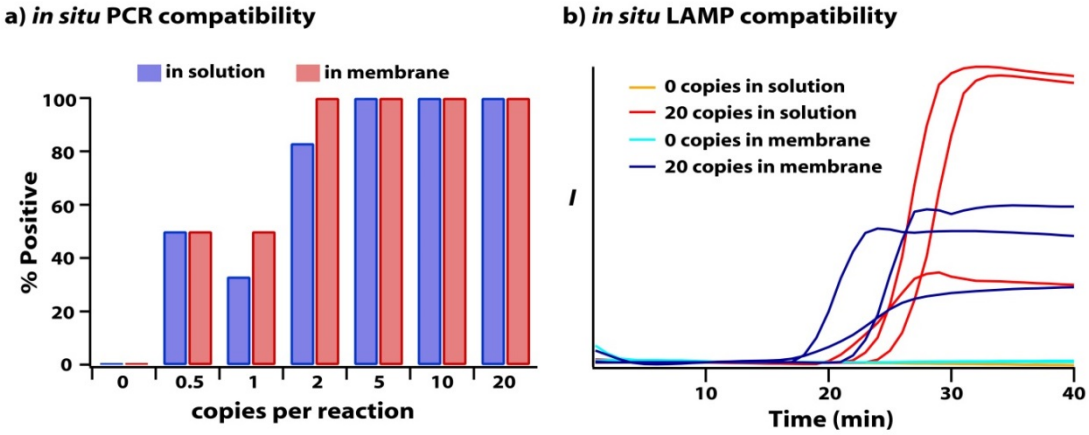

Figure 8-S8. Compatibility of chitosan membranes with PCR and LAMP amplification. a) Dilutions of λ DNA were wetted onto chitosan membranes or placed into a well plate without a membrane; PCR mix was added and amplification was detected via melt curve analysis. Six replicates were run at each dilution; the percent of replicates positive for λ DNA product is shown (n = 6). b) 20 copies of λ DNA were wetted onto chitosan membranes within a well plate, or placed into a well plate without a membrane; LAMP mix was added and amplification was detected via real-time fluorescence. Three

replicates were run for each sample; the fluorescent traces as a function of time are plotted.

LAMP reagents were purchased from Eiken Chemical (Tokyo, Japan), product code LMP207. The LAMP mixture used for amplification of λ-phage DNA contained the following: 5 μL Reaction Mixture, 0.4 μL of Enyzme Mixture, 0.5 μL of 20X LAMP primer mixture (Table 4-S6), 0.25 μL of Calcein (Fd), and 3.85 μL of nuclease-free water.

Details of capture and in situ *amplification (Figure 4-5)*

Figure 8-S9 is a schematic of the syringe/luer lock system used to flow mL-scale volumes through chitosan membranes with a radius of 2 mm. Syringes were purchased from BD (Franklin Lakes, NJ) and luer locks (Catalog #LC78-J1A) were purchased from Nordson Medical (Westlake, Ohio). Table 4-S4 shows all the quantities of λ DNA, volumes of 10 mM MES buffer, and amounts of background DNA used to generate Figure 4-5. Salmon sperm DNA from Invitrogen (Carlsbad, CA) was used as "background DNA".

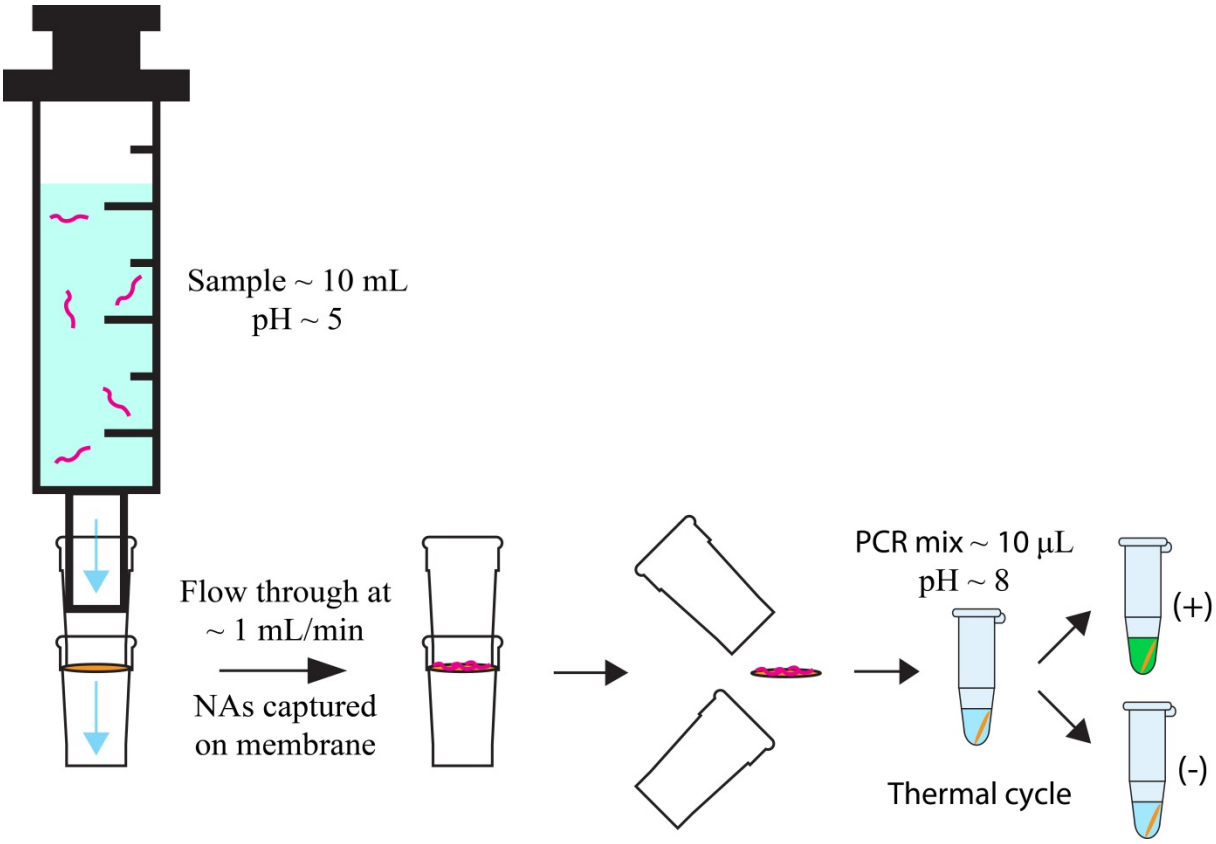

Figure 8-S9. Schematic of syringe/luer lock system used to flow mL-scale volumes through the chitosan membrane with a radius of 2 mm. A chitosan membrane is placed in between two luer locks. A syringe containing a nucleic acid sample is connected to the top luer lock and the plunger is compressed to flush the sample through the membrane. Then, the luer locks are disconnected from the syringe, and taken apart, and the membrane containing captured nucleic acids is placed in a PCR tube along with amplification mix for thermal cycling.

Table 4-S4. Volumes of 10 mM MES (2-(N-morpholino)ethanesulfonic acid) buffer and final concentrations of λ DNA used for Figure 4-5a. The two fabrication methods are described in the Experimental Section.

Copies of λ DNA	Volume of 10 mM MES buffer (mL)	λ DNA Concentration (cop/mL)	Background DNA added to MES buffer (ng)	Positive membranes	Total membranes tested	Fabrication Method

0	1	0	100	0	3	A
0	3	0	100	0	3	B
10	50	0.2	100	1	1	B
10	50	0.2	100	1	4	A
5	15	0.3	100	2	2	A
10	30	0.3	100	1	2	A
10	25	0.4	100	1	2	A
5	10	0.5	100	2	2	A
10	20	0.5	100	3	4	A
25	50	0.5	100	1	1	B
25	50	0.5	0	1	1	B
9	10	0.9	10	6	6	B
5	5	1.0	100	2	2	A
10	10	1.0	100	1	2	A
10	10	1.0	50	3	3	B
9	5	1.8	0	6	6	B
6	3	2.0	100	2	3	B
10	5	2.0	50	2	3	B
12	5	2.4	100	3	3	A
10	4	2.5	100	2	2	A
5	1	5.0	100	5	5	A
10	2	5.0	100	4	4	A
6	1	6.0	100	3	3	B
10	1	10.0	100	3	4	A
20	2	10.0	100	2	2	A
10	1	10.0	0	2	3	B
20	1	20.0	100	5	5	A
20	1	20.0	0	3	3	B

To detect λ DNA product after *in situ* amplification, two methods were used. i) After thermal cycling the membrane with PCR mix in a well plate, an appropriate amount of 6x gel loading dye and TE buffer was added to each well and pipette mixed. Then, 5 μL of this solution was removed from the well, placed in a 1.2% agarose gel, and run for 50 min at 80V. Samples with DNA product at the same length as the λ PCR amplicon (322 base pairs) were considered positive. An example of a gel image is shown in Figure 8-S10a. ii) After thermal cycling, the PCR reaction mixture was transferred to an empty well and an appropriate amount of 20X Evagreen dye (Biotium) and 10X TE buffer was

added. A continuous melt curve was then obtained from 65–95 ˚C; samples with a peak around ~85 ˚C (the melting temperature of the λ PCR amplicon) were considered positive. (Figure 8-S10b).

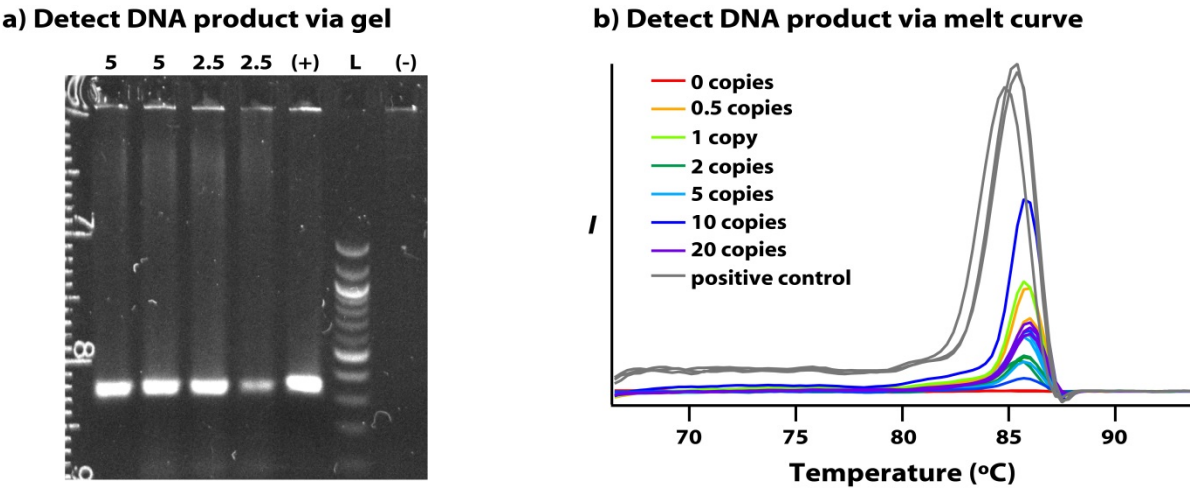

Figure 8-S10. DNA detection after *in situ* amplification. a) Varying concentrations of λ DNA in 10 mM MES buffer were flowed through chitosan membranes. The membranes were then placed in a well plate and thermal cycled. After thermal cycling, each sample was run on a gel. Lanes 1–2: 5 copies/mL; Lanes 3–4: 2.5 copies/mL; Lane 5: positive control (10 copies of λ DNA in PCR mix, no membrane); Lane 6: negative control (0 copies of λ DNA in PCR mix, no membrane). b) Dilutions of λ DNA were wetted onto chitosan membranes; PCR mix was added and melt curve fluorescent traces are plotted. Three replicates were run at each dilution.

It is important to note that while Table 4-S4 includes experiments done on multiple batches of membranes over 8 months, it does not include all experiments that we performed with chitosan-coated nylon membranes. Using binding capacity measurements (described in Experimental Section) and DNA capture experiments (described in S-IV), we determined that there was batch-to-batch variation in the fabrication process. Therefore, only those batches with consistent performance were analyzed and other batches that did not meet our standards were excluded from analysis.

Table 4-S5 summarizes Table 4-S4 by binning the various experiments into concentration ranges and reporting a "% Positive membranes" along with the standard error. This data is then plotted in Figure 4-5a of the manuscript.

Table 4-S5. Histogram of Table 4-S4 with concentration bins and standard error.

Concentration (cop/mL)	positive	total	positive/total	SE
0	0	6	0.00	0.00
0.2 - 0.5	5	10	0.50	0.16
0.5 - 0.9	6	7	0.86	0.13
0.9 - 2.0	22	25	0.88	0.06
2.0 - 10.0	24	26	0.92	0.05
10.0 - 20.0	8	8	1.00	0.00

To reliably detect ultra-low concentrations of nucleic acids from large volumes, we reduced the background DNA amount to 10 ng and relaxed the constraint imposed on the experiments for Figure 4-5a that the solution be flowed through the membrane at 1 mL/min. We instead flowed through at ~0.3 mL/min and compared 50 mL solutions with 100 ng background DNA to 50 mL solutions with 10 ng background DNA. These experiments showed that 25 copies in 50 mL can be consistently detected when the flow rate and background DNA are reduced from the previous constraints of 1 mL/min and 100 ng. The data is shown in
Table **4-S6** below and summarized in the manuscript with Figure 4-5b.

Table 4-S6. Volumes of 10 mM MES (2-(N-morpholino)ethanesulfonic acid) buffer and final concentrations of λ DNA used for Figure 4-5b. The two fabrication methods are described in the Experimental Section.

Copies of λ DNA	Volume of 10 mM MES buffer (mL)	λ DNA Concentration (cop/mL)	Background DNA added to MES buffer (ng)	Positive membranes	Total membranes tested	Fabrication Method
25	50	0.5	100	6	10	B

25	50	0.5	10	9	9	B

Primer sequences for $\boldsymbol{\lambda}$-phage DNA PCR amplification and $\boldsymbol{\lambda}$-phage DNA LAMP amplification

A mixture of primers from Table 4-S7 was made at 5 μM each in nuclease-free water and used for the PCR amplification reactions described in this manuscript.

Table 4-S7. Sequences for λ-phage DNA PCR primers.

forward	CGTTGCAGCAATATCTGGGC
reverse	TATTTTGCATCGAGCGCAGC

A mixture of each primer from
Table **4-S8** was made in nuclease-free water and used for the LAMP amplification reactions described in S-IV. The concentration of each primer in the 20X mixture is also listed.

Table 4-S8. Sequences for λ-phage DNA LAMP primers[5] and their concentration in the 20X primer mix.

Name	**Sequence**	**Conc.**
FOP	GGCTTGGCTCTGCTAACACGTT	4 μM
BOP	GGACGTTTGTAATGTCCGCTCC	4 μM
FIP	CAGCCAGCCGCAGCACGTTCGCTCATAGGAGATATGGTAGAGCCGC	32 μM
BIP	GAGAGAATTTGTACCACCTCCCACCGGGCACATAGCAGTCCTAGGGACAGT	32 μM
LOOPF	CTGCATACGACGTGTCT	8 μM
LOOPR	ACCATCTATGACTGTACGCC	8 μM

CDI functionalization of nylon membrane

Before coating with chitosan, the LoProdyne membrane was functionalized with N,N carbonyldiimidazole (CDI) in methylene chloride according to the manufacturer's protocol. The protocol is found at this website (http://www.pall.com/main/oem-materials-and-devices/literature-library-details.page?id=4765) and is also copied below:

LoProdyne LP membrane has hydroxyl surface chemistry. The membrane binds very little protein in standard binding tests using IgG or BSA. The membrane can be activated for covalent attachment using N, N® carbonyldiimidazole (CDI) in methylene chloride as follows:

Dissolve 0.49 g CDI in 45 mL MeCl2.
Add to a glass dish under a fume hood.
Immerse sheet of LoProdyne LP membrane in this solution for 15 minutes, RT.
Wash membrane 4X with 40 mL per wash MeCl2, 5 minutes per wash.
Air dry at 60 °C for 3 minutes.
Store in vacuum desiccator until use.

Complex solutions

To test whether salts in solution could interfere with electrostatic binding and decrease the ability of chitosan membranes to capture and detect nucleic acids, we performed preliminary experiments in complex solutions. Ringer's solution was used to mimic the salt concentration of plasma and was made according to the instructions at the following website: http://cshprotocols.cshlp.org/content/2008/1/pdb.rec11273.full?text_only=true. The information from the website is also pasted below:

Ringer's solution (pH 7.3-7.4)
Reagent (amount to add): NaCl (7.2 gm), CaCl2 (0.17 gm), KCl (0.37 gm).

Dissolve all reagents into reagent-grade H2O, and bring the final volume to 1 L. Adjust the pH to 7.3-7.4. Once thoroughly dissolved, filter through a 0.22-μm filter, aliquot into single-use volumes (25-50 mL), and autoclave.

The final salt concentration of the Ringer's solution is ~125 mM. 5 mM EDTA was also tested because plasma is often processed and stored in an anticoagulant such as EDTA.

References

(1) Thömmes, J.; Kula, M. R. *Biotechnol. Prog.* 1995, *11*, 357-367.
(2) Lukacs, G. L.; Haggie, P.; Seksek, O.; Lechardeur, D.; Freedman, N.; Verkman, A. *J. Biol. Chem.* 2000, *275*, 1625-1629.
(3) Wink, T.; de Beer, J.; Hennink, W. E.; Bult, A.; van Bennekom, W. P. *Anal. Chem.* 1999, *71*, 801-805.
(4) Kamm, R. C.; Smith, A. G. *Clin. Chem.* 1972, *18*, 519-522.
(5) Nagamine, K.; Hase, T.; Notomi, T. *Mol. Cell. Probes* 2002, *16*, 223-229.

Author Contributions

Contributions of non-corresponding authors:

Travis S. Schlappi:

- Contributor to method/protocol development for capture experiments and in situ amplification experiments.
- Major contributor to simulation and theory development.
- Performed all simulations for Figures 1 and 2.
- Developed protocol for DNA capacity measurements and performed all experiments for Figure 3.
- Contributed to experiments and data accumulation for Figure 5.
- Major contributor to outline, manuscript, and supporting information writing.

- Major contributor to figure and manuscript revisions.
- Made all figures and tables in the manuscript and supporting information.

Stephanie E. McCalla:

- Major contributor to concept of chitosan-based flow-through capture and in situ amplification for low concentration detection.
- Major contributor to method/protocol development for chitosan functionalization (hydrogel and monolayer), capture experiments, and in situ amplification experiments.
- Major contributor to simulation and theory development.
- Performed preliminary experimental work on in situ amplification and flow-through capture.
- Performed preliminary simulations for Figure 1c.
- Contributed to outline writing.
- Contributed to manuscript revisions.

Nathan G. Schoepp:

- Major contributor to method/protocol development for chitosan hydrogel synthesis.
- Contributor to method/protocol development for capture experiments, and in-situ amplification.
- Contributor to experiments and data accumulation for Figure 5.
- Minor contributor to manuscript writing.
- Minor contributor to manuscript revisions.

Chapter IX

Real-time, digital LAMP with commercial microfluidic chips reveals the interplay of efficiency, speed, and background amplification as a function of reaction temperature and time[8]

Abstract

Real-time, isothermal, digital nucleic acid amplification is emerging as an attractive approach for a multitude of applications including diagnostics, mechanistic studies, and assay optimization. Unfortunately, there is no commercially available and affordable real-time, digital instrument validated for isothermal amplification; thus, most researchers have not been able to apply digital, real-time approaches to isothermal amplification. Here, we generate an approach to real-time digital loop-mediated isothermal amplification (LAMP) using commercially available microfluidic chips and reagents, and open-source components. We demonstrate this approach by testing variables that influence LAMP reaction speed and the probability of detection. By analyzing the interplay of amplification efficiency, background, and speed of amplification, this real-time digital method enabled us to test enzymatic performance over a range of temperatures, generating high-precision kinetic and endpoint measurements. We were able to identify the unique optimal temperature for two polymerase enzymes, while accounting for amplification efficiency, non-specific background, and time to threshold. We validated this digital LAMP assay and pipeline by performing a phenotypic antibiotic susceptibility test on 17 archived clinical urine samples from patients diagnosed with urinary tract infections. We provide all the necessary workflows to perform digital LAMP using standard laboratory equipment and commercially available materials. This

[8]This chapter was first published in *Analytical Chemistry* with authorship belonging to Justin C. Rolando, Erik Jue, Nathan G. Schoepp, and Rustem F. Ismagilov. The original manuscript can be found at: http://dx.doi.org/10.1021/acs.analchem.8b04324.

real-time digital approach will be useful to others in the future to understand the fundamentals of isothermal chemistries—including which components determine amplification fate, reaction speed, and enzymatic performance. Researchers can also adapt this pipeline, which uses only standard equipment and commercial components, to quickly study and optimize assays using precise, real-time digital quantification—accelerating development of critically needed diagnostics.

Introduction

In this paper, we describe a methodology to use commercially available chips, reagents, and microscopes to perform real-time digital LAMP. We use this methodology to perform a mechanistic study of digital isothermal amplification, and apply the lessons learned to perform a phenotypic antibiotic susceptibility test (AST).

Microfluidics-based diagnostics for infectious diseases are advancing as a result of using nucleic acid testing, making them amenable to the point of care (POC) and limited-resource settings where they will have clinical impact. Isothermal amplification methods in particular show promise for simplifying nucleic-acid-based POC diagnostics by circumventing the stringent thermal cycling requirements of PCR.[1] One isothermal method that is being actively pursued in bioanalytical chemistry and the field of diagnostics is loop-mediated isothermal amplification (LAMP).[2-6]

LAMP and other isothermal technologies are fast and sensitive, but when performed in a bulk format in microliter volumes (e.g., in a tube) they provide only semi-quantitative (log-scale) resolution or presence/absence measurements.[7-15] As a result, when optimizing an assay, it is difficult to quantify how small changes in assay conditions (e.g., in primers, reagents, or temperature) impact the reaction's speed and analytical sensitivity. To reliably understand these effects with high precision would require hundreds of bulk experiments per condition.[16] For the field to be able to take full advantage of the capabilities of LAMP, researchers need to be able to optimize reaction

conditions by understanding and testing the variables that may influence reaction speed and probability of detection. Furthermore, the semi-quantitative measurements yielded by bulk isothermal methods are insufficient for analyses requiring precise quantification, such as phenotypic antibiotic susceptibility testing.[17,18]

These problems can be solved using "digital" approaches, which partition single target molecules in large numbers of compartments and give a binary (presence/absence) readout for each compartment. These "digital" approaches thus allow determination of the efficiency of the amplification reaction[19] and provide absolute quantification with high resolution. Digital isothermal measurements have been used to quantify viral load for HCV,[16,20,21] HIV,[19,20] and influenza,[22] perform bacterial enumeration,[23-25] optimize primers,[16] and test for phenotypic antibiotic susceptibility[18] using LAMP[18-28] and RPA.[29]

Real-time digital formats are especially valuable for examining the variables that most affect non-specific amplification and the speed of amplification. Many excellent approaches for end-point[19,20,22-28] and real-time[16,18,21] digital LAMP (dLAMP) have been published. Despite the value that real-time dLAMP can bring to diagnostics, this method is difficult to implement—especially for those without a background in micro-electro-mechanical systems or microfluidics—because there is no commercial system for real-time, digital isothermal amplification. To achieve statistical significance, a meaningful study might require dozens of experiments; such studies are difficult to perform without a commercial source of chips. Consequently, the few LAMP mechanistic studies that have been performed were not done with high precision. Further, those who would most benefit from optimized digital isothermal reactions (e.g. those working on POC diagnostics) cannot efficiently improve them.

Here, we demonstrate how to generate high-precision kinetic and endpoint measurements using a real-time dLAMP assay that is performed completely with commercially available and open-source components (**Figure 1**). We use this real-time information to investigate dLAMP reactions mechanistically, including the interplay of efficiency,

speed, and background amplification as a function of reaction temperature and time on two enzymes. To illustrate one application of using real-time dLAMP to improve a clinically relevant assay, we optimized the assay conditions for a phenotypic AST using the real-time dLAMP pipeline and used the optimized protocol to compare our AST of 17 clinical urine samples to the gold-standard method.

Experimental Section

Microfluidic chips used in this paper were sourced from Applied Biosystems, Foster City, CA, USA) Ref A26316, "QuantStudio 3D Digital PCR 20k Chip Kit V2."

LAMP reagents

Our amplification target was the *E. coli* 23S ribosomal gene, which we used previously as a target to perform rapid AST on clinical samples.[18] Primers were purchased through Integrated DNA Technologies (San Diego, CA, USA) and were described previously.[18] Final primer concentrations were identical for all experiments: 1.6 μM FIP/BIP, 0.2 μM FOP/BOP, and 0.4 μM LoopF/LoopB.

LAMP experiments using *Bst* 3.0 **(Figure 2; Figure 3b d, e, f, h-j; Figure 4)** contained the following final concentrations, optimized previously[18]: 1x Isothermal Amplification Buffer II (New England BioLabs (NEB), Ipswich, MA, USA; Ref. B0374S; containing 20 mM Tris-HCl 10 mM $(NH_4)_2SO_4$ 150 mM KCl, 2 mM $MgSO_4$, 0.1% Tween 20 pH 8.8 at 25 °C), 4 mM additional $MgSO_4$ (beyond 2 mM from buffer), 1.4 mM Deoxynucleotide Solution Mix, primers: 1.6 μM FIP/BIP, 0.2 μM FOP/BOP, and 0.4 μM LoopF/LoopB, 1 mg/mL BSA (New England BioLabs, Ref B90005), 320 U/mL *Bst* 3.0, Ambion RNAse cocktail (ThermoFisher, Waltham, MA, USA; Ref AM2286, 5 U/mL RNase A, 400 U/mL TNase T1), 2 μM SYTO 9 (ThermoFisher, Reference S34854), and approximately 660 copies/μL template in Ambion nuclease-free water (ThermoFisher, Ref AM9932).

LAMP experiments using *Bst* 2.0 **(Figure 3a, c, e, g)** contained the following final concentrations, optimized as shown in **Figure S3**: 1x Isothermal Amplification Buffer (New England BioLabs, Ref. B0537S; containing 20 mM Tris-HCl 10 mM $(NH_4)_2SO_4$, 50 mM KCl 2 mM $MgSO_4$ 0.1% Tween 20 pH 8.8 at 25 °C), additional 6 mM $MgSO_4$ (New England BioLabs, Ref. B1003S), 1.4 mM Deoxynucleotide Solution Mix (New England BioLabs, Ref N0447S), primers: 1.6 µM FIP/BIP, 0.2 µM FOP/BOP, and 0.4 µM LoopF/LoopB, 1 mg/mL BSA (New England BioLabs, Ref B90005), 320 U/mL *Bst* 2.0 (New England BioLabs, Ref M0537S), Ambion RNAse cocktail (ThermoFisher, Ref AM2286, 5 U/mL RNase A, 400 U/mL TNase T1), 2 µM SYTO 9 (ThermoFisher, Ref S34854), and approximately 660 copies/µL template in Ambion nuclease-free water (ThermoFisher, Ref AM9932).

Template *E. coli* DNA was extracted from exponential-phase cultures grown in BBL Brain-Heart Infusion media (BD, Franklin Lakes, NJ, USA; Ref. 221813) using QuickExtract DNA Extraction Solution (Lucigen, Middleton, WI, USA; Ref. QE09050) as described previously.[18] Serial 10-fold dilutions were prepared in Tris-EDTA buffer (5 mM Tris-HCl, 0.5 mM EDTA, pH 8.0) containing 2 U/mL RNase A and 80 U/mL RNase T1 (ThermoFisher, Ref AM2286). DNA dilutions were quantified as described previously[18] using the QX200 Droplet Digital PCR (ddPCR) system (Bio-Rad Laboratories, Hercules, CA, USA).

Phenotypic antibiotic susceptibility testing (AST) on clinical samples

For the phenotypic AST, we adopted a workflow described previously,[17,18] and used archived nucleic-acid extractions from a previous study.[18] Briefly, clinical urine samples from patients with urinary tract infections (UTI) were split and diluted into equal volumes of media with or without the presence of an antibiotic. Samples were incubated for 15 min at 37 °C, a nucleic-acid extraction was preformed, and these samples were

archived at -80 °C until use. LAMP was performed on the archived samples to quantify the number of copies of the *E. coli* 23S ribosomal gene.

We tested our optimized assay on 17 archived clinical UTI samples containing $\geq 5 \times 10^4$ CFU/ml *E. coli* that had been categorized previously using the gold-standard broth microdilution AST (5 ciprofloxacin-susceptible, 5 ciprofloxacin-resistant, 4 nitrofurantoin-susceptible, and 3 nitrofurantoin-resistant).

We assessed samples as phenotypically "resistant" or "susceptible" by calculating the ratio of the concentration of 23S in the control and antibiotic-treated sample, which we call the control:treated (C:T) ratio. The C:T ratio was calculated 10 min after beginning to heat the LAMP reaction. A threshold of 1.1 was established previously,[17,18] so samples with C:T ratios >1.1 indicated that there was DNA replication in the untreated (control) group but not in the antibiotic-treated samples; these samples were identified as susceptible to the antibiotic. Samples with C:T ratios of <1.1 indicated that DNA replication occurred in both the control and antibiotic-treated samples; these samples were identified as resistant to the antibiotic.

Results and Discussion

Workflow summary of real-time digital LAMP

To evaluate a pipeline for real-time dLAMP experiments, we chose commercially sourced microfluidic chips sold for endpoint digital PCR applications. The chips consist of an array of 20,000 uniform partitions (**Figure 1**), each 60 μm in diameter and an estimated 0.75 nL internal volume, which is similar to the volumes typically used in dLAMP.[16,18,20-23,25,26,28] These chips are loaded by pipetting the sample mixture (in our case containing the LAMP reagents: buffer components, enzymes, template, and primers) into the plastic "blade" provided with the chips, and dragging the blade at a 70–80° angle to the chip to load the sample mixture by capillarity. This is followed by drying and

evaporation of the surface layer for 20 sec at 40 °C, and application of the immersion fluid. Manual loading requires some skill, though a machine can be purchased to perform the task; typically, we were able to load ~18,000 out of the 20,000 partitions. We performed our evaluation using two different enzyme mixtures, *Bst* 2.0 and *Bst* 3.0 . Our amplification target (**Figure 1**) was the *E. coli* 23S ribosomal gene that we previously used as a target to perform rapid AST on clinical samples.[18]

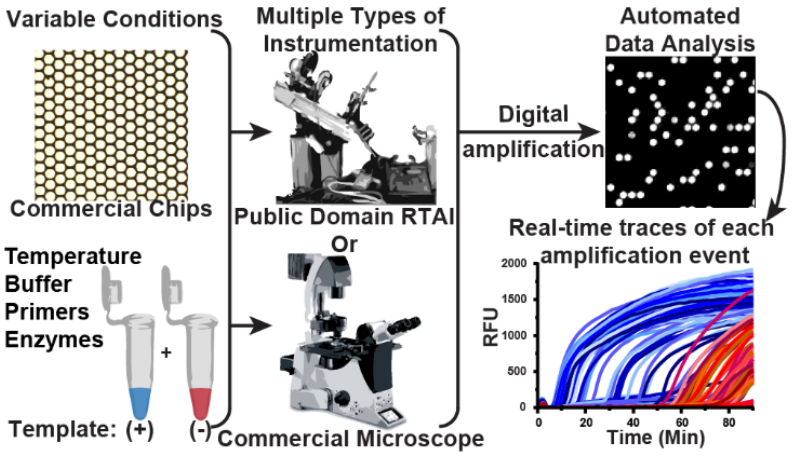

Figure 9-1. A schematic of the pipeline for performing multiplexed, real-time, digital loop-mediated isothermal amplification (LAMP) using only commercially available and/or open source components. Microfluidic chips and reagents (e.g. primers, enzymes, buffer composition) can be purchased commercially. Multiple instrument configurations can be used to capture results. e.g. a customized real-time instrument (instructions for building publicly available[30]) or any commercial microscope. Data analysis is automated using a MATLAB script (Supporting Information, S-I).

The instrumentation requirements for real-time isothermal capabilities include a heater that can hold a stable temperature, and optical components with high spatial resolution that are capable of imaging the fluorescence intensity of the 20,000 individual partitions of the chip over time (**Figure 2a**). Here, we investigated two approaches: using a standard laboratory microscope (Leicia DMI-6000B), and using the RTAI,[30] which is composed of a thermocycler, optical components, a camera, and a light source.

We generated a custom MATLAB script to analyze the digital real-time data (details in **Supporting Information, S-I**). The software follows the change in fluorescence in individual partitions over time. From these data, we extract each partition's time to a fluorescence intensity threshold and calculate the bulk template concentration. In our demonstration, we loaded the acquired images into FIJI[31] as a time-stack series and manually separated the images of the individual chips to be analyzed separately. To process each chip's image stack, we used the custom MATLAB script that tracks the mean intensity of each partition over the course of each experiment. This script could be run with only minor modifications with images obtained from different instruments.

To calculate the bulk template concentration over time, we (1) identified the partitions that did or did not contain reaction solution, (2) tracked the partitions that met a minimum fluorescence intensity and (3) used the previous information to calculate the concentration of template in the bulk solution.

A summary of the script is as follows: (i) load the images into memory, (ii) count the total number of partitions before heating (iii) identify positive partitions after the conclusion of the experiment, (iv) track the intensity of positive partitions for each image frame, (v) apply Gaussian smoothing and baseline subtraction, (vi) save the data, and (vii) repeat for each image stack. The output of the script contains: the raw traces of individual partitions over time, baseline corrected traces of individual partitions over time (**Figure 2b**), the number of partitions exceeding the manually defined minimum fluorescence intensity threshold with time (**Figure 2f**), and the maximum relative rate in RFU per 30 sec for individual partitions (**Figure 2d**). These data provide all the necessary information to conduct the analyses detailed in **Figure 2**.

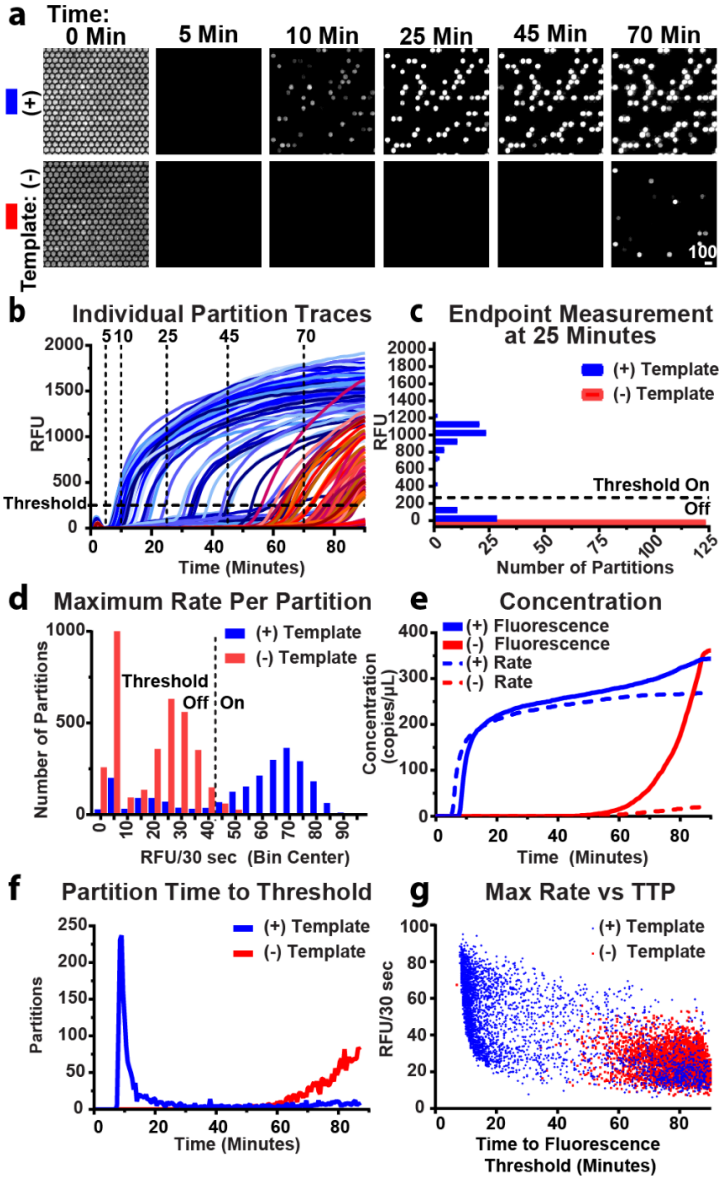

Figure 2. Experimental demonstration of the real-time digital LAMP (dLAMP) approach using the commercially available enzyme *Bst* 3.0. Experiments were run at 70 °C and imaged using a commercial microscope. (a) A time course of fluorescence images from a subset of 350 partitions out of 20,000 partitions undergoing dLAMP reactions. (Intensity range 920-1705 RFU). (b) Fluorescence intensity for a subset of partitions over time. Blue traces indicate partitions containing template; red traces indicate fluorescence in the absence of template (i.e. non-specific amplification). Partitions turn "on" at the time point when the curve passes the threshold at 250 RFU. Vertical traces correspond to time

points illustrated in panel (a) and generate endpoint measurements. (c) An "endpoint" measurement taken on a subset of partitions at 25 min. Bin width is 100 RFU. Fluorescence threshold is 250 RFU. (d) A histogram of the maximum observed change in fluorescence of individual partitions using the full chip. Rate threshold is 45 RFU/30 sec. (e) Change in observed bulk concentration over time from the full chip using fluorescence intensity as threshold (solid lines) and rate (dashed lines). (f) Time at which individual partitions in panel (b) cross the fluorescence intensity threshold. (g) Maximum rate per partition plotted by time to fluorescence intensity threshold.

Digital, real-time experiments to quantify LAMP performance

We next sought to experimentally evaluate this pipeline (**Figure 1**). First, we established whether the fluorescence from LAMP reactions could be reliably measured from individual partitions over time (**Figure 2a**). We used LAMP reagents for *Bst* 3.0, commercial chips, a resistive heater held at 70 °C, and a commercial microscope. Although the microscope is capable of collecting all 20,000 partitions on one chip in a single image, for simplicity, in **Figure 2a**, we cropped the image to include only 350 of the 20,000 partitions. Before turning on the heater (t = 0), we measured the autofluorescence from SYTO 9 to quantify the total number of partitions loaded with reaction solution. (To calculate template concentration using the Poisson distribution[32,33], we must know the total number of partitions containing the reaction mixture.) Autofluorescence from SYTO 9 decreases as the chip is heated and is completely eliminated within 3 min. The heater used on the microscope reaches reaction temperature within 120 sec. In less than 10 min, an increase in fluorescence was observed within some of the individual partitions, indicating amplification of individual template molecules inside those partitions. Due to the stochastic nature of amplification initiation, some of the partitions fluoresced later.

In the negative-control (no template) partitions, fluorescence was not observed for the first 45 min. However, we began to observe non-specific amplification after ~60 min. In

these experiments, the negative control contains only 0.05x Tris-EDTA buffer in place of template and represents a best-case scenario. We attribute amplification in the absence of template to primer dimers and other non-specific LAMP products.

Second, we asked if the signal from non-specific amplification was sufficiently delayed to differentiate it from the signal arising from specific amplification in the presence of template. To answer this question, we generated real-time fluorescence curves by plotting the change in fluorescence of individual partitions as a function of time (**Figure 2b**). We observed specific amplification (blue curves) beginning to initiate at ~7 min and non-specific amplification beginning to initiate at ~50 min (red curves) and concluded that we could discriminate specific and non-specific amplification by time.

Third, we asked whether enzymatic heterogeneity[16,21,34] of specific amplification can be quantified to differentiate specific from non-specific amplification. We plotted the maximum change of fluorescence achieved by each partition of the full chip per 30-sec interval (**Figure 2d)**. For the negative-control sample (red bars), we observed non-specific amplification following a bimodal distribution of rates, with a first peak with little to no rate of fluorescence increase and a second peak at ~25 RFU per 30 sec. For the sample containing template (blue bars), rates for specific amplification were heterogeneous and centered around a rate of 70 RFU/30 sec. We note that in PCR, which is gated by temperature cycling, there is no equivalent concept of "rate" as long as replication of DNA occurs faster that the duration of each elongation step. We found in our dLAMP experiments that the rate of specific amplification was greater than non-specific amplification. Hence, tracking amplification in real-time made it possible to distinguish true positives from false positives (non-specific amplification).

Fourth, we asked if the distribution in time to fluorescence threshold is sufficiently narrow to discriminate specific and non-specific amplification. By plotting the number of "on" partitions (i.e. partitions that crossed the fluorescence intensity threshold defined in **Figure 2b)** against time, we generated a distribution curve (**Figure 2f**) that illustrates the

number of partitions that turn on per time point. This is related to the derivative of the change in concentration over time. This plot contains the time to threshold of all partitions within the entire chip, rather than a subset, to minimize sampling bias**.** In the sample containing template (blue curve), most partitions reached the threshold in 7–20 min, whereas the negative-control sample (red curve) had little non-specific amplification until approximately 60 min. Graphing time to threshold illustrates the overall reaction's speed (defined as the location of the peak or mode time to threshold) and efficiency (proportional to the area under the curve and illustrated in **Figure 2f** as the calculated concentration). In our experiment, the peak of the sample containing template was narrow and well separated from the non-specific amplification of the negative control (**Figure 2f**), indicating sufficiently low heterogeneity in amplification rate and time to initiation of the reaction.

Fifth, we asked how the calculated bulk concentration changes over time. To answer this question, we generated endpoint-style measurements for each 30-sec time point, and calculated how the concentration changed over time. To demonstrate how to generate a single endpoint-style measurement, we selected one time point (25 min) and plotted RFU as a factor of the number of partitions (**Figure 2c**). Partitions were classified as either "on" (>250 RFU threshold) or "off" (<250 RFU threshold). Partitions that are defined as having turned "on" contain a template molecule that amplified, whereas partitions that are "off" either lack a template molecule or have not yet begun amplification. The sum of the partitions passing the threshold out of the total number of partitions with solution was used to determine a precise bulk concentration of template in the sample using the Poisson equation, as has been documented elsewhere.[32,33] We plotted the calculated concentration as it changed over time in **Figure 2e** (solid lines).

When the aim is to determine a precise concentration, we need to determine the best time at which to stop the assay. Deciding the best time to end the assay is complicated because each reaction initiates stochastically,[16,21] causing the calculated concentration to asymptotically approach the true concentration (**Figure 2e**). It would be ideal for the

calculated concentration to rapidly rise to the true bulk concentration and plateau near the true concentration; however, the reaction should be stopped before the rise in non-specific amplification (observed in our example starting at 60 min; red curves, **Figure 2e–f**). We tested whether there is heterogeneity in amplification rate (i.e. whether partitions with slow amplification rates take longer to reach the fluorescence intensity threshold than partitions with fast amplification rates) and found that initiation time was stochastic, but the reaction rates for true and false positives were consistent (**Figure 2g**). Hence, two molecules could have the same TTP, yet initiate at different moments, resulting in variable amplification rates.

Combining information about the concentration of template (**Figure 2e**) and the time it takes for partitions to turn "on" (**Figure 2f**) can be used to inform the choice of an optimal assay length for endpoint measurements, for situations where real-time quantification is not feasible. For example, in **Figure 2**, the optimal assay length for an endpoint readout would be ~45 min. This approach allows one to balance stochastic initiation of amplification, overcome enzymatic heterogeneity, and reduce the incidence of false positives caused by non-specific amplification.

However, in cases where real-time measurements are desirable, thresholding by rate may be used to separate specific and non-specific amplification. For example, to correct for the observed increase in non-specific amplification (after 45 min), we implemented a threshold (**Figure 2d**) on the maximum rate per partition, thus eliminating some of the non-specific amplification in both the presence and absence of template (compare solid and dashed lines in **Figure 2e).** For example, the measured value at 60 min is 280 copies per μL (solid line), and the corrected value is 258 copies per μL (dashed line). In the no-template control, at 60 min, the measured value is 16 copies per μL (solid line), whereas the corrected value is 3 copies per μL (dashed line). The correction is more pronounced at 80 min where non-specific amplification is greater. At 80 min, the measured value in the presence of template is 325 copies per μL and the corrected value 266 copies per μL—indicating that almost 20% of the signal could arise from non-specific amplification.

In the absence of template, the uncorrected value at 80 min is 187 copies per μL; however if rate is accounted for, then the value can be corrected to 16 copies per μL, thus eliminating the majority of the false positives.

Finally, we note that although we calculated template concentration, the value is precise but could be inaccurate if not all target molecules loaded into the chip undergo amplification (in other words, if efficiency of amplification is not 100%). Thus, we next sought to measure the absolute likelihood of detecting a molecule as a function of reaction condition**.**

Evaluation of the effect of temperature on dLAMP with two different enzymes to analyze the interplay of amplification efficiency, background, and speed of amplification

After establishing a protocol for generating real-time, digital measurements, we evaluated the absolute amplification efficiency of LAMP as a function of temperature for two different enzymes. We selected two commercial polymerases that worked well for us previously. Both enzymes are *in silico* homologues on the *Bacillus* stearothermophilus DNA Polymerase I and Large Fragment. NEB describes *Bst* 3.0 as an improvement of *Bst* 2.0 by adding reverse transcriptase activity, increased amplification speed, and increased thermostability. We sought to understand the differences in performance between these two enzymes at the single template level. For this experiment, we used the previously described RTAI.[30] The field of view for this instrument is larger than a microscope, allowing up to six samples to be observed concurrently. Hence, both the positive and negative controls could be collected in triplicate simultaneously. We expect some differences in measurements made on different instruments as a result of differing camera sensitivities and differences in the heating mechanism. Indeed, when we ran a single-concentration amplification reaction under identical conditions and compared measurements from the microscope and the RTAI, we found that there was significant difference ($P = 0.03$) in amplification efficiency between the two instruments (**Figure**

S2), with the RTAI generating higher amplification efficiency. Hence, we performed all enzyme-performance comparisons on a single instrument.

Amplification efficiency

First, we sought to establish the amplification efficiency of dLAMP, i.e. the fraction of template copies loaded that are detected (**Figure 3a-b**). We calculated the bulk concentration of template molecules from the digital measurement and plotted the observed template concentration as a fraction of template molecules loaded. To calculate the amplification efficiency, we determined template concentration using ddPCR and assumed all template molecules amplified. Using the real-time component of our measurements, we plotted the percent of copies detected over time compared with ddPCR.

We next asked how temperature impacts amplification efficiency. In general, we observed greater amplification efficiency at longer amplification times, which aligned with our previous observation (**Figure 2d–e)**. Second, when observing at a fixed time, increasing temperature increased amplification efficiency to an optimum (green box in **Figure 3a-b**) before activity decreased.

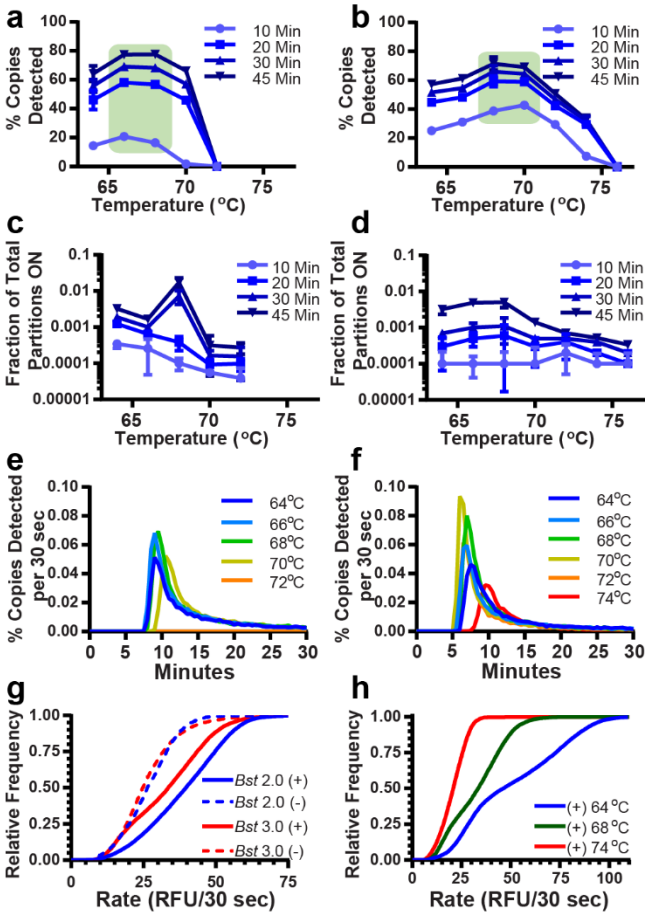

Figure 3. Evaluation of reaction conditions (enzymes and temperature) using real-time digital LAMP. (a-b) Amplification efficiency (percent template copies detected out of copies loaded) of *Bst* 2.0 (a) and *Bst* 3.0 (b) as a function of temperature. Green boxes indicate the optimal temperature range for the greatest probability of template detection. (c-d) Non-specific amplification in template-free buffer samples using *Bst* 2.0 (c) and *Bst* 3.0 (d) for conditions matching panels a-b. (e-f) Distribution of time to fluorescence threshold using *Bst* 2.0 (e) and *Bst* 3.0 (f). (g) The fractional cumulative distribution function (CDF) compares the enzymes at their optimal temperatures (68 °C). (h) Fractional CDF plots of *Bst* 3.0 rate at three temperatures. Error bars are S.D. For all datasets, N = 3 chips (technical replicates). CDF plots are the sum of 3 technical replicates.

Several observations can be made by comparing the results from *Bst* 2.0 and *Bst* 3.0 (**Figure 3a-b**). Although *Bst* 2.0 and *Bst* 3.0 have an identical reported optimal incubation temperature in bulk (65°C), we observed they had different optimal temperature ranges for amplification efficiency (*Bst* 2.0 at 66–68 °C; *Bst* 3.0 at 68–70 °C). We detected lower amplification efficiency at higher temperatures with *Bst* 2.0 compared with *Bst* 3.0. *Bst* 2.0 failed to amplify at 72 °C, whereas *Bst* 3.0 continued amplifying until 76 °C. At short amplification times, (such as 10 min), *Bst* 3.0 had greater amplification efficiency than *Bst* 2.0 (42.8% vs 20.8%, respectively). In contrast, at longer amplification times, such at 30 or 45 min, efficiency for the enzymes was similar (77.6% vs 71.5% at 45 min, respectively), though *Bst* 2.0 had slightly greater amplification efficiency than *Bst* 3.0.

We hypothesize that increased temperature improved amplification efficiency (presumably by increasing the breathing of dsDNA and facilitating primer annealing) until, at higher temperatures, a combination of enzyme denaturation or failure of the primers to anneal occurred. Our primers had melting temperatures ranging from 56–61 °C, when excluding the secondary FIP and BIP anealing regions, as calculated using OligoCalc.[35] We found that chip-to-chip variability was extremely low. Relative error for *Bst* 2.0 at optimal temperature (68 °C) and 45 min of amplification was ~2% (**Figure 2a**), whereas the predicted Poisson noise for a single chip is 0.7%. Achieving such high precision using bulk measurements would require hundreds of experiments. The low variability among these measurements indicates that we were correctly determining whether a partition contained solution and whether it amplified.

Non-specific background amplification

Next, we quantified the amount of non-specific amplification (**Figure 3 c-d)** as a function of time and temperature. We plotted the number of wells that turned “on” in the absence of template relative to the total number of wells filled with LAMP solution. As previously stated, these non-specific amplification reactions included buffer in place of

template and represent a best-case scenario. We concluded that at least for these idealized conditions, non-specific amplification in dLAMP was extremely low. For example, a fraction of 0.001 could correspond to 20 partitions turning on from among a total of 20,000 possible partitions. For both enzymes, we found the maximum fraction of non-specific amplification per total partitions was 0.0012 for times 20 min or less. The highest fraction of non-specific amplification observed was 0.017 at 45 min, corresponding to fewer than 350 non-specific partitions of the 20,000 total (**Figure 3c-d**). Furthermore, we observed higher temperatures resulted in lower non-specific amplification (**Figure 3c-d**). Finally, at extremely long amplification times (e.g. 60 min amplification, data not shown) *Bst* 2.0 had lower background than *Bst* 3.0.

Variations in speed and amplification efficiency

Third, we quantified the variation in speed and amplification efficiency across partitions in the time to reach fluorescence intensity threshold (**Figure 3e-f**). We first plotted the percent copies detected as a function of time for each temperature. As described previously, these curves represent the distribution in the time to threshold across all partitions and thus illustrate the interplay of (i) detecting a molecule (area under the curve from zero to a given time corresponding to the values plotted in **Figure 3a-b**), (ii) the speed of the reaction (the time at which the peak reaches a maxima) and (iii) several parameters of peak width summarized in **Table S1**. We hypothesize peak width is related to both the enzyme amplification rate, overall amplification efficiency, and the time at which the reaction initiates. Next, we plotted the peak time to threshold (**Figure S1)**. Images were collected in 30-sec intervals and we report the average of three trials. In some cases, the difference in time to threshold was less than the imaging time interval. For each time point, if fewer than 15 partitions (0.075% of total partitions) were "on," that time point was not included in the calculation of the mode. For these measurements, at the start of the reaction, the heat block was at 25 °C and the time to threshold included the time for the heat block to come to reaction temperature (~70 sec). Hence, there will be minor differences (seconds) in the time for each reaction to reach the fixed

temperature. We do not see evidence that this difference manifests in the mode time to positive (TTP) measurements.

In reactions with *Bst* 2.0, below 68 °C, mode TTP was narrowly clustered around 9.5 min. At 70 °C, mode TTP increased, and the reaction failed to amply beyond 72 °C. In reactions with *Bst* 3.0, the mode TTP decreased from 8.2 ± 0.3 (mode ± S.D.) min at 64 °C to 6.6 ± 0.3 min at 70 °C, then increased with increasing temperature until amplification failed for all partitions at temperatures ≥76 °C. In the negative controls for both enzymes (**Figure S1**), amplification either failed or started after 75 min.

Several observations can be made by comparing the results from **Figure 3e-f.** We found that the optimal temperature for time to threshold corresponded with the optimal temperature for amplification efficiency (**Figure 3a-b)**, and that the optimal temperatures also had the smallest tailing factors, Full Width at Half Maximum (FWHM) and asymmetric factor (i.e. narrowest peak widths) **(Figure 3e-f; Table S1)**. At optimal efficiency, *Bst 3*.0 was approximately 2 min faster in mode TTP, had much narrower FWHM, smaller tailing factor, and lower asymmetry than *Bst* 2.0. Finally, as efficiency decreases, measurements of peak shape and width increase. To the best of our knowledge, this is the first published quantification that explicitly tests and quantifies the time dependence of LAMP efficiency using these enzymes. Real-time digital enables us to identify the time point at which the observed concentration most closely approximates the true concentration thus optimizing the assay duration.

Rates of amplification (specific and non-specific)

Fourth, we compared the rates of specific and non-specific amplification between *Bst* 2.0 and *Bst* 3.0. The data shown represent the combined rates of three separate trials. We found that non-specific amplification rates were similar for the two enzymes (**Figure 3g**, dashed lines), whereas in the presence of template, amplification rates were faster for *Bst* 2.0 than *Bst* 3.0 (**Figure 3g**, solid lines), despite lower efficiency at short times.

Differences in camera sensitivity between the microscope (used for real-time images in **Figure 2**) and the RTAI (used for **Figure 3**) result in different apparent amplification rates.

We also examined the relationship between temperature, efficiency, and maximum rate. In the case of *Bst* 3.0, maximum reaction amplification rate does not correspond with optimal efficiency (**Figure 3h**). 64 °C had the fastest amplification rates, but suboptimal efficiency (57.3% at 45 min). Optimal amplification efficiency occurs at 68 °C (71.5% at 45 min), but slightly slower amplification rate than 64 °C. At 74 °C, we observed both poor efficiency (32.7% at 45 min) and slowest reaction rate. We attribute this to a combination of decreased enzymatic velocity and decreased primer annealing. Additionally, we note that different thresholds for amplification rate would be needed for each temperature. This is expected given changes in enzymatic velocity.

Application of the pipeline to a phenotypic antibiotic susceptibility test (AST) using clinical samples

We next asked whether we could apply the output of this digital real-time pipeline to perform a rapid phenotypic AST. Specifically, we aimed to categorically sort clinical samples as phenotypically "susceptible" or "resistant" to an antibiotic in agreement with the gold-standard reference method. This study was constructed as a demonstration of the capability of the microfluidic chips and the value gained from using this digital real-time pipeline to optimize reaction conditions—it was not an assessment of the digital AST (dAST) methodology established previously.[17,18] We selected the optimal dLAMP conditions for *Bst* 3.0 based on the measurements of mode TTP and amplification efficiency established in the previous experiments (**Figure 3b**)—70 °C and a reaction time of 10 min. We used archived clinical urine samples from patients diagnosed with urinary tract infections (UTI) containing *E. coli.* These samples had been categorized as phenotypically susceptible or resistant to the antibiotics ciprofloxacin or nitrofurantoin using the gold-standard (broth microdilution) method.[18] We tested exactly 17 samples

and observed 100% categorical agreement with the gold-standard method (0 major errors; 0 minor errors). We conclude that the pipeline presented in this paper performs well and could be used, among other applications, to optimize reaction conditions for speed and sensitivity and apply those conditions to a determination of phenotypic antibiotic susceptibility in clinical samples.

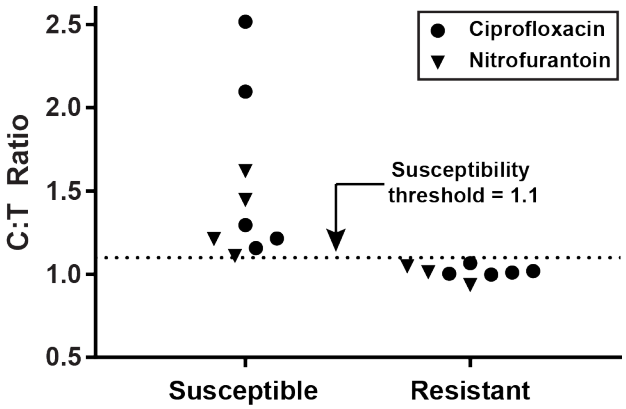

Figure 4. Phenotypic antibiotic susceptibility tests of 17 clinical urine samples from patients infected with a urinary tract infection containing *E. coli*. Susceptibility to the antibiotics nitrofurantoin and ciprofloxacin were tested using dLAMP conditions optimized using digital real-time experiments (Figure 3). Urine samples were exposed to media without antibiotic (control) or media with an antibiotic (treated) for 15 min and then concentrations of nucleic acids were quantified to calculate a control:treated (C:T) ratio. Samples were categorized by dLAMP as susceptible (above the susceptibility threshold) or resistant (below the threshold). All samples were categorized in agreement with the clinical gold-standard method.

Conclusion

We have presented a pipeline to generate real-time, digital isothermal amplification measurements using only commercial and open-source components. We used this pipeline to examine how small changes in reaction conditions influence the interplay of LAMP efficiency, speed, and background by performing 124 real-time dLAMP

experiments. As one practical application of this approach, we determined the optimal reaction conditions for a phenotypic test of antibiotic susceptibility using 17 clinical urine samples from patients diagnosed with urinary tract infections. In all cases, the results of the optimized dLAMP assays were in agreement with the clinical gold-standard AST.

These experiments validate that real-time digital measurements enable tests of enzymatic performance in dLAMP. Generally, we found that each enzyme had a unique optimal temperature for amplification efficiency (probability of detecting a target molecule) and for eliminating non-specific amplification. This "optimal" temperature produced the fastest mode TTP and the narrowest, most symmetrical distribution curves; interestingly, the optimal temperature did not necessarily yield the fastest amplification rate. Together, these data suggest that amplification efficiency is an interplay of enzymatic rate, diffusive transport, and DNA breathing. When reactions are performed away from optimal temperature, the distribution curves broaden and decrease in total area, resulting in reduced overall amplification efficiency and slower mode TTP; whereas amplification rate decreases with increasing temperature. With regard to the specific enzymes in this study, although efficiency was similar at long amplification times (> 20 min), *Bst* 3.0 had a faster mode TTP than *Bst* 2.0 by approximately 2 min, and more narrow and symmetrical distribution curves. However, *Bst* 2.0 had faster amplification rates than *Bst* 3.0, so reactions with *Bst* 2.0 took longer to initiate, but proceeded more rapidly. For both polymerases, non-specific amplification in buffer was extremely low.

In the future, this pipeline can be used to understand the fundamental pieces of LAMP. The field of diagnostics would benefit from a thorough mechanistic study of LAMP asking which components determine amplification fate, and how components, such as primers and heating rate (**Figure S2**), impact reaction and enzymatic speed. This pipeline makes such a mechanistic study possible. For example, in this study we corrected the observed concentration by separating true positives from background amplification using rate and fluorescence, but we did not explore the origins of non-specific amplicons—which deserves its own study and development of more precise tools for studies of non-

specific amplification. Finally, this pipeline can be extended to optimize other isothermal amplification chemistries that could be suited to other types of diagnostic assays.

Ultimately, this pipeline will make digital real-time measurements more accessible to researchers, even those who lack microfluidic expertise or specialized equipment. The commercially available chips and reagents used here could be coupled with many combinations of standard laboratory or field equipment, such as a hot plate and a fluorescent stereoscope, or a chemical heater and a cell phone camera. While we believe the general trends found in this manuscript will extend to other primer sets, we hope this pipeline will enable others to study other primer sets and conditions of interest to them.

Acknowledgments

This research was supported in part by the Burroughs Wellcome Fund Innovation in Regulatory Science Award (to R.F.I.) and a grant from the Jacobs Institute for Molecular Engineering for Medicine. Research reported in this publication was also supported by the Department of Health and Human Services (HHS) Office of the Assistant Secretary for Preparedness and Response (ASPR) and the Wellcome Trust under the CARB-X program (federal award number IDSEP160030-02); the content is solely the responsibility of the authors and does not necessarily represent the official views of the Department of HHS Office of the ASPR. This work is funded in part by CARB-X as a collaboration between Talis Biomedical Corp. and Caltech. This project benefited from the use of instrumentation at the Jim Hall Design and Prototyping Lab at the California Institute of Technology. We thank Travis Schlappi for performing the extractions of the archived clinical samples and Natasha Shelby for contributions to writing and editing this manuscript.

References

(1) Heid, C. A.; Stevens, J.; Livak, K. J.; Williams, P. M. *Genet. Res.* **1996**, *6*, 986-994.

(2) Tanner, N. A.; Zhang, Y.; Evans, T. C. *BioTechniques* **2012**, *53*, 81-89.

(3) Tanner, N. A.; Zhang, Y.; Evans, T. C. *BioTechniques* **2015**, *58*, 59-68.

(4) Notomi, T.; Okayama, H.; Masubuchi, H.; Yonekawa, T.; Watanabe, K.; Amino, N.; Hase, T. *Nucleic Acids Res.* **2000**, *28*, e63-e63.

(5) Tanner, N. A.; Evans, T. C. *Curr. Protoc. Mol. Biol.* **2014**, *105*, 15.14.11-15.14.14.

(6) Becherer, L.; Bakheit, M.; Frischmann, S.; Stinco, S.; Borst, N.; Zengerle, R.; von Stetten, F. *Anal. Chem.* **2018**, *90*, 4741-4748.

(7) Aoi, Y.; Hosogai, M.; Tsuneda, S. *J. Biotechnol.* **2006**, *125*, 484-491.

(8) Drame, P. M.; Fink, D. L.; Kamgno, J.; Herrick, J. A.; Nutman, T. B. *J. Clin. Microbiol.* **2014**, *52*, 2071-2077.

(9) Mori, Y.; Kitao, M.; Tomita, N.; Notomi, T. *J. Biochem. Bioph. Meth.* **2004**, *59*, 145-157.

(10) Ball, C. S.; Light, Y. K.; Koh, C.-Y.; Wheeler, S. S.; Coffey, L. L.; Meagher, R. J. *Anal. Chem.* **2016**, *88*, 3562-3568.

(11) Calvert, A. E.; Biggerstaff, B. J.; Tanner, N. A.; Lauterbach, M.; Lanciotti, R. S. *PLOS One* **2017**, *12*, e0185340.

(12) Poole, C. B.; Ettwiller, L.; Tanner, N. A.; Evans, T. C., Jr.; Wanji, S.; Carlow, C. K. S. *PLOS One* **2015**, *10*, e0139286.

(13) Poole, C. B.; Tanner, N. A.; Zhang, Y.; Evans, T. C., Jr.; Carlow, C. K. S. *PLOS Neglect. Trop. D.* **2012**, *6*, e1948.

(14) Wheeler, S. S.; Ball, C. S.; Langevin, S. A.; Fang, Y.; Coffey, L. L.; Meagher, R. J. *PLOS One* **2016**, *11*, e0147962.

(15) Bhadra, S.; Jiang, Y. S.; Kumar, M. R.; Johnson, R. F.; Hensley, L. E.; Ellington, A. D. *PLoS One* **2015**, *10*, e0123126.

(16) Khorosheva, E. M.; Karymov, M. A.; Selck, D. A.; Ismagilov, R. F. *Nucleic Acids Res.* **2016**, *44*, e10.

(17) Schoepp, N. G.; Khorosheva, E. M.; Schlappi, T. S.; Curtis, M. S.; Humphries, R. M.; Hindler, J. A.; Ismagilov, R. F. *Angew. Chem. Int. Edit.* **2016**, 9557-9561.

(18) Schoepp, N. G.; Schlappi, T. S.; Curtis, M. S.; Butkovich, S. S.; Miller, S.; Humphries, R. M.; Ismagilov, R. F. *Sci. Trans. Med.* **2017**, *9*, eaal3693.

(19) Sun, B.; Shen, F.; McCalla, S. E.; Kreutz, J. E.; Karymov, M. A.; Ismagilov, R. F. *Anal. Chem.* **2013**, *85*, 1540-1546.

(20) Rodriguez-Manzano, J.; Karymov, M. A.; Begolo, S.; Selck, D. A.; Zhukov, D. V.; Jue, E.; Ismagilov, R. F. *ACS Nano* **2016**, *10*, 3102-3113.

(21) Sun, B.; Rodriguez-Manzano, J.; Selck, D. A.; Khorosheva, E.; Karymov, M. A.; Ismagilov, R. F. *Angew. Chem. Int. Edit.* **2014**, *53*, 8088-8092.

(22) Hu, Y.; Xu, P.; Luo, J.; He, H.; Du, W. *Anal. Chem.* **2017**, *89*, 745-750.

(23) Ma, Y.-D.; Chang, W.-H.; Luo, K.; Wang, C.-H.; Liu, S.-Y.; Yen, W.-H.; Lee, G.-B. *Biosens. Bioelectron.* **2018**, *99*, 547-554.

(24) Ma, Y.-D.; Luo, K.; Chang, W.-H.; Lee, G.-B. *Lab Chip* **2018**, *18*, 296-303.

(25) Schuler, F.; Siber, C.; Hin, S.; Wadle, S.; Paust, N.; Zengerle, R.; von Stetten, F. *Anal. Methods-UK* **2016**, *8*, 2750-2755.

(26) Gansen, A.; Herrick, A. M.; Dimov, I. K.; Lee, L. P.; Chiu, D. T. *Lab Chip* **2012**, *12*, 2247-2254.

(27) Rane, T. D.; Chen, L.; Zec, H. C.; Wang, T.-H. *Lab Chip* **2015**, *15*, 776-782.

(28) Zhu, Q.; Gao, Y.; Yu, B.; Ren, H.; Qiu, L.; Han, S.; Jin, W.; Jin, Q.; Mu, Y. *Lab Chip* **2012**, *12*, 4755-4763.

(29) Shen, F.; Davydova, E. K.; Du, W.; Kreutz, J. E.; Piepenburg, O.; Ismagilov, R. F. *Anal. Chem.* **2011**, *83*, 3533-3540.

(30) Selck, D. A.; Ismagilov, R. F. *PLOS One* **2016**, *11*, e0163060.

(31) Schindelin, J.; Arganda-Carreras, I.; Frise, E.; Kaynig, V.; Longair, M.; Pietzsch, T.; Preibisch, S.; Rueden, C.; Saalfeld, S.; Schmid, B.; Tinevez, J.-Y.; White, D. J.; Hartenstein, V.; Eliceiri, K.; Tomancak, P.; Cardona, A. *Nat. Methods* **2012**, *9*, 676.

(32) Kreutz, J. E.; Munson, T.; Huynh, T.; Shen, F.; Du, W.; Ismagilov, R. F. *Anal. Chem.* **2011**, *83*, 8158-8168.

(33) Rissin, D. M.; Walt, D. R. *Nano Lett.* **2006**, *6*, 520-523.

(34) Rojek, M. J.; Walt, D. R. *PLOS One* **2014**, *9*, e86224.

(35) Kibbe, W. A. *Nucleic Acids Res.* **2007**, *35*, W43-W46.

S-I Summary of MATLAB script functions

In order to quantify the reactions on chips using the Poisson distribution, we needed to know the number of partitions that contained solution and the number of partitions that were empty. (It would be naïve to assume that all 20,000 partitions were loaded with solution; visual inspection shows that was rare.) We counted the total number of partitions with solution using the image of the autofluorescence of SYTO 9 dye before heating at time 0 (**Figure 2a**). SYTO 9 had uniform autofluorescence independent of template presence, making it easy to count all partitions loaded with solution.

To track the mean fluorescence intensity of each partition over time, we solved two challenges. First, when the microfluidic chip was heated (especially during the first 2 min) the chip moved. As the chip heated, it lost the initial autofluorescence from SYTO 9. Consequently, it was not possible to track this movement with the fluorescence of a single fluorophore. We solved this challenge by creating a mask (using image segmentation) that outlined each detectable partition at the chip's final position using a frame at the end of amplification. An advantage to using only the detectable partitions that met a minimum fluorescence intensity (out of a total of 20,000 partitions per chip) was reduced overall computation time because only a fraction of the total partitions were tracked in real-time.

A second challenge when tracking mean fluorescence intensity of each partition over time using only the detectable partitions is that partitions can appear to be different sizes because of differences in fluorescence intensity (dark partitions can appear artificially smaller and bright partitions can appear artificially larger). To counteract the effect of each partition having a different average intensity, we performed multi-level thresholding with tight restrictions for the area and major axis filters. We set a minimum fluorescence intensity (threshold) for each pixel at a given time and used this information to segment (define the perimeter) each individual partition. This threshold was combined with

selection criteria for the area and major axis. The area filter defined the smallest and largest partitions while the major axis filter ensured that detected regions were circular. We repeated this for different threshold values and merged the resulting partitions. This technique restricted partitions to a specific size and shape while enabling detection over many intensity values.

Finally, we used the information from quantifying the number of partitions containing solution and tracking mean fluorescence of each partition over time to calculate the concentration of template in the bulk solution. To smooth the traces and reduce the noise, we first applied a Gaussian-weighted moving average filter with window length 10 frames to each intensity curve. To ensure all partitions start at zero intensity, we determined the baseline intensity by calculating the average partition intensity for selected frames after heating but prior to detectable amplification (between 2.5 min and 5 min). The baseline intensity was subtracted from all frames. Finally, we manually defined a threshold to determine whether a partition would be counted as a "positive" or "negative." Using the adjusted traces, threshold, and the total number of partitions, we determined the fraction of partitions that were "on" for any given time. Using the fraction of partitions that were "off," we calculated via the Poisson distribution the concentration of template detected in the bulk solution for any given time point. From this measurement of concentration, we can calculate the amplification efficiency by dividing the measured concentration by the known (true) concentration.

The MATLAB script described here has been deposited in the open-access online repository GitHub and may be accessed using the following direct link: https://github.com/IsmagilovLab/Digital_NAAT_Analyzer

S-II Real-time data acquisition parameters

Acquiring real-time data using microscopy

Images were acquired in 30-sec intervals on a Leica DMI-6000B (Leica, Buffalo Grove, IL, USA) with a 1.25x 0.04NA HCX PL FLUOTAR Objective (506215) and 0.55x coupler (Leica C-mount 11541544) using a 1-sec exposure through the L5 (GFP) Nomarski prism and a Hamamatsu ORCA-ER CCD camera (Hamamatsu Photonics K.K., Hamamatsu City, Shizuoka, Japan; Ref. C4742-80-12AG). Heating was performed using an integrated circuit (IC) board prototype for temperature control developed by Green Domain Design (San Diego, CA, USA). The IC board was connected to a DC power supply (Model 3670; Electro Industries, Monticello, MN, USA), a Nichrome wire (12 ohm) attached to a 5 x 25 x 25 mm aluminum block. A thermistor was mounted within the block to measure the temperature of the heating block. When the temperature of the heating block was lower than the set-point temperature, the IC board supplied current to the Nichrome wire resistive heater. With this setup, heating was achieved to 70.0 ± 2 °C within 2 min. Images obtained on the microscope were processed with our MATLAB script (**Supporting Information, S-I**) using the following parameters: Area Bound [5 40] pixels, Major Axis [2 9] pixels, Threshold [250] Relative Fluorescence Units (RFU), Baseline Smoothing Frames [6 11], Masking Image Frame [175].

Acquiring data using a custom large-format real-time amplification instrument (RTAI)

Images were acquired in 30-sec intervals on a custom-built, public-domain real-time amplification instrument (RTAI), described previously,[30] using the FAM channel with a 15-sec exposure at *f*/5.6. Heating was achieved using the built-in PCT-200 thermocycler, which heats to 70.0 ± 0.3 °C within 70 sec. The temperature of the thermocycler block was held at 25 °C to start all reactions, with the exception of an experiment where the block was preheated to the optimal temperature (**Figure S2b**). We equipped the thermocycler with an aluminum block with two sloped planes (each set at 11°, an angle defined by the microfluidic chip manufacturer's requirements), to segregate bubbles formed during the reaction to a specifically designed bubble trap. It was advantageous to

use this instrument to analyze up to six chips in parallel in a single field of view and under a uniform temperature. By running multiple chips on a real-time instrument we achieved "multiplexed" assays (wherein multiple measurements are made simultaneously). Images obtained on the RTAI were processed through our MATLAB script (**Supporting Information, S-I**) using the following parameters: Area Bound [4 12] pixels, Major Axis [2 5] pixels, Threshold [100] RFU, Baseline Smoothing frames [6 11], Masking Image Frame [175].

S-III Limitations of chips used

A limitation of chips that discretize by capillary action is that solution can spread among the partitions. For example, during dLAMP quantification of extractions for three of the clinical samples, we observed spreading of one positive partition to its adjacent partitions. We attribute this spreading to liquid bridges forming among adjacent wells, resulting in transfer of the amplicon among compartments. These bridges could arise from defects in surface coatings of commercial chips or from an excess of surface active molecules present in some clinical samples. To test whether spreading was due to surface active impurities in the samples, samples were diluted in Tris-EDTA (TE) buffer and in the subsequent test, spreading was eliminated for one sample. For the remaining samples, dilution reduced the spreading enough that quantification at 10 min was not hindered, although some spreading was observed at later times. Quantification of the C:T ratio remained consistent (and the susceptibility call the same) because we use a ratiometric calculation.

S-IV Calculation of Peak width metrics

The average distribution curve (averaged over three trials) was calculated for each temperature and all values normalized to the peak prominence. Time resolution was estimated to the nearest 15 second interval. Calculations were based on: John V.

Hinshaw. "How Do Your Peaks Measure Up?" Oct 01, 2013, LCGC Europe, Volume 26, Issue 10, pg 575–582.

Full Width at Half Maximum was calculated at the time difference between the leading at tailing edges at 50% peak prominence.

Asymmetric factor was calculated by dividing the time between the peak prominence and the tailing edge ("$b_{0.1}$") by the time between the peak prominence and the leading edge at 10% peak height ("$f_{0.1}$"). (Eq. S1)

$$Asymmetric\ Factor = \frac{b_{0.1}}{f_{0.1}}$$

Tailing factor was calculated as the total peak width at 5% of the prominence (or the distance from the leading edge to the time of peak prominence ("$f_{0.05}$") plus the distance from the time of peak prominence to the tailing edge ("$b_{0.05}$")) divided by twice the distance from the leading edge to the time of peak prominence. (Eq. S2)

$$Tailing\ Factor = \frac{f_{0.05} + b_{0.05}}{2f_{0.05}}$$

Table 9-S1. Tabular quantification of the time to threshold distribution curves.

Bst 2.0						*Bst* 3.0					
Temp (°C)	Efficiency at 45 min (%)	Mode TTP (min)	FWHM (min)	Asymmetric Factor	Tailing Factor	Temp (°C)	Efficiency at 45 min (%)	Mode TTP (min)	FWHM (min)	Asymmetric Factor	Tailing Factor
64.0	64±8	9.5±0.0	2.5	10.2	14.8	64.0	57±2	8.2±0.3	3.0	8.0	14.2
66.0	78±2	9.3±0.3	2.3	7.6	11.7	66.0	61±2	7.3±0.3	2.3	5.6	11.4
68.0	78±2	9.8±0.3	2.3	7.2	14.3	68.0	71±6	7.6±0.3	2.3	6.0	9.2
70.0	66±1	11.0±0.0	2.8	8.8	9.1	70.0	69±3	6.7±0.3	1.5	7.3	3.7
						72.0	51±3	7.2±0.3	2.0	8.3	4.3
						74.0	33±9	10.2±0.6	2.8	5.7	13.1

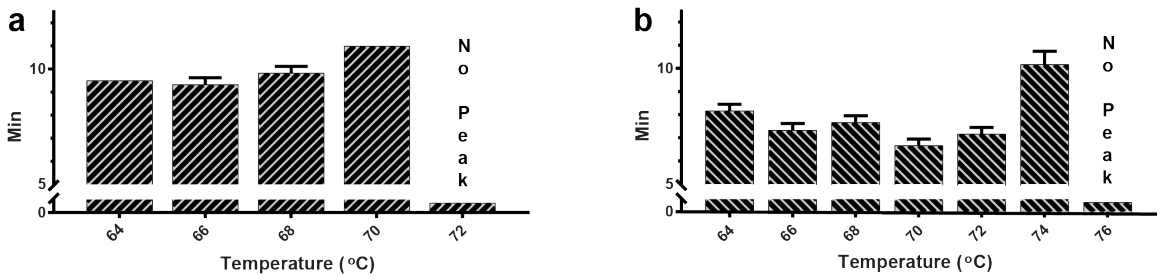

Figure 9-S1. Bar graphs of the time location of the peak of the distribution curve (time to mode positive) using *Bst* 2.0 (a) and *Bst* 3.0 (b). We required 15 or greater partitions turn on at a given time (0.075% of total partitions), to include the time point for the mode. Data are summarized in Table S1 in S-III.

S-VI Hardware and pre-heating considerations

We asked if multiple instrumentation formats could be used to collect the data and if hardware format impacted the amplification efficiency. We used the optimal conditions for *Bst* 3.0. First, we compared the performance of the large-format real-time amplification instrument (RTAI) to a wide-field microscope fitted with a heat block—a set-up that would be accessible to most laboratories. We found that the heater ramp rate was slower on the microscope than the RTAI (120 sec versus 70 sec) resulting in 9.0 ±1.0 min time to mode positive (**Figure S2a)**.

Next, we looked at the effect of pre-heating using the RTAI. We compared the optimal conditions using *Bst* 3.0 and starting from 25 °C (green curve) with the same instrument and heating block already at the optimal reaction temperature of 70 °C (orange curve). When the block is preheated, we observed the mode time to threshold reduced from 6.7 ±0.3 min to 6.0 ±0.0 min (**Figure S2a**).

Next, we asked if differences in hardware configuration and the heating rates between the instruments would also correspond to differences in probability of detection. We observed significant variation in amplification efficiency (RTAI vs RTAI with preheating $P = 0.002$; RTAI vs microscope with heater $P = 0.031$, RTAI with preheating vs

microscope with heater $P < 0.001$) and concluded that heating rate may impact probability of amplification (**Figure S2b**). Hence, all comparisons made in this study were instrument specific. Though it remains to be tested, we suspect more precise hardware, with improved heating control, could improve device performance.

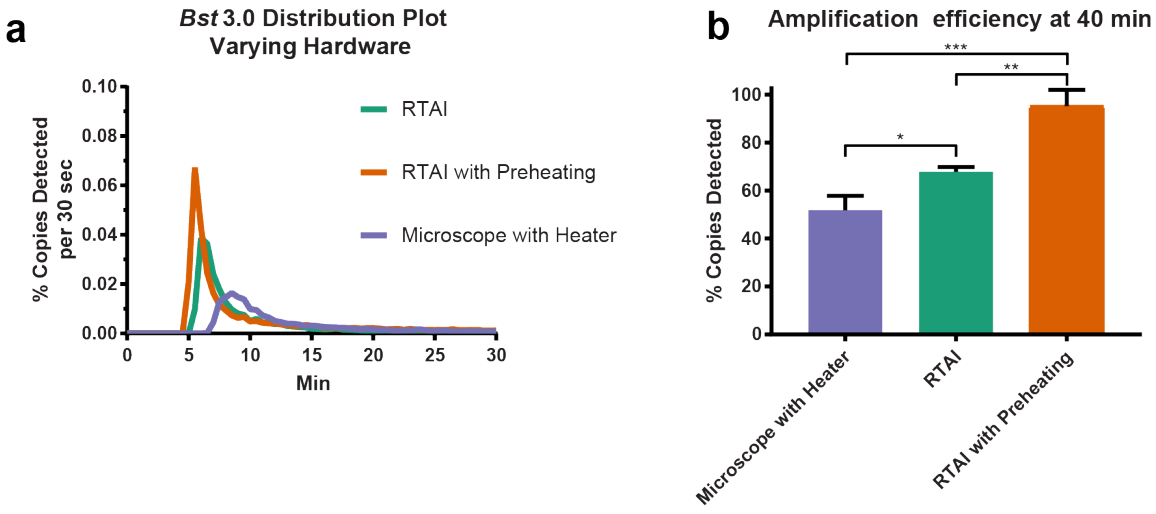

Figure 9-S2. Effect of hardware and heating on (a) the distribution in time to fluorescence threshold and (b) quantification of amplification efficiency (mean percentage copies detected ± S.D.) at 40 min.

S-VII Optimization of *Bst* 2.0 buffer composition

Following the protocol described previously[18], buffer conditions for *Bst* 2.0 were optimized in bulk at 713 copies/uL (e.g. ~4,280 or 0 copies per 6 µL reaction). Optimal buffer composition was selected based on fastest bulk time to positive.

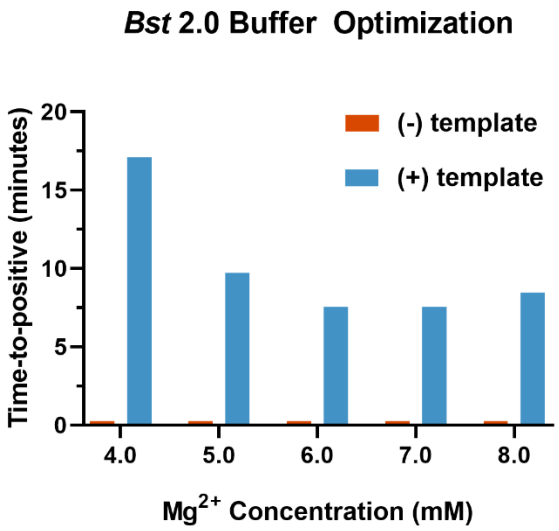

Figure 9-S3. Magnesium optimization for *Bst* 2.0. A value of 0.25 indicates that no amplification was observed. Amplification was performed at 67.5° C. N=1 for all TTP values.

S-VIII Contributions of non-corresponding authors

J.C.R. conceptualized the method, generated and analyzed data. Wrote the paper, constructed figures, and performed all revisions.

E.J. wrote the MATLAB software script for automated analysis of digital LAMP image sequences. Provided minor input to experimental design; and minor edits and inputs to the figures and manuscript.

N.G.S. prepared and quantified nucleic acid stocks. Optimized buffer conditions for *Bst* 2.0. Provided minor input to experimental design and minor edits and inputs to the figures and manuscript.